

INTERNATIONAL UNIVERSITY LIAISON INDONESIA (IULI)

BACHELOR'S THESIS

STABILITY ANALYSIS AND CONTROL DESIGN OF BARUNA-1

By

I Made Pradana Kusuma Putra

11201801015

Presented to the Faculty of Engineering

In Partial Fulfilment Of the Requirements for the Degree of

SARJANA TEKNIK

In

AVIATION ENGINEERING

FACULTY OF ENGINEERING

BSD City 15345

Indonesia

July 2022

APPROVAL PAGE

STABILITY ANALYSIS AND CONTROL DESIGN OF BARUNA-1

I MADE PRADANA KUSUMA PUTRA

11201801015

Presented to the Faculty of Engineering

In Partial Fulfillment of the Requirements for the Degree of

SARJANA TEKNIK

In

AVIATION ENGINEERING

FACULTY OF ENGINEERING

Triwanto Simanjuntak, PhD

Thesis Advisor

Date

Dipl.-Ing. Sentot Wahjoe Georitno, MSi

Dean of Faculty of Engineering

Date

EXAMINERS APPROVAL PAGE

Ressa Octavianty, PhD

Date

Ir. Setyo Utomo Soekarsono, MSc. MM

Date

STATEMENT BY THE AUTHOR

I declare that this submission is my own work and to the best of my knowledge, it contains no material previously published or written by another person, nor material which to a substantial extent has been accepted for the award of any other degree or diploma at any educational institution, except where due acknowledgement is made in the thesis.

I Made Pradana Kusuma Putra _____

Student

Date

ABSTRACT

Stability Analysis and Control Design of Baruna-1

by

I Made Pradana Kusuma Putra

Triwanto Simanjuntak, PhD, Advisor

In this thesis, the static and dynamic stability of Baruna-1 — a firefighting aircraft proposed by IULI Design Team to respond the [2021 - 2022 AIAA Aircraft Design Competition](#) — at take-off and cruise conditions are analyzed. The Linear Quadratic Regulator (LQR) control technique of Stability Augmentation System is applied in order to ensure the aircraft is stable and controllable during missions. The dynamic characteristics of Baruna-1 are evaluated based on the American Military Specification MIL-F-8785C.

The static stability is analyzed based on the C_{m_α} , C_{l_β} and C_{n_β} derivatives and the static margin. The dynamic stability is analyzed by using the State Space model, where the aerodynamic coefficients and stability derivatives of Baruna-1 are calculated by using Approach 1 (based on literature's methodologies) and Approach 2 (the combination of Approach 1 and USAF Digital DATCOM data).

The result shows that Baruna-1 aircraft is longitudinal, lateral and directional statically stable with 24.1743% static margin. However, the result of Approach 1 at take-off conditions shows that the aircraft is lateral statically unstable with the value of C_{l_β} is 0.023283. Baruna-1 is natural dynamically unstable with the positive sign of the eigenvalues. The implementation of lqr control technique successfully stabilized the aircraft, indicated by the negative sign of all the eigenvalues, where the aircraft is asymptotically stable with the curve converges to the steady-state conditions.

The dynamic characteristics of Baruna-1 aircraft have met the Level I of MIL-F-8785C flying and handling quality requirements. However, the dutch roll natural frequency did not meet the minimum level requirements.

Keyword: *Stability, Control, SAS, LQR*

ACKNOWLEDGEMENTS

First, I would want to thank God for blessed me with good health during the whole process of writing my thesis. Throughout the completion of this thesis, I have faced many obstacles that I could not have handled on my own. I would like to express my deepest appreciation for:

- Triwanto Simanjuntak, PhD, as my supervisor. His support and guidance throughout this thesis from you all has been invaluable. First time when i discussed with him about thesis topic, i was trying to avoid writing a bachelor thesis about flight dynamics and flight control. However, he has shown his support and insight at the beginning what should i prepare to do this thesis. This made me more confident and helped me push myself to complete this thesis.
- My parents and my family, especially my mother and grandmother, who always supports and push me. Their supports gave me a lot of energy to complete my thesis and fight during my thesis journey.
- My best friends, Hendy, Prameswara, Yona, Galuh and Bandem, who always support me by their own ways. A lot of discussions and laugh happened during my thesis writing with them that gave me spirit and a great mood to complete my thesis. Also Richard, Felix and Satria that willing to help me on my thesis.
- Last but not least, for all of the people that I am regrettably not able to mention who kept on believing in me.

Contents

Approval Page	i
EXAMINERS APPROVAL PAGE	ii
Statement by The Author	iii
Abstract	iv
Acknowledgements	v
Contents	vi
List of Figures	xi
List of Tables	xv
1 Introduction	1
1.1 Background	1
1.2 The Overview of Baruna-1	4
1.3 Problem Statement	7
1.4 Research Questions	8
1.5 Research Objectives	9
1.6 Research Scope and Limitation	9
1.7 Significance of the Study	10
2 Literature Review	11
2.1 The Aircraft Equation of Motion	11
2.1.1 Body Reference Frame, Inertial Frame and Stability Axes	13
2.1.2 Linear Momentum	14

2.1.3	Angular Momentum	16
2.1.4	Euler Angles	17
2.1.5	Flight Path Equations	18
2.1.6	Kinematic Equations	20
2.1.7	Gravitational Equations	22
2.2	Steady State and Perturbation Equations of Motion	23
2.2.1	Overview	23
2.2.2	Steady State Equations of Motion	24
2.2.3	Perturbation Equations of Motion	25
2.2.4	Small Perturbation Equations of Motion	27
2.3	Aerodynamic and Thrust Forces and Moments	28
2.3.1	Longitudinal Aerodynamic Forces and Moment	28
2.3.2	Lateral Directional Aerodynamic Forces and Moments	31
2.3.3	Thrust Forces and Moments	33
2.3.4	Longitudinal Aerodynamic Forces and Moment at Small Per- turbation Condition	34
2.3.5	Lateral Directional Aerodynamic Force and Moments at Small Perturbation Condition	35
2.3.6	Thrust Forces and Moments at Small Perturbation Condition	36
2.4	The Equations of Motion Laplace Transformations at Small Pertur- bation	37
2.4.1	The Longitudinal Equations of Motion Laplace Transforma- tions at Small Perturbation	38
2.4.2	The Lateral Directional Equations of Motion Laplace Trans- formations at Small Perturbation	41
2.5	Aircraft Stability	44
2.5.1	Static Stability and Control	45
	Longitudinal Static Stability and Trim Condition	45
	Lateral Static Stability	47
	Directional Static Stability	47
2.5.2	Dynamic Stability Stability and Control	48
	The Short Period and Phugoid Modes	49
	The Rolling, Spiral and Dutch Roll Modes	50

2.6	The Dynamics Systems State Variables Model	51
2.6.1	The Longitudinal State Variable Model	51
2.6.2	The Lateral Directional State Variable Model	54
2.7	Flying and Handling Qualities	56
2.7.1	Longitudinal Flying Quality Requirements	56
	Phugoid Mode Damping Ratio	56
	The Short Period Mode Damping Ratio	56
2.7.2	Lateral Directional Flying Quality Requirements	59
	The Dutch Roll Mode Damping Ratio and Natural Frequency	59
	The Spiral Mode Time Constant	59
	The Rolling Mode Time Constant	60
2.8	Stability Augmentations System	60
2.8.1	The LQR Control Technique	61
3	Research Methodology	64
3.1	Reserach Overview	64
3.2	Tails and Control Surfaces Design	68
3.2.1	Tail Arm Calculation	68
3.2.2	Horizontal and Vertical Tail Design	69
3.2.3	Control Surfaces Design	71
3.3	MATLAB	72
3.4	Stability and Control Derivatives Calculation	72
3.4.1	Steady-State Lift Coefficient	72
3.4.2	Steady-State Drag Coefficient	74
3.4.3	Steady-State Pitching Moment Coefficient	75
3.4.4	Steady-State Lateral Force Coefficient	76
3.4.5	Steady-State Rolling Moment Coefficient	81
3.4.6	Steady-State Yawing Moment Coefficient	86
3.4.7	Steady-State Thrust Coefficient	89
3.4.8	Speed Derivatives	90
3.4.9	Rate of Angle of Attack Derivatives	91
3.4.10	Pitch Rate Derivatives	91
3.4.11	Roll Rate Derivatives	92

3.4.12	Yaw Rate Derivatives	96
3.5	State Space Model	100
3.5.1	State Space Model of Longitudinal Dynamics	100
3.5.2	State Space Model of Lateral Directional Dynamic	100
3.5.3	Longitudinal Modes Calculations	101
3.6	USAF Digital DATCOM	102
3.6.1	drawDATCOMaircraft	102
3.6.2	USAF Digital DATCOM Input Definition	102
	FLTCON Namelist	103
	OPTINS and SYNTHS Namelist	104
	BODY Namelist	104
	WGPLNF, HTPLNF and VTPLNF Namelists	105
	WGSCHR, HTSCHR, VTSCHR Namelists	106
	SYMFLP and ASYFLP Namelists	107
	Case Control Cards	109
3.6.3	Output Definitions	110
4	Results and Discussions	114
4.1	Tail and Control Surfaces Design	114
4.2	Analysis Overview	116
4.3	Stability and Control Analysis	117
4.3.1	The Steady State Aerodynamic Coefficient and the Stability and Control Derivatives	117
4.3.2	Static Stability Analysis	117
	Longitudinal Static Stability and Trim Condition Analysis	117
	Lateral Directional Static Stability Analysis	122
4.3.3	Dynamic Stability	123
	Longitudinal Dynamic Stability	123
	Lateral Directional Dynamic Stability	128
4.4	Application of Stability Augmentation System for Dynamics Stability	132
4.4.1	Application of Stability Augmentation System for Longitu- dinal Dynamics Stability	132

4.4.2	Application of Stability Augmentation System for Lateral Directional Dynamics Stability	139
4.5	Baruna-1 Flying and Handling Quality Evaluation	150
4.5.1	Baruna-1 Short Period Mode Flying Qualities	150
4.5.2	Baruna-1 Phugoid Mode Flying Qualities	151
4.5.3	Baruna-1 Dutch Roll Mode Flying Qualities	151
4.5.4	Baruna-1 Roll Mode Flying Qualities	152
4.5.5	Baruna-1 Spiral Mode Flying Qualities	152
5	Summary, Conclusion, Recommendation	153
5.1	Summary	153
5.2	Conclusion	154
5.3	Recommendations	156
	Bibliography	157
	Appendices	160
	Turnitin Report	227
	Curriculum Vitae	229

List of Figures

1.1	Burned area (Mkm^2) 1982-2018 showing the FireCCI51 (based on AVHRR-LTDR data) alongside FireCCI51 and MCD64A19 [3]	1
1.2	Comparison of burned area trends from satellite observations (GFED4s) and prognostic fire models from FireMIP [4]	2
1.3	Annual burned areas extracted for Indonesia from GFED4s for total area, wildland and peatland [4]	3
1.4	The Evergreen Boeing 747 Aircraft [14]	4
1.5	AIAA Undergraduate Design Competition	5
1.6	The Final Design of Baruna-1	6
1.7	Baruna-1 Mission Profile	7
1.8	Baruna-1 Wing	8
2.1	Aircraft Equations of Motion Flowchart	11
2.2	Forces and Moments, Linear and Angular Velocity and Gravitational Components Acting on the Body Axes	12
2.3	Body Axes and Earth Based Inertial Frame (Reproduced from [16])	13
2.4	Aircraft Body and Stability Axes (Reproduced from [16])	14
2.5	The North-East-Down frame (Reproduced from [16])	17
2.6	Introduction of the Euler Angles Ψ (Reproduced from [16])	18
2.7	Introduction of the Euler Angles Θ (Reproduced from [16])	19
2.8	Introduction of the Euler Angles Φ (Reproduced from [16])	19
2.9	Longitudinal Aerodynamic Forces and Moment (Reproduced from [16])	28
2.10	Wetted Area of the Elevator and Stabilator (Reproduced from [16])	29
2.11	Longitudinal Steady-State Aerodynamic Forces and Moments (Reproduced from [16])	31

2.12	The Installed Thrust Directions in accordance with Body and Stability Axes (Reproduced from [16])	33
2.13	Concept of Transfer Function (Reproduced from [16])	41
2.14	Pitching Moment Coefficient vs Angle of Attack [19]	46
2.15	Static Margin of an Aircraft (Reproduced from [16])	47
2.16	Rolling Moment Coefficient vs Sideslip Angle [19]	48
2.17	Yawing Moment Coefficient vs Sideslip Angle [19]	49
2.18	Longitudinal Characteristic Equations Root Locations (Reproduced from [16])	50
2.19	Lateral Directional Characteristic Equations Root Locations (Reproduced from [16])	51
2.20	Longitudinal Feedback Options [15]	61
2.21	Lateral Directional Feedback Options [15]	61
3.1	Research Methodology Flowchart	64
3.2	Tail and Control Surfaces Design Flowchart	65
3.3	Aerodynamic Coefficients Flowchart	65
3.4	Stability and Control Derivatives Flowchart	66
3.5	Static Stability Analysis Flowchart	66
3.6	Dynamic Stability Analysis Flowchart	67
3.7	Stability Augmentation System Flowchart	68
3.8	Dynamic Stability Characteristic Evaluations Flowchart	69
3.9	Fuselage Section Radius Definition for Tail Arm Calculation [19]	70
3.10	The Location of Aircraft Aerodynamic Center and Center of Gravity (Reproduced from [16])	77
3.11	Wing Body Interference Factor [16]	79
3.12	Rudder Effectiveness τ_R as a result of $\vec{c}_{rudder}/\vec{c}_{vtail}$ [16]	80
3.13	Span Factor between Rudder and Vertical Tail [16]	80
3.14	Contribution to $c_{l_{\beta_{WB}}}$ due to Wing Twist Angle [16]	82
3.15	Identification of the Vertical Tail Z_V and X_V (Reproduced from [16])	83
3.16	Location of the Ailerons along the Wing Span (Reproduced from [16])	84
3.17	Rolling Moment Effectiveness for $AR = 8$ and $\lambda = 0.5$ [16]	84
3.18	Identification of the Rudder Z_R and X_R (Reproduced from [16])	86

3.19 Geometric Parameter of the XZ Cross Section of the Fuselage (Re-	
produced from [16])	87
3.20 Empirical Factor K_N for Wing-Body Interface [16]	88
3.21 Effect of Reynolds Number on Wing-Body Interface [16]	88
3.22 Yawing Moment Correlation Coefficient due to Aileron Deflections	
[16]	89
3.23 K_q Correction Coefficient [16]	92
3.24 Rolling Damping Parameters for $\lambda = 0.5$ [16]	93
3.25 Effect of Wing Twist on c_{n_p} [16]	95
3.26 Evaluation of $\left(\frac{c_{l_r}}{c_{L_1}}\right)\bigg _{\kappa}$ [16]	97
3.27 Effect of Wing Twist on c_{l_r} [16]	98
3.28 Effect of Lift on c_{n_r} [16]	99
3.29 Baruna-1 Aircraft DATCOM Model	103
3.30 FLTCON Namelist	104
3.31 OPTINS and SYNTHS Namelists	104
3.32 BODY Namelist	105
3.33 WGPLNF, HTPLNF and VTPLNF Namelists	106
3.34 WGSCHR, HTSCHR and VTSCHR Namelists	107
3.35 SYMFLP and ASYFLP Namelists	109
3.36 Case Control Cards	110
3.37 Aerodynamic Coefficient and Stability Derivatives DATCOM Output	110
3.38 Aerodynamic Coefficient and Stability Derivatives DATCOM Out-	
put (Cont')	111
4.1 Elevator and Rudder Design	114
4.2 Aileron Design	115
4.3 The Pitching Moment Coefficient vs Angle of Attack	120
4.4 Trim Diagram for Approach 1 and Approach 2	121
4.5 Location of the CG, AC, Neutral Point and the Static Margin of	
Baruna-1	122
4.6 The Location of Short Period and Phugoid Mode Eigenvalues	127
4.7 The Location of Dutch Roll, Rolling and Spiral Mode Eigenvalues .	131

4.8	The Location of Short Period and Phugoid Mode State Feedback Eigenvalues	136
4.9	The Response of Speed Perturbation $u(s)$ to Elevator $\delta_e(s)$ Step Input	137
4.10	The Response of Angle of Attack $\alpha(s)$ to Elevator $\delta_e(s)$ Step Input	137
4.11	The Response of Pitch Rate $q(s)$ to Elevator $\delta_e(s)$ Step Input . . .	138
4.12	The Response of Pitch Angle $\theta(s)$ to Elevator $\delta_e(s)$ Step Input . . .	138
4.13	The Location of Dutch Roll, Rolling and Spiral Mode State Feedback Eigenvalues	143
4.14	The Response of Sideslip Angle $\beta(s)$ to Aileron $\delta_a(s)$ Step Input . .	144
4.15	The Response of Roll Rate $p(s)$ to Aileron $\delta_a(s)$ Step Input	145
4.16	The Response of Yaw Rate $r(s)$ to Aileron $\delta_a(s)$ Step Input	145
4.17	The Response of Bank Angle $\phi(s)$ to Aileron $\delta_a(s)$ Step Input . . .	146
4.18	The Response of Sideslip Angle $\beta(s)$ to Rudder $\delta_r(s)$ Step Input . .	147
4.19	The Response of Roll Rate $p(s)$ to Rudder $\delta_r(s)$ Step Input	147
4.20	The Response of Yaw Rate $r(s)$ to Rudder $\delta_r(s)$ Step Input	148
4.21	The Response of Bank Angle $\phi(s)$ to Rudder $\delta_r(s)$ Step Input . . .	149

List of Tables

1.1	Design requirements as per specified in the Request for Proposal for Responsive Aerial Fire Fighting Aircraft by AIAA	5
1.2	Fuselage Length and the Location of CG and AC of Baruna-1	7
1.3	Wing Geometric Parameter	8
2.1	The Longitudinal Dimensional Stability and Control Derivatives	40
2.2	Lateral Directional Dimensional Stability and Control Derivatives	43
2.3	Classes of Military Aircraft along with Examples of Civilian Equivalent	57
2.4	Categories of Aircraft Maneuvers	58
2.5	Requirements for the Phugoid Damping	58
2.6	Requirements for the Short Period Damping (Military Aircraft)	58
2.7	Dutch Roll Damping and Natural Frequency Requirements (Military Aircraft)	59
2.8	Requirements for the Spiral Mode (Military Aircraft)	59
2.9	Requirements for the Rolling Mode (Military Aircraft)	60
3.1	Typical Value for Horizontal and Vertical Tail Volume Coefficients [25]	70
3.2	Typical Value for Aircraft Control Surfaces [25]	71
4.1	Geometric Properties of the Horizontal and Vertical Tails	115
4.2	Geometric Properties of the Aircraft Control Surfaces	115
4.3	The Steady-State Aerodynamic Coefficient of Baruna-1 at Take-off and Cruise Conditions	117
4.4	Longitudinal Stability and Control Derivative of Baruna-1 at Take-off and Cruise Conditions ($\alpha_{to} = 12.0856^\circ$ and $\alpha_{cruise} = 1.344^\circ$)	118

4.5	Lateral Directional Stability and Control Derivative of Baruna-1 at Take-off and Cruise Conditions ($\alpha_{to} = 12.0856^\circ$ and $\alpha_{cruise} = 1.344^\circ$)	119
4.6	Longitudinal Transfer Function of Baruna-1 at Take-off and Cruise Conditions	126
4.7	Longitudinal Eigenvalues of Baruna-1 at Take-off and Cruise Conditions	126
4.8	The Natural Frequency ω , Damping ζ and Time Constant T of Baruna-1 at Take-off and Cruise Conditions	126
4.9	Lateral Directional Transfer Function of Baruna-1 at Take-off and Cruise Conditions	130
4.10	Lateral Directional Eigenvalues of Baruna-1 at Take-off and Cruise Conditions	130
4.11	Longitudinal State Feedback Transfer Function of Baruna-1 at Take-off and Cruise Conditions	134
4.12	Longitudinal State Feedback Eigenvalues of Baruna-1 at Take-off and Cruise Conditions	135
4.13	The State Feedback Natural Frequency ω , Damping ζ and Time Constant T of Baruna-1 at Take-off and Cruise Conditions	139
4.14	Lateral Directional State Feedback Transfer Function of Baruna-1 at Take-off and Cruise Conditions	141
4.15	Lateral Directional State Feedback Eigenvalues of Baruna-1 at Take-off and Cruise Conditions	142
4.16	Baruna-1 Short Period Mode Damping Evaluation at Take-off and Cruise Conditions	150
4.17	Baruna-1 Phugoid Mode Damping Evaluation at Take-off and Cruise Conditions	151
4.18	Baruna-1 Dutch Roll Mode Damping Evaluation at Take-off and Cruise Conditions	151
4.19	Baruna-1 Dutch Roll Mode Natural Frequency Evaluation at Take-off and Cruise Conditions	152
4.20	Baruna-1 Rolling Mode Time Constant Evaluation at Take-off and Cruise Conditions	152

4.21 Baruna-1 Spiral Mode Double Amplitude Time Constant Evaluation at Take-off and Cruise Conditions	152
--	-----

List of Abbreviations

AC	Aerodynamic Center
COG	Center Of Gravity
KE	Kinematic Equation
IKE	Inverted Kinematic Equation
LQR	Linear Quadratic Regulator

Dedicated to my parents

CHAPTER 1

INTRODUCTION

1.1 Background

Wildfires are acknowledged as a global environmental phenomenon that had impacts on the Earth's atmosphere[1], where these problems have been a difficult and unpredictable issue that necessitates lots of attention to the changing of individuals, landscapes and ecosystems which occur in all over the world[2]. Every year, wildfires affect approximately 4 million km² of Earth's land as shown in Fig. 1.1, which shows the burned area between 1982-2018[3].

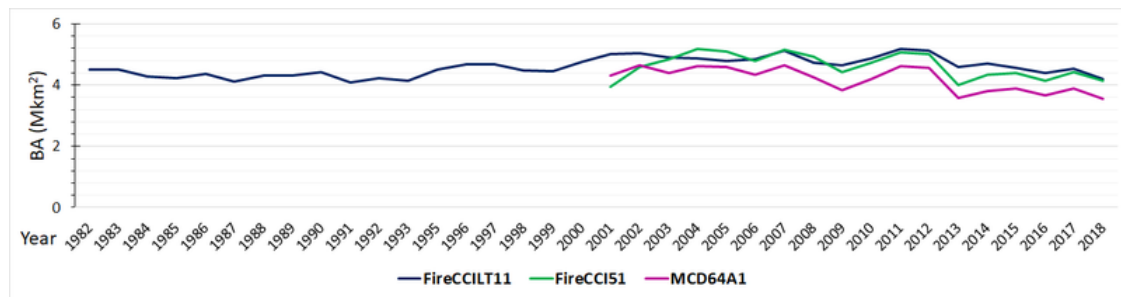


FIGURE 1.1: Burned area (Mkm^2) 1982-2018 showing the FireC-CILT11 (based on AVHRR-LTDR data) alongside FireCCI51 and MCD64A19 [3]

The trend in global burned area declined about $-1.35 \pm 0.49\%$ year⁻¹ between 1998 - 2005 with significant declines occurred in tropical savannas of South America and Africa and grasslands across the Asian based on the Global Fire Emissions Database version 4 (GFED4s). FireMIP models ($n = 9$) predicted a mean trend of $-0.13 \pm 0.56\%$ year⁻¹ in comparison to the observed trend $-1.09 \pm 0.61\%$ year⁻¹ in global burned area in 1997 - 2013 as shown in Fig. 1.2[4].

Forest and peatland fires in Indonesia are a significant worldwide issue because to the high greenhouse gas emissions and detrimental effects of ensuing aerosol

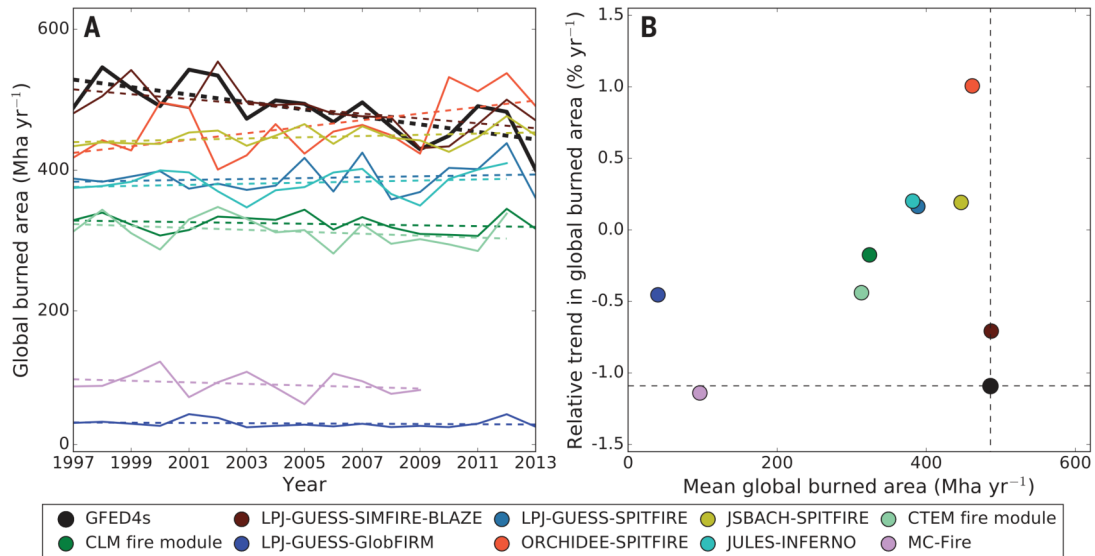


FIGURE 1.2: Comparison of burned area trends from satellite observations (GFED4s) and prognostic fire models from FireMIP [4]

emissions on human health, transportation, tourism, and economic activity in the Southeast Asian area[5]. The majority of wildfires in Indonesia are caused by human activities[6], where the burned area in Indonesia from year 2000 to 2016 based on Global Fire Emission Database GFEDv4 are shown in Fig. 1.3. According to World Bank[7], 2.6 million hectares land are burned between June - October 2015 with the total costs of USD 16.1 billion. From January to September 2019, Indonesia has 857 756 hectares of land and forest fire coverage, with 1464 hot spots[8].

Certainly, wildfires have negative impacts on many aspect of life, from environmental problems to health issues. Air pollution, respiratory issues, flame and thermal burns, head induced illness, cardiovascular effects, as well as psychological effects[9]. In combating wildfires, the use of firefighting aircraft is one of the common approach that used in Australia, where it can assist ground forces be more effective and efficient[10]. Currently, the majority of aerial firefighting services are used to extinguish fires outside of inhabited areas, such as forests and grasslands. The reasons for using aerial firefighting are time constraints and limited terrain access for ground firefighting mechanisms[11]. To support fire operations, a variety

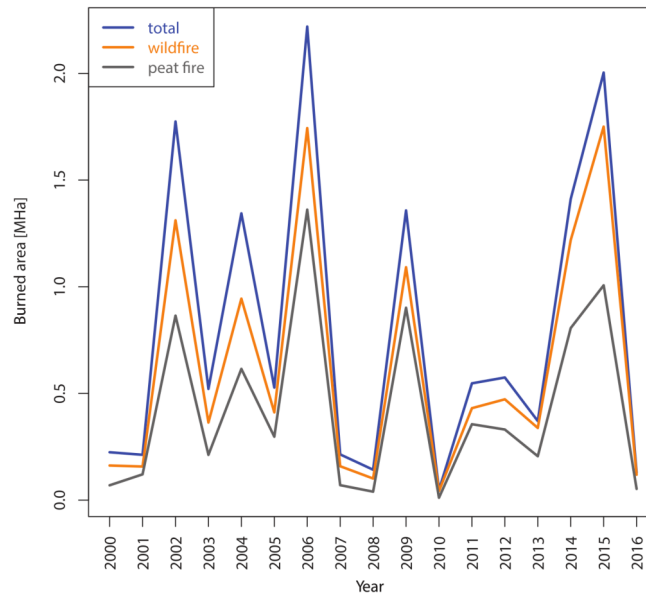


FIGURE 1.3: Annual burned areas extracted for Indonesia from GFED4s for total area, wildland and peatland [4]

of fixed and rotary wing aircrafts are used. Due to their ability to react quickly and prevent flames from spreading, Single Engine Air Tankers (SEATs) are widely utilized for firefighting operations[12].

The most commonly used in order of firefighting aircraft are water bombers, including helitack and scoopers, and land-based air tankers. Helitack focuses mostly on the use of helicopters to transfer water from adjacent water sources into storage tanks. Scoopers work by scooping water from nearby bodies of water (lakes, rivers, etc.). An example of a firefighting aircraft is the Evergreen Boeing 747 as shown in Fig. 1.4, a big water tanker with a fire retardant capacity of 78 000 gallons. Large-capacity tankers are also quicker and have more endurance than their smaller equivalents, which improves reaction time and enables the aircraft to remain stationed for prolonged durations[12].

The majority of the aircraft used for firefighting services are military or commercial aircrafts that have been modified. The equipment required for firefighting purposes is integrated into the aircraft structure, although compromises and inefficiencies are introduced as a result of changes in aerial firefighting payload delivery compared to the aircraft's original design objectives[13]. The massive payload

carried by the Aerial Firefighting Aircraft will have an impact on the aircraft's stability during take-off, cruising, and critical missions. In order to achieve the



FIGURE 1.4: The Evergreen Boeing 747 Aircraft [14]

aircraft stability, understanding the aircraft equations of motion is critical. Since it provides the foundation for the entire flight dynamic framework, providing an understanding of flight and handling quality. The aircraft equations of motion for a particular aircraft design may be fully descriptive in terms of static stability, dynamic stability, and control system.

By this study, the author aims to calculate and analyze the static and dynamic stability of Baruna-1, with the application of the stability augmentation system in order to improve the dynamic stability characteristic of the Baruna-1 and ensure the aircraft remain in stable condition during missions.

1.2 The Overview of Baruna-1

Baruna-1, is a firefighting aircraft designed by Inferno Team International University Liaison Indonesia, which participated in AIAA Undergraduate Aircraft Design Competition 2022 which has an ultimate goal to ensure superiority over the fire and maintain low operational costs. There are several requirements to be met in designing the firefighting aircraft for AIAA Undergraduate Design Competition 2022 shown in Tab. 1.1

STABILITY ANALYSIS AND CONTROL DESIGN OF BARUNA-1

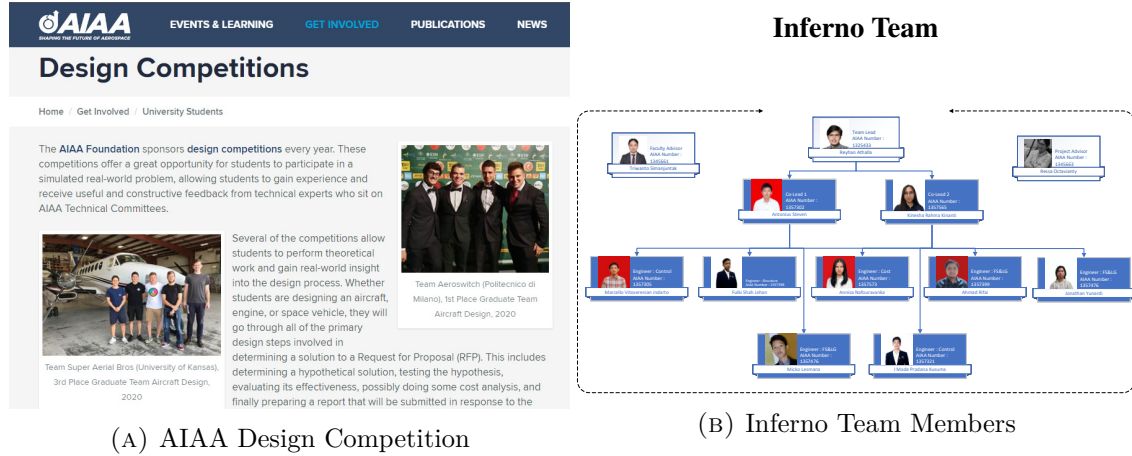


FIGURE 1.5: AIAA Undergraduate Design Competition

Code	RFP	Mandatory	Goal
R0	Entry into service (EIS)	Year 2030	Year 2030
R1	Engine readiness year	≤ Year 2028	≤ Year 2028
R2	Specific fuel consumption/ efficiency, thrust/power and weight	Assumptions must be documented	
R3	Fire retardant capacity (gallons)	4000	8000
R4	Multi-drop capability	Yes	Yes
R5	Volume per drop	≥ 2000	≥ 3000
R6	Fire retardant reload rate	≥ 500 gal / min	750 gal / min
R7	Retardant density	≥ 9 lbs/gal	9 lbs / gal
R8	Drop speed	≤ 150 kts	≤ 125 kts
R9	Drop altitude	≤ 300 ft AGL	150 ft AGL
R10	Design radius with full payload (n mi)	200	400
R11	Design ferry range (kts)	2000	4000
R12	Dash speed (kts)	300	400
R13	Balanced field length	≤ 8000 ft @ 5,000 ft MSL elevation on a +35°F hot day	≤ 5000 ft @ 5,000 ft MSL elevation on a +35°F hot day
R14	Certification	VFR and IFR flight with an autopilot	VFR and IFR flight with an autopilot
R15		Flight in known icing conditions	Flight in known icing conditions
R16		FAA 14 CFR Part 25	FAA 14 CFR Part 25
R17		Autonomous operations	

TABLE 1.1: Design requirements as per specified in the Request for Proposal for Responsive Aerial Fire Fighting Aircraft by AIAA

The Baruna-1 is powered by four Europrop TP400-D6 engines with a combined power of 44 260 horsepower and a fire retardant capacity of 8000 gallons. The ground support for the Baruna-1 will be provided by two pumps, one for water and one for vacuum, with fire retardant reloads of 1761 gal/min and 924.6 gal/min, respectively. At maximum performance, Baruna-1 can drop eight times, and the amount of retardant released in each drop can be adjusted. The Baruna-1 has a drop speed of 60 meters per second and a drop altitude of 50 m. With full fuel capacity, Baruna-1 has a maximum mission range of 4500 m and a ferry range of 12 500 m.

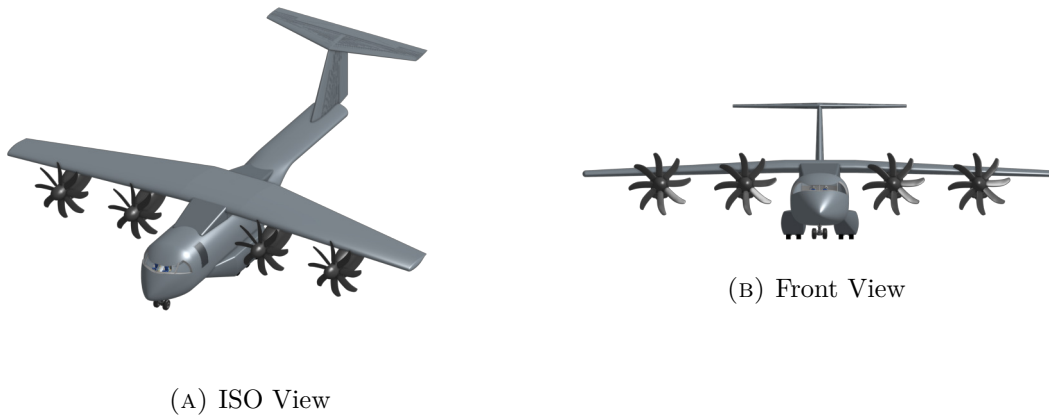
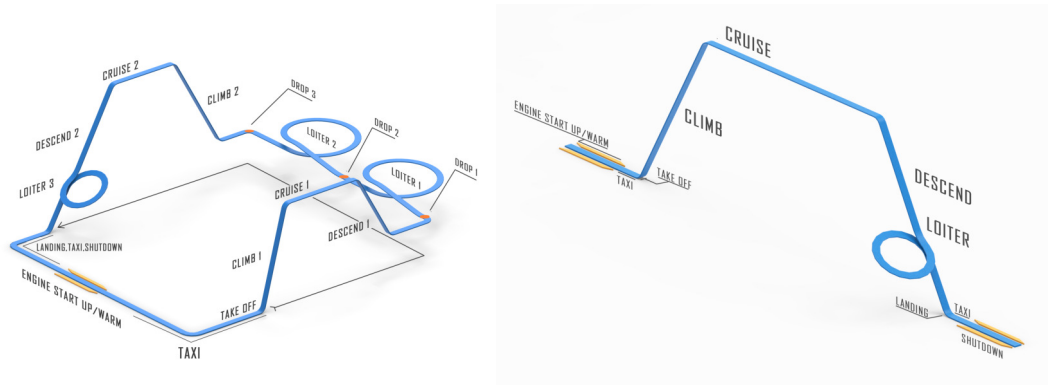


FIGURE 1.6: The Final Design of Baruna-1

Furthermore, the mission profiles of the Baruna-1 are similar to those of a military bomber aircraft. Instead of bombs, Baruna-1 will drop fire retardants onto burning areas. The fire-fighting mission profile is shown in Fig. 1.7a, where Baruna-1 will drop three separate batches of fire retardants at an altitude of about 100 meters (300 feet). Each drop phase will last approximately one minute, while the loiter phase following the Drop 1 and Drop 2 phases will last approximately fifteen minutes each. Furthermore, due to the critical Mach Number of the airfoil, the aircraft will maintain an altitude of 3,500 m (11,500 ft) during both cruising phases. During the Cruise 2 phase, the aircraft will cruise at 206 m/s (400 knots). Finally, if the aircraft makes an Instrument approach, it will remain in the Loiter 3 phase for approximately 45 minutes. For the ferry mission profile is shown in Fig. 1.7b, where this mission profile is similar to that of a typical commercial aircraft mission profile. Like the firefighting mission profile, the aircraft will cruise

at 3,500 m (11,500 ft) and will remain in the air for approximately 45 minutes if an instrument approach is used.



(A) Firefighting Mission

(B) Ferry Mission

FIGURE 1.7: Baruna-1 Mission Profile

The geometry of Baruna-1 are shown below. The location of Baruna-1 center of gravity and the aerodynamic center are shown in Table 1.2. The geometry of the wing is shown in Table 1.3 and Fig. 1.8.

Parameter	Value
Location of the Aircraft CG from Nose (m)	10.5734
Location of the Aircraft CG (% MAC)	-10.1400
Wing Apex (m)	10.4392
Location of the Wing AC (% MAC)	0.2200
Location of the Wing-Fuselage AC (% MAC)	0.1282
Location of the Horizontal Tail AC from Nose (m)	32.8371
Location of the Horizontal Tail AC from Wing Leading Edge (% MAC)	447.9600
Fuselage Length (m)	32.7778

TABLE 1.2: Fuselage Length and the Location of CG and AC of Baruna-1

1.3 Problem Statement

The aircraft control surfaces are important for the stability and controllability of the aircraft. The static and dynamic stability have to be analyzed in order to find out



FIGURE 1.8: Baruna-1 Wing

Parameter	Value
Wing Planform Area (S_{ref}) (m^2)	200.00
Wing Span (m)	40.02
Aspect Ratio	8.00
Taper Ratio	0.50
Twist Angle ($^\circ$)	-2.00
Dihedral Angle ($^\circ$)	-2.00
Wing Airfoil	MS(1)-0317

TABLE 1.3: Wing Geometric Parameter

the aircraft stability during missions. It is important to design the aircraft control surfaces based on the Baruna-1 wing and body configurations and to analyze the aircraft stability that meet the flying and handling quality requirements.

1.4 Research Questions

- What are the dimensions of the aircraft control surfaces required to be designed based on the Baruna-1 wing and body configurations?
- Is Baruna-1 stable in Longitudinal and Lateral Directional motion during take-off and cruise conditions?
- How to make Baruna-1 stable and controllable during take-off and cruise conditions?
- Are the dynamic characteristics of Baruna-1 meet the American Military Specification MIL-F-8785C flying and handling quality?

1.5 Research Objectives

The aims of this study are to:

- Design the aircraft control surfaces based on the Baruna-1 wing and body configurations.
- Calculate and analyze the stability of Baruna-1.
 - Longitudinal Static Stability;
 - Lateral Static Stability;
 - Directional Static Stability;
 - Longitudinal Dynamic Stability; and
 - Lateral Directional Dynamic Stability;
- Implement the lqr control technique of stability augmentation system to ensure Baruna-1 is stable and controllable during take-off and cruise conditions.
- Evaluate the dynamic characteristics of Baruna-1 based on the American Military Specification MIL-F-8785C flying and handling quality.

1.6 Research Scope and Limitation

The Author established the following scopes and limitations for the research:

1. The static and dynamic stability of Baruna-1 are analyzed at take-off and cruise condition.
2. The linear control theory is used to analyze the static and dynamic stability of Baruna-1.
3. The aerodynamic coefficients and stability derivatives are calculated using two approaches: the analytical approach and the combination of analytical approach and USAF Digital DATCOM as a comparison control.
4. The Linear Quadratic Regulator (LQR) control technique is used for Stability Augmentation System.

5. The flying and handling quality requirements are analyzed based on the MIL-F-8785C American Military Specification.

1.7 Significance of the Study

The results of this research are expected:

- Can be used as a proof of the Baruna-1 static and dynamic stability with the implementation of the lqr control technique of stability augmentation system in improving the dynamic stability characteristics of Baruna-1 to meet the flying and handling quality requirements.
- The methods that have been used in this thesis can be implemented in other types of aircraft design process to analyze the stability of an aircraft.
- Became a baseline for flight dynamics and control students which are interested in designing an aircraft in evaluating the static and dynamic stability of aircrafts.

CHAPTER 2

LITERATURE REVIEW

2.1 The Aircraft Equation of Motion

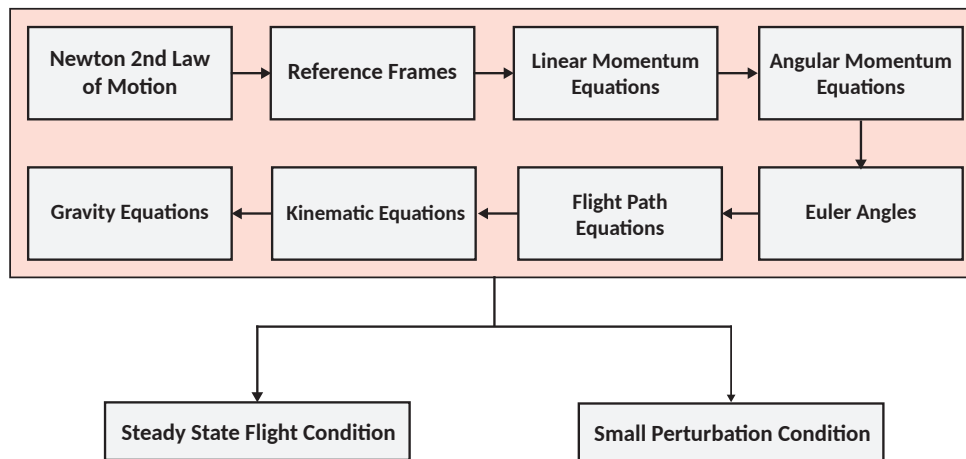


FIGURE 2.1: Aircraft Equations of Motion Flowchart

Different sets of equations derived from the simplest form of Newton 2nd law shown in Eq. 2.1 for each of the aircraft's degree of freedom define its equations of motion [15], that will leads to six fundamental equations: the linear momentum and angular momentum equations, euler angles, flight path equations, kinematic equations and gravitational equations which described the aircraft dynamic system [16], where forces and moments, linear and angular velocity and gravitational components that corresponding to each fundamental equations acting on the body axes are shown in Fig. 2.2,

$$\vec{F} = m\vec{a} \quad (2.1)$$

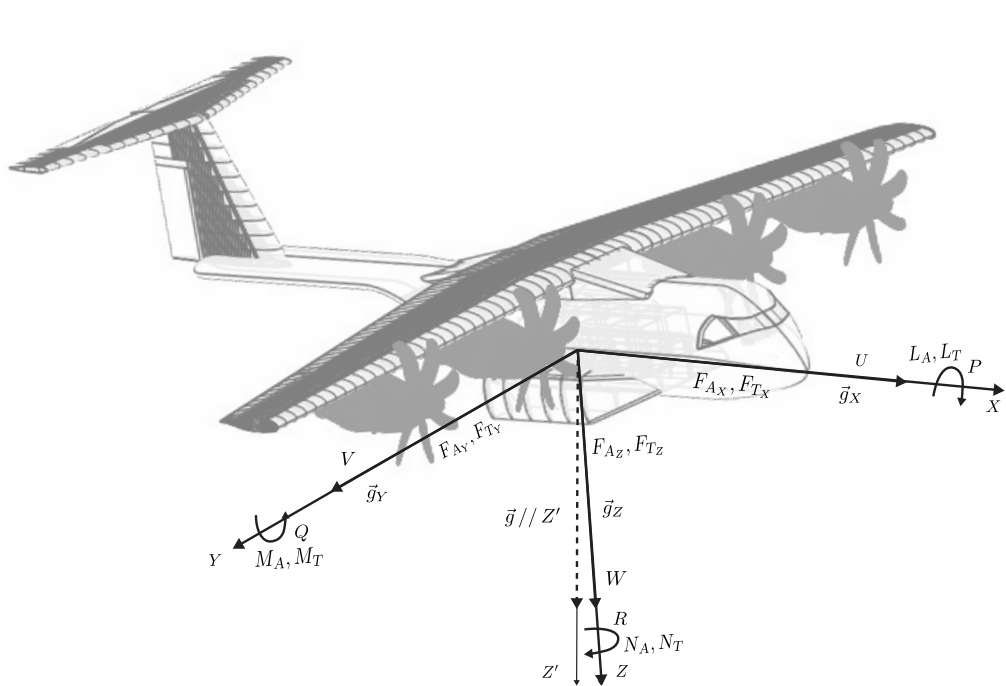


FIGURE 2.2: Forces and Moments, Linear and Angular Velocity and Gravitational Components Acting on the Body Axes

2.1.1 Body Reference Frame, Inertial Frame and Stability Axes

A body reference frame and an Earth-based inertial frame are introduced in deriving the aircraft equation of motion. As shown in Fig. 2.3, the location of the body frame is at the aircraft CG denoted as X, Y, Z , and at the center of Earth for the Earth-based inertial frame denoted as X', Y', Z' with the condition that the inertia frame does not rotate with Earth. The \vec{r}' component is defined as the distance between inertial frame and a generic point on the aircraft known as the moment arm. Additionally, the aircraft body is assumed to be rigid, with the mass of the aircraft and the distribution of the aircraft mass are constant which appropriate for a limited time period $\frac{dm}{dt} = 0$ in accordance with the fuel consumptions during flight [16].

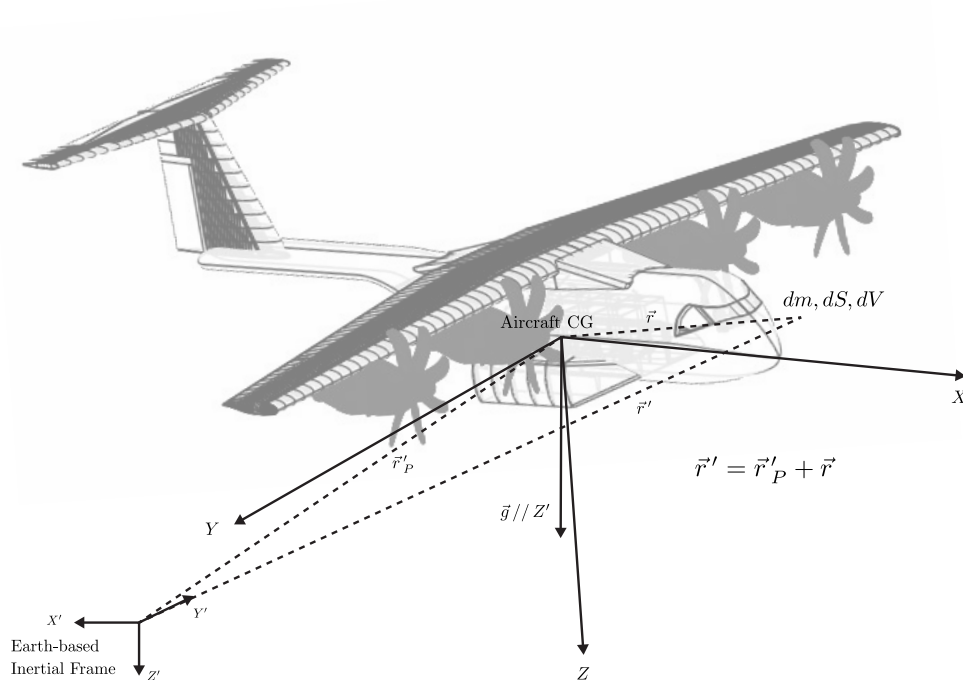


FIGURE 2.3: Body Axes and Earth Based Inertial Frame (Reproduced from [16])

The aircraft stability axes, labeled X_S, Y_S, Z_S , are used to model the aircraft aerodynamic forces and moments, with X_S being associated with the steady-state

airspeed direction and Z_S being zero. By definitions, can be expressed by

$$\begin{aligned} V_{P_1} &= U_{1_S} \\ W_{1_S} &= 0 \end{aligned}$$

with the angle between X_S and X as shown in Fig. 2.4 is the angle of attack α_1 at steady state condition, which is described the body frame and the stability axes relationships.

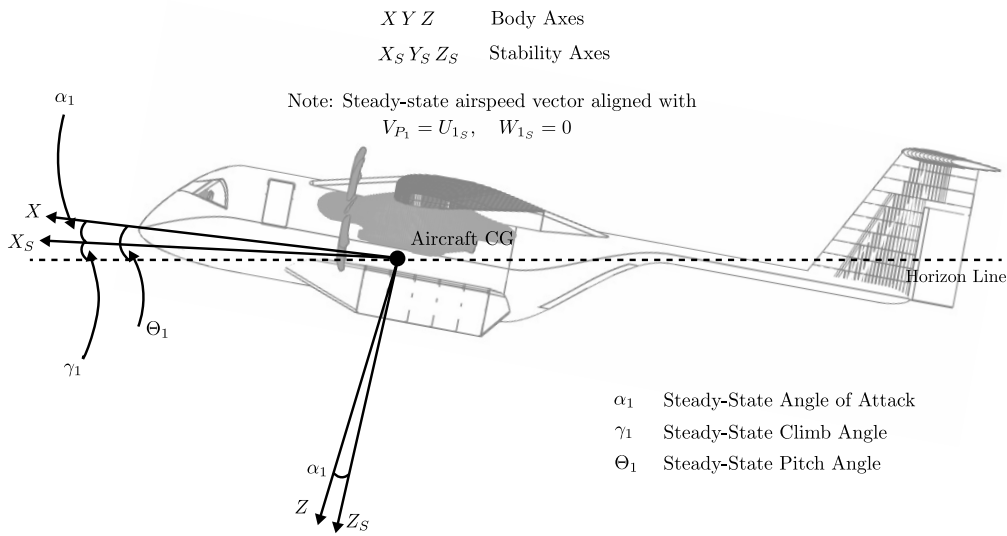


FIGURE 2.4: Aircraft Body and Stability Axes (Reproduced from [16])

2.1.2 Linear Momentum

The initial point is considering the aircraft as a continuous system with the each components are mass m , density ρ_A , volume V and surface S , which can be expressed as [16]

$$m = \int_V \rho_A dV \tag{2.2}$$

The general relationship of the linear momentum equations in vectorial form in accordance with the Earth-based inertial frame is expressed in Eq. 2.1

$$\frac{d}{dt} \int_V \rho_A \frac{d\vec{r}}{dt} dV = \int_V \rho_A \vec{g} dV + \int_S (\vec{F}_A + \vec{F}_T) dS \tag{2.3}$$

The gravitational force, aerodynamic and thrust forces are acting on the body frame which located at the aircraft CG. This condition leads to the first linear momentum equations vectorial relationship in accordance with the Earth-based inertial frame shown in Eq. 2.4.

$$m \frac{d\vec{V}_P}{dt} = m\vec{g} + (\vec{F}_A + \vec{F}_T) \quad (2.4)$$

In addition, the relative motion of a body frame in accordance with the inertial frame is expressed to express the aircraft dynamics relative to the body frame. A generic vector \vec{C} in accordance with the inertial frame is introduced that will be expressed in body frame by introducing the the body frame angular velocity $\vec{\omega}$ in accordance with the Earth-based inertial frame. The relationship can be mathematically expressed as [16]

$$\frac{d\vec{C}}{dt} = \frac{\partial \vec{C}}{\partial t} + \vec{\omega} \times \vec{C} \quad (2.5)$$

Recall the Eq. 2.4 where the generic vector relationship is applied, leads to

$$m (\vec{\dot{V}}_P + \vec{\omega} \times \vec{V}_P) = m\vec{g} + (\vec{F}_A + \vec{F}_T) \quad (2.6)$$

This relationship should be expressed in accordance with the body frame which leads to the linear momentum equations in accordance with the body reference frame X, Y, Z ,

$$\begin{aligned} m(\dot{U} + QW - RV) &= mg_X + (F_{Ax} + F_{Tx}) \\ m(\dot{V} + UR - PW) &= mg_Y + (F_{Ay} + F_{Ty}) \\ m(\dot{W} + PV - QU) &= mg_Z + (F_{Az} + F_{Tz}) \end{aligned} \quad (2.7)$$

where

- The U, V, W components of the linear velocity vector in accordance with the body frame;
- The g_X, g_Y, g_Z is the gravitational components; and
- The P, Q, R components of the angular velocity vector in accordance with the body frame.

2.1.3 Angular Momentum

The development of angular momentum equations starting from Eq. 2.3, where the initial conservation of the angular momentum equations in vectorial form is expressed by [16]

$$\frac{d}{dt} \int_V \vec{r} \times \rho_A \frac{d\vec{r}}{dt} dV = \vec{M}_A + \vec{M}_T \quad (2.8)$$

where

$$\vec{M}_A + \vec{M}_T = \int_S \vec{r} \times (\vec{F}_A + \vec{F}_T) dS$$

Due to the initial angular momentum equations is expressed in accordance with the inertial frame, the following relationship is introduced in accordance with the body reference frame in order to represent the aircraft rotational dynamics in accordance with the center of gravity. Reformulate the expression into the volumetric integral leads to

$$\frac{d}{dt} \int_V \vec{r} \times \rho_A \frac{d\vec{r}}{dt} dV = \int_V \vec{r} \times \rho_A \frac{d}{dt} \frac{d\vec{r}}{dt} dV \quad (2.9)$$

The relative motion relationship is used to differentiate the \vec{r} twice in accordance with the body frame. The first differentiation which is called as a generic vector \vec{c} is given by

$$\frac{d\vec{r}}{dt} = \dot{\vec{r}} + \vec{\omega} \times \vec{r} \quad (2.10)$$

leads to

$$\int_V \vec{r} \times \rho_A \frac{d}{dt} \frac{d\vec{r}}{dt} dV = \int_V \vec{r} \times \rho_A \frac{d}{dt} (\dot{\vec{r}} + \vec{\omega} \times \vec{r}) dV \quad (2.11)$$

Next, the second differentiation of the generic vector \vec{c} is expressed by

$$\begin{aligned} \frac{d\vec{c}}{dt} &= \frac{\partial(\dot{\vec{r}} + \vec{\omega} \times \vec{r})}{\partial t} + \vec{\omega} \times (\dot{\vec{r}} + \vec{\omega} \times \vec{r}) \\ &= \left((\ddot{\vec{r}} + \dot{\vec{\omega}} \times \vec{r} + \vec{\omega} \times \dot{\vec{r}}) + \vec{\omega} \times (\dot{\vec{r}} + \vec{\omega} \times \vec{r}) \right) \end{aligned} \quad (2.12)$$

Thus, the angular momentum equation becomes

$$\begin{aligned} \int_V \vec{r} \times \rho_A \frac{d}{dt} (\dot{\vec{r}} + \vec{\omega} \times \vec{r}) dV &= \vec{M}_A + \vec{M}_T \\ \int_V \vec{r} \times \left((\ddot{\vec{r}} + \dot{\vec{\omega}} \times \vec{r} + \vec{\omega} \times \dot{\vec{r}}) + \vec{\omega} \times (\dot{\vec{r}} + \vec{\omega} \times \vec{r}) \right) \rho_A dV &= \vec{M}_A + \vec{M}_T \end{aligned} \quad (2.13)$$

This can be solved using BAC/CAB rule for the double cross product with a rigid body aircraft is assumed $\dot{\vec{r}} = \ddot{\vec{r}} = 0$ which leads to the angular momentum equations in accordance with the body frame as shown in Eq. 2.14, where these expressions show how rotations in two axes generate a rotational motion within the remaining axis where the magnitude is precisely proportional to the moments and product of inertia differences.

$$\begin{aligned}
 \dot{P} I_{XX} - \dot{R} I_{XZ} - PQ I_{XZ} + RQ(I_{ZZ} - I_{YY}) &= L_A + L_T \\
 \dot{Q} I_{YY} + PR(I_{XX} - I_{ZZ}) + (P^2 - R^2) I_{XZ} &= M_A + M_T \\
 \dot{R} I_{ZZ} - \dot{P} I_{XZ} + PQ(I_{YY} - I_{XX}) + QR I_{XZ} &= N_A + N_T
 \end{aligned} \tag{2.14}$$

2.1.4 Euler Angles

The euler angles Ψ, Θ, Φ are used to represent the body frame orientations in accordance with the inertial frame, which is based on a strict sequence of sequential rotations and the addition of a number of reference frames. There are four step processes in determining the Euler angles as described below [16].

1. Introduce the North-East-Down frame, where X_1, Y_1, Z_1 moves with the aircraft CG while being parallel to the inertial frame as shown in Fig. 2.5

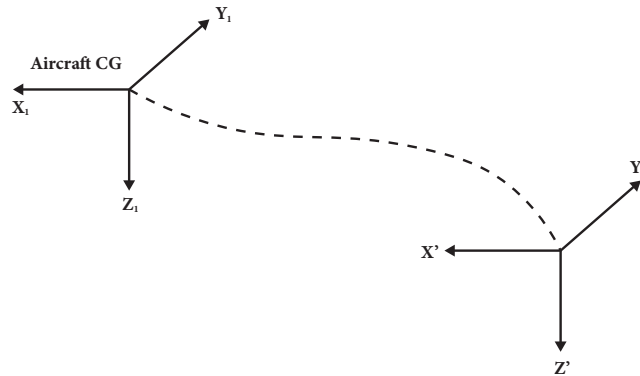


FIGURE 2.5: The North-East-Down frame (Reproduced from [16])

2. Yawing angle Ψ rotation around Z_1 from X_1, Y_1, Z_1 to X_2, Y_2, Z_2 with $Z_1 = Z_2$ as shown in the Figure 2.6

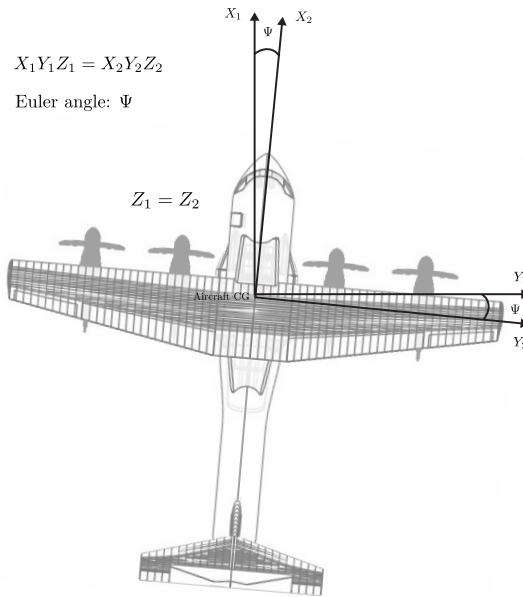


FIGURE 2.6: Introduction of the Euler Angles Ψ (Reproduced from [16])

3. Pitch angle Θ rotation around Y_2 from X_2, Y_2, Z_2 to X_3, Y_3, Z_3 with $Y_2 = Y_3$ as shown in the Figure 2.7
4. Roll angle Φ rotation around X_3 from X_3, Y_3, Z_3 to X, Y, Z with $X_3 = X$ as shown in the Figure 2.8

2.1.5 Flight Path Equations

The flight path expressions are used to represent the aircraft trajectory in the inertial frame, and their solution gives the whole three-dimensional trajectory of the aircraft's motion in the inertial frame [16].

Using the relationship for the linear velocity components between the different frames as determined in Euler angles, with the Earth-based inertial frame X', Y', Z' is parallel to X_1, Y_1, Z_1 , leading to the following relationships

$$\begin{aligned} U_1 &= \dot{X}_1 = \dot{X}' \\ V_1 &= \dot{Y}_1 = \dot{Y}' \\ W_1 &= \dot{Z}_1 = \dot{Z}' \end{aligned}$$

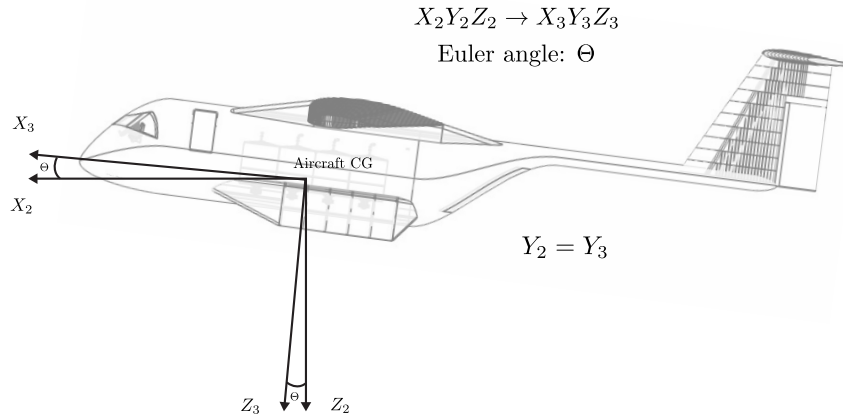


FIGURE 2.7: Introduction of the Euler Angles Θ (Reproduced from [16])

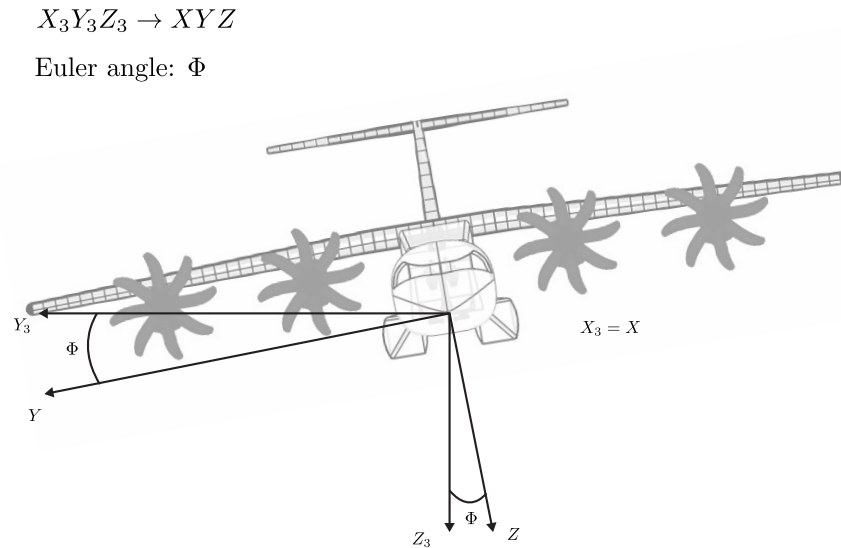


FIGURE 2.8: Introduction of the Euler Angles Φ (Reproduced from [16])

The transformations described in euler angles with the previous relationships are applied to the components of the linear velocities is sequentially shown in Eq. 2.15, Eq. 2.16 and Eq. 2.17.

$$\begin{bmatrix} U_1 \\ V_1 \\ W_1 \end{bmatrix} = \begin{bmatrix} \cos \Psi & -\sin \Psi & 0 \\ \sin \Psi & \cos \Psi & 0 \\ 0 & 0 & 1 \end{bmatrix} \begin{bmatrix} U_2 \\ V_2 \\ W_2 \end{bmatrix} \quad (2.15)$$

$$\begin{bmatrix} U_2 \\ V_2 \\ W_2 \end{bmatrix} = \begin{bmatrix} \cos \Theta & 0 & \sin \Theta \\ 0 & 1 & 0 \\ -\sin \Theta & 0 & \cos \Theta \end{bmatrix} \begin{bmatrix} U_3 \\ V_3 \\ W_3 \end{bmatrix} \quad (2.16)$$

$$\begin{bmatrix} U_3 \\ V_3 \\ W_3 \end{bmatrix} = \begin{bmatrix} 1 & 0 & 0 \\ 0 & \cos \Phi & -\sin \Phi \\ 0 & \sin \Phi & \cos \Phi \end{bmatrix} \begin{bmatrix} U \\ V \\ W \end{bmatrix} \quad (2.17)$$

Leading to the general expression corresponds the linear velocity component in accordance with Earth-based inertial frame with the linear velocity components in accordance with the body frame is shown in Eq. 2.25.

$$\begin{bmatrix} \dot{X}' \\ \dot{Y}' \\ \dot{Z}' \end{bmatrix} = \begin{bmatrix} \cos \Psi & -\sin \Psi & 0 \\ \sin \Psi & \cos \Psi & 0 \\ 0 & 0 & 1 \end{bmatrix} \begin{bmatrix} \cos \Theta & 0 & \sin \Theta \\ 0 & 1 & 0 \\ -\sin \Theta & 0 & \cos \Theta \end{bmatrix} \begin{bmatrix} 1 & 0 & 0 \\ 0 & \cos \Phi & -\sin \Phi \\ 0 & \sin \Phi & \cos \Phi \end{bmatrix} \begin{bmatrix} U \\ V \\ W \end{bmatrix} \quad (2.18)$$

Furthermore, the final expression for the Flight Path Equations is shown in Eq. 2.19

$$\begin{bmatrix} \dot{X}' \\ \dot{Y}' \\ \dot{Z}' \end{bmatrix} = \begin{bmatrix} \cos \Psi \cos \Theta & -\sin \Psi \cos \Phi + \cos \Psi \sin \Theta \sin \Phi & \sin \Psi \sin \Phi + \cos \Psi \sin \Theta \cos \Psi \\ \sin \Psi \cos \Theta & \cos \Psi \cos \Phi + \sin \Psi \sin \Theta \sin \Phi & -\sin \Phi \cos \Psi + \sin \Psi \sin \Theta \cos \Phi \\ -\sin \Theta & \cos \Theta \sin \Phi & \cos \Theta \cos \Phi \end{bmatrix} \begin{bmatrix} U \\ V \\ W \end{bmatrix} \quad (2.19)$$

2.1.6 Kinematic Equations

The KEs are purposed to derive an expression for the aircraft's angular velocity components P, Q, R of the euler angles. Based on the four-step process introduced in Euler angles, the expression for the angular velocity vector is given by [16]

$$\vec{\omega} = \dot{\Psi} + \dot{\Theta} + \dot{\Phi} \quad (2.20)$$

By definition in the angular momentum equations, the angular velocity vector is also given by

$$\vec{\omega} = P\vec{i} + Q\vec{j} + R\vec{k}$$

leads to

$$P\vec{i} + Q\vec{j} + R\vec{k} = \dot{\vec{\Psi}} + \dot{\vec{\Theta}} + \dot{\vec{\Phi}} \quad (2.21)$$

The derivation of the kinematic equations is based on the transformation stated in Euler angles. The transformation of the angular velocity vector is described below.

1. In term of unity vector of the first transformation in the euler angles indicates $\vec{k}_1 = \vec{k}_2$ (see Figure 2.5), leading to

$$\dot{\vec{\Psi}} = \dot{\Psi}\vec{k}_1 = \dot{\Psi}\vec{k}_2$$

2. In term of unity vector of the second transformation in the euler angles indicates $\vec{j}_2 = \vec{j}_3$ (see Figure 2.6), leading to

$$\dot{\vec{\Theta}} = \dot{\Theta}\vec{j}_2 = \dot{\Theta}\vec{j}_3$$

3. In term of unity vector of the third transformation in the euler angles indicates $\vec{i}_3 = \vec{i}$ (see Figure 2.7), leading to

$$\dot{\vec{\Phi}} = \dot{\Phi}\vec{i}_3 = \dot{\Phi}\vec{i}$$

Additionally, the derivation of the expressions for \vec{k}_2, \vec{j}_3 with regard to $\vec{i}, \vec{j}, \vec{k}$ are expressed below, which the transformation applied in terms of the unity vectors.

$$\begin{bmatrix} \vec{i}_2 \\ \vec{j}_2 \\ \vec{k}_2 \end{bmatrix} = \begin{bmatrix} \cos \Theta & 0 & \sin \Theta \\ 0 & 1 & 0 \\ -\sin \Theta & 0 & \cos \Theta \end{bmatrix} \begin{bmatrix} \vec{i}_3 \\ \vec{j}_3 \\ \vec{k}_3 \end{bmatrix} \quad (2.22)$$

$$\begin{bmatrix} \vec{i}_3 \\ \vec{j}_3 \\ \vec{k}_3 \end{bmatrix} = \begin{bmatrix} 1 & 0 & 0 \\ 0 & \cos \Phi & -\sin \Phi \\ 0 & \sin \Phi & \cos \Phi \end{bmatrix} \begin{bmatrix} \vec{i} \\ \vec{j} \\ \vec{k} \end{bmatrix} \quad (2.23)$$

The previous matrices, leads to the following relationships for \vec{k}_2, \vec{j}_3

$$\vec{k}_2 = -\sin \Theta \vec{i} + \cos \Theta \vec{k}_3 \quad (2.24)$$

$$\vec{j}_3 = \cos \Phi \vec{j} - \sin \Phi \vec{k} \quad (2.25)$$

where the \vec{k}_3 is expressed by

$$\vec{k}_3 = \sin \Phi \vec{j} + \cos \Phi \vec{k} \quad (2.26)$$

Leading to the Inverse Kinematic Equations (IKEs) relationship,

$$P\vec{i} + Q\vec{j} + R\vec{k} = \dot{\Psi} \left(-\sin \Theta \vec{i} + \cos \Theta \sin \Phi \vec{j} + \cos \Theta \cos \Phi \vec{k} \right) + \dot{\Theta} \cos \Phi \vec{j} - \sin \Phi \vec{k} + \dot{\Phi} \vec{i} \quad (2.27)$$

The Inverse Kinematic Equations (IKEs) relationship above is rearranged in form of matrix leads to

$$\begin{bmatrix} P \\ Q \\ R \end{bmatrix} = \begin{bmatrix} 1 & 0 & -\sin \Theta \\ 0 & \cos \Phi & \cos \Theta \sin \Phi \\ 0 & -\sin \Phi & \cos \Theta \cos \Phi \end{bmatrix} \begin{bmatrix} \dot{\Phi} \\ \dot{\Theta} \\ \dot{\Psi} \end{bmatrix} \quad (2.28)$$

The KEs are calculated by inverting the Inverse Kinematic Equations in matrix form, leading to the final expression of the Kinematic Equations as shown in Eq. 2.29.

$$\begin{bmatrix} \dot{\Phi} \\ \dot{\Theta} \\ \dot{\Psi} \end{bmatrix} = \begin{bmatrix} 1 & \sin \Phi \tan \Theta & \cos \Phi \tan \Theta \\ 0 & \cos \Phi & -\sin \Phi \\ 0 & \sin \Phi \sec \Theta & \cos \Phi \sec \Theta \end{bmatrix} \begin{bmatrix} P \\ Q \\ R \end{bmatrix} \quad (2.29)$$

2.1.7 Gravitational Equations

The gravitational equations are designed to represent the component of gravitational vector in the body frame that parallel to the Z' axis in the inertial frame. The initial relationships for gravity equations using the transformation in Euler angles are given by [16]

$$\vec{g} = g\vec{k}' = g\vec{k}_1 = g\vec{k}_2 = g_X\vec{i} + g_Y\vec{j} + g_Z\vec{k} \quad (2.30)$$

where the \vec{k}_2 has been expressed in Eq. 2.24.

Leading to the following relationship,

$$\begin{aligned} g\vec{k}_2 &= g_X\vec{i} + g_Y\vec{j} + g_Z\vec{k} \\ -\sin\Theta\vec{i} + \cos\Theta\sin\Phi\vec{j} + \cos\Theta\cos\Phi\vec{k} &= g_X\vec{i} + g_Y\vec{j} + g_Z\vec{k} \end{aligned} \quad (2.31)$$

The previous relationship is grouped in terms of $\vec{i}, \vec{k}, \vec{j}$, the final expression of gravitational equations are shown below and this is purposed to provide one of the three input sets in the linear momentum equations.

$$\begin{aligned} g_X &= -g\sin\Theta \\ g_Y &= g\cos\Theta\sin\Phi \\ g_Z &= g\cos\Theta\cos\Phi \end{aligned} \quad (2.32)$$

2.2 Steady State and Perturbation Equations of Motion

2.2.1 Overview

According to Napolitano [16], the conditions in which the linear and angular accelerations related to the body axes are zero known as the steady state flight condition. By definition, this can be expressed as

$$\begin{aligned} \vec{V}_P = 0 &\quad \rightarrow \quad \vec{V}_P = \text{constant} \\ \vec{\omega} = 0 &\quad \rightarrow \quad \vec{\omega} = \text{constant} \end{aligned}$$

Perturbed flight conditions are the conditions where all the aircraft dynamics motion variables deviate from an initial set of steady-state values.

Furthermore, the following expressions describe the motion variables of the aircraft at steady-state and perturbation conditions.

$$\begin{aligned}
 U &= U_1 + u, \quad V = V_1 + v, \quad W = W_1 + w \\
 P &= P_1 + p, \quad Q = Q_1 + q, \quad R = R_1 + r \\
 \Phi &= \Phi_\phi + u, \quad \Theta = \Theta_1 + \theta, \quad \Psi = \Psi_1 + \psi \\
 F_{AX} &= F_{AX_1} + f_{AX}, \quad F_{AY} = F_{AY_1} + f_{AY}, \quad F_{AZ} = F_{AZ_1} + f_{AZ} \\
 F_{TX} &= F_{TX_1} + f_{TX}, \quad F_{TY} = F_{TY_1} + f_{TY}, \quad F_{TZ} = F_{TZ_1} + f_{TZ} \\
 L_A &= L_{A_1} + l_A, \quad M_A = M_{A_1} + m_A, \quad N_A = N_{A_1} + n_A \\
 L_T &= L_{T_1} + l_T, \quad M_T = M_{T_1} + m_T, \quad N_T = N_{T_1} + n_T
 \end{aligned} \tag{2.33}$$

The linear and angular accelerations in accordance with the body frame are zero, can be expressed by

$$\begin{aligned}
 \dot{U}_1 &= \dot{V}_1 = \dot{W}_1 = 0 \\
 \dot{P}_1 &= \dot{Q}_1 = \dot{R}_1 = 0 \\
 \dot{U} &= \dot{u}, \quad \dot{V} = \dot{v}, \quad \dot{W} = \dot{w} \\
 \dot{P} &= \dot{p}, \quad \dot{Q} = \dot{q}, \quad \dot{R} = \dot{r} \\
 \dot{\Phi} &= \dot{\phi}, \quad \dot{\Theta} = \dot{\theta}, \quad \dot{\Psi} = \dot{\psi}
 \end{aligned} \tag{2.34}$$

2.2.2 Steady State Equations of Motion

Recall the relationship for the introduction of the steady state conditions in Eq. 2.34,

$$\begin{aligned}
 \dot{U}_1 &= \dot{V}_1 = \dot{W}_1 = 0 \\
 \dot{P}_1 &= \dot{Q}_1 = \dot{R}_1 = 0
 \end{aligned}$$

leads to the linear momentum equations, angular momentum equations and KEs at steady-state conditions,

$$\begin{aligned}
 m(Q_1W_1 - R_1V_1) &= -mg \sin \Theta_1 + (F_{Ax_1} + F_{Tx_1}) \\
 m(U_1R_1 - P_1W_1) &= mg \cos \Theta_1 \sin \Phi_1 + (F_{Ay_1} + F_{Ty_1}) \\
 m(P_1V_1 - Q_1U_1) &= mg \cos \Theta_1 \cos \Phi_1 + (F_{Az_1} + F_{Tz_1}) \\
 P_1Q_1 I_{XZ} + R_1Q_1(I_{ZZ} - I_{YY}) &= L_{A_1} + L_{T_1} \\
 P_1R_1(I_{XX} - I_{ZZ}) + (P_1^2 - R_1^2) I_{XZ} &= M_{A_1} + M_{T_1} \\
 P_1Q_1(I_{YY} - I_{XX}) + Q_1R_1 I_{XZ} &= N_{A_1} + N_{T_1}
 \end{aligned} \tag{2.35}$$

$$\begin{bmatrix} \dot{\Phi}_1 \\ \dot{\Theta}_1 \\ \dot{\Psi}_1 \end{bmatrix} = \begin{bmatrix} 1 & \sin \Phi_1 \tan \Theta_1 & \cos \Phi_1 \tan \Theta_1 \\ 0 & \cos \Phi_1 & -\sin \Phi_1 \\ 0 & \sin \Phi_1 \sec \Theta_1 & \cos \Phi_1 \sec \Theta_1 \end{bmatrix} \begin{bmatrix} P_1 \\ Q_1 \\ R_1 \end{bmatrix} \tag{2.36}$$

The steady-state reclinear flight condition is applied to the actual flight conditions with the mathematical expressions written in Eq. 2.36. Furthermore,

$$P_1 = Q_1 = R_1 = 0$$

leads to the expression for linear momentum equations and angular momentum equations at steady-state conditions expressed in Eq. 2.37.

$$\begin{aligned}
 0 &= -mg \sin \Theta_1 + (F_{Ax_1} + F_{Tx_1}) \\
 0 &= mg \cos \Theta_1 \sin \Phi_1 + (F_{Ay_1} + F_{Ty_1}) \\
 0 &= mg \cos \Theta_1 \cos \Phi_1 + (F_{Az_1} + F_{Tz_1}) \\
 0 &= L_{A_1} + L_{T_1} \\
 0 &= M_{A_1} + M_{T_1} \\
 0 &= N_{A_1} + N_{T_1}
 \end{aligned} \tag{2.37}$$

2.2.3 Perturbation Equations of Motion

The analysis of the equation of motion of the aircraft at perturbed conditions provides a crucial analysis of the dynamics of an aircraft when applied to atmospheric turbulence [16].

By applying the steady-state flight condition:

$$\begin{aligned}\dot{U} &= \dot{U}_1 + \dot{u}, \quad \dot{V} = \dot{V}_1 + \dot{v}, \quad \dot{W} = \dot{W}_1 + \dot{w} \\ \dot{P} &= \dot{P}_1 + \dot{p}, \quad \dot{Q} = \dot{Q}_1 + \dot{q}, \quad \dot{R} = \dot{R}_1 + \dot{r}\end{aligned}$$

For small perturbation conditions, the following assumptions are applied:

$$\begin{aligned}\psi\theta &= \psi\phi = \theta\phi \approx 0 \\ \sin\psi &\approx \psi, \quad \sin\theta \approx \theta, \quad \sin\phi \approx \phi \\ \cos\psi &\approx 1, \quad \cos\theta \approx 1, \quad \cos\phi \approx 1\end{aligned}$$

Leading to the linear and angular momentum equation at the small perturbations, as shown in Eq. 2.38

$$\begin{aligned}m(\dot{u} + Q_1w + qW_1 - R_1v - rV_1) &= -mg\theta \cos\Theta_1 + (f_{A_X} + f_{T_X}) \\ m(\dot{v} + U_1r + uR_1 - P_1w + pW_1) &= -mg\theta \sin\Phi_1 \sin\Theta_1 + mg\phi \cos\Phi_1 \cos\Theta_1 + (f_{A_Y} + f_{T_Y}) \\ m(\dot{w} + P_1v + pV_1 - Q_1u + qU_1) &= -mg\theta \cos\Phi_1 \sin\Theta_1 - mg\phi \sin\Phi_1 \cos\Theta_1 + (f_{A_Z} + f_{T_Z}) \\ \dot{p}I_{XX} - \dot{r}I_{XZ} - (P_1q + Q_1p)I_{XZ} + (R_1q + Q_1r)(I_{ZZ} - I_{YY}) &= (l_A + l_T) \\ \dot{q}I_{YY} + (P_1r + pR_1)(I_{XX} - I_{ZZ}) + (2P_1p - 2R_1r)I_{XZ} &= (m_A + m_T) \\ \dot{r}I_{ZZ} - \dot{p}I_{XZ} + (P_1q - pQ_1)(I_{YY} - I_{XX}) + (Q_1r + R_1q)I_{XZ} &= (n_A + n_T)\end{aligned}\tag{2.38}$$

Furthermore, for the inverted kinematic equations at small perturbations, starting from the expressions,

$$\begin{aligned}P &= \dot{\Phi} - \sin\Theta \dot{\Psi} \\ Q &= \cos\Phi \dot{\Theta} + \cos\Theta \sin\Phi \dot{\Psi} \\ R &= \cos\Theta \cos\Phi \dot{\Psi} - \sin\Phi \dot{\Theta}\end{aligned}\tag{2.39}$$

with the additional relationships,

$$\begin{aligned}P &= P_1 + p, \quad Q = Q_1 + q, \quad R = R_1 + r \\ \dot{P} &= \dot{p}, \quad \dot{Q} = \dot{q}, \quad \dot{R} = \dot{r} \\ \Phi &= \Phi_1 + \phi, \quad \Theta = \Theta_1 + \theta, \quad \Psi = \Psi_1 + \psi \\ \dot{\Phi} &= \dot{\phi}, \quad \dot{\Theta} = \dot{\theta}, \quad \dot{\Psi} = \dot{\psi}\end{aligned}\tag{2.40}$$

Leading to the inverted kinematic equations at small perturbations as shown in Eq. 2.41

$$\begin{aligned}
 p &= \dot{\phi} - \dot{\Psi}_1 \theta \cos \Theta_1 - \dot{\psi} \sin \Theta_1 \\
 q &= -\dot{\Theta}_1 \phi \sin \Phi_1 + \dot{\theta} \cos \Phi_1 - \dot{\Psi}_1 \theta \sin \Phi_1 \sin \Theta_1 + \dot{\Psi}_1 \phi \cos \Phi_1 \cos \Theta_1 + \dot{\psi} \sin \Phi_1 \cos \Theta_1 \\
 r &= -\dot{\Psi}_1 \theta \cos \Phi_1 \sin \Theta_1 - \dot{\Psi}_1 \phi \sin \Phi_1 \cos \Theta_1 + \dot{\psi} \cos \Phi_1 \cos \Theta_1 - \dot{\Theta}_1 \phi \cos \Phi_1 - \dot{\theta} \sin \Phi_1
 \end{aligned} \tag{2.41}$$

2.2.4 Small Perturbation Equations of Motion

The solution of the small perturbation linear and angular momentum equations and inverted kinematic equations at the steady-state rectilinear condition, the following relationships applies [16]:

- $P_1 = Q_1 = R_1 = 0$;
- $\Phi_1 = \text{constant}$, $\Theta_1 = \text{constant}$, $\Psi_1 = \text{constant}$;
- $V_1 = 0$;
- $\Phi_1 = 0$, $\sin \Phi_1 = 0$, $\cos \Phi_1 = 1$.

Leading to the simplified small perturbation linear and angular momentum equations and inverted kinematic equations as shown in Eq. 2.42.

$$\begin{aligned}
 m[\dot{u} + qW_1] &= -mg\theta \cos \Theta_1 + (f_{A_x} + f_{T_x}) \\
 m[\dot{v} + U_1 r - pW_1] &= mg\theta + \cos \Theta_1 + (f_{A_y} + f_{T_y}) \\
 m[\dot{w} - Q_1 u] &= -mg\theta \sin \Phi_1 + (f_{A_z} + f_{T_z}) \\
 \dot{p}I_{XX} - \dot{r}I_{XZ} &= (l_A + l_T) \\
 \dot{q}I_{YY} &= (m_A + m_T) \\
 \dot{r}I_{ZZ} - \dot{p}I_{XZ} &= (n_A + n_T) \\
 p &= p\dot{h}i - \dot{\psi} \sin \Theta_1 \\
 q &= \dot{\theta} \\
 r &= \dot{\psi} \cos \Theta_1
 \end{aligned} \tag{2.42}$$

2.3 Aerodynamic and Thrust Forces and Moments

2.3.1 Longitudinal Aerodynamic Forces and Moment

In analyzing the longitudinal aerodynamic forces and moments, the configuration of the horizontal tail is need to be specified. Elevators are considered to be utilized for longitudinal control of the aircraft. The longitudinal aircraft aerodynamic forces and moments as shown in Fig. 2.9 are given by

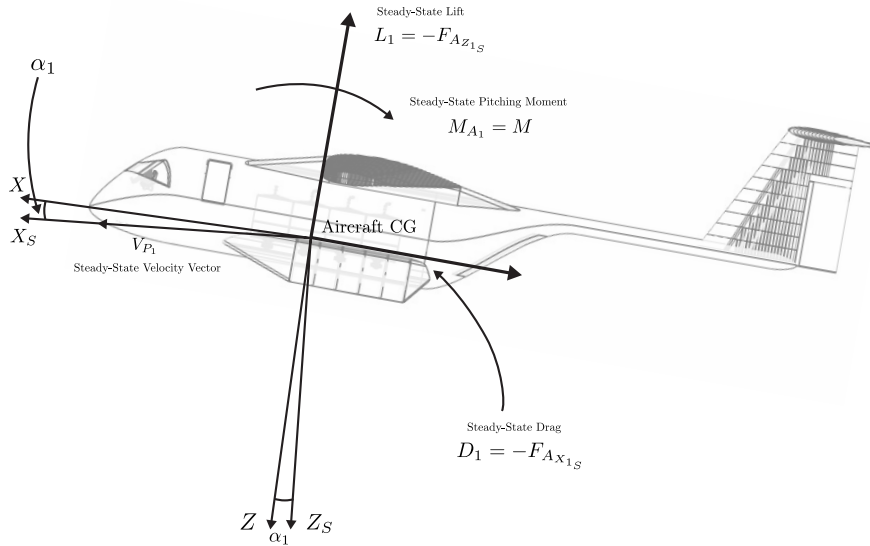


FIGURE 2.9: Longitudinal Aerodynamic Forces and Moment (Reproduced from [16])

- $D_1 \triangleq$ Drag, the force acting on the X_S axis. It is expressed by

$$D_1 = C_{D_1} \bar{q} S \quad (2.43)$$

where, $C_{D_1} \triangleq$ the dimensionless drag coefficient given in Eq. 2.44; $\bar{q} \triangleq$ the aircraft dynamic pressure; $S \triangleq$ the wing area.

$$C_{D_1} = C_{D_0} + C_{D_\alpha} \alpha + C_{D_{\delta_E}} \delta_E \quad (2.44)$$

where,

- $C_{D_0} = C_D|_{\alpha=\delta_E=0^\circ} \triangleq$ the drag coefficient analyzed under the initial state.
- $C_{D_\alpha} \triangleq$ the drag stability derivatives in accordance with the angle of attack.
- $C_{D_{\delta_E}} \triangleq$ the drag stability derivatives in accordance with the elevator deflection.

However, $C_{D_{\delta_E}}$ can be assumed to be negligible, because of the longitudinal control surfaces typically have limited cross sections subjected to the air-flow, which is referred as the wetted area as shown in Fig. 2.10 Furthermore,

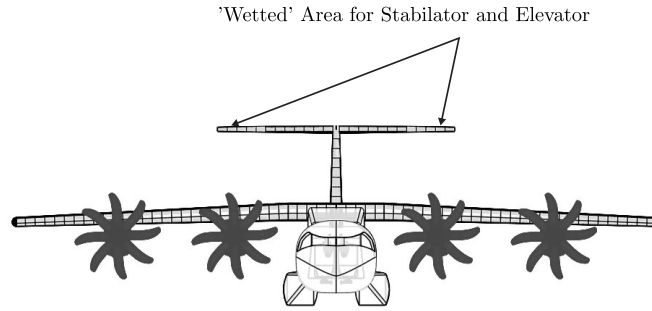


FIGURE 2.10: Wetted Area of the Elevator and Stabilator (Reproduced from [16])

the modeling of the C_{D_1} can be approximated using a conceptual approach provided by the Prandtl relationship as shown in Eq. 2.45.

$$C_{D_1} = C_{D_0} + \frac{C_L^2}{\pi AR e} \quad (2.45)$$

where,

- $AR \triangleq$ the wing aspect ratio.
- $e \triangleq$ the Oswald Efficiency factor
- $L_1 \triangleq$ Lift, the force acting on the Z_S axis. It is expressed by

$$L_1 = C_{L_1} \bar{q} S \quad (2.46)$$

where, $C_{L_1} \triangleq$ the dimensionless lift coefficient given in Eq. 2.47.

$$C_{L_1} = C_{L_0} + C_{L_\alpha} \alpha + C_{L_{\delta_E}} \delta_E \quad (2.47)$$

where,

- $C_{L_0} = C_L|_{\alpha=\delta_E=0^\circ} \triangleq$ the lift coefficient analyzed under the initial state.
- $C_{L_\alpha} \triangleq$ the lift stability derivatives in accordance with the angle of attack.
- $C_{L_{\delta_E}} \triangleq$ the lift stability derivatives in accordance with the elevator deflection.

At trim condition, the dimensionless lift coefficient C_{L_1} can be assumed to be [17]:

$$C_{L_1} = \frac{W}{\bar{q}S} \quad (2.48)$$

- $M_1 \triangleq$ Pitching moment, the steady-state pitching moment acting on the Y_S axis. It is expressed by

$$M_1 = C_{m_1} \bar{q} S \bar{c} \quad (2.49)$$

where, C_{m_1} is the dimensionless pitching moment coefficient given in Eq. 2.50; \bar{c} is the wing mean aerodynamic center (MAC).

$$C_{m_1} = C_{m_0} + C_{m_\alpha} \alpha + C_{m_{\delta_E}} \delta_E \quad (2.50)$$

where,

- $C_{m_0} = C_m|_{\alpha=\delta_E=0^\circ} \triangleq$ the pitching moment coefficient analyzed under the initial state.
- $C_{m_\alpha} \triangleq$ the pitching moment stability derivatives in accordance with the angle of attack.
- $C_{m_{\delta_E}} \triangleq$ the pitching moment stability derivatives in accordance with the elevator deflection.

At trim condition,

$$C_{m_1} = 0$$

2.3.2 Lateral Directional Aerodynamic Forces and Moments

In analyzing the lateral directional aerodynamic forces and moments at steady-state and perturbed conditions, the ailerons δ_A and rudder δ_R control surfaces are assumed to be used by the aircraft for lateral and directional control. Furthermore, the introduction of the sideslip angle β and sidewash angle σ are important to understand [16].

The sideslip angle β is the lateral angle of attack which measured the deviation of the airspeed V_∞ in accordance with the longitudinal stability axes. The sidewash angle σ is a cost in effective sideslip angle when approaching the aircraft tails. It is frequently referred as the lateral counterpart to the longitudinal downwash angle ε .

The lateral directional aircraft aerodynamic forces and moments as shown in Fig. 2.11 are given by

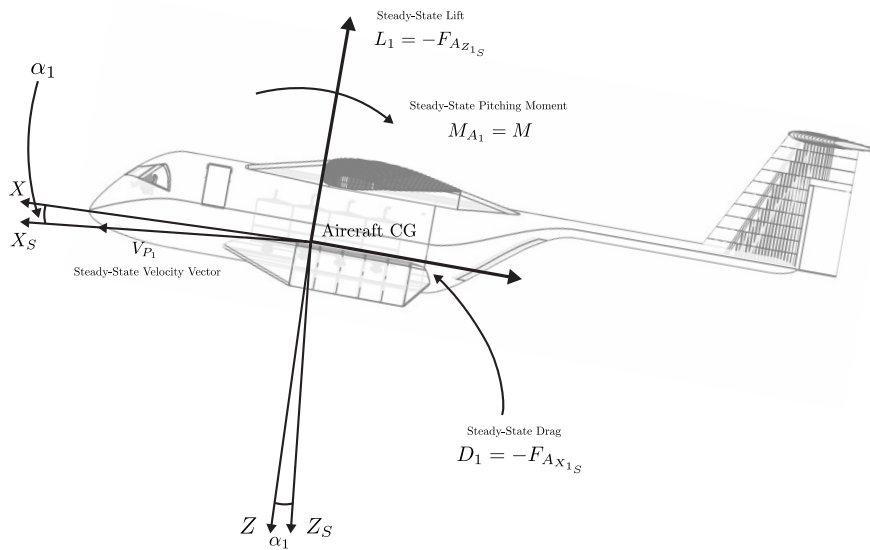


FIGURE 2.11: Longitudinal Steady-State Aerodynamic Forces and Moments (Reproduced from [16])

- $F_{A_{Y_1}} \triangleq$ Lateral force, the aerodynamic force acting on the Y_S axis. It is expressed by

$$F_{A_{Y_1}} = C_{y_1} \bar{q} S \quad (2.51)$$

w where, $C_{y_1} \triangleq$ the lateral force coefficient given in Eq. 2.52.

$$C_{y_1} = C_{y_0} + C_{y_\beta}\beta + C_{y_{\delta_A}}\delta_A + C_{y_{\delta_R}}\delta_R \quad (2.52)$$

where,

- C_{y_0} is the residual sideforce, with the condition of the aircraft is symmetry in accordance with the XZ plane, it is assumed to be

$$C_{y_0} = c_Y|_{\beta=\delta_A=\delta_R=0^\circ} = 0$$

- $C_{y_\beta} \triangleq$ the sideforce in accordance with the sideslip angle.
- $C_{y_{\delta_A}} \triangleq$ the sideforce in accordance with the ailerons deflection.
- $C_{y_{\delta_R}} \triangleq$ the sideforce in accordance with the rudder deflection.
- $L_{A_1} \triangleq$ Rolling moment, the rolling moment acting on the X_S axis. It is expressed by

$$L_{A_1} = C_{l_1}\vec{q}Sb \quad (2.53)$$

w where, $C_{l_1} \triangleq$ the rolling moment coefficient given in Eq. 2.54.

$$C_{l_1} = C_{l_0} + C_{l_\beta}\beta + C_{l_{\delta_A}}\delta_A + C_{l_{\delta_R}}\delta_R \quad (2.54)$$

where,

- $C_{l_\beta} \triangleq$ the rolling moment in accordance with sideslip angle.
- $C_{l_{\delta_A}} \triangleq$ the rolling moment in accordance with the ailerons deflection.
- $C_{l_{\delta_R}} \triangleq$ the rolling moment in accordance with the rudder deflection.
- $N_{A_1} \triangleq$ Yawing moment, the yawing moment acting on the Z_S axis. It is expressed by

$$N_{A_1} = C_{n_1}\vec{q}Sb \quad (2.55)$$

where, $C_{n_1} \triangleq$ the yawing moment coefficient given in Eq. 2.46

$$C_{n_1} = C_{n_0} + C_{n_\beta}\beta + C_{n_{\delta_A}}\delta_A + C_{n_{\delta_R}}\delta_R \quad (2.56)$$

where,

- $C_{n_0} \triangleq$ the residual yawing moment coefficient, assumed to be negligible.

$$C_{n_0} = c_n|_{\beta=\delta_A=\delta_R=0^\circ} = 0$$

- $C_{n_\beta} \triangleq$ the yawing moment in accordance with sideslip angle, also known as the directional stability derivative.
- $C_{n_{\delta_A}} \triangleq$ the yawing moment in accordance with the ailerons deflection.
- $C_{n_{\delta_R}} \triangleq$ the yawing moment in accordance with the rudder deflection.

2.3.3 Thrust Forces and Moments

In the usual case of a multi-engine aircraft, each installed thrust may be represented by the i -th generic vector of T_i , (with $i = 1, \dots, N$, N is the number of engines). The orientation of the T_i vector in accordance with body frame and stability axes is shown in Fig. 2.12

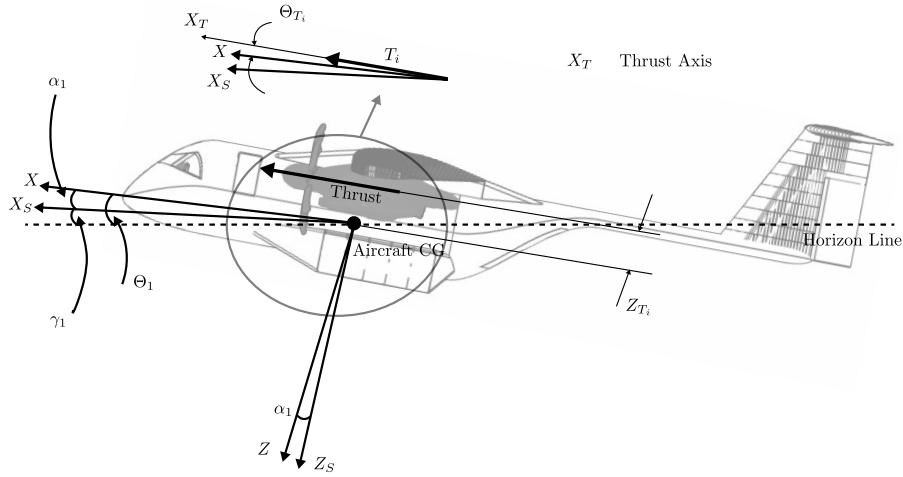


FIGURE 2.12: The Installed Thrust Directions in accordance with Body and Stability Axes (Reproduced from [16])

At steady-state conditions, it is assumed that all engines are operating at nominal conditions with identical throttle settings.

$$\text{rbation } \sin(\Theta_T) \approx \Theta_T, \sin(\Psi_T) \approx \Psi_T, \sin(\alpha_1) \approx \alpha_1, \alpha_1 \Psi_T \approx 0, \alpha_1 \Theta_T \approx 0$$

The thrust forces and moments are given by

$$\begin{aligned}
 F_{T_{X_1}} &= \left(\sum_{i=1}^N T_i \cos(\Theta_{T_i}) \right) \cos(\alpha_1) \\
 M_{T_1} &= \left(\sum_{i=1}^N T_i (z_{T_i} \cos(\Theta_{T_i})) \right) \\
 F_{T_{X_1}} &= - \left(\sum_{i=1}^N T_i (\Theta_{T_i}) \right) \cos(\alpha_1) - \left(\sum_{i=1}^N T_i \cos(\Theta_{T_i}) \right) \sin(\alpha_1) \\
 L_{T_1} &= 0 \\
 F_{T_{Y_1}} &= 0 \\
 N_{T_1} &= 0
 \end{aligned} \tag{2.57}$$

2.3.4 Longitudinal Aerodynamic Forces and Moment at Small Perturbation Condition

In analyzing the longitudinal aerodynamic forces and moment at small perturbation condition, the following relationships are introduced as the aerodynamic stability derivatives are analyzed in accordance with the angle of attack α [16].

$$\begin{aligned}
 f_{A_x} &= f_{A_x}(u, \alpha, \dot{\alpha}, q, \delta_E) \\
 f_{A_z} &= f_{A_z}(u, \alpha, \dot{\alpha}, q, \delta_E) \\
 m_A &= f_{m_A}(u, \alpha, \dot{\alpha}, q, \delta_E)
 \end{aligned}$$

For the $u, \dot{\alpha}, q$ coefficients to be dimensionless, an ad hoc non-dimensionalization procedure is presented using transformation variables given below.

$$u \left(\frac{ft}{sec} \right) \rightarrow \frac{u}{V_{P_1}}, \quad \dot{\alpha} \left(\frac{rad}{sec} \right) \rightarrow \frac{\dot{\alpha} \vec{c}}{2V_{P_1}}, \quad q \left(\frac{rad}{sec} \right) \rightarrow \frac{q \vec{c}}{2V_{P_1}}$$

The relationships for the small perturbation forces and moment in longitudinal motion are given by

$$\begin{aligned}
 f_{A_X} &= \bar{q}S \left(-(C_{D_u} + 2C_{D_1}) \left(\frac{u}{V_{P_1}} \right) + (-C_{D_\alpha} + C_{L_1})\alpha - C_{D_{\dot{\alpha}}} \left(\frac{\dot{\alpha}\vec{c}}{2V_{P_1}} \right) \right. \\
 &\quad \left. - C_{D_q} \left(\frac{q\vec{c}}{2V_{P_1}} \right) - C_{D_{\delta_E}} \delta_E \right) \\
 f_{A_Z} &= \bar{q}S \left(-(C_{L_u} + 2C_{L_1}) \left(\frac{u}{V_{P_1}} \right) - (-C_{L_\alpha} + C_{D_1})\alpha - C_{L_{\dot{\alpha}}} \left(\frac{\dot{\alpha}\vec{c}}{2V_{P_1}} \right) \right. \\
 &\quad \left. - C_{L_q} \left(\frac{q\vec{c}}{2V_{P_1}} \right) - C_{L_{\delta_E}} \delta_E \right) \\
 M_A &= \bar{q}S\vec{c} \left((C_{m_u} + 2C_{m_1}) \left(\frac{u}{V_{P_1}} \right) + C_{m_\alpha}\alpha + C_{m_{\dot{\alpha}}} \left(\frac{\dot{\alpha}\vec{c}}{2V_{P_1}} \right) \right. \\
 &\quad \left. - C_{m_q} \left(\frac{q\vec{c}}{2V_{P_1}} \right) + C_{m_{\delta_E}} \delta_E \right)
 \end{aligned} \tag{2.58}$$

where,

- $C_{D_u}, C_{L_u}, C_{m_u} \triangleq$ Speed derivatives.
- $C_{D_{\dot{\alpha}}}, C_{L_{\dot{\alpha}}}, C_{m_{\dot{\alpha}}} \triangleq$ Rate of angle of attack derivatives.
- $C_{D_q}, C_{L_q}, C_{m_q} \triangleq$ Pitch rate derivatives.

2.3.5 Lateral Directional Aerodynamic Force and Moments at Small Perturbation Condition

In analyzing the lateral directional aerodynamic force and moments at small perturbation condition at small perturbation condition, the following relationships are introduced as the lateral aerodynamic stability coefficients are analyzed in accordance with the sideslip angle β [16].

$$\begin{aligned}
 f_{A_Y} &= f_{A_Y}(\beta, \dot{\beta}, p, r, \delta_A, \delta_R) \\
 l_A &= l_A(\beta, \dot{\beta}, p, r, \delta_A, \delta_R) \\
 n_A &= n_A(\beta, \dot{\beta}, p, r, \delta_A, \delta_R)
 \end{aligned}$$

For the $\dot{\beta}, p, r$ coefficients to be dimensionless, an ad hoc non-dimensionalization procedure is presented using transformation variables as given below.

$$\dot{\beta} \left(\frac{rad}{sec} \right) \rightarrow \frac{\dot{\beta}b}{2V_{P_1}}, p \left(\frac{rad}{sec} \right) \rightarrow \frac{pb}{2V_{P_1}}, r \left(\frac{rad}{sec} \right) \rightarrow \frac{rb}{2V_{P_1}}$$

The relationships for the small perturbation force and moments in lateral directional motions are given by

$$\begin{aligned} f_{A_Y} &= \vec{q}S \left(C_{Y_\beta} \beta + C_{Y_{\dot{\beta}}} \left(\frac{\dot{\beta}b}{2V_{P_1}} \right) + C_{Y_p} \left(\frac{pb}{2V_{P_1}} \right) + C_{Y_r} \left(\frac{rb}{2V_{P_1}} \right) + C_{Y_{\delta_A}} \delta_A + C_{Y_{\delta_R}} \delta_R \right) \\ l_A &= \vec{q}S \left(C_{l_\beta} \beta + C_{l_{\dot{\beta}}} \left(\frac{\dot{\beta}b}{2V_{P_1}} \right) + C_{l_p} \left(\frac{pb}{2V_{P_1}} \right) + C_{l_r} \left(\frac{rb}{2V_{P_1}} \right) + C_{l_{\delta_A}} \delta_A + C_{l_{\delta_R}} \delta_R \right) \\ n_A &= \vec{q}S \left(C_{n_\beta} \beta + C_{n_{\dot{\beta}}} \left(\frac{\dot{\beta}b}{2V_{P_1}} \right) + C_{n_p} \left(\frac{pb}{2V_{P_1}} \right) + C_{n_r} \left(\frac{rb}{2V_{P_1}} \right) + C_{n_{\delta_A}} \delta_A + C_{n_{\delta_R}} \delta_R \right) \end{aligned} \quad (2.59)$$

where,

- $C_{Y_{\dot{\beta}}}, C_{l_{\dot{\beta}}}, C_{n_{\dot{\beta}}} \triangleq$ Rate of sideslip angle derivatives. For most aircraft, $\dot{\beta}$ -derivatives are negligible.
- $C_{Y_p}, C_{l_p}, C_{n_p} \triangleq$ Roll rate derivatives.
- $C_{Y_r}, C_{l_r}, C_{n_r} \triangleq$ Yaw rate derivatives.

2.3.6 Thrust Forces and Moments at Small Perturbation Condition

The thrust forces and moments at small perturbation condition are divided into

- Longitudinal f_{T_X}, f_{T_Z}, m_T
- Lateral directional l_T, f_{T_Y}, n_T

In analyzing the longitudinal and lateral directional thrust forces and moments at small perturbation condition, the nondimensional small perturbation are used, as described previously for longitudinal and lateral directional aerodynamic forces

[16].

$$\begin{aligned}
 f_{T_X} &= f\left(\frac{u}{V_{P_1}}, \alpha\right), f_{T_Z} = f\left(\frac{u}{V_{P_1}}, \alpha\right), m_T = f\left(\frac{u}{V_{P_1}}, \alpha\right) \\
 f_{T_Y} &= f(\beta), l_T = f(\beta), n_T = f(\beta)
 \end{aligned}$$

By considering small perturbation occurred, the expressions of small perturbation longitudinal thrust forces and moment are given by

$$\begin{aligned}
 f_{T_X} &= \left(\vec{q}_1 S(C_{T_{X_U}} + 2C_{T_{X_1}})\right) \left(\frac{u}{V_{P_1}}\right) + (\vec{q}_1 S C_{T_{X_\alpha}}) \alpha \\
 f_{T_Z} &= \left(\vec{q}_1 S(C_{T_{Z_U}} + 2C_{T_{Z_1}})\right) \left(\frac{u}{V_{P_1}}\right) + (\vec{q}_1 S C_{T_{Z_\alpha}}) \alpha \\
 m_T &= \left(\vec{q}_1 S(C_{m_{T_U}} + 2C_{m_{T_1}})\right) \left(\frac{u}{V_{P_1}}\right) + (\vec{q}_1 S C_{m_{T_\alpha}}) \alpha
 \end{aligned} \tag{2.60}$$

where,

- $C_{T_{X_1}} \triangleq$ the coefficient countering C_{D_1} to achieve $T = D$ equilibrium.
- $C_{T_{X_U}} \triangleq$ the thrust coefficient in accordance with speed derivative.
- $C_{m_{T_u}} \triangleq$ the thrust moment in accordance with speed derivative.
- $C_{m_{T_\alpha}} \triangleq$ the thrust versus angle of attack derivative.
- For most aircraft, $C_{T_{Z_1}} \approx 0, C_{T_{Z_u}} \approx 0, C_{T_{Z_\alpha}} \approx 0$.
- For most aircraft propulsive configurations, $C_{T_{Y_\beta}} \approx 0, C_{l_{T_\beta}} \approx 0, C_{n_{T_\beta}} \approx 0$.

2.4 The Equations of Motion Laplace Transformations at Small Perturbation

The Laplace transform is crucial in control theory. It indicates in the description of linear time invariant systems, where it converts convolution operators to multiplication operators and enables the definition of a system's transfer function. System properties can then be translated into transfer function properties. The Laplace transform is used to solve the linearized equations that have been calculated previously. Recall the small perturbations linear and angular momentums and inverted

kinematic equations in Eq. 2.42, and decoupling into two sets of equations in longitudinal and lateral directional, as expressed below [16].

Longitudinal Equations

$$\begin{aligned}
 m(\dot{u} + qW_1) &= -mg\theta \cos \Theta_1 + (f_{A_X} + f_{T_X}) \\
 m(\dot{w} - U_1q) &= -mg\theta \sin \Theta_1 + (f_{A_Z} + f_{T_Z}) \\
 \dot{q}I_{YY} &= (m_A + m_T) \\
 q &= \dot{\theta}
 \end{aligned} \tag{2.61}$$

Lateral Directional Equations

$$\begin{aligned}
 m(\dot{v} + U_1r - pW_1) &= mg\Phi \cos \Theta_1 + (f_{A_X} + f_{T_X}) \\
 \dot{p}I_{XX} - \dot{r}I_{XZ} &= (l_A + l_T) \\
 \dot{r}I_{ZZ} - \dot{p}I_{XZ} &= (n_A + n_T) \\
 p &= \dot{\Phi} - \dot{\psi} \sin \Theta_1 \\
 r &= \dot{\psi} \cos \Theta_1
 \end{aligned} \tag{2.62}$$

2.4.1 The Longitudinal Equations of Motion Laplace Transformations at Small Perturbation

The expression for the aerodynamic and thrust forces and moment in longitudinal motion are given by

$$\begin{aligned}
 (f_{A_X} + f_{T_X}) &= \vec{q}_1 S \left(-(C_{D_u} + 2C_{D_1}) \frac{u}{V_{P_1}} + (C_{T_{X_u}} + 2C_{T_{X_1}}) \frac{u}{V_{P_1}} - (C_{D_\alpha} - C_{L_1}) \alpha - C_{D_{\delta_E}} \delta_E \right) \\
 (f_{A_Z} + f_{T_Z}) &= \vec{q}_1 S \left(-(C_{L_u} + 2C_{L_1}) \frac{u}{V_{P_1}} + (C_{L_\alpha} + C_{D_1}) \alpha - C_{L_{\dot{\alpha}}} \frac{\dot{\alpha} \vec{c}}{2V_{P_1}} - C_{L_q} \frac{q \vec{c}}{2V_{P_1}} - C_{L_{\delta_E}} \delta_E \right) \\
 (m_A + m_T) &= \vec{q}_1 S \vec{c} \left((C_{m_u} + 2C_{m_1}) \frac{u}{V_{P_1}} + (C_{m_{T_u}} + 2C_{m_{T_1}}) \frac{u}{V_{P_1}} + (C_{m_\alpha} + C_{m_{T_\alpha}}) \alpha + C_{m_{\dot{\alpha}}} \frac{\dot{\alpha} \vec{c}}{2V_{P_1}} \right. \\
 &\quad \left. + C_{m_q} \frac{q \vec{c}}{2V_{P_1}} + C_{m_{\delta_E}} \delta_E \right)
 \end{aligned} \tag{2.63}$$

The aerodynamic forces and moment are defined in the stability axes (X_S, Y_S, Z_S). The only nonzero component of the linear velocity is along the X_S axis with

$$U_{1S} = V_{P_1}, \quad W_{1S} = 0$$

Redefined the linear momentum equations in the stability axes along with the IKEs about the pitch axis $q = \dot{\theta}$, which originally derived in the body axes, and given by

$$\begin{aligned}
 m\dot{u} &= -mg\theta \cos \Theta_1 + \bar{q}_1 S \left(-(C_{D_u} + 2C_{D_1}) \frac{u}{V_{P_1}} + (C_{T_{X_u}} + 2C_{T_{X_1}}) \frac{u}{V_{P_1}} - (C_{D_\alpha} - C_{L_1}) \alpha - C_{D_{\delta_E}} \delta_E \right) \\
 m(\dot{w} - V_{P_1}q) &= -mg\theta \sin \Theta_1 + \bar{q}_1 S \left(-(C_{L_u} + 2C_{L_1}) \frac{u}{V_{P_1}} + (C_{L_\alpha} + C_{D_1}) \alpha - C_{L_{\dot{\alpha}}} \frac{\dot{\alpha} \bar{c}}{2V_{P_1}} - C_{L_q} \frac{q \bar{c}}{2V_{P_1}} - C_{L_{\delta_E}} \delta_E \right) \\
 I_{Y_Y} \dot{q} &= \bar{q}_1 S \bar{c} \left((C_{m_u} + 2C_{m_1}) \frac{u}{V_{P_1}} + (C_{m_{T_u}} + 2C_{m_{T_1}}) \frac{u}{V_{P_1}} + (C_{m_\alpha} + C_{m_{T_\alpha}}) \alpha + C_{m_{\dot{\alpha}}} \frac{\dot{\alpha} \bar{c}}{2V_{P_1}} \right. \\
 &\quad \left. + C_{m_q} \frac{q \bar{c}}{2V_{P_1}} + C_{m_{\delta_E}} \delta_E \right)
 \end{aligned} \tag{2.64}$$

For aerodynamic modeling purposes, it is necessary to identify an inconsistency in the equations setup [16], where the second equation is analyzed in accordance with the small perturbation vertical velocity w and the aircraft stability derivatives are analyzed in accordance with the angle of attack α . The following variable transformations are introduced

$$w \rightarrow \alpha, \quad q \rightarrow \theta$$

with

$$\begin{aligned}
 q &= \dot{\theta}, \quad \dot{q} = \ddot{\theta} \\
 w &\approx V_{P_1} \alpha, \quad \dot{w} \approx V_{P_1} \dot{\alpha}
 \end{aligned}$$

resulting in a various set of equations, which given by

$$\begin{aligned}
 \dot{u} &= -g\theta \cos \Theta_1 + \frac{\bar{q}_1 S}{m} \left(-(C_{D_u} + 2C_{D_1}) \frac{u}{V_{P_1}} + (C_{T_{X_u}} + 2C_{T_{X_1}}) \frac{u}{V_{P_1}} - (C_{D_\alpha} - C_{L_1}) \alpha - C_{D_{\delta_E}} \delta_E \right) \\
 (V_{P_1} \dot{\alpha} - V_{P_1} q) &= -g\theta \sin \Theta_1 + \frac{\bar{q}_1 S}{m} \left(-(C_{L_u} + 2C_{L_1}) \frac{u}{V_{P_1}} + (C_{L_\alpha} + C_{D_1}) \alpha - C_{L_{\dot{\alpha}}} \frac{\dot{\alpha} \bar{c}}{2V_{P_1}} - C_{L_q} \frac{q \bar{c}}{2V_{P_1}} - C_{L_{\delta_E}} \delta_E \right) \\
 I_{Y_Y} \ddot{\theta} &= \bar{q}_1 S \bar{c} \left((C_{m_u} + 2C_{m_1}) \frac{u}{V_{P_1}} + (C_{m_{T_u}} + 2C_{m_{T_1}}) \frac{u}{V_{P_1}} + (C_{m_\alpha} + C_{m_{T_\alpha}}) \alpha + C_{m_{\dot{\alpha}}} \frac{\dot{\alpha} \bar{c}}{2V_{P_1}} \right. \\
 &\quad \left. + C_{m_q} \frac{q \bar{c}}{2V_{P_1}} + C_{m_{\delta_E}} \delta_E \right)
 \end{aligned} \tag{2.65}$$

The longitudinal dimensional stability and control derivatives are expressed below in Tabel.2.1

$X_u = \frac{-\vec{q}_1 S (C_{D_U} + 2C_{D_1})}{mU_1}$	$M_u = \frac{\vec{q}_1 S \vec{c} (C_{m_U} + 2C_{m_1})}{U_1 I_{YY}}$
$X_\alpha = \frac{-\vec{q}_1 S (C_{D_\alpha} - C_{L_1})}{m}$	$M_\alpha = \frac{\vec{q}_1 S \vec{c} C_{m_\alpha}}{I_{YY}} \cdot (sec^{-2})$
$X_{T_u} = \frac{\vec{q}_1 S (C_{T_{X_u}} + 2C_{T_{X_1}})}{mU_1}$	$M_{\dot{\alpha}} = \frac{\vec{q}_1 S \vec{c} C_{m_{\dot{\alpha}}}}{I_{YY}} \cdot \frac{\vec{c}}{2U_1}$
$X_{\delta_E} = \frac{-\vec{q}_1 S C_{D_{\delta_E}}}{m}$	$M_{\delta_E} = \frac{\vec{q}_1 S \vec{c} C_{m_{\delta_E}}}{I_{YY}}$
$Z_u = -\frac{\vec{q}_1 S (C_{L_U} + 2C_{L_1})}{mU_1}$	$M_{T_u} = \frac{\vec{q}_1 S \vec{c} (C_{m_{T_U}} + 2C_{m_{T_1}})}{U_1 I_{YY}}$
$Z_\alpha = -\frac{\vec{q}_1 S (C_{L_\alpha} + C_{D_1})}{m}$	$M_{T_\alpha} = \frac{\vec{q}_1 S \vec{c} C_{m_{T_\alpha}}}{I_{YY}}$
$Z_{\dot{\alpha}} = -\frac{\vec{q}_1 S \vec{c} C_{L_{\dot{\alpha}}}}{2mU_1}$	$M_q = \frac{\vec{q}_1 S \vec{c} C_{m_q}}{I_{YY}} \cdot \frac{\vec{c}}{2U_1}$
$Z_q = -\frac{\vec{q}_1 S \vec{c} C_{L_q}}{2mU_1}$	
$Z_{\delta_E} = \frac{-\vec{q}_1 S C_{L_{\delta_E}}}{m}$	

TABLE 2.1: The Longitudinal Dimensional Stability and Control Derivatives

Based on the expression of the longitudinal dimensional stability and control derivatives, substitute to the new set of equations 2.65 leads to

$$\begin{aligned}
 \dot{u} &= -g\theta \cos \Theta_1 + (X_u + X_{T_u})u + X_\alpha \alpha + X_{\delta_E} \delta_E \\
 V_{P_1} \dot{\alpha} &= -g\theta \sin \Theta_1 + Z_u u + Z_\alpha \alpha + Z_{\dot{\alpha}} \dot{\alpha} + (Z_q + V_{P_1}) \dot{\theta} + Z_{\delta_E} \delta_E \\
 \ddot{\theta} &= (M_u + M_{T_u})u + (M_\alpha + M_{T_\alpha})\alpha + M_{\dot{\alpha}} \dot{\alpha} + M_q \dot{\theta} + M_{\delta_E} \delta_E
 \end{aligned} \tag{2.66}$$

Assuming zero initial condition with Laplace transformation is applied to the Eq. 2.66 and the coefficients of the equations are grouped in terms of $(u(s), \alpha(s), \theta(s))$, and expressed by

$$\begin{aligned}
 X_{\delta_E} \delta_E &= (s - (X_u + X_{T_u}))u(s) - X_\alpha \alpha(s) + g \cos \Theta_1 \theta(s) \\
 Z_{\delta_E} \delta_E &= -Z_u u(s) + (s(V_{P_1} - Z_{\dot{\alpha}}) - Z_\alpha) \alpha(s) + (-s(Z_q + V_{P_1}) + g \sin \Theta_1) \theta(s) \\
 M_{\delta_E} \delta_E &= -(M_u + M_{T_u})u(s) - (M_{\dot{\alpha}} s + (M_\alpha + M_{T_\alpha})) \alpha(s) + s(s - M_q) \theta(s)
 \end{aligned} \tag{2.67}$$

The transfer function concept is shown below in Fig. 2.13
 For longitudinal dynamics, the deflection of the elevator $\delta_E(t)$ is represented

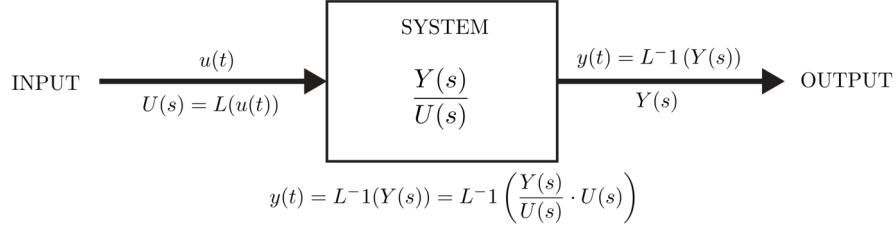


FIGURE 2.13: Concept of Transfer Function (Reproduced from [16])

the input and the small perturbation variables ($u(t)$, $\alpha(t)$, $\theta(t)$) are represented the individual outputs. Using the transfer functions $\left(\frac{u(s)}{\delta_E(s)}, \frac{\alpha(s)}{\delta_E(s)}, \frac{\theta(s)}{\delta_E(s)}\right)$, Eq. 2.67 are converted into matrix format.

$$\begin{bmatrix} (s - (X_u + X_{T_u})) & -X_\alpha & g \cos \Theta_1 \\ -Z_u & (s(V_{P_1} - Z_{\dot{\alpha}}) - Z_\alpha) & (-s(Z_q + V_{P_1}) + g \sin \Theta_1) \\ -(M_u + M_{T_u}) & -(M_{\dot{\alpha}}s + (M_\alpha + M_{T_\alpha})) & s(s - M_q) \end{bmatrix} \begin{bmatrix} \frac{u(s)}{\delta_E(s)} \\ \frac{\alpha(s)}{\delta_E(s)} \\ \frac{\theta(s)}{\delta_E(s)} \end{bmatrix} = \begin{bmatrix} X_{\delta_E} \\ Z_{\delta_E} \\ M_{\delta_E} \end{bmatrix} \quad (2.68)$$

2.4.2 The Lateral Directional Equations of Motion Laplace Transformations at Small Perturbation

The expression for the lateral force, rolling and yawing moments at small perturbation condition are given by

$$\begin{aligned}
 (f_{A_Y} + f_{T_Y}) &= \vec{q}_1 S \left((c_{Y_\beta} + c_{Y_{T_\beta}}) \beta + c_{Y_p} \frac{pb}{2V_{P_1}} + c_{Y_r} \frac{rb}{2V_{P_1}} + c_{Y_{\delta_A}} \delta_A + c_{Y_{\delta_R}} \delta_R \right) \\
 (l_A + l_T) &= \vec{q}_1 S b \left((c_{l_\beta} + c_{l_{T_\beta}}) \beta + c_{l_p} \frac{pb}{2V_{P_1}} + c_{l_r} \frac{rb}{2V_{P_1}} + c_{l_{\delta_A}} \delta_A + c_{l_{\delta_R}} \delta_R \right) \\
 (n_A + n_T) &= \vec{q}_1 S b \left((c_{n_\beta} + c_{n_{T_\beta}}) \beta + c_{n_p} \frac{pb}{2V_{P_1}} + c_{n_r} \frac{rb}{2V_{P_1}} + c_{n_{\delta_A}} \delta_A + c_{n_{\delta_R}} \delta_R \right)
 \end{aligned} \quad (2.69)$$

These expressions are expressed in the stability axes shown in Eq. 2.70 along with the Inverted Kinematic equations around the roll and yaw axes with the thrust

induced rolling and yawing moments and lateral force are negligible.

$$\begin{aligned}
 m(\dot{v} + V_{P_1}r) &= mg\phi + \vec{q}_1 S \left(c_{Y_\beta} \beta + c_{Y_p} \frac{pb}{2V_{P_1}} + c_{Y_r} \frac{rb}{2V_{P_1}} + c_{Y_{\delta_A}} \delta_A + c_{Y_{\delta_R}} \delta_R \right) \\
 I_{XX}\dot{p} - I_{XZ}\dot{r} &= \vec{q}_1 S b \left(c_{l_\beta} \beta + c_{l_p} \frac{pb}{2V_{P_1}} + c_{l_r} \frac{rb}{2V_{P_1}} + c_{l_{\delta_A}} \delta_A + c_{l_{\delta_R}} \delta_R \right) \\
 I_{ZZ}\dot{r} - I_{XZ}\dot{p} &= \vec{q}_1 S b \left(c_{n_\beta} \beta + c_{n_p} \frac{pb}{2V_{P_1}} + c_{n_r} \frac{rb}{2V_{P_1}} + c_{n_{\delta_A}} \delta_A + c_{n_{\delta_R}} \delta_R \right)
 \end{aligned} \tag{2.70}$$

The transformation shown below is introduced to represent (I_{XX}, I_{YY}, I_{XZ}) in accordance with the stability axes, given by

$$\begin{bmatrix} I_{XX} \\ I_{ZZ} \\ I_{XZ} \end{bmatrix}_{\text{Stability axes}} = \begin{bmatrix} \cos^2 \alpha_1 & \sin^2 \alpha_1 & -\sin(2\alpha_1) \\ \sin^2 \alpha_1 & \cos^2 \alpha_1 & \sin(2\alpha_1) \\ 0.5 \sin(2\alpha_1) & -0.5 \sin(2\alpha_1) & \cos(2\alpha_1) \end{bmatrix} \begin{bmatrix} I_{XX} \\ I_{ZZ} \\ I_{XZ} \end{bmatrix}_{\text{Body axes}} \tag{2.71}$$

Furthermore, a variable transformation is introduced to express \dot{v} with regards to $\dot{\beta}$,

$$v \approx V_{P_1} \beta \rightarrow \beta \approx \frac{v}{V_{P_1}}, \quad \dot{v} \approx V_{P_1} \dot{\beta} \rightarrow \dot{\beta} \approx \frac{\dot{v}}{V_{P_1}}$$

and substituting

$$p \approx \dot{\phi}, \quad \dot{p} \approx \ddot{\phi}, \quad r \approx \dot{\psi}, \quad \dot{r} \approx \ddot{\psi}$$

Leading to a new set of small perturbation lateral directional equations in Eq. 2.72, which the right-hand side of Eq. 2.70 contains a combination of aerodynamic coefficients, aircraft geometrics (b, S) and inertial moments (I_{XX}, I_{YY}, I_{XZ}) , also flight conditions (\vec{q}_1) .

$$\begin{aligned}
 (V_{P_1}\dot{\beta} + V_{P_1}\dot{\psi}) &= g\phi + \frac{\vec{q}_1 S}{m} \left(c_{Y_\beta} \beta + c_{Y_p} \frac{pb}{2V_{P_1}} + c_{Y_r} \frac{rb}{2V_{P_1}} + c_{Y_{\delta_A}} \delta_A + c_{Y_{\delta_R}} \delta_R \right) \\
 \ddot{\phi} - \frac{I_{XZ}}{I_{XX}} \ddot{\psi} &= \frac{\vec{q}_1 S b}{I_{XX}} \left(c_{l_\beta} \beta + c_{l_p} \frac{pb}{2V_{P_1}} + c_{l_r} \frac{rb}{2V_{P_1}} + c_{l_{\delta_A}} \delta_A + c_{l_{\delta_R}} \delta_R \right) \\
 \ddot{\psi} - \frac{I_{XZ}}{I_{ZZ}} \ddot{\phi} &= \frac{\vec{q}_1 S b}{I_{ZZ}} \left(c_{n_\beta} \beta + c_{n_p} \frac{pb}{2V_{P_1}} + c_{n_r} \frac{rb}{2V_{P_1}} + c_{n_{\delta_A}} \delta_A + c_{n_{\delta_R}} \delta_R \right)
 \end{aligned} \tag{2.72}$$

Moreover, the lateral directional dimensional stability and control derivatives are introduced based on Eq. 2.72 as shown in Tabel 2.2.

$Y_\beta = \frac{\vec{q}_1 S c_{Y_\beta}}{m}$	$L_\beta = \frac{\vec{q}_1 S b c_{l_\beta}}{I_{XX}}$
$Y_r = \frac{\vec{q}_1 S c_{Y_r} b}{m 2U_1}$	$L_r = \frac{\vec{q}_1 S b c_{l_r}}{I_{XX}}$
$Y_p = \frac{\vec{q}_1 S c_{Y_p} b}{m 2U_1}$	$L_p = \frac{\vec{q}_1 S b c_{l_p} b}{I_{XX} 2U_1}$
$Y_{\delta_R} = \frac{\vec{q}_1 S c_{Y_{\delta_R}}}{m}$	$L_{\delta_R} = \frac{\vec{q}_1 S b c_{l_{\delta_R}}}{I_{XX}}$
$Y_{\delta_A} = \frac{\vec{q}_1 S c_{Y_{\delta_A}}}{m}$	$L_{\delta_A} = \frac{\vec{q}_1 S b c_{l_{\delta_A}}}{I_{XX}}$
$N_\beta = \frac{\vec{q}_1 S b c_{n_\beta}}{I_{ZZ}}$	$N_{T_\beta} = \frac{I_{ZZ}}{\vec{q}_1 S b c_{n_{T_\beta}}}$
$N_r = \frac{\vec{q}_1 S b c_{n_r} b}{I_{ZZ} 2U_1}$	$N_{\delta_R} = \frac{\vec{q}_1 S b c_{n_{\delta_R}}}{I_{ZZ}}$
$N_p = \frac{\vec{q}_1 S b c_{n_p} b}{I_{ZZ} 2U_1}$	$N_{\delta_A} = \frac{\vec{q}_1 S b c_{n_{\delta_A}}}{I_{ZZ}}$

TABLE 2.2: Lateral Directional Dimensional Stability and Control Derivatives

Based on the expression of the lateral directional dimensional stability and control derivatives, substitute to the new set of equations 2.72 leads to

$$\begin{aligned}
 (V_{P_1} \dot{\beta} + V_{P_1} \dot{\psi}) &= g\phi + Y_\beta \beta + Y_{\dot{\phi}} \dot{\phi} + Y_{\dot{\psi}} \dot{\psi} + Y_{\delta_A} \delta_A + Y_{\delta_R} \delta_R \\
 \ddot{\phi} - \frac{I_{XZ}}{I_{XX}} \ddot{\psi} &= L_\beta \beta + L_{\dot{\phi}} \dot{\phi} + L_{\dot{\psi}} \dot{\psi} + L_{\delta_A} \delta_A + L_{\delta_R} \delta_R \\
 \ddot{\psi} - \frac{I_{XZ}}{I_{ZZ}} \ddot{\phi} &= N_\beta \beta + N_{\dot{\phi}} \dot{\phi} + N_{\dot{\psi}} \dot{\psi} + N_{\delta_A} \delta_A + N_{\delta_R} \delta_R
 \end{aligned} \tag{2.73}$$

where,

$$Y_{\dot{\phi}} = Y_p, \quad Y_{\dot{\psi}} = Y_r, \quad L_{\dot{\phi}} = L_p, L_{\dot{\psi}} = L_r, \quad N_{\dot{\phi}} = N_p, \quad N_{\dot{\psi}} = N_r$$

Furthermore, assuming zero initial condition with Laplace transformation is applied, also the inertia ratios are introduced,

$$I_1 = \frac{I_{XZ}}{I_{XX}}, I_2 = \frac{I_{XZ}}{I_{ZZ}}$$

leads to

$$\begin{aligned}
 Y_\delta \delta(s) &= (sV_{P_1} - Y_\beta) \beta(s) - (sY_p + g \cos \Theta_1) \theta(s) + s(V_{P_1} - Y_r) \psi(s) \\
 L_\delta \delta(s) &= -L_\beta \beta(s) + s(s - L_p) \phi(s) - s(sI_1 + L_r) \psi(s) \\
 N_\delta \delta(s) &= -N_\beta \beta(s) - s(sI_2 + N_p) \phi(s) + s(s - N_r) \psi(s)
 \end{aligned} \tag{2.74}$$

Transfer functions for lateral directional dynamics are introduced with ailerons and rudder are considered to be used, resulting in the six transfer functions shown below [16].

$$\left\{ \frac{\beta(s)}{\delta_A(s)}, \frac{\phi(s)}{\delta_A(s)}, \frac{\psi(s)}{\delta_A(s)} \right\} \left\{ \frac{\beta(s)}{\delta_R(s)}, \frac{\phi(s)}{\delta_R(s)}, \frac{\psi(s)}{\delta_R(s)} \right\}$$

Leading to a matrix form of Eq. 2.75,

$$\begin{bmatrix} (sV_{P_1} - Y_\beta) & -(sY_p + g) & s(V_{P_1} - Y_r) \\ -L_\beta & s(s - L_p) & -s(sI_1 + L_r) \\ -N_\beta & -s(sI_2 + N_p) & s(s - N_r) \end{bmatrix} \begin{bmatrix} \frac{\beta(s)}{\delta(s)} \\ \frac{\phi(s)}{\delta(s)} \\ \frac{\psi(s)}{\delta(s)} \end{bmatrix} = \begin{bmatrix} Y_\delta \\ L_\delta \\ N_\delta \end{bmatrix} \tag{2.75}$$

2.5 Aircraft Stability

It is essential to evaluate an aircraft's stability under trimmed conditions. Trimmed condition occurs when the airplane is flying in a straight line at a constant speed and all forces operating on the aircraft are in equilibrium. According to the general definition, stability is the tendency of an aircraft to return to the trim state when it is disturbed while in the trim condition [18].

The static stability of an aircraft is typically regarded as its tendency to return to its initial equilibrium condition after a small perturbation from trim conditions. On the other hand, dynamic stability describes the short-term motions that occur as the system recovers to equilibrium condition after a perturbation [15].

2.5.1 Static Stability and Control

Longitudinal Static Stability and Trim Condition

To fly, an aircraft must be stable and capable of being trimmed, where the aircraft must generate lift equal to its weight while generating zero moment [19]. The longitudinal static stability is characterized by

- The pitching moment coefficient changes with the angle of attack (C_{m_α}).
- The aircraft neutral point (\vec{X}_{np}) or also known as the aircraft aerodynamic center (\vec{X}_{AC}).
- The static margin (SM)

The requirement for the aircraft to be longitudinal statically stable is given by

$$C_{m_\alpha} = \frac{\partial C_m}{\partial \alpha} < 0 \quad (2.76)$$

where C_{m_α} is calculated at trim condition. The C_{m_α} requirement shows that the aircraft required a negative pitching moment curve slope to be longitudinal statically stable. Transport aircraft have "high" pitch stability, indicated in a low C_{m_α} value from -1.2 to -1.7 per radian [19].

The airplane aerodynamic center is the point where the aircraft pitching moment does not vary with angle of attack, mathematically expressed as

$$C_{m_\alpha} = 0$$

The expression for the aircraft aerodynamic center is expressed below in Eq. 2.77.

$$\vec{x}_{AC} = \frac{\vec{x}_{ACWB} + \frac{C_{L\alpha H}}{C_{L\alpha W}} \eta_H \frac{S_H}{S} \left(1 - \frac{d\varepsilon}{d\alpha}\right) \vec{x}_{ACH}}{1 + \frac{C_{L\alpha H}}{C_{L\alpha W}} \eta_H \frac{S_H}{S} \left(1 - \frac{d\varepsilon}{d\alpha}\right)} \quad (2.77)$$

The typical ranges for the aircraft aerodynamic center are [16]

- [0.4 – 0.6] for general aviation aircraft.

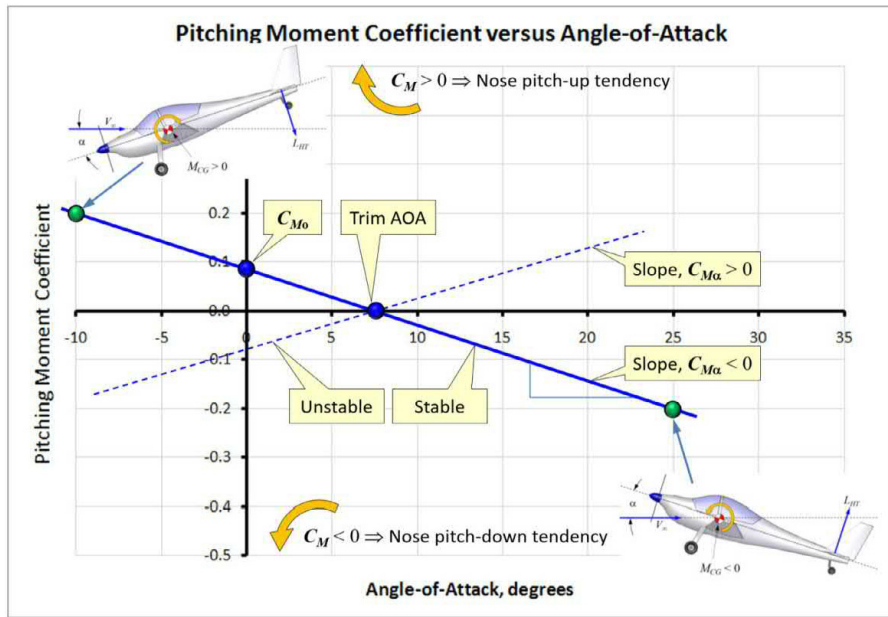


FIGURE 2.14: Pitching Moment Coefficient vs Angle of Attack [19]

- [0.35 – 0.45] for commercial and military transport aircrafts.
- [0.3 – 0.35] for fighter aircraft.

The aircraft aerodynamic center is important to calculate, because it is required to calculate the Static Margin of the aircraft. The Static Margin describe the distance between the aircraft aerodynamic center (also called the aircraft neutral point) and the aircraft center of gravity in accordance with the mean aerodynamic chord \bar{c} . The Static Margin in mathematical form can be expressed by

$$SM = -100 (\bar{x}_{CG} - \bar{x}_{AC}) \quad (2.78)$$

The figure shown below describes the aircraft aerodynamic center and center of gravity which described the static margin.

The typical ranges of the Static Margin are given by

- [0.15 – 0.25] for commercial and military transport aircrafts.
- [0.05 – 0.15] for open loop stable fighter aircraft.

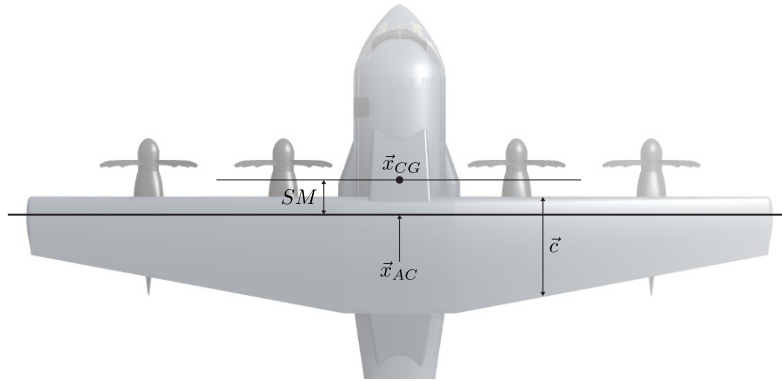


FIGURE 2.15: Static Margin of an Aircraft (Reproduced from [16])

Lateral Static Stability

Lateral stability is the tendency of an aircraft to level its wing during yaw and the aircraft is lateral statically stable if it generates a negative rolling moment when subjected to a positive sideslip angle β [19]. The lateral static stability is calculated at cruise condition with the requirement for the the aircraft to be lateral statically stable is given by [19],

$$C_{l_\beta} = \frac{\partial C_l}{\partial \beta} < 0 \quad \text{and} \quad C_l = 0 \quad \text{if} \quad \beta = 0 \quad (2.79)$$

The C_{l_β} requirement shows that the aircraft required a negative slope to restore the rolling moment and become lateral statically stable. A typical range of C_{l_β} is $-0.03 < C_{l_\beta} < -0.12$ per radian [19].

Directional Static Stability

Directional stability is the capability of the aircraft to weathervane with the slope of the yawing moment curve must have a positive slope. The directional static stability is calculated at cruise condition with the aircraft to be directional statically stable is given by [19],

$$C_{n_\beta} = \frac{\partial C_n}{\partial \beta} > 0 \quad \text{and} \quad C_n = 0 \quad \text{if} \quad \beta = 0 \quad (2.80)$$

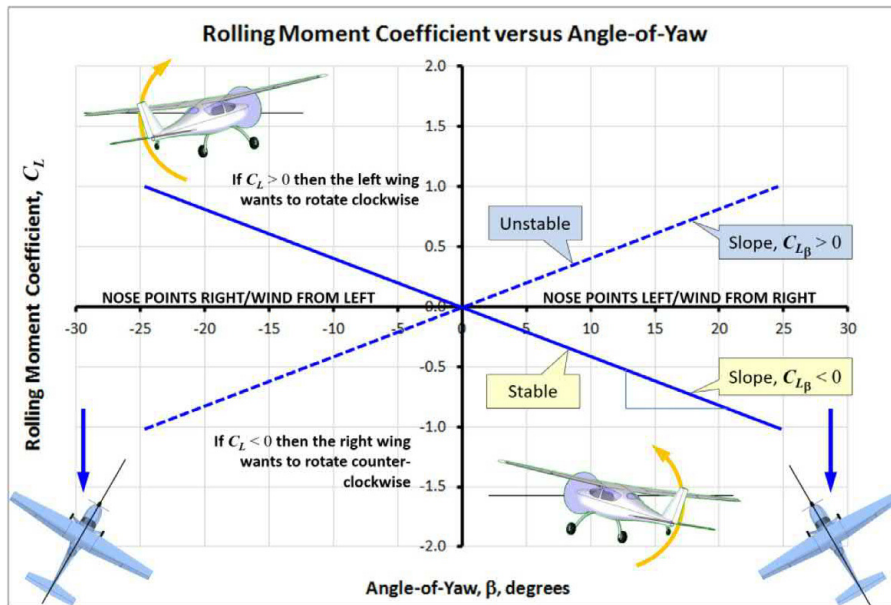


FIGURE 2.16: Rolling Moment Coefficient vs Sideslip Angle [19]

The C_{n_β} requirement shows that the aircraft required a positive yawing moment curve to be directional statically stable. A typical ranges of C_{n_β} is $0.03 < C_{n_{\beta W}} < 0.2$ per radian, where multiengine aircraft tend toward greater values.

2.5.2 Dynamic Stability Stability and Control

The aircraft is said to be longitudinal and lateral directional dynamically stable, if:

1. The longitudinal characteristic equation (CE) has two pairs of complex conjugate roots with a negative real part, where each pair is correlated with a specific dynamic mode, known as short period mode and phugoid mode.
2. The lateral directional characteristic equation (CE) has a pair of complex conjugate root along with two real roots with a negative real part, where the roots are associated with lateral dynamics mode, known as dutch roll mode, spial mode and roll mode.

The longitudinal and lateral directional characteristic equation is calculated by using the longitudinal dynamic in matrix form in Eq. 2.68 and lateral directional dynamics in matrix form in Eq. 2.75.

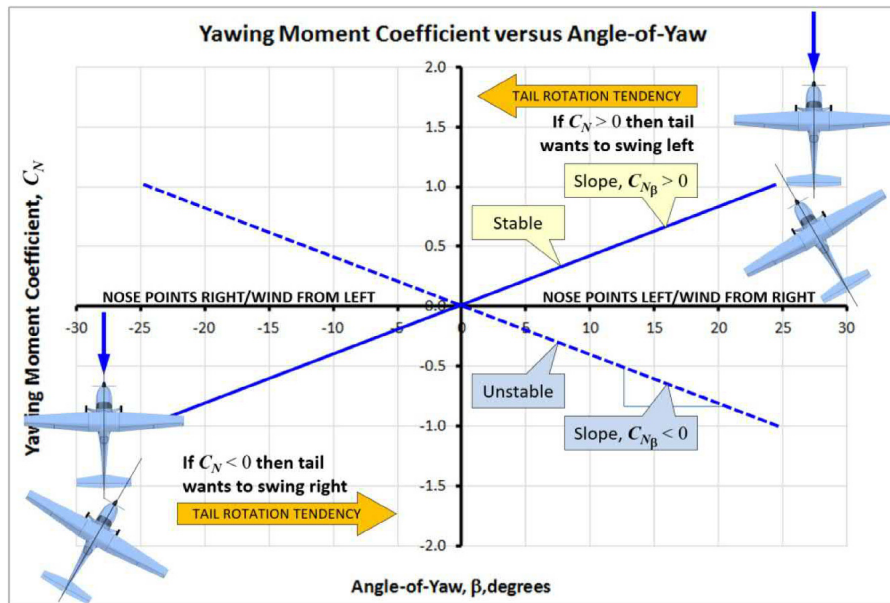


FIGURE 2.17: Yawing Moment Coefficient vs Sideslip Angle [19]

The Short Period and Phugoid Modes

Typically, the short period mode is a damped oscillation in pitch about the oy axis. When an aircraft is perturbed from its pitch equilibrium state, the short period mode is stimulated and manifests as a classical second-order oscillation with the major variables are incidence $\alpha(w)$, pitch rate q , and pitch attitude θ [15].

The phugoid mode is typically a lightly damped low-frequency oscillation in velocity u that relates into pitch attitude θ and altitude h . During a disturbance, this mode's incidence $\alpha(w)$ remains relatively constant. Consequently, the phugoid is a classically damped harmonic motion that results in the aircraft following a lightly sinusoidal flight path around the nominal trimmed height datum. As strong inertia and momentum effects are present, the motion must be slow enough that the angular accelerations, q and $\alpha(w)$ are negligibly small. As a result, the mode's natural frequency is low, and because drag is supposed to be low, damping is similarly low.

The typical locations of the characteristic equations roots associated with these modes are shown in Fig. 2.18

However, the short period and phugoid modes are characterised by

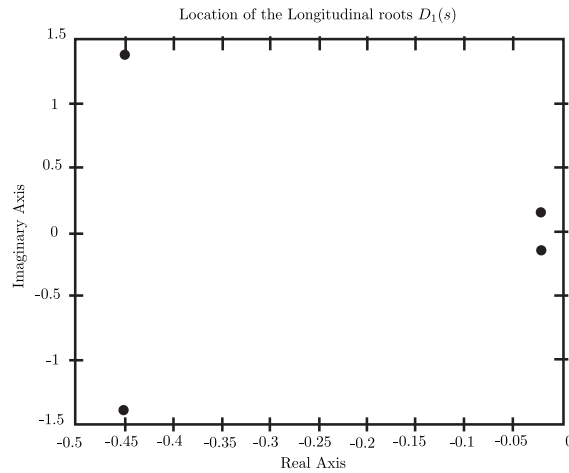


FIGURE 2.18: Longitudinal Characteristic Equations Root Locations (Reproduced from [16])

- The short period is identified by relatively high damping ratio ζ_{SP} and high natural frequency values $\omega_{n_{SP}}$.
- The phugoid has low damping coefficient ζ_{PH} and natural frequency $\omega_{n_{PH}}$.

The relationship below is applied to the longitudinal dynamic modes:

$$\omega_{n_{SP}} \gg \omega_{n_{PH}} \quad \zeta_{SP} \gg \zeta_{PH}$$

The Rolling, Spiral and Dutch Roll Modes

The dutch roll mode is a classically damped yaw oscillation on the aircraft's main axis that links into roll and, to a lesser extent, sideslip. Therefore, the motion represented by the dutch roll mode involves a complicated relationship between the three lateral degrees of freedom. The pair of complex roots in its characteristic polynomial describe its properties. Fundamentally, the dutch roll mode corresponds to the longitudinal short period mode in the lateral direction.

The roll mode is a non-oscillatory lateral characteristic that is often significantly separated from the spiral and dutch roll modes, characterized by a single real root of the characteristic polynomial and appears in rolling motion as an exponential lag. Also non-oscillatory, the spiral mode is determined by the other real root of the characteristic polynomial. The spiral mode is frequently triggered by a sideslip disturbance that follows a roll disturbance that causes a wing to drop [15].

The typical locations of the characteristic equations roots associated with these modes [16] are shown below in Fig. 2.19

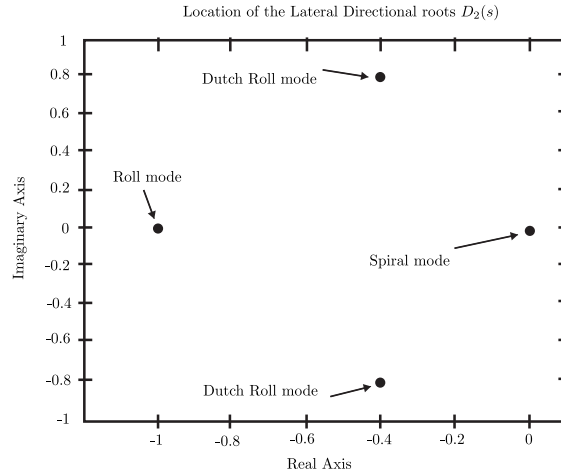


FIGURE 2.19: Lateral Directional Characteristic Equations Root Locations (Reproduced from [16])

However, these modes are characterized by

- The dutch roll is defined by moderate levels of the damping ratio ζ_{DR} and the natural frequency $\omega_{n_{DR}}$. Majority of aircraft, $\omega_{n_{PH}} < \omega_{n_{DR}} < \omega_{n_{SP}}$ with regards to $\zeta_{PH} < \zeta_{DR} < \zeta_{SP}$.
- The spiral is an extremely slow mode of the first order with the root at $-\lambda_S$, typically positioned near the origin of the s -plane, resulting in a relatively high value for the related time constant $T_S = -\frac{1}{\lambda_S}$.
- The rolling is a rather fast first order mode, with the root at $-\lambda_R$ correlated with the constant time $T_R = -\frac{1}{\lambda_R}$.

2.6 The Dynamics Systems State Variables Model

2.6.1 The Longitudinal State Variable Model

The set of longitudinal equations in Eq. 2.66 provides a framework for the creation of the SV model of longitudinal dynamics, which can be rewritten using the

relationship

$$q = \dot{\theta}, \dot{q} = \ddot{\theta}$$

leads to

$$\begin{aligned} \dot{u} &= (X_u + X_{T_u})u + X_\alpha \alpha - g \cos \Theta_1 \theta + X_{\delta_E} \delta_E \\ (V_{P_1} - Z_{\dot{\alpha}}) \dot{\alpha} &= Z_u u + Z_\alpha \alpha - g \sin \Theta_1 \theta + (Z_q + V_{P_1}) q + Z_{\delta_E} \delta_E \\ \dot{q} &= (M_u + M_{T_u})u + (M_\alpha + M_{T_\alpha}) \alpha + M_{\dot{\alpha}} \dot{\alpha} + M_q \dot{\theta} + M_{\delta_E} \delta_E \\ \dot{\theta} &= q \end{aligned} \quad (2.81)$$

These equations show that $\dot{\alpha}$ equation can be integrated into \dot{q} equation, also the propulsive dimensional derivatives contribution (M_{T_u}, M_{T_α}) can be neglected, leads to the following expression as shown in Eq. 2.82.

$$\begin{aligned} \dot{u} &= (X_u + X_{T_u})u + X_\alpha \alpha - g \cos \Theta_1 \theta + X_{\delta_E} \delta_E \\ \dot{\alpha} &= \frac{Z_u}{(V_{P_1} - Z_{\dot{\alpha}})}u + \frac{Z_\alpha}{(V_{P_1} - Z_{\dot{\alpha}})}\alpha - \frac{g \sin \Theta_1}{(V_{P_1} - Z_{\dot{\alpha}})}\theta + \frac{(Z_q + V_{P_1})}{(V_{P_1} - Z_{\dot{\alpha}})}q + \frac{Z_{\delta_E}}{(V_{P_1} - Z_{\dot{\alpha}})}\delta_E \\ \dot{q} &= \left(M_{\dot{\alpha}} \frac{Z_u}{(V_{P_1} - Z_{\dot{\alpha}})} + M_u \right) u + \left(M_{\dot{\alpha}} \frac{Z_\alpha}{(V_{P_1} - Z_{\dot{\alpha}})} + M_\alpha \right) \alpha + \left(M_{\dot{\alpha}} \frac{-g \sin \Theta_1}{(V_{P_1} - Z_{\dot{\alpha}})} \right) \theta \\ &\quad + \left(M_{\dot{\alpha}} \frac{Z_q + V_{P_1}}{(V_{P_1} - Z_{\dot{\alpha}})} + M_q \right) q + \left(M_{\dot{\alpha}} \frac{Z_{\delta_E}}{(V_{P_1} - Z_{\dot{\alpha}})} + M_{\delta_E} \right) \delta_E \\ \dot{\theta} &= q \end{aligned} \quad (2.82)$$

The State Variable model for the longitudinal dynamics is shown in Eq. 2.83,

$$\begin{aligned} \dot{x}_{Long} &= A_{Long} x_{Long} + B_{Long} u_{Long} \\ y_{Long} &= C_{Long} x_{Long} + D_{Long} u_{Long} \end{aligned} \quad (2.83)$$

where,

- The $(x_{Long}) \triangleq$ the set of longitudinal state variables;
- The $(u_{Long}) \triangleq$ the longitudinal input column;
- If only (δ_E) is used for the longitudinal control surface, (u_{Long}) reduces themselves to a scalar $(u_{Long} = (\delta_E))$

with the (x_{Long}) is given by

$$x_{Long} = \begin{bmatrix} u \\ \alpha \\ q \\ \theta \end{bmatrix}$$

Leading to the longitudinal state equations in matrix form as expressed in Eq. 2.84.

$$\begin{aligned} \begin{bmatrix} \dot{u} \\ \dot{\alpha} \\ \dot{q} \\ \dot{\theta} \end{bmatrix} &= A_{Long} \begin{bmatrix} u \\ \alpha \\ q \\ \theta \end{bmatrix} + B_{Long}(\delta_E) \\ &= \begin{bmatrix} X'_u & X'_\alpha & X'_q & X'_\theta \\ Z'_u & Z'_\alpha & Z'_q & Z'_\theta \\ M'_u & M'_\alpha & M'_q & M'_\theta \\ 0 & 0 & 1 & 0 \end{bmatrix} \begin{bmatrix} u \\ \alpha \\ q \\ \theta \end{bmatrix} + \begin{bmatrix} X'_{\delta_E} \\ Z'_{\delta_E} \\ M'_{\delta_E} \\ 0 \end{bmatrix} (\delta_E) \end{aligned} \quad (2.84)$$

where,

- $(A_{Long}) \triangleq$ the longitudinal state matrix;
- $(B_{Long}) \triangleq$ the longitudinal input matrix.

The coefficient of (A_{Long}) and (B_{Long}) are calculated using the following expressions.

$$\begin{aligned} X'_u &= (X_u + X_{T_u}), & X'_\alpha &= X_\alpha, & X'_q &= 0, & X'_\theta &= -g \cos \Theta_1, & X'_{\delta_E} &= X_{\delta_E} \\ Z'_u &= \frac{Z_u}{(V_{P_1} - Z_{\dot{\alpha}})}, & Z'_\alpha &= \frac{Z_\alpha}{(V_{P_1} - Z_{\dot{\alpha}})}, & Z'_q &= \frac{(Z_q + V_{P_1})}{(V_{P_1} - Z_{\dot{\alpha}})}, \\ Z'_\theta &= -\frac{g \sin \Theta_1}{(V_{P_1} - Z_{\dot{\alpha}})}, & Z'_{\delta_E} &= \frac{Z_{\delta_E}}{(V_{P_1} - Z_{\dot{\alpha}})} \\ M'_u &= M_{\dot{\alpha}} Z'_u + M_u, & M'_\alpha &= M_{\dot{\alpha}} Z'_\alpha + M_\alpha, & M'_\theta &= M_{\dot{\alpha}} Z'_\theta, \\ M'_q &= M_{\dot{\alpha}} Z'_q + M_q, & M'_{\delta_E} &= M_{\dot{\alpha}} Z'_{\delta_E} + M_{\delta_E} \end{aligned} \quad (2.85)$$

The output vector (y_{Long}) in the SV model second Eq. 2.83 represents the longitudinal properties of the aircraft as recorded by onboard sensors.

2.6.2 The Lateral Directional State Variable Model

Recall the lateral directional equations in Eq. 2.73 with the following relationship applied

$$r \approx \dot{\psi}, \dot{r} \approx \ddot{\psi}, p \approx \dot{\phi}, \dot{p} \approx \ddot{\phi}$$

The lateral directional equations are rewritten as shown in Eq. 2.86.

$$\begin{aligned} (V_{P_1} \dot{\beta}) &= Y_{\beta} \beta + Y_p p + (Y_r - V_{P_1}) r + g \cos \Theta_1 \phi + Y_{\delta_A} \delta_A + Y_{\delta_R} \delta_R \\ \dot{p} - \frac{I_{XZ}}{I_{XX}} \dot{r} &= L_{\beta} \beta + L_p p + L_r r + L_{\delta_A} \delta_A + L_{\delta_R} \delta_R \\ \dot{r} - \frac{I_{XZ}}{I_{ZZ}} \dot{p} &= N_{\beta} \beta + N_p p + N_r r + N_{\delta_A} \delta_A + N_{\delta_R} \delta_R \end{aligned} \quad (2.86)$$

The second and third equations of Eq. 2.86 are integrated in terms of solving the equations, these have to be solved separately. However, the final equation of lateral directional equations are given in Eq. 2.87 along with the kinematic relationship $\dot{\phi} = p + \tan \Theta_1 r$

$$\begin{aligned} \dot{\beta} &= \frac{Y_{\beta}}{V_{P_1}} \beta + \frac{Y_p}{V_{P_1}} p + \frac{(Y_r - V_{P_1})}{V_{P_1}} r + \frac{g \cos \Theta_1}{V_{P_1}} \phi + \frac{Y_{\delta_A}}{V_{P_1}} \delta_A + \frac{Y_{\delta_R}}{V_{P_1}} \delta_R \\ \dot{p} &= \frac{(L_{\beta} + I_1 N_{\beta})}{(1 - I_1 I_2)} \beta + \frac{(L_p + I_1 N_p)}{(1 - I_1 I_2)} p + \frac{(L_r + I_1 N_r)}{(1 - I_1 I_2)} r + L'_{\delta_A} \delta_A + \frac{(L_{\delta_R} + I_1 N_{\delta_R})}{(1 - I_1 I_2)} \delta_R \\ \dot{r} &= \frac{(I_2 L_{\beta} + N_{\beta})}{(1 - I_1 I_2)} \beta + \frac{(I_2 L_p + N_p)}{(1 - I_1 I_2)} p + \frac{(I_2 L_r + N_r)}{(1 - I_1 I_2)} r + \frac{(I_2 L_{\delta_A} + N_{\delta_A})}{(1 - I_1 I_2)} \delta_A + \frac{(I_2 L_{\delta_R} + N_{\delta_R})}{(1 - I_1 I_2)} \delta_R \end{aligned} \quad (2.87)$$

The general relationships for Lateral-Directional equations in SV model are given by

$$\begin{aligned} \dot{x}_{Lat Dir} &= A_{Lat Dir} x_{Lat Dir} + B_{Lat Dir} u_{Lat Dir} \\ y_{Lat Dir} &= C_{Lat Dir} x_{Lat Dir} + D_{Lat Dir} u_{Lat Dir} \end{aligned} \quad (2.88)$$

where,

- The $\dot{x}_{Lat Dir} \triangleq$ the lateral directional state equation.
- The $y_{Lat Dir} \triangleq$ the lateral directional output equation.

with $(x_{Lat Dir})$ and $(u_{Lat Dir})$ are given by

$$x_{Lat Dir} = \begin{bmatrix} \beta \\ p \\ r \\ \phi \end{bmatrix}, \quad u_{Lat Dir} = \begin{bmatrix} \delta_A \\ \delta_R \end{bmatrix}$$

Leading to the lateral directional state variable model are given by

$$\begin{aligned} \begin{bmatrix} \dot{\beta} \\ \dot{p} \\ \dot{r} \\ \dot{\phi} \end{bmatrix} &= A_{Lat Dir} \begin{bmatrix} \beta \\ p \\ r \\ \phi \end{bmatrix} + B_{Lat Dir} \begin{bmatrix} \delta_A \\ \delta_R \end{bmatrix} \\ &= \begin{bmatrix} Y'_\beta & Y'_p & Y'_r & Y'_\phi \\ L'_\beta & L'_p & L'_r & 0 \\ N'_\beta & N'_p & N'_r & 0 \\ 0 & 1 & \tan \Theta_1 & 0 \end{bmatrix} \begin{bmatrix} \beta \\ p \\ r \\ \phi \end{bmatrix} + \begin{bmatrix} Y'_{\delta_A} & Y'_{\delta_R} \\ L'_{\delta_A} & L'_{\delta_R} \\ N'_{\delta_A} & N'_{\delta_R} \\ 0 & 0 \end{bmatrix} \begin{bmatrix} \delta_A \\ \delta_R \end{bmatrix} \end{aligned} \quad (2.89)$$

where,

- $A_{Lat Dir} \triangleq$ the lateral directional state matrix;
- $B_{Lat Dir} \triangleq$ the lateral directional input matrix.

The coefficient of $A_{Lat Dir}$ and $B_{Lat Dir}$ are calculated using the following expressions.

$$\begin{aligned} Y'_\beta &= \frac{Y_\beta}{V_{P1}}, \quad Y'_p = \frac{Y_p}{V_{P1}}, \quad Y'_r = \frac{(Y_r - V_{P1})}{V_{P1}}, \quad Y'_\phi = \frac{g \cos \Theta_1}{V_{P1}}, \quad Y'_{\delta_A} = \frac{Y_{\delta_A}}{V_{P1}}, \quad Y'_{\delta_R} = \frac{Y_{\delta_R}}{V_{P1}} \\ L'_\beta &= \frac{(L_\beta + I_1 N_\beta)}{(1 - I_1 I_2)}, \quad L'_p = \frac{(L_p + I_1 N_p)}{(1 - I_1 I_2)}, \quad L'_r = \frac{(L_r + I_1 N_r)}{(1 - I_1 I_2)}, \quad L'_{\delta_A} = \frac{(L_{\delta_R} + I_1 N_{\delta_R})}{(1 - I_1 I_2)}, \quad L'_{\delta_R} = \frac{(L_{\delta_R} + I_1 N_{\delta_R})}{(1 - I_1 I_2)} \delta_R \\ N'_\beta &= \frac{(I_2 L_\beta + N_\beta)}{(1 - I_1 I_2)}, \quad N'_p = \frac{(I_2 L_p + N_p)}{(1 - I_1 I_2)}, \quad N'_r = \frac{(I_2 L_r + N_r)}{(1 - I_1 I_2)}, \quad N'_{\delta_A} = \frac{(I_2 L_{\delta_A} + N_{\delta_A})}{(1 - I_1 I_2)}, \quad N'_{\delta_R} = \frac{(I_2 L_{\delta_R} + N_{\delta_R})}{(1 - I_1 I_2)} \delta_R \end{aligned} \quad (2.90)$$

The lateral directional output derivation equations $(y_{Lat Dir})$ is dependent on the elements selection on the output column which includes the lateral direction sensor parameters.

2.7 Flying and Handling Qualities

There are three levels of flying qualities [16]:

1. Level I: Under the specified flying conditions, satisfactory and optimal for the specified maneuver.
2. Level II: Acceptable and suitable for the specified maneuver under the current flying conditions, but with higher effort and pilot correction, resulting in a slight decrease in mission effectiveness.
3. Level III: Control and navigation of the aircraft safely, but with a large increase in effort and pilot compensation, resulting in a significant decrease in mission effectiveness.

Moreover, the aircraft dynamic characteristics requirements are depends on the specific class of the aircraft. As shown in Table 2.3, the different classes of military aircraft according to MIL-F-878SC are divided to four classes which also compared to the civiliant equivalent aircrafts [16].

Moreover, the mission profile of each types of aircrafts should be specified, in order to analyze the flying and handling qualities of the aircraft. A mission profile is a typical sequence of maneuvers (from Categories A, B, and C) for a particular aircraft of a particular class as shown in Table 2.4.

2.7.1 Longitudinal Flying Quality Requirements

Phugoid Mode Damping Ratio

The phugoid mode damping ratio ζ_{PH} requirements are shown in Table 2.5 [20].

Within the military specifications for Level III, the parameter T_{2Ph} implies that phugoid mode oscillations may double their amplitudes if the necessary duration exceeds 55 seconds.

The Short Period Mode Damping Ratio

The short period mode damping ratio ζ_{SP} requirements are shown in Table 2.6 [20].

Classes of Military Aircraft (according to MIL-F-878SC)	Examples	Civilian Equivalent
Class I: Small and Light Airplanes.		
Light utility;	Cessna T-41;	Cessna 210;
Primary trainer;	Beech T-34C.	Piper Tomahawk.
Light observation and/or reconnaissance.		
Class II: Medium weight, low-to-medium maneuverability airplanes.		
Heavy utility/search and rescue;	Fairchild C-119;	Boeing 727;
Light or medium transport/cargo/tanker;	Grumman E-2C;	Boeing 737;
Early warning/Electronic counter-measures/	Boeing E-3A;	McDD DC-9;
Airborne command, control or communications relay;	Lockheed S-3A;	McDD MD-80;
Anti-submarine;	Lockheed C-130;	Airbus A320.
Assault transport;	Fairchild A-10;	
Reconnaissance;	Aeritalia G222;	
Tactical Bomber;	Douglas B -60;	
Heavy Attack;	Grumman A-6;	
Trainer for Class II aircraft.	Beech T-1A.	
Class III: Large, heavy; low-to-medium maneuverability airplanes.		
Heavy transport/cargo/tanker;	McDD C-17;	McDD MD-11;
Heavy bomber;	Boeing B-S2H;	Boeing 747;
Patrol/Early warning/Electronic counter-measures/	Lockheed P-3;	Boeing 777;
Airborne command, control or communications relay;	Lockheed C-S;	Airbus 330;
Trainer for Class III.	Boeing B-3D;	Airbus 340;
	Boeing KC-135.	Airbus 380.
Class IV: High maneuverability airplanes.		
Fighter/interceptor;	Lockheed F-22;	Pitts Special.
Attack;	McDDF-4;	
Tactical reconnaissance;	McDDF-15;	
Observation;	Lockheed SR-71;	
Trainer for Class IV aircraft.	Northrop T-38.	

TABLE 2.3: Classes of Military Aircraft along with Examples of Civilian Equivalent

"Non-Terminal" Maneuvers		"Terminal" Maneuvers
Category A	Category B	Category C
Air-to-air combat;	Climb;	Takeoff;
Ground attack;	Cruise;	Carrier and/or catapult takeoff;
Weapon delivery/launch;	Loiter;	Approach;
Aerial recovery;	In-flight refueling (as tanker);	Wave-off/go-around;
Reconnaissance;	Descent;	Landing.
In-flight refueling (as receiver aircraft);	Emergency descent;	
Terrain following;	Emergency deceleration;	
Anti-submarine search;	Aerial delivery.	
Close formation flying.		

TABLE 2.4: Categories of Aircraft Maneuvers

MIL-F-8785C	VAL, FAR 23 and FAR 25
Level I $\zeta_{PH} \geq 0.04$	Level I No requirement
Level II $\zeta_{PH} \geq 0$	Level II No requirement
Level III $T_{2PH} \geq 55$ sec	Level III No requirement

TABLE 2.5: Requirements for the Phugoid Damping

Category A & C Maneuvers	Category B Maneuvers
Level I $\zeta_{SP} > 0.35$	Level I $\zeta_{SP} > 0.35$
Level II $\zeta_{SP} > 0.25$	Level II $\zeta_{SP} > 0.2$
Level III $\zeta_{SP} > 0.15$	Level III $\zeta_{SP} > 0.15$

TABLE 2.6: Requirements for the Short Period Damping (Military Aircraft)

2.7.2 Lateral Directional Flying Quality Requirements

The Dutch Roll Mode Damping Ratio and Natural Frequency

The MIL-F-8785C specifies the dutch roll mode ζ_{DR} and $\omega_{n_{DR}}$ requirements for military aircraft as shown in Table 2.7 [20].

Level	Category of Maneuvers	Class of Aircraft	Minimum ζ_{DR}	Minimum $\zeta_{DR}\omega_{n_{DR}}$	Minimum $\omega_{n_{DR}}$
Level I	A (Combat and Ground Attack)	IV	0.4	-	1.0
	A (All Others)	I, IV	0.19	0.35	1.0
		II, III	0.19	0.35	0.4
	B	All	0.08	0.15	0.4
	C	I, II-C, IV	0.08	0.15	1.0
II-L, III		0.08	0.10	0.4	
Level II	All	All	0.05	0.05	0.4
Level III	All	All	0	-	0.4

TABLE 2.7: Dutch Roll Damping and Natural Frequency Requirements (Military Aircraft)

The Spiral Mode Time Constant

The spiral mode time constant requirements for military aircraft are shown in Table 2.8 [20].

Category of Maneuvers	Level I	Level II	Level III
A, C	$T_{2s} > 12sec$	$T_{2s} > 8sec$	$T_{2s} > 4sec$
B	$T_{2s} > 20sec$	$T_{2s} > 12sec$	$T_{2s} > 12sec$

TABLE 2.8: Requirements for the Spiral Mode (Military Aircraft)

The parameter T_{2s} is defined as the amount of time necessary to double the spiral's amplitude.

The Rolling Mode Time Constant

For fighter aircraft, the requirements for the rolling mode are critical. A pilot’s ability to roll quickly is a valuable asset in air combat. The rolling mode time constant requirements for military aircraft are shown in Table 2.9 [20].

Category of Maneuvers	Class of Aircraft	Level I	Level II	Level III
A, C	I, IV	$T_R < 1sec$	$T_R < 1.4sec$	$T_R < 10sec^*$
	II, III	$T_R < 1.4sec$	$T_R < 3sec$	-
B	ALL	$T_R < 1.4sec$	$T_R < 3sec$	$T_R < 10sec$
C	I, II-C, IV	$T_R < 1sec$	$T_R < 1.4sec$	$T_R < 10sec^*$
	II-L, III	$T_R < 1.4sec$	$T_R < 3sec$	-

*for Class IV only

TABLE 2.9: Requirements for the Rolling Mode (Military Aircraft)

2.8 Stability Augmentations System

If the aircraft does not fulfill the specifications in any manner, corrective measures must be considered, where Stability Augmentation System is introduced. The stability augmentation system primary function is to reduce response transients after an upset from equilibrium. The design of the inner loop control law is the most critical aspect of FCS design. The goal of the design is to give the aircraft good stability, control, and handling characteristics throughout its flight envelope.

Due to the fact that each variable generates an unique combination of changes, the choice of feedback variable is crucial for defining the type of the change in the aircraft’s stability characteristics. The longitudinal stability augmentation options are shown in Fig. 2.20. The idea is that any of the motion variables and the elevator may complete a negative feedback loop. The evaluation is conducted by assessing the effect of each motion variable on the closed-loop stability characteristics as a function of the closed loop gain K .

In addition to the longitudinal stability augmentation options described previously, it is useful to evaluate all of the lateral-directional single loop feedback options. The options for lateral-directional stability augmentation are shown in

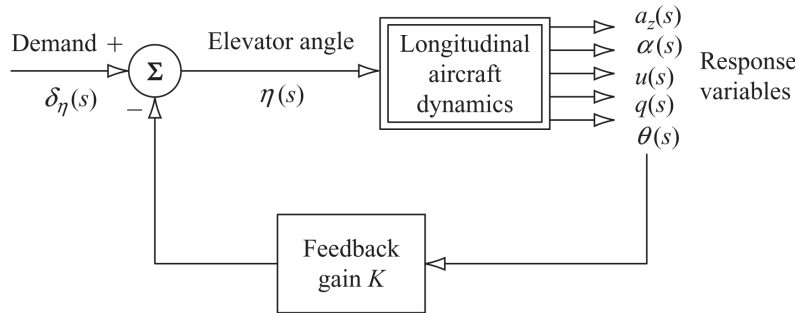


FIGURE 2.20: Longitudinal Feedback Options [15]

Fig. 2.21, where it is implied that a negative feedback loop can be closed between any of the motion variables and either the ailerons or the rudder.

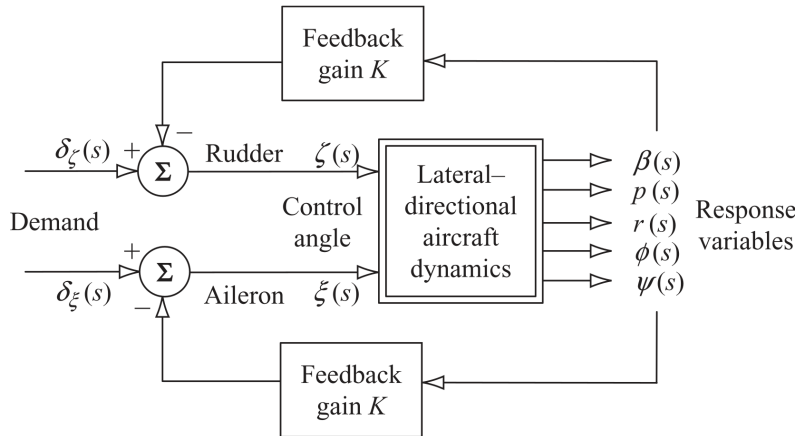


FIGURE 2.21: Lateral Directional Feedback Options [15]

2.8.1 The LQR Control Technique

To reach a certain objective, instead of choosing the closed-loop eigenvalue locations, the gains for a state feedback controller can be chosen by trying to optimize a cost function. This can be especially helpful for balancing the system’s performance with the size of the inputs it needs to reach that level of performance [21]. Modern control theory has a method called linear quadratic regulator (LQR), which is an alternative and very powerful way to design flight control systems. The method is based on manipulating the equations of motion in state space form, and the analysis process makes full use of the appropriate computational tools [22].

Starting from the state variable model general expression,

$$\dot{x} = Ax + Bu$$

with initial condition $x(0) = x_0$, the following cost function (also known as the quadratic performance index) must be reduced in order to identify the best control inputs while simultaneously optimizing the state variables [23].

$$J(x_0) = \int_0^{t_f} (x^T Q x + u^T R u) dt + x^T(t_f) S(t_f) x(t_f) \quad (2.91)$$

where, Q and R are the weighting matrices with Q is a semi-positive definite symmetric matrix, while R is a positive definite symmetric matrix.

This cost function represents a balance between the deviation of the state from the origin and the cost of the control input. The solution to the LQR problem is provided by the linear control law of the form [21],

$$u = -Kx \quad (2.92)$$

where,

$$K = R^{-1} B^T S \quad (2.93)$$

The S component is a positive definite symmetric matrix, given by

$$-\dot{S} = A^T S + S A - S B R^{-1} B^T S + Q \quad (2.94)$$

This equation known as the Riccati differential equation, which integrated backwards in time. The minimal cost function, representing the optimal cost, can be expressed as

$$\min \int_0^{t_f} (x^T Q x + u^T R u) dt + x^T(t_f) S(t_f) x(t_f) = x^T(0) S(0) x(0) \quad (2.95)$$

If the Riccati equation has a unique positive solution, then the optimum control problem can be solved. The LQR problem is significantly simplified with the condition of the time frame is infinite and the matrices are constant, in that circumstance S is a constant matrix provided by the steady-state solution of Eq. 2.94, which is

known as the algebraic Riccati equation as expressed below.

$$A^T S + SA - SBR^{-1}B^T S + Q = 0 \quad (2.96)$$

If the system is solvable, there exists a unique positive definite matrix S fulfilling Eq. 2.96 that turns the closed loop system stable. In choosing the value for the cost function weighting matrices Q and R , a particularly simple solution is by using diagonal weight as shown below.

$$Q = \begin{bmatrix} Q_1 & & 0 \\ & \ddots & \\ 0 & & Q_n \end{bmatrix} \quad R = \begin{bmatrix} R_1 & & 0 \\ & \ddots & \\ 0 & & R_n \end{bmatrix} \quad (2.97)$$

Moreover, the following conditions have to be considered in choosing the value of Q and R . The higher the weight matrices Q , the greater the gain feedback K value, which may allow a faster response system to reach an intermediate state cost function. The higher the weight matrices R , the lower the gain feedback (K) value, which might impede steady state (energy drive) [24].

CHAPTER 3

RESEARCH METHODOLOGY

3.1 Reserach Overview

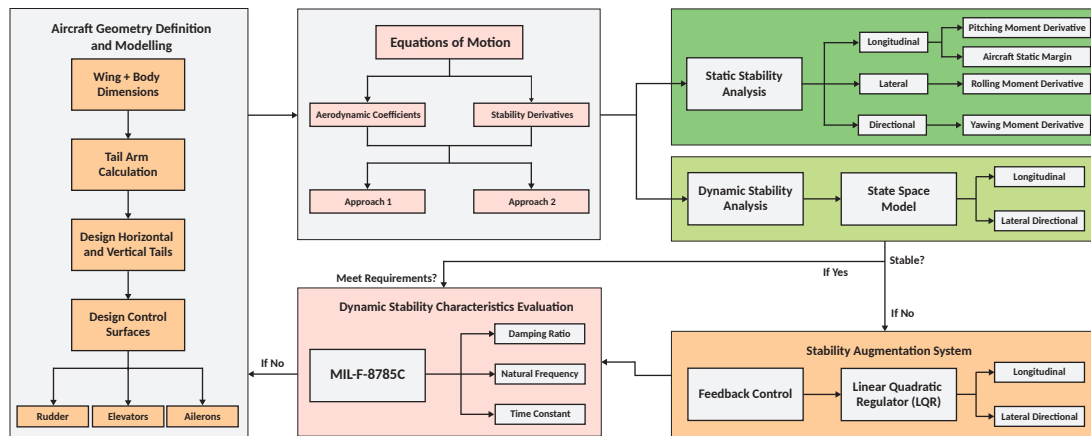


FIGURE 3.1: Research Methodology Flowchart

This thesis begins by defining and modeling the Baruna-1 geometry, starting from defining the wing and body dimensions definitions, tail arm calculation, horizontal and vertical tail design and control surfaces (elevators, rudder and ailerons) design as shown in Fig. 3.2.

The aerodynamic coefficients and stability and control derivatives are calculated using two approaches as shown in Fig. 3.3 for the aerodynamic coefficients and Fig. 3.4 for the stability and control derivatives:

1. Approach 1: Analytical method based on the Marcello's[16], Snorri's[19], Sadrey's[25], and Roskam's[17] methodologies.

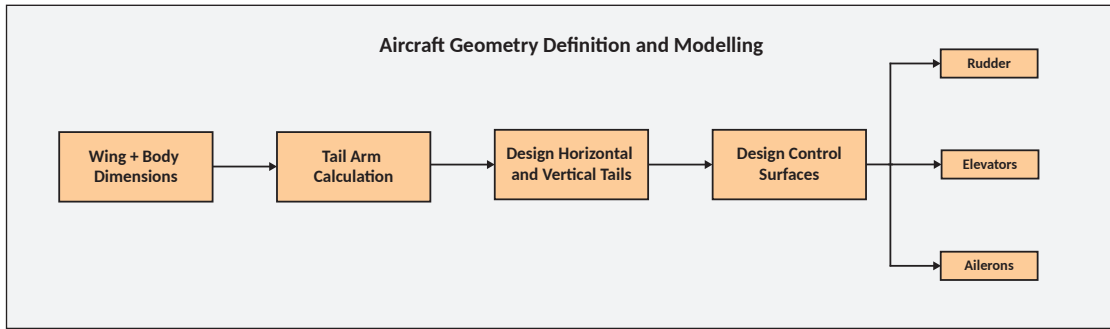


FIGURE 3.2: Tail and Control Surfaces Design Flowchart

2. Approach 2: The combination of the aerodynamic coefficients calculated using Approach 1 and the aerodynamic coefficients calculated using USAF Digital DATCOM. There are several aerodynamic coefficients that can't be calculated by USAF Digital DATCOM shown in Fig. 3.3 for the aerodynamic coefficients and Fig. 3.4 for the stability and control derivatives,

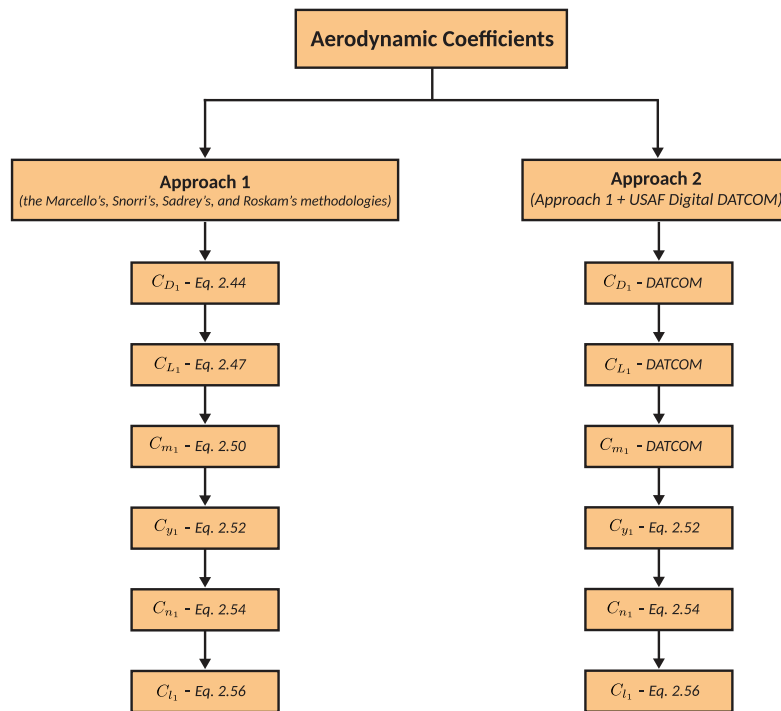


FIGURE 3.3: Aerodynamic Coefficients Flowchart

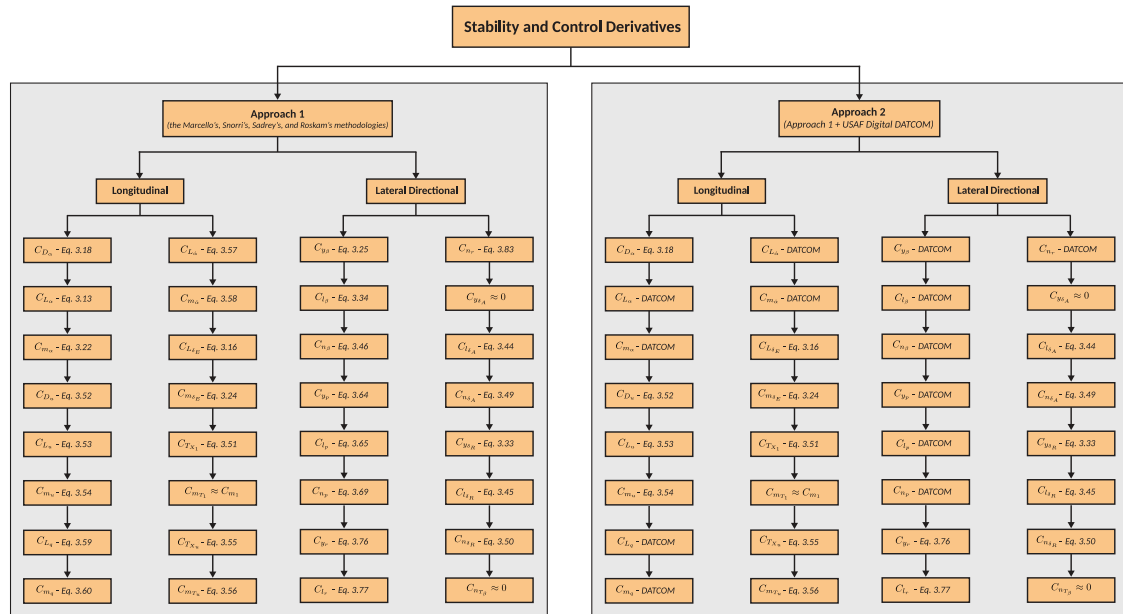


FIGURE 3.4: Stability and Control Derivatives Flowchart

The static stability of Baruna-1 in longitudinal, lateral and directional motions are analyzed based on pitching moment derivatives C_{m_α} , Static Margin SM , rolling moment derivatives C_{y_β} and yawing moment derivative C_{l_β} as shown in Fig. 3.5

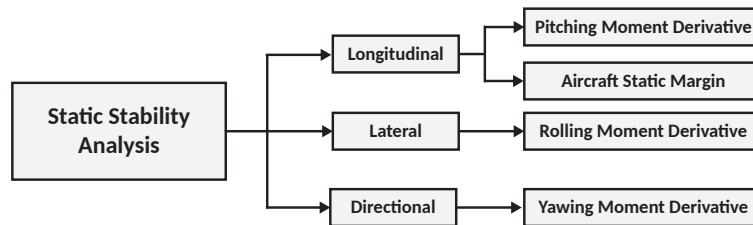


FIGURE 3.5: Static Stability Analysis Flowchart

The dynamic stability of Baruna-1 in longitudinal and lateral directional motions are analyzed using state space model. The state space model will leads to the characteristic equations and transfer functions. The transfer functions represent the dynamic behaviour of the aircraft in the time series. The characteristic equations are solved to achieve the eigenvalues. The eigenvalues of the aircraft in longitudinal and lateral directional motions describe the dynamic characteristic of the aircraft that corresponding to each mode as shown in Fig.3.6

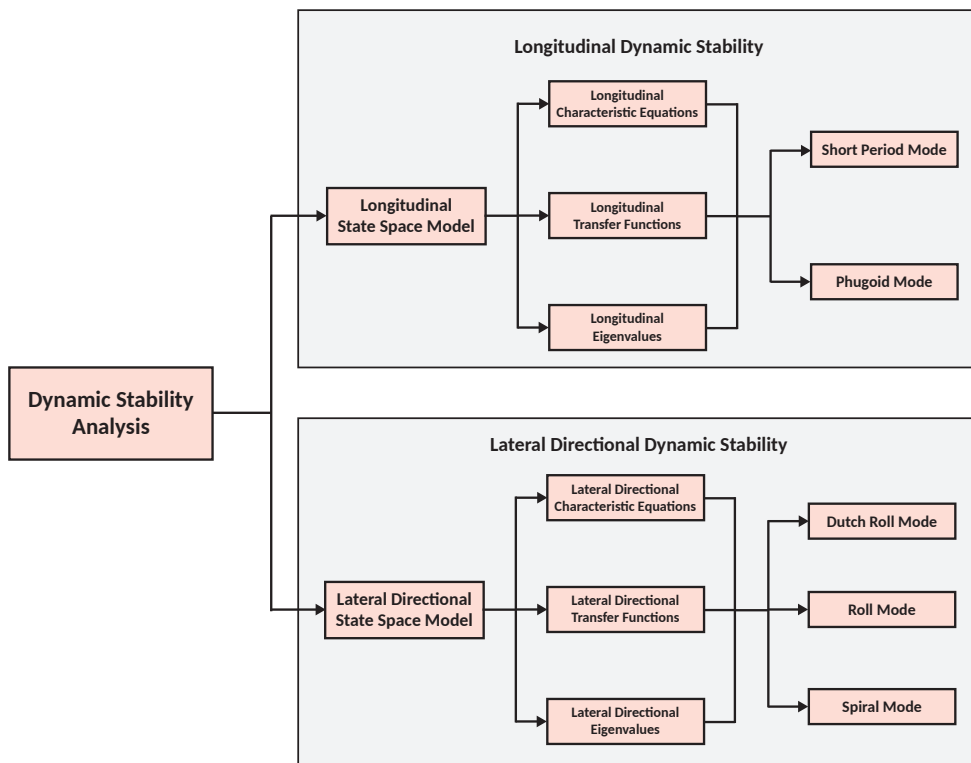


FIGURE 3.6: Dynamic Stability Analysis Flowchart

The stability augmentation system is necessary in order to improve or stabilize the aircraft if the aircraft isn't stable or the aircraft dynamic characteristics doesn't meet the flying and handling requirements. The linear quadratic regulator (LQR) control technique is used to achieve the optimum feedback control gains K for stability augmentation system as shown in Fig.3.7.

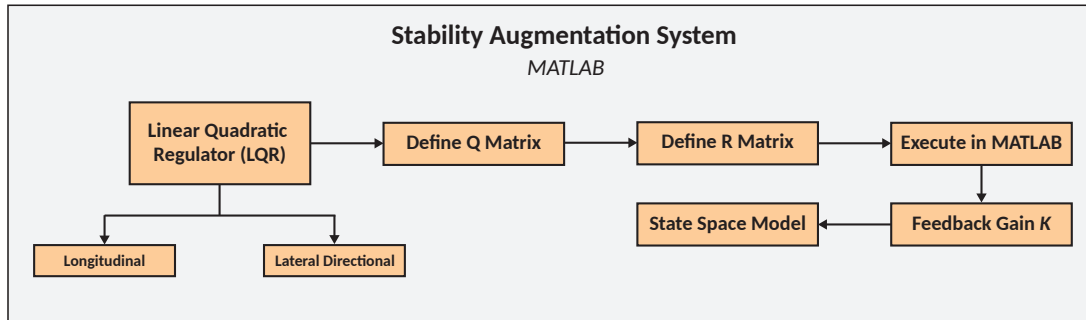


FIGURE 3.7: Stability Augmentation System Flowchart

The flying and handling quality evaluations will be based on the American Military Specification MIL-F-8785C. The damping ratio of short period and phugoid modes, the damping ratio and natural frequency of dutch roll mode, and the time constant of spiral and roll modes will be analyzed based on the requirement available in MIL-F-8785C.

3.2 Tails and Control Surfaces Design

3.2.1 Tail Arm Calculation

The tail arm is defined as the distance between the quarter chord of wing mean aerodynamic chord and the quarter chord of the horizontal and vertical tails, where this can be calculated by using the following relationship[19]:

$$l_T = \sqrt{\frac{2 \cdot S (V_{HT} \cdot \bar{c} + V_{VT} \cdot b)}{\pi (R_1 + R_2)}} \quad (3.1)$$

where,

- $S \triangleq$ Wing planform area;

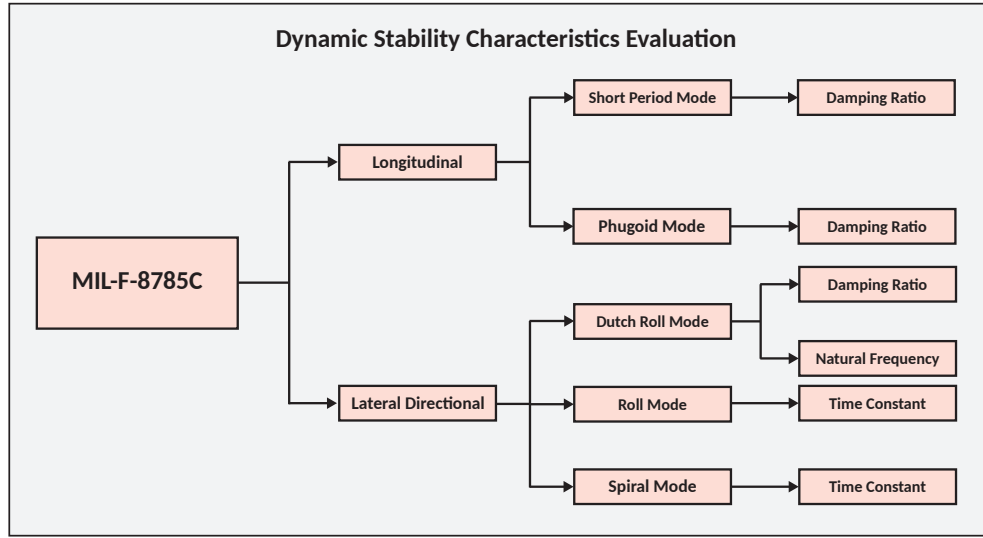


FIGURE 3.8: Dynamic Stability Characteristic Evaluations Flowchart

- $V_{HT} \triangleq$ Horizontal tail volume coefficient;
- $V_{VT} \triangleq$ Horizontal tail volume coefficient;
- $\bar{c} \triangleq$ Wing Mean Aerodynamic Chord;
- R_1 and $R_2 \triangleq$ The fuselage radius on the quarter chord of wing mean aerodynamic chord section and the quarter chord tail section as shown in Fig. 3.9

The horizontal and vertical tail volume coefficients are provided by Sadrey[25] shown in Tab. 3.1

3.2.2 Horizontal and Vertical Tail Design

The horizontal tail planform area S_{HT} can be calculated by using[19]:

$$S_{HT} = \frac{V_{HT} \cdot S \cdot \bar{c}}{l_T} \quad (3.2)$$

and the horizontal tail span b_{HT} and mean aerodynamic chord \bar{c}_{HT} can be calculated by using:

$$b_{HT} = \sqrt{AR_{HT} \times S_{HT}} \quad (3.3)$$

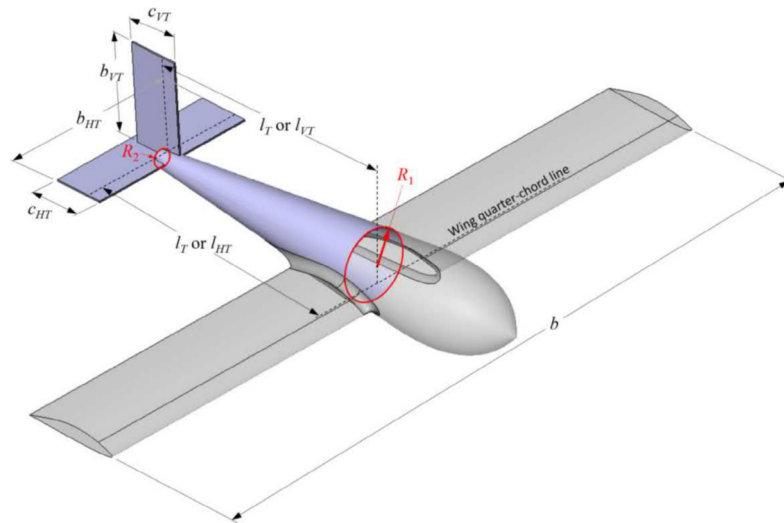


FIGURE 3.9: Fuselage Section Radius Definition for Tail Arm Calculation [19]

No.	Aircraft	Horizontal tail volume coefficient (\bar{V}_H)	Vertical tail volume coefficient (\bar{V}_V)
1	Glider and motor glider	0.6	0.03
2	Home-built	0.5	0.04
3	GA single prop-driven engine	0.7	0.04
4	GA twin prop-driven engine	0.8	0.07
5	GA with canard	0.6	0.05
6	Agricultural	0.5	0.04
7	Twin turboprop	0.9	0.08
8	Jet trainer	0.7	0.06
9	Fighter aircraft	0.4	0.07
10	Fighter (with canard)	0.1	0.06
11	Bomber/military transport	1	0.08
12	Jet transport	1.1	0.09

TABLE 3.1: Typical Value for Horizontal and Vertical Tail Volume Coefficients [25]

$$\vec{c}_{HT} = \frac{b_{HT}}{AR_{HT}} \quad (3.4)$$

The vertical tail planform area S_{VT} can be calculated by using[19]:

$$S_{VT} = \frac{V_{VT} \cdot S \cdot b}{l_T} \quad (3.5)$$

and the horizontal tail span b_{VT} and mean aerodynamic chord \vec{c}_{VT} can be calculated by using:

$$b_{VT} = \sqrt{AR_{VT} \times S_{VT}} \quad (3.6)$$

$$\vec{c}_{VT} = \frac{b_{VT}}{AR_{VT}} \quad (3.7)$$

3.2.3 Control Surfaces Design

According to Sadrey[25], the typical value for the aircraft control surfaces geometry are shown in Tab. 3.2 where the general relationship for the control surface area is

Control surface	Elevator	Aileron	Rudder
Control surface area/lifting surface area	$S_E/S_h = 0.15-0.4$	$S_A/S = 0.03-0.12$	$S_R/S_V = 0.15-0.35$
Control surface span/lifting surface span	$b_E/b_h = 0.8-1$	$b_A/b = 0.2-0.40$	$b_R/b_V = 0.7-1$
Control surface chord/lifting surface chord	$C_E/C_h = 0.2-0.4$	$C_A/C = 0.15-0.3$	$C_R/C_V = 0.15-0.4$
Control surface maximum deflection (negative)	-25 deg (up)	25 deg (up)	-30 deg (right)
Control surface maximum deflection (positive)	+20 deg (down)	20 deg (down)	+30 deg (left)

TABLE 3.2: Typical Value for Aircraft Control Surfaces [25]

given by

$$S_{CS} = b_{CS} \times \vec{c}_{CS} \quad (3.8)$$

where,

- $b_{CS} \triangleq$ Control surface span;

- $\vec{c}_{CS} \triangleq$ Control surface chord;

3.3 MATLAB

MATLAB is a programming and numerical computing platform from Mathworks, Inc. MATLAB has many build-in tools which provides more functionalities to the users. MATLAB has capabilities to data computational and analysis, mathematical computational, data simulation and visualization. Based on the features available on MATLAB, the Author is decided to use MATLAB as the main scientific computing. This will help the Author to calculate and analyze the stability of Baruna-1 accurately and less human error calculation and analysis.

In this thesis, MATLAB is used to calculate the stability and control derivatives, longitudinal and lateral directional dynamic calculation in form of state space model, the transfer functions, the eigenvalues, damping, natural frequency and time constant for the longitudinal and lateral directional state space model. The application of lqr method of Stability Augmentation System to obtain the optimum feedback control gain is conducted in MATLAB. The MATLAB scripts of Baruna-1 are provided in Appendix 5.3 for Approach 1 and Appendix 5.3 for Approach 2. The longitudinal and lateral directional dynamic calculation in form of state space model are described in the following sections.

3.4 Stability and Control Derivatives Calculation

3.4.1 Steady-State Lift Coefficient

The calculation of steady-state lift coefficient starts from:

1. Recall the general expression of steady state lift coefficient in Eq. 2.47, as shown below.

$$C_{L_1} = C_{L_0} + C_{L_\alpha} \alpha + C_{L_{\delta_E}} \delta_E$$

2. Calculate C_{L_0} using the following expression [19],

$$C_{L_0} = |\alpha_{C_L=0}| \cdot C_{L_{\alpha_{WB}}} \tag{3.9}$$

The zero lift angle of attack $\alpha_{C_L=0}$ is estimated using

$$|\alpha_{C_L=0}| = -\frac{C_{l_0}}{C_{l_{\alpha_W}}} \quad (3.10)$$

where, C_{l_0} is the wing airfoil lift coefficient at zero angle of attack; $C_{l_{\alpha_W}}$ is the wing airfoil lift curve slope. The wing fuselage lift curve slope $C_{L_{\alpha_{WB}}}$ can be approximated using the expression below,

$$C_{L_{\alpha_{WB}}} \approx K_{WB} C_{L_{\alpha_W}} \quad (3.11)$$

where,

$$K_{WB} = 1 + 0.025 \left(\frac{d}{b}\right) - 0.25 \left(\frac{d}{b}\right)^2$$

with the approximation of K_{WB} can be used only if $\left(\frac{d}{b}\right) > 4$. However, K_{WB} can be assumed as $K_{WB} \approx 1$. Furthermore, the wing lift curve slope $C_{L_{\alpha_W}}$ can be calculated using the following expression [25],

$$C_{L_{\alpha_W}} = \frac{C_{l_{\alpha_W}}}{1 + \frac{C_{l_{\alpha_W}}}{\pi AR_W e}} \quad (3.12)$$

3. Calculate $C_{L_{\alpha}}$ using the following expression.

$$C_{L_{\alpha}} = C_{L_{\alpha_{WB}}} + C_{L_{\alpha_H}} \eta_H \frac{S_H}{S} \left(1 - \frac{d\varepsilon}{d\alpha}\right) \quad (3.13)$$

The $C_{L_{\alpha_H}}$ is expressed using the similar approach as $C_{L_{\alpha_W}}$, which is given by

$$C_{L_{\alpha_H}} = \frac{C_{l_{\alpha_H}}}{1 + \frac{C_{l_{\alpha_H}}}{\pi AR_H}} \quad (3.14)$$

where,

- $C_{l_{\alpha_H}} \triangleq$ the horizontal tail airfoil lift curve slope.
- $AR_H \triangleq$ the horizontal tail aspect ratio.

The η_H is the dynamic pressure ratio at the horizontal tail, for T-Tail aircraft $\eta_H \approx 1$. S_H and S is the horizontal tail and wing planform area.

The downwash effect $\frac{d\varepsilon}{d\alpha}$ is calculated by using the following expression [19],

$$\frac{d\varepsilon}{d\alpha} = \frac{2C_{L\alpha W}}{\pi AR_W} \quad (3.15)$$

4. Calculate $C_{L\delta_E}$ using the following expression.

$$C_{L\delta_E} = \eta_H \frac{S_H}{S} C_{L\alpha_H} \tau_E \quad (3.16)$$

where, $\tau_E \triangleq$ the elevator effectiveness, can be approximated using the polynomial equation below [19].

$$\tau_E \approx -4.66r_e^4 + 8.79r_e^3 - 6.44r_e^2 + 2.85r_e + 0.0316 \quad (3.17)$$

where, the $r_e \triangleq$ the elevator area ratio $r_e = \frac{S_e}{S_H}$

3.4.2 Steady-State Drag Coefficient

The calculation of steady-state drag coefficient starts from:

1. Recall the general expression of stedy state drag coefficient in Eq. 2.44, as shown below.

$$C_{D_1} = C_{D_0} + C_{D_\alpha} \alpha + C_{D_{\delta_E}} \delta_E$$

2. Calculate C_{D_0} using CFD method.
3. Calculate C_{D_α} using the following expression.

$$C_{D_\alpha} \approx \left(\frac{2C_{L_1}}{\pi AR_e} \right) C_{L_\alpha} \quad (3.18)$$

4. $C_{D_{\delta_E}}$ is assumed to be negligible. $C_{D_{\delta_E}} \approx 0$.

3.4.3 Steady-State Pitching Moment Coefficient

The calculation of steady-state pitching moment coefficient starts from:

1. Recall the general expression of steady state pitching moment coefficient in Eq. 2.50, as shown below.

$$C_{m_1} = C_{m_0} + C_{m_\alpha} \alpha + C_{m_{\delta_E}} \delta_E$$

2. Calculate C_{m_0} using the following expression [19].

$$C_{m_0} = C_{m_{0W}} + C_{m_{0HT}} \quad (3.19)$$

where, the wing contribution $C_{m_{0W}}$ is calculated using,

$$C_{m_{0W}} = C_{m_{ACW}} + C_{L_{0W}} (\vec{x}_{CG} - \vec{x}_{ACWB}) \quad (3.20)$$

with $C_{m_{ACW}}$ is extracted from the airfoil data, when C_m at zero angle of attack.

The horizontal tail contribution is calculated using,

$$C_{m_{0HT}} = C_{m_{ACHT}} + C_{L_{0HT}} (\vec{x}_{ACH}) \quad (3.21)$$

3. Calculate C_{m_α} using the following expression.

$$C_{m_\alpha} = C_{L_{\alpha W}} (\vec{x}_{CG} - \vec{x}_{ACWB}) - C_{L_{\alpha H}} \left(1 - \frac{d\varepsilon}{d\alpha} \right) (\vec{x}_{ACH} - \vec{x}_{CG}) \quad (3.22)$$

where,

- $\vec{x}_{ACWB} \triangleq$ the location of the wing-body contribution aerodynamic center in accordance with the wing mean aerodynamic chord \vec{c} , can be calculated using the Torenbeek's methodology [26], given by

$$\left(\frac{X_{ac}}{\vec{c}} \right)_{WB} = \left(\frac{X_{ac}}{\vec{c}} \right)_w + \frac{\Delta_{f1} X_{ac}}{\vec{c}} + \frac{\Delta_{f2} X_{ac}}{\vec{c}} \quad (3.23)$$

where,

– $\frac{\Delta_{f1}X_{ac}}{\bar{c}}$ is calculated by

$$\frac{\Delta_{f1}X_{ac}}{\bar{c}} = -\frac{1.8}{C_{L\alpha_{WB}}} \frac{b_f h_f l_{fn}}{S\bar{c}}$$

where, $b_f \triangleq$ the fuselage width, h_f is the fuselage height, l_{fn} is the wing apex.

– $\frac{\Delta_{f2}X_{ac}}{\bar{c}}$ is calculated by

$$\frac{\Delta_{f2}X_{ac}}{\bar{c}} = \frac{0.273}{1 + \lambda} \frac{b_f c_g (b - b_f)}{(\bar{c})^2 (b + 2.15b_f)} \quad \text{for } \frac{b_f}{b} < 2$$

- $\vec{x}_{CG} \triangleq$ the location of the aircraft center of gravity in accordance with the wing mean aerodynamic chord \bar{c} .
- $\vec{x}_{AC_H} \triangleq$ the location of the horizontal tail aerodynamic center in accordance with the mean aerodynamic chord \bar{c} , refers to the Fig. 3.10

4. Calculate $C_{m\delta_E}$

$$C_{m\delta_E} = -C_{L\alpha_H} \eta_H \frac{S_H}{S} (\vec{x}_{AC_H} - \vec{x}_{CG}) \tau_E \quad (3.24)$$

3.4.4 Steady-State Lateral Force Coefficient

The calculation of steady-state lateral force coefficient starts from:

1. Recall the general expression of steady state lateral force coefficient in Eq. 2.52, as shown below.

$$C_{y1} = C_{y0} + C_{y\beta} \beta + C_{y\delta_A} \delta_A + C_{y\delta_R} \delta_R$$

2. C_{y0} is zero at initial condition,

$$C_{y0} = c_Y|_{\beta=\delta_A=\delta_R=0^\circ} = 0$$

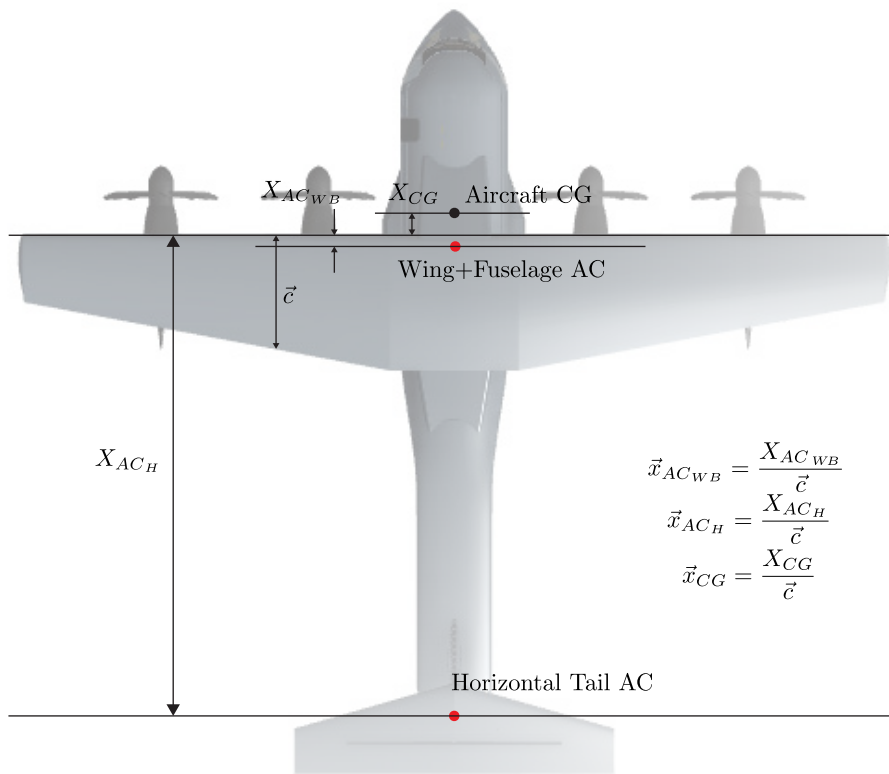


FIGURE 3.10: The Location of Aircraft Aerodynamic Center and Center of Gravity (Reproduced from [16])

3. Calculate C_{y_β} using the following expression.

$$C_{y_\beta} = C_{y_{\beta_W}} + C_{y_{\beta_H}} + C_{y_{\beta_V}} + C_{y_{\beta_{FUS}}} \quad (3.25)$$

where,

- The wing contribution $C_{y_{\beta_W}}$ is expressed by

$$C_{y_{\beta_W}} \approx -0.00573 |\Gamma_{W_{deg}}| + \text{sgn}(\beta) \frac{C_{L1}^2}{30} \frac{\tan \Lambda_{c/4} \sin \Lambda_{c/4}}{AR (AR + 4 \cos \Lambda_{c/4})} \quad (3.26)$$

where,

- $\Gamma_{W_{deg}} \triangleq$ the wing dihedral angle in degrees and $\text{sgn}()$ is the sign function.
- $\tan \Lambda_x = \tan \Lambda_{LE} - \frac{4x(1-\lambda)}{AR(1+\lambda)}$, where $x = [0-1]$, 0 at leading edge and 1 at trailing edge.

- The horizontal tail contribution $C_{y_{\beta_H}}$ is expressed by

$$C_{y_{\beta_H}} \approx -0.00573 |\Gamma_{H_{deg}}| \eta_H \left(1 + \frac{\partial \sigma}{\partial \beta} \right) \frac{S_H}{S} \quad (3.27)$$

where, $\Gamma_{H_{deg}}$ is the horizontal tail dihedral angle in degrees and the sidewash contribution by the horizontal tail is expressed by

$$\eta_H \left(1 + \frac{\partial \sigma}{\partial \beta} \right) = 0.724 + 3.06 \frac{S_H/S}{1 + \cos \Lambda_{c/4}} + 0.4 \frac{Z_W}{d_{FUS}} \quad (3.28)$$

where $Z_W \triangleq$ the vertical distance from fuselage centerline to 25% of the wing root[16].

- The vertical tail contribution $C_{y_{\beta_V}}$ is expressed by

$$C_{y_{\beta_V}} \approx -K_{Y_V} |C_{L_{\alpha_V}}| \eta_V \left(1 + \frac{\partial \sigma}{\partial \beta} \right) \frac{S_V}{S} \quad (3.29)$$

where, K_{Y_V} is given by

$$K_{Y_V} = \begin{cases} 0.76 & \text{if } b_V/2r_1 < 2 \\ 0.4 + 0.16(b_V/2r_1) & \text{if } 2 \leq b_V/2r_1 \leq 3.5 \\ 1 & \text{if } b_V/2r_1 \geq 3.5 \end{cases} \quad (3.30)$$

and the sidewash contribution by the vertical tail is expressed by

$$\eta_V \left(1 + \frac{\partial \sigma}{\partial \beta} \right) = 0.724 + 3.06 \frac{S_V/S}{1 + \cos \Lambda_{c/4}} + 0.4 \frac{Z_W}{d_{FUS}} + 0.009 A R_W \quad (3.31)$$

- The fuselage contribution $C_{y\beta_{FUS}}$ is expressed by

$$C_{y\beta_{FUS}} \approx -2 \cdot K_i \frac{S_{P \rightarrow V}}{S} \quad (3.32)$$

where, K_i can be approximated using Fig. 3.11 and $S_{P \rightarrow V}$ is the cross section at the location of the fuselage X_0

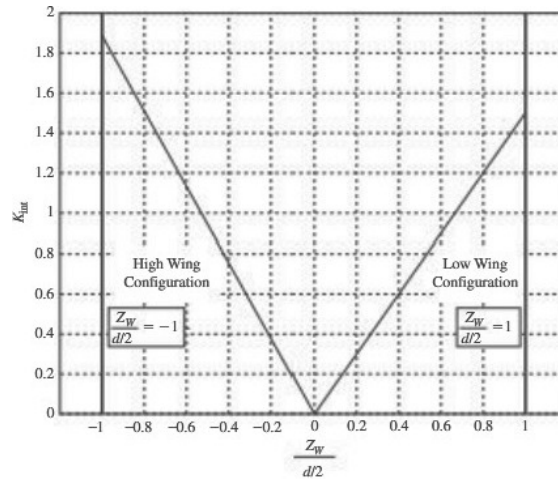


FIGURE 3.11: Wing Body Interference Factor [16]

4. Calculate $C_{y\delta_A}$ can be neglected $C_{y\delta_A} \approx 0$ due to the asymmetric deflections of the left and right ailerons act along the vertical and horizontal tail directions [16].

5. Calculate $C_{y\delta_R}$ using the following expression.

$$C_{y\delta_R} = |C_{L\alpha_V}| \eta_V \frac{S_V}{S} \Delta(K_R) \tau_R \quad (3.33)$$

where, $\tau_R \triangleq$ rudder effectiveness factor, is found using Fig. 3.12 and K_R is a correction factor associated with the rudder span within the vertical tail span, and calculated using Fig. 2.11.

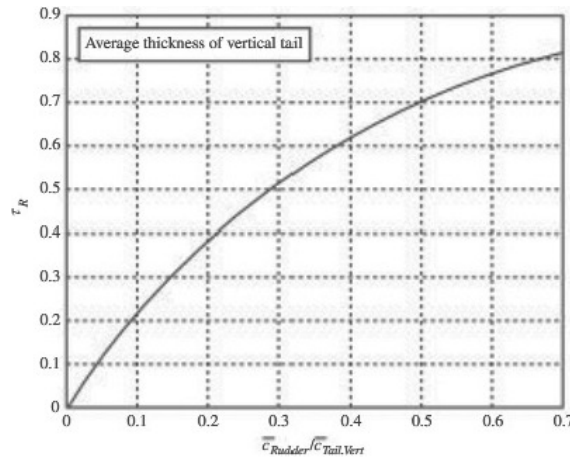


FIGURE 3.12: Rudder Effectiveness τ_R as a result of $\bar{c}_{rudder}/\bar{c}_{vtail}$ [16]

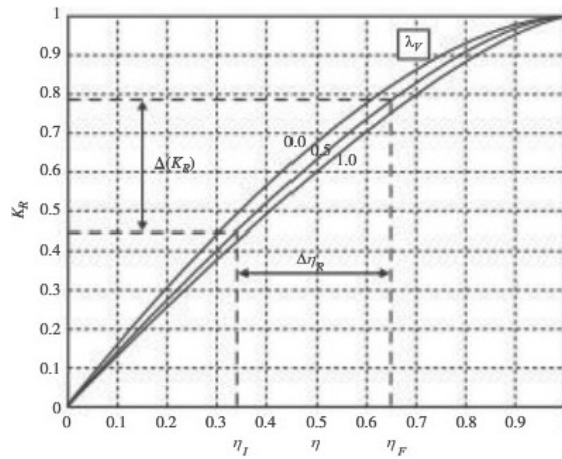


FIGURE 3.13: Span Factor between Rudder and Vertical Tail [16]

3.4.5 Steady-State Rolling Moment Coefficient

The calculation of steady-state rolling moment coefficient starts from:

1. Recall the general expression of steady state rolling moment coefficient in Eq. 2.54, as shown below.

$$C_{l_1} = C_{l_0} + C_{l_\beta}\beta + C_{l_{\delta_A}}\delta_A + C_{l_{\delta_R}}\delta_R$$

2. C_{l_0} is zero at initial condition,

$$C_{l_0} = c_Y|_{\beta=\delta_A=\delta_R=0^\circ} = 0$$

3. Calculate C_{l_β} using the following expression.

$$C_{l_\beta} = C_{l_{\beta_W}} + C_{l_{\beta_H}} + C_{l_{\beta_V}} \quad (3.34)$$

where, $C_{l_{\beta_W}}$ is consist of several contributions from each components of the wing, it is expressed by

$$C_{l_{\beta_W}} = C_{L_1} \left(\left(\frac{C_{l_\beta}}{C_l} \right)_{\Lambda_{c/2}} K_{M_\Lambda} + \left(\frac{C_{l_\beta}}{C_l} \right)_{AR} \right) + \Gamma \left(\frac{C_{l_\beta}}{\Gamma} K_{M_\Gamma} \right) + \varepsilon_W \tan \Lambda_{\Lambda_{c/4}} \left(\frac{\Delta C_{L_\beta}}{\varepsilon_W \tan \Lambda_{\Lambda_{c/4}}} \right) \quad (3.35)$$

where,

- $\left(\frac{C_{l_\beta}}{C_l} \right)_{\Lambda_{c/2}}$ is calculated using the polynomial equation shown below (valid for $AR = 8, \lambda = 0.5$).

$$C_{l_{\beta_{\Lambda_{c/2}}}} = -2.8639 \times 10^{-8} \Lambda_{c/2}^3 + 5.7675 \times 10^{-7} \Lambda_{c/2}^2 - 7.4987 \times 10^{-5} \Lambda_{c/2} - 8.2421 \times 10^{-5}$$

- K_{M_Λ} is calculated using the polynomial equation shown below (valid for $AR = 8, \lambda = 0.5$).

$$K_{M_\Lambda} = 0.7766 + 1.3372x - 2.3077x^2 + 2.0271x^3$$

where, $x = M_{infly} \cos \Lambda_{c/2}$

- $\left(\frac{C_{l_\beta}}{C_l}\right)_{AR}$ is calculated using the polynomial equation shown below (for $\lambda = 0.5$).

$$\left(\frac{C_{l_\beta}}{C_l}\right)_{AR} = -\frac{0.009804}{AR} + \frac{0.001}{AR^{0.005}}$$

- $\frac{C_{l_\beta}}{\Gamma}$ is calculated using the polynomial equation shown below (valid for $AR \leq 8, \lambda = 0.5$).

$$\frac{C_{l_\beta}}{\Gamma} = (-2.786 - 50.46AR + 2.653AR^2) \times 10^{-6} \quad \text{if } \Lambda_{c/2} = 0$$

$$\frac{C_{l_\beta}}{\Gamma} = (-2.706 - 47.47AR + 4.618AR^2) \times 10^{-6} \quad \text{if } \Lambda_{c/2} = \pm 40$$

- K_{M_Γ} is calculated using the polynomial equation shown below (valid for $AR = 8, \lambda = 0.5$).

$$K_{M_\Gamma} = 1 + (-0.1969x + 1.6231x^2 - 2.8513x^3 + 2.1992x^4) \times (0.1193AR - 0.1961)$$

- $\frac{\Delta C_{L_\beta}}{\varepsilon_W \tan \Lambda_{c/4}}$ is approximated using Fig. 3.14 [16]

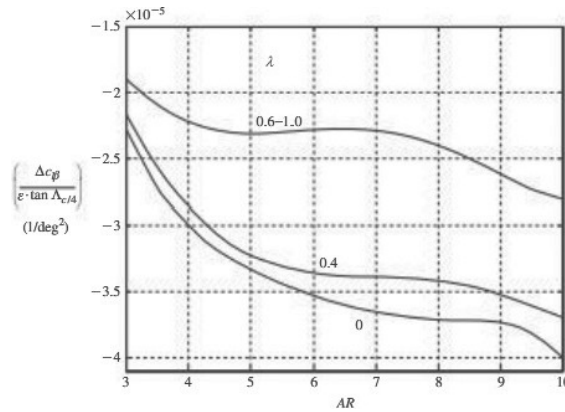


FIGURE 3.14: Contribution to $c_{l_{\beta WB}}$ due to Wing Twist Angle [16]

The horizontal tail contribution $C_{l_{\beta H}}$ for most aircraft can be neglected
 $C_{l_{\beta H}} \approx 0$.

The vertical tail contribution $C_{l_{\beta V}}$ is calculated using the following expression 3.36 [16].

$$C_{l_{\beta V}} = C_{y_{\beta V}} \frac{Z_V \cos \alpha_1 - X_V \sin \alpha_1}{b} \quad (3.36)$$

where, the understanding of Z_V and X_V are shown in Fig. 3.15.

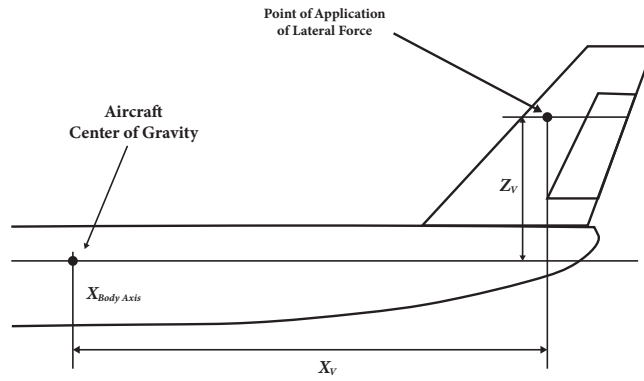


FIGURE 3.15: Identification of the Vertical Tail Z_V and X_V (Reproduced from [16])

4. The expression for the rolling moment due to the aileron deflections $C_{l_{\delta_A}}$ is conducted into five steps, starting from:
 - (a) The in-board and out-board locations of the left and right ailerons y_{AI} and y_{AO} as fraction of the semi-wing span $b/2$ determination as shown in Fig. 3.16

$$\eta_I = \frac{y_{AI}}{b/2}, \quad \eta_O = \frac{y_{AO}}{b/2} \quad (3.37)$$

- (b) Using η_I, η_O find the ΔRME parameter based on Fig. 3.17 for taper ratio $\lambda = 0.5$. RME is a function of the parameter:

$$\Lambda_\beta = \tan^{-1} \left(\frac{\tan \Lambda_{c/4}}{\beta} \right) = \tan^{-1} \left(\frac{\tan \Lambda_{c/4}}{\sqrt{1 - Mach^2}} \right) \quad (3.38)$$

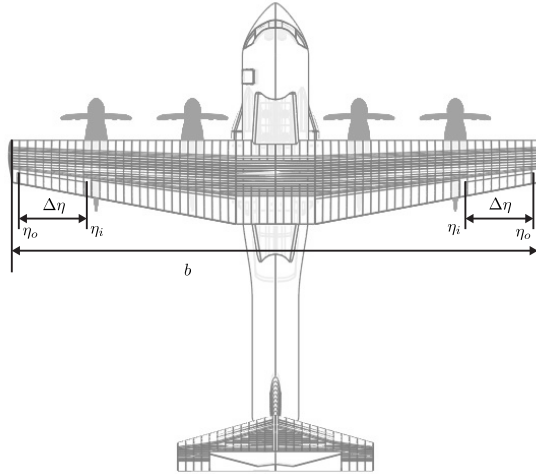


FIGURE 3.16: Location of the Ailerons along the Wing Span (Reproduced from [16])

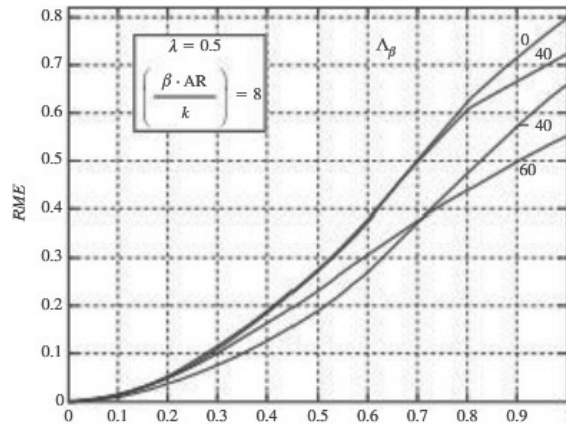


FIGURE 3.17: Rolling Moment Effectiveness for $AR = 8$ and $\lambda = 0.5$ [16]

The plots in Fig. 2.14 are given for different values of $\beta \cdot AR/k$, where k is given by

$$k = \frac{(C_{L\alpha})_{W|Mach} \cdot \beta}{2\pi} \quad (3.39)$$

By definition, RME is given by

$$RME = \frac{C_{l\delta} \cdot \beta}{k} \quad (3.40)$$

Based on Fig. 2.14, the calculation of $\Delta(RME)$ is given by

$$\Delta(RME) = RME|_{\eta_O} - RME|_{\eta_I} \quad (3.41)$$

- (c) Based on the value of $\Delta(RME)$ in Step 2, $C'_{l\delta}$ is relative to two full chord sections of the wing being deflected asymmetrically and given by

$$C'_{l\delta} = \frac{\Delta(RME) \cdot k}{\beta} \quad (3.42)$$

- (d) Consider only a chord section is deflected, $C_{l\delta}$ is calculated using

$$C_{l\delta} = \tau_A \cdot C'_{l\delta} \quad (3.43)$$

- (e) The influence of the asymmetric nature of the ailerons deflections is accounted by considering $C_{l\delta_{R,L}}$ as 50% of the previous calculated $C_{l\delta}$ value, leads to the expression for $C_{l\delta_A}$.

$$C_{l\delta_A} = \frac{1}{2} \left((C_{l\delta})|_{Left} + (C_{l\delta})|_{Right} \right) \quad (3.44)$$

5. Calculate $C_{l\delta_R}$ using the following expression.

$$C_{l\delta_R} = C_{y\delta_R} \left(\frac{Z_R \cos \alpha_1 - X_R \sin \alpha_1}{b} \right) \quad (3.45)$$

where, Z_R and X_R are identified using Fig. 3.18.

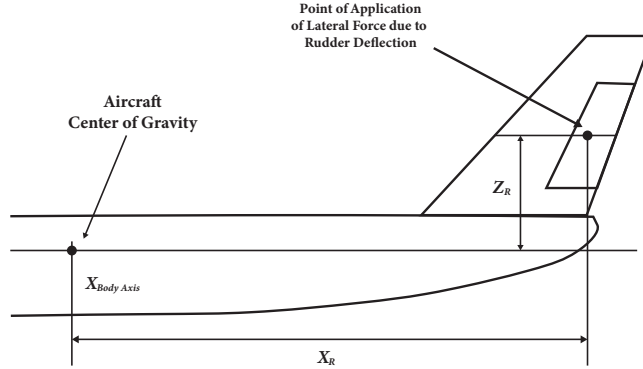


FIGURE 3.18: Identification of the Rudder Z_R and X_R (Reproduced from [16])

3.4.6 Steady-State Yawing Moment Coefficient

The calculation of steady-state yawing moment coefficient starts from:

1. Recall the general expression of steady state yawing moment coefficient in Eq. 2.56, as shown below.

$$C_{n_1} = C_{n_0} + C_{n_\beta} \beta + C_{n_{\delta_A}} \delta_A + C_{n_{\delta_R}} \delta_R$$

2. C_{y_0} is zero at initial condition,

$$C_{n_0} = c_n|_{\beta=\delta_A=\delta_R=0^\circ} = 0$$

3. Calculate C_{n_β} using the following expression.

$$C_{n_\beta} = C_{n_{\beta_W}} + C_{n_{\beta_B}} + C_{n_{\beta_H}} + C_{n_{\beta_V}} \quad (3.46)$$

The contribution of the wing $C_{n_{\beta_W}}$ is negligible for any aircraft configurations $C_{n_{\beta_W}} \approx 0$ and the horizontal tail contribution also consider to be negligible $C_{n_{\beta_H}} \approx 0$

The body contribution $C_{n_{\beta_B}}$ is calculated using the following expression.

$$C_{n_{\beta_B}} = -57.3 \cdot K_N K_{R_l} \frac{S_{B_S} l_B}{S b} \quad (3.47)$$

where,

- S_{B_S} and l_B are defined in Fig. 3.19
- K_N is an empirical factor related to the geometric coefficient of the axial cross section of the fuselage, estimated through Fig. 3.20
- K_{R_l} is a factor related to Reynolds number, estimated through Fig. 3.21

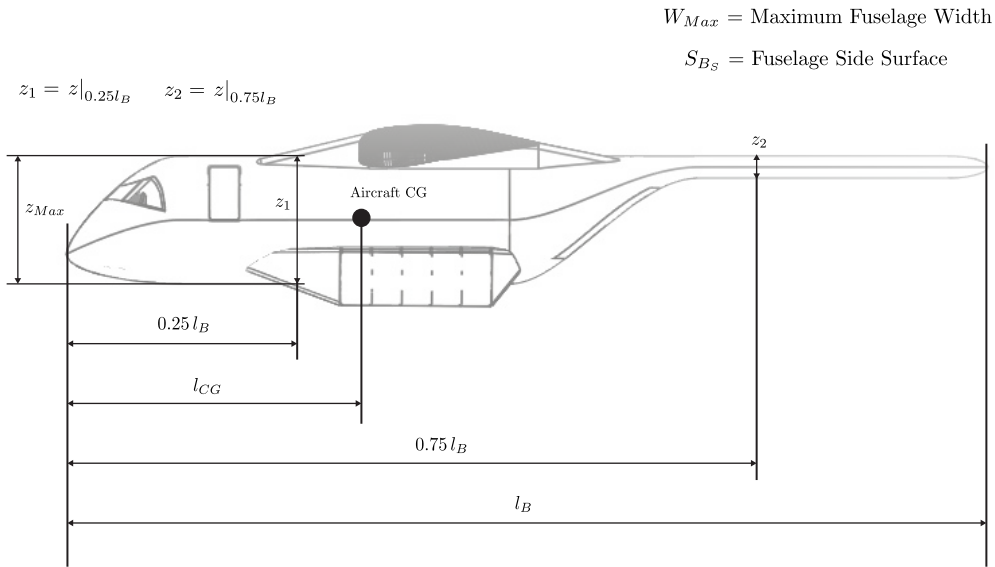


FIGURE 3.19: Geometric Parameter of the XZ Cross Section of the Fuselage (Reproduced from [16])

The vertical tail contribution $C_{n_{\beta_V}}$ is significant in preliminary analysis, meaning that $C_{n_{\beta}}$ can be approximated equals to $C_{n_{\beta_V}}$, with the expression

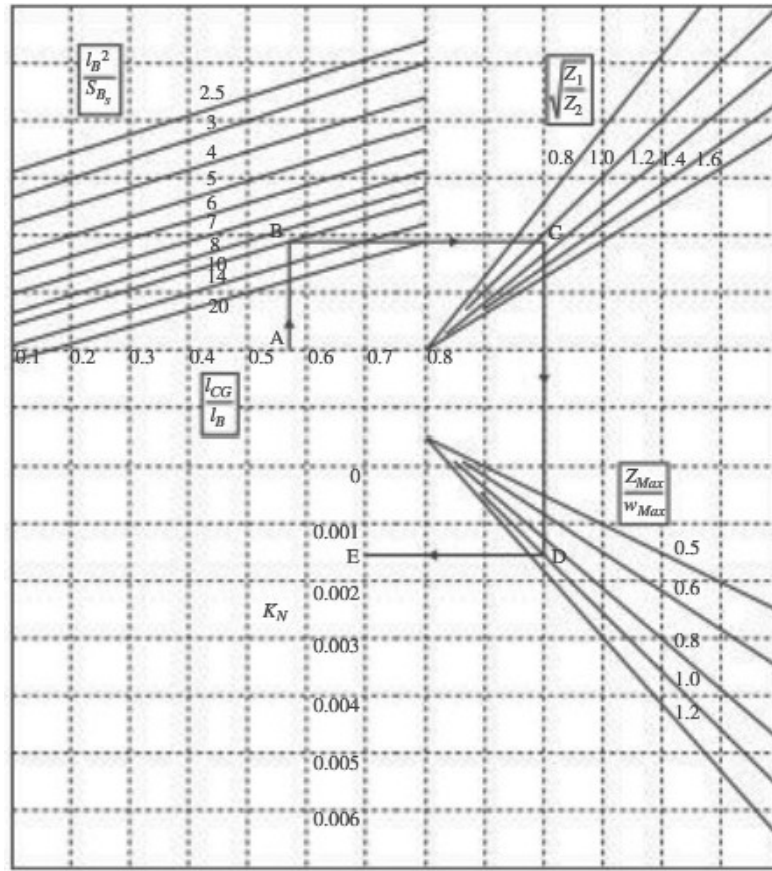


FIGURE 3.20: Empirical Factor K_N for Wing-Body Interface [16]

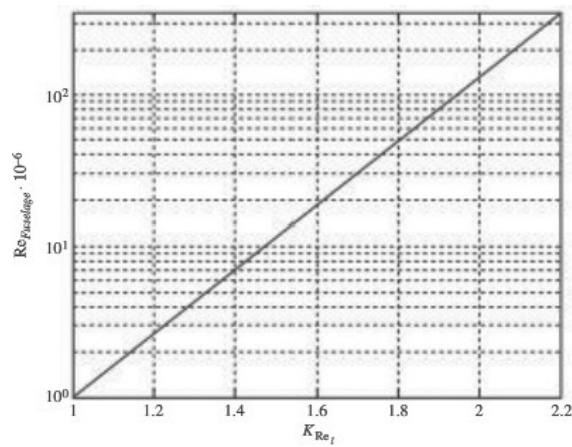


FIGURE 3.21: Effect of Reynolds Number on Wing-Body Interface [16]

is given by

$$C_{n_{\beta_V}} = -C_{y_{\beta_V}} \frac{(X_V \cos \alpha_1 + Z_V \sin \alpha_1)}{b} \quad (3.48)$$

4. Calculate $C_{n_{\delta_A}}$ using the following expression.

$$C_{n_{\delta_A}} = \Delta(K_{n_A}) C_{L_1} C_{l_{\delta_A}} \quad (3.49)$$

where, $\Delta(K_{n_A})$ is defined as the difference between the value of K_{n_A} associated with $\eta_I = \frac{y_{A_I}}{b/2}$, $\eta_O = \frac{y_{A_O}}{b/2}$ and calculated using Fig. 3.22

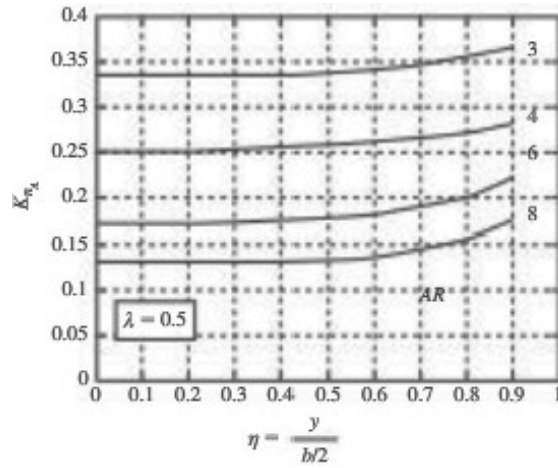


FIGURE 3.22: Yawing Moment Correlation Coefficient due to Aileron Deflections [16]

5. Calculate $C_{n_{\delta_R}}$ using the following expression.

$$C_{n_{\delta_R}} = -C_{y_{\delta_R}} \left(\frac{X_R \cos \alpha_1 + Z_R \sin \alpha_1}{b} \right) \quad (3.50)$$

3.4.7 Steady-State Thrust Coefficient

The calculation of steady-state thrust coefficient is given by

$$C_{T_{X_1}} = C_{D_1} \quad (3.51)$$

where, $C_{T_{X_1}}$ is the coefficient opposing C_{D_1} to ensure $T = D$ equilibrium.

3.4.8 Speed Derivatives

The calculation of speed derivatives starts from:

- Calculate C_{D_u} using the following expression.

$$C_{D_u} = Mach \cdot \frac{\partial C_D}{\partial Mach} \quad (3.52)$$

where, $C_{D_u} \triangleq$ the change in drag for small, positive increment in forward speed.

- Calculate C_{L_u} using the following expression.

$$C_{L_u} = \left(\frac{Mach^2}{1 - Mach^2} \right) \cdot C_{L_1} \quad (3.53)$$

where, $C_{L_u} \triangleq$ the change in lift for small, positive increment in forward speed.

- Calculate C_{m_u} using the following expression.

$$C_{m_u} = -C_{L_1} \frac{\partial \vec{X}_{ACWB}}{\partial Mach} \quad (3.54)$$

where, $C_{m_u} \triangleq$ the change in pitching moment for small, positive increment in forward speed.

- Calculate $C_{T_{X_U}}$ using the following expression for variable pitch propeller.

$$C_{T_{X_U}} = -3C_{T_{X_1}} \quad (3.55)$$

where, $C_{T_{X_U}} \triangleq$ the thrust variation coefficient along X_S with small variations in the linear speed in forward direction.

- Calculate $C_{m_{T_u}}$ using the following expression.

$$C_{m_{T_u}} = \left(\frac{dT}{\vec{c}} \right) C_{T_{X_U}} \quad (3.56)$$

where, $d_T \triangleq$ the thrust moment arm in accordance with aircraft center of gravity.

3.4.9 Rate of Angle of Attack Derivatives

The calculation of rate of angle of attack derivatives starts from:

1. At subsonic conditions, $C_{D_{\dot{\alpha}}} \approx 0$
2. Calculate $C_{L_{\dot{\alpha}}}$ using the following expression.

$$C_{L_{\dot{\alpha}}} \approx 2C_{L_{\alpha_H}} \eta_H \frac{S_H}{S} (\vec{X}_{AC_H} - \vec{X}_{CG}) \frac{d\varepsilon}{d\alpha} \quad (3.57)$$

3. Calculate $C_{m_{\dot{\alpha}}}$ using the following expression.

$$C_{m_{\dot{\alpha}_H}} \approx 2C_{L_{\alpha_H}} \eta_H \frac{S_H}{S} (\vec{X}_{AC_H} - \vec{X}_{CG})^2 \frac{d\varepsilon}{d\alpha} \quad (3.58)$$

3.4.10 Pitch Rate Derivatives

The calculation of pitch rate derivatives starts from:

1. At subsonic conditions, $C_{D_q} \approx 0$
2. Calculate C_{L_q} using the following expression.

$$C_{L_q} \approx \left(\frac{AR + 2 \cos \Lambda_{c/4}}{AR \cdot (\sqrt{1 - Mach^2 (\cos \Lambda_{c/4})^2}) + 2 \cos \Lambda_{c/4}} \right) \cdot \left(\frac{1}{2} + 2 \cdot |\vec{x}_{AC_W} - \vec{x}_{CG}| \right) C_{L_{\alpha_W}}|_{Mach=0} + 2C_{L_{\alpha_H}} \eta_H \frac{S_H}{S} (\vec{X}_{AC_H} - \vec{X}_{CG}) \quad (3.59)$$

3. Calculate C_{m_q} using the following expression.

$$C_{m_q} = C_{m_{q_W}} + C_{m_{q_H}} \quad (3.60)$$

The wing contribution $C_{m_{qW}}$ is calculated using

$$m_{qW} = \left(\frac{\left(\frac{AR^3 + \tan^2 \Lambda_{c/4}}{AR \cdot B + 6 \cos \Lambda_{c/4}} \right) + \frac{3}{B}}{\left(\frac{AR^3 + \tan^2 \Lambda_{c/4}}{AR + 6 \cos \Lambda_{c/4}} \right) + 3} \right) \cdot C_{m_{qW}} \Big|_{Mach=0} \quad (3.61)$$

where,

$$B = \sqrt{1 - Mach^2 (\cos \Lambda_{c/4})^2}$$

$$C_{m_{qW}} \Big|_{Mach=0} = -K_q C_{L\alpha W} \Big|_{Mach=0} \cos \Lambda_{c/4} \cdot C$$

$$C = \left(\frac{AR (0.5 |\vec{x}_{ACW} - \vec{x}_{CG}| + 2 |\vec{x}_{ACW} - \vec{x}_{CG}|^2)}{AR + 2 \cos \Lambda_{c/4}} \right) + \frac{1}{24} \left(\frac{AR^3 + \tan^2 \Lambda_{c/4}}{AR + 6 \cos \Lambda_{c/4}} \right) + \frac{1}{8} \quad (3.62)$$

with K_q is evaluated using Fig. 3.23

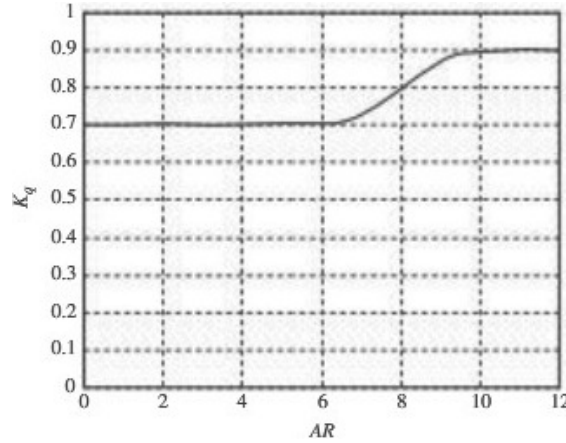


FIGURE 3.23: K_q Correction Coefficient [16]

The horizontal tail contribution $C_{m_{qH}}$ is calculated using

$$C_{m_{qH}} \approx -2C_{L\alpha H} \eta_H \frac{S_H}{S} (\vec{X}_{AC_H} - \vec{X}_{CG})^2 \quad (3.63)$$

3.4.11 Roll Rate Derivatives

The calculation of roll rate derivatives starts from:

1. Calculate C_{y_p} using the following expression.

$$C_{y_p} \approx C_{y_{\beta V}} \frac{(Z_V \cos \alpha_1 - X_V \sin \alpha_1)}{b} \quad (3.64)$$

where, $C_{y_p} \triangleq$ contribution of the roll rate to the lateral force with the vertical tail only is contributed,

$$C_{y_p} \approx C_{y_{pV}}$$

2. Calculate C_{l_p} using the following expression.

$$C_{l_p} = C_{l_{pWB}} + C_{l_{pH}} + C_{l_{pV}} \quad (3.65)$$

- The wing body contribution $C_{l_{pWB}}$ is calculated by

$$C_{l_{pWB}} = RDP \cdot \frac{k}{\beta} \quad (3.66)$$

with RDP is the rolling damping parameter, evaluated using Fig. 3.24

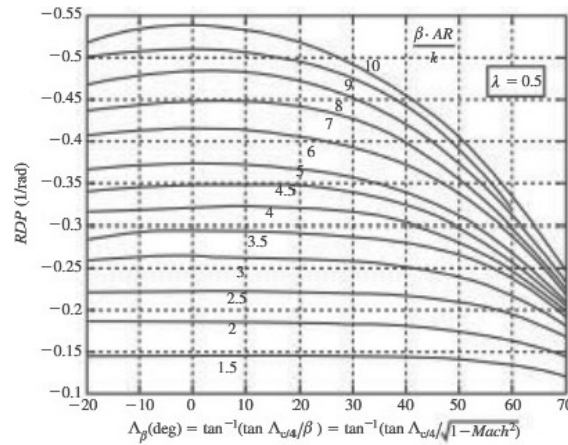


FIGURE 3.24: Rolling Damping Parameters for $\lambda = 0.5$ [16]

- The horizontal tail contribution $C_{l_{pH}}$ is calculated by

$$C_{l_{pH}} = \frac{1}{2} (C_{l_{pW}})|_H \frac{S_H}{S} \left(\frac{b_H}{b} \right)^2 \quad (3.67)$$

with

$$(C_{l_{pW}})|_H \approx C_{l_{pW}}$$

However, the horizontal contribution is often negligible due to the low numerical value of the product of $\frac{S_H}{S} \cdot \left(\frac{b_H}{b}\right)^2$

- The vertical tail contribution $C_{l_{pV}}$ is calculated by

$$C_{l_{pV}} \approx 2C_{y_{\beta V}} \left(\frac{Z_V}{b}\right)^2 \quad (3.68)$$

3. Calculate C_{n_p} using the following expression.

$$C_{n_p} = C_{n_{pWB}} + C_{n_{pH}} + C_{n_{pV}} \quad (3.69)$$

where, $C_{n_p} \triangleq$ the contribution to the yawing moment due to the roll rate.

However, the contribution of the fuselage and horizontal tail is not considerable to the C_{n_p} , leads to

$$C_{n_p} = C_{n_{pW}} + C_{n_{pV}} \quad (3.70)$$

where,

- The wing contribution $C_{n_{pW}}$ is calculated using

$$C_{n_{pW}} = -C_{l_{pW}} \tan(\alpha_1) + C_{l_p} \tan(\alpha_1) + \left(\frac{C_{n_p}}{C_{L_1}}\right) \Big|_{\substack{Mach \\ c_L=0}} C_{L_1} + \left(\frac{\Delta C_{n_p}}{\varepsilon_W}\right) \varepsilon_W \quad (3.71)$$

Where, the coefficient $\left(\frac{C_{n_p}}{C_{L_1}}\right) \Big|_{\substack{Mach \\ c_L=0}}$ is calculated using

$$\left(\frac{C_{n_p}}{C_{L_1}}\right) \Big|_{\substack{Mach \\ c_L=0}} = C \left(\frac{C_{n_p}}{C_{L_1}}\right) \Big|_{\substack{Mach=0 \\ c_L=0}} \quad (3.72)$$

where,

$$\left(\frac{C_{n_p}}{C_{L_1}}\right)\bigg|_{\substack{Mach=0 \\ C_L=0}} = -\frac{1}{6} \cdot \frac{AR + 6(AR + \cos(\Lambda_{c/4})) \cdot \left((\bar{x}_{CG} - \bar{x}_{AC}) \frac{\tan(\Lambda_{c/4})}{AR} + \frac{\tan^2(\Lambda_{c/4})}{12} \right)}{(AR + \cos(\Lambda_{c/4}))} \quad (3.73)$$

$$C = \frac{(AR + 4 \cos(\Lambda_{c/4}))}{(AR \cdot B + 4 \cos(\Lambda_{c/4}))} \cdot \left(\frac{AR \cdot B + \frac{1}{2}(AR \cdot B + 4 \cos(\Lambda_{c/4})) \tan^2(\Lambda_{c/4})}{AR + \frac{1}{2}(AR + 4 \cos(\Lambda_{c/4})) \tan^2(\Lambda_{c/4})} \right) \quad (3.74)$$

and $\left(\frac{\Delta C_{n_p}}{\varepsilon_W}\right)$ is evaluated using Fig. 3.25

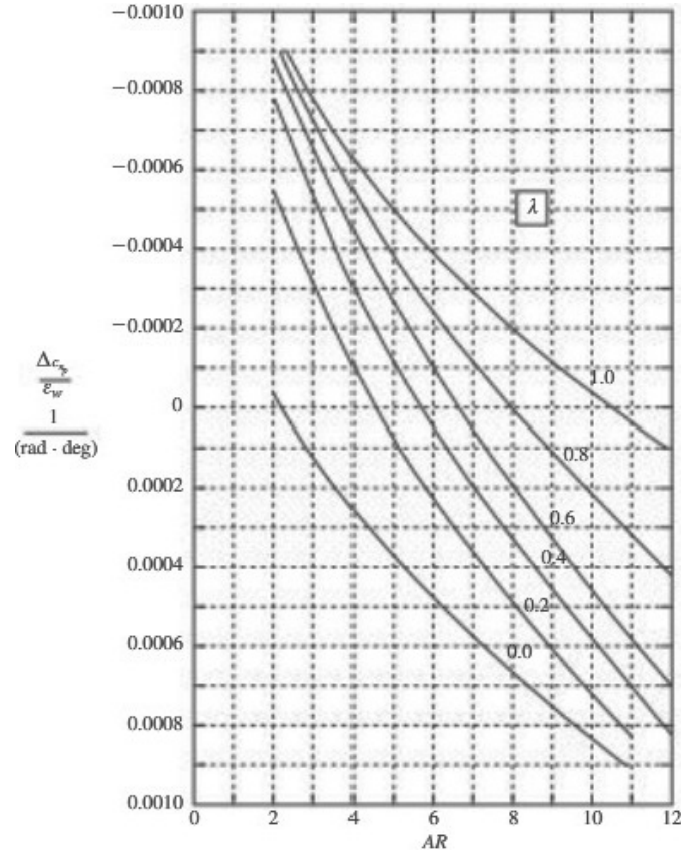


FIGURE 3.25: Effect of Wing Twist on c_{n_p} [16]

- The vertical tail contribution $C_{n_{pV}}$ is calculated using

$$C_{n_{pV}} \approx -2C_{y_{\beta V}} \cdot \frac{(X_V \cos \alpha_1 + Z_V \sin \alpha_1)}{b} \cdot \frac{(Z_V \cos \alpha_1 - X_V \sin \alpha_1 - Z_V)}{b} \quad (3.75)$$

3.4.12 Yaw Rate Derivatives

The calculation of rate of angle of attack derivatives starts from:

1. Calculate C_{y_r} using the following expression.

$$C_{y_r} \approx -2C_{y_{\beta_V}} \frac{(X_V \cos \alpha_1 + Z_V \sin \alpha_1)}{b} \quad (3.76)$$

where, $C_{y_r} \triangleq$ the contribution of the yaw rate to the lateral force with only the vertical tail is contributed,

$$C_{y_r} \approx C_{y_{r_V}}$$

2. Calculate C_{l_r} using the following expression.

$$C_{l_r} \approx C_{l_{r_W}} + C_{l_{r_V}} \quad (3.77)$$

where, $C_{l_r} \triangleq$ the contribution of the yaw rate to the rolling moment with The contributions of the fuselage and horizontal tail are not considerably influential to the C_{l_r} .

- The wing contribution $C_{l_{r_W}}$ is calculated using

$$C_{l_{r_W}} \approx \left(\frac{C_{l_r}}{C_{L_1}} \right) \Big|_{\substack{Mach \\ C_L=0}} \cdot C_{L_1} + \left(\frac{\Delta C_{l_r}}{\Gamma} \right) \cdot \Gamma + \left(\frac{\Delta C_{l_r}}{\varepsilon_W} \right) \cdot \varepsilon_W \quad (3.78)$$

where,

$$\left(\frac{C_{l_r}}{C_{L_1}} \right) \Big|_{\substack{Mach \\ C_L=0}} = D \left(\frac{C_{l_r}}{C_{L_1}} \right) \Big|_{\substack{Mach=0 \\ C_L=0}} \quad (3.79)$$

$$D = \frac{1 + \frac{AR(1 - B^2)}{2B(AR \cdot B + 2 \cos(\Lambda_{c/4}))} + \frac{(AR + 2 \cos(\Lambda_{c/4}))}{(AR + 4 \cos(\Lambda_{c/4}))} \cdot \frac{\tan^2(\Lambda_{c/4})}{8}}{1 + \frac{(AR + 2 \cos(\Lambda_{c/4}))}{(AR + 4 \cos(\Lambda_{c/4}))} \cdot \frac{\tan^2(\Lambda_{c/4})}{8}} \quad (3.80)$$

with

$$- \left(\frac{C_{l_r}}{C_{L_1}} \right) \Big|_{\substack{Mach=0 \\ C_L=0}} \text{ is evaluated through Fig. 3.26}$$

– $\left(\frac{\Delta C_{l_r}}{\Gamma}\right)$ is a factor related to the wing dihedral angle Γ , calculated using

$$\left(\frac{\Delta C_{l_r}}{\Gamma}\right) \approx \left(\frac{1}{12}\right) \cdot \frac{(\pi \cdot AR \cdot \sin(\Lambda_{c/4}))}{(AR + 4 \cdot \cos(\Lambda_{c/4}))} \quad (3.81)$$

– $\left(\frac{\Delta C_{l_r}}{\varepsilon_W}\right)$ is a factor related to the wing twist angle ε_W modeled using Fig. 3.27

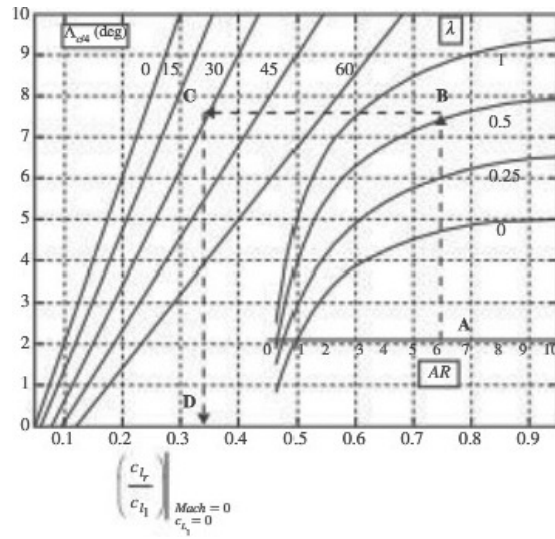


FIGURE 3.26: Evaluation of $\left(\frac{c_{l_r}}{c_{L1}}\right)\bigg|_{\kappa}$ [16]

where $\kappa = \frac{Mach=0}{c_L=0}$.

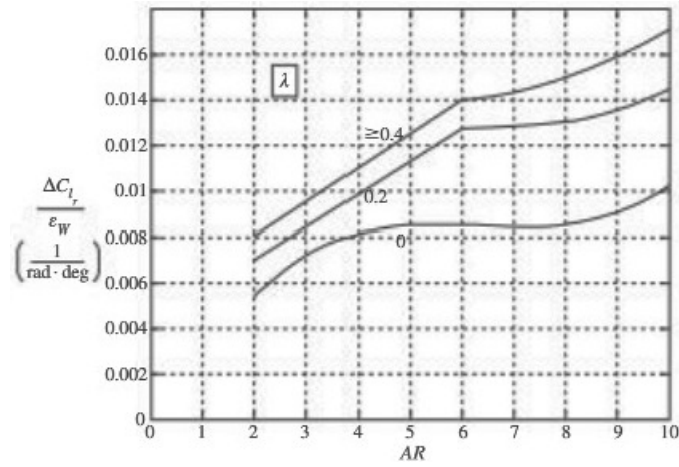
- The vertical tail contribution $C_{l_{rV}}$ is calculated using

$$C_{l_{rV}} = -2C_{y\beta_V} \frac{(X_V \cos \alpha_1 + Z_V \sin \alpha_1)}{b} \cdot \frac{(Z_V \cos \alpha_1 - X_V \sin \alpha_1)}{b} \quad (3.82)$$

3. Calculate C_{n_r} using the following expression.

$$C_{n_r} \approx C_{n_{rW}} + C_{n_{rV}} \quad (3.83)$$

where, C_{n_r} defines the contribution to the yawing moment due to the yaw rate with the fuselage and horizontal tail contributions do not significantly impact to the C_{n_r}


 FIGURE 3.27: Effect of Wing Twist on c_{l_r} [16]

- The wing contribution $C_{n_{rW}}$ is calculated using

$$C_{n_{rW}} \approx \left(\frac{C_{n_r}}{C_{L_1}} \right) \cdot C_{L_1}^2 + \left(\frac{C_{n_r}}{\bar{C}_{D_0}} \right) \bar{C}_{D_0} \quad (3.84)$$

For the majority of configurations, the $\left(\frac{C_{n_r}}{\bar{C}_{D_0}} \right)$ contribution is negligible, leads to

$$C_{n_{rW}} \approx \left(\frac{C_{n_r}}{C_{L_1}} \right) \cdot C_{L_1}^2 \quad (3.85)$$

where the $\left(\frac{C_{n_r}}{C_{L_1}} \right)$ is evaluated using Fig. 3.28

- The vertical tail contribution $C_{n_{rV}}$ is calculated using

$$C_{n_{rV}} \approx 2C_{Y_{\beta V}} \cdot \frac{(X_V \cos \alpha_1 + Z_V \sin \alpha_1)^2}{b^2} \quad (3.86)$$

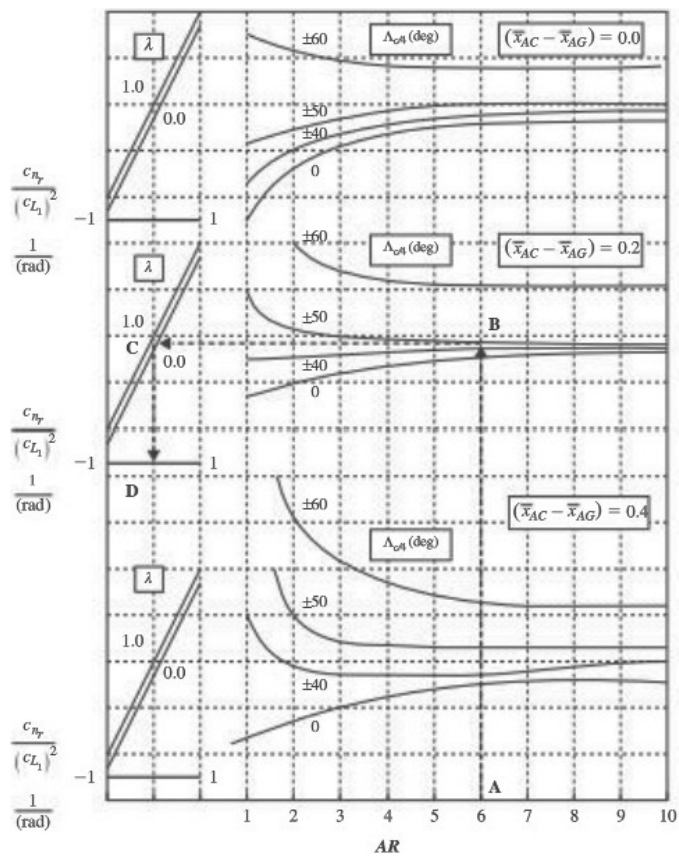


FIGURE 3.28: Effect of Lift on c_{n_r} [16]

3.5 State Space Model

3.5.1 State Space Model of Longitudinal Dynamics

The longitudinal dynamics of Baruna-1 is calculated using the state variable model as given below.

$$\begin{aligned}\dot{x}_{Long} &= A_{Long}x_{Long} + B_{Long}u_{Long} \\ y_{Long} &= C_{Long}x_{Long} + D_{Long}u_{Long}\end{aligned}$$

The step-by-step calculations of the longitudinal dynamics are given by

1. Recall the longitudinal state equations in matrix form in Eq. 2.84, as shown below.

$$\begin{aligned}\begin{bmatrix} \dot{u} \\ \dot{\alpha} \\ \dot{q} \\ \dot{\theta} \end{bmatrix} &= A_{Long} \begin{bmatrix} u \\ \alpha \\ q \\ \theta \end{bmatrix} + B_{Long}(\delta_E) \\ &= \begin{bmatrix} X'_u & X'_\alpha & X'_q & X'_\theta \\ Z'_u & Z'_\alpha & Z'_q & Z'_\theta \\ M'_u & M'_\alpha & M'_q & M'_\theta \\ 0 & 0 & 1 & 0 \end{bmatrix} \begin{bmatrix} u \\ \alpha \\ q \\ \theta \end{bmatrix} + \begin{bmatrix} X'_{\delta_E} \\ Z'_{\delta_E} \\ M'_{\delta_E} \\ 0 \end{bmatrix} (\delta_E)\end{aligned}$$

2. Calculate the inputs in the longitudinal state equations in matrix form using equations in Tab.2.1.
3. Input the identity matrix I for the output matrix C in the output vector y_{Long} .
4. Input the zero value for the direct matrix D in the output vector y_{Long} .

3.5.2 State Space Model of Lateral Directional Dynamic

The lateral directional dynamic stability of Baruna-1 is calculated using the state variable model of lateral directional dynamics in Eq. 2.88 as shown below.

$$\begin{aligned}\dot{x}_{Lat Dir} &= A_{Lat Dir}x_{Lat Dir} + B_{Lat Dir}u_{Lat Dir} \\ y_{Lat Dir} &= C_{Lat Dir}x_{Lat Dir} + D_{Lat Dir}u_{Lat Dir}\end{aligned}$$

The step-by-step calculations of the lateral directional dynamics are given by

1. Recall the lateral directional state equations in matrix form in Eq. 2.89, as shown below.

$$\begin{aligned} \begin{bmatrix} \dot{\beta} \\ \dot{p} \\ \dot{r} \\ \dot{\phi} \end{bmatrix} &= A_{Lat Dir} \begin{bmatrix} \beta \\ p \\ r \\ \phi \end{bmatrix} + B_{Lat Dir} \begin{bmatrix} \delta_A \\ \delta_R \end{bmatrix} \\ &= \begin{bmatrix} Y'_\beta & Y'_p & Y'_r & Y'_\phi \\ L'_\beta & L'_p & L'_r & 0 \\ N'_\beta & N'_p & N'_r & 0 \\ 0 & 1 & \tan \Theta_1 & 0 \end{bmatrix} \begin{bmatrix} \beta \\ p \\ r \\ \phi \end{bmatrix} + \begin{bmatrix} Y'_{\delta_A} & Y'_{\delta_R} \\ L'_{\delta_A} & L'_{\delta_R} \\ N'_{\delta_A} & N'_{\delta_R} \\ 0 & 0 \end{bmatrix} \begin{bmatrix} \delta_A \\ \delta_R \end{bmatrix} \end{aligned}$$

2. Calculate the inputs in the lateral directional state equations in matrix form using equations in Tab.2.2
3. Input the identity matrix I for the output matrix C in the output vector $y_{Lat Dir}$.
4. Input the zero value for the direct matrix D in the output vector $y_{Lat Dir}$.

3.5.3 Longitudinal Modes Calculations

The longitudinal characteristic equation is calculated using the longitudinal dynamics in matrix form in Eq. 2.68. Two sets of complex conjugate roots comprise the longitudinal characteristic equation. Each pair is associated with a unique set of dynamic modes associated with a second-order system. The equation for longitudinal characteristics is given by

$$\begin{aligned} \vec{D}_1(s) &= A_1 s^4 + B_1 s^3 + C_1 s^2 + D_1 s + E_1 \\ &= (s^2 + 2\zeta_{SP}\omega_{n_{SP}}s + \omega_{n_{SP}}^2) (s^2 + 2\zeta_{PH}\omega_{n_{PH}}s + \omega_{n_{PH}}^2) \end{aligned} \quad (3.87)$$

The longitudinal short period and phugoid modes are calculated using MATLAB-based solution based on the location of roots which associated with short period

and phugoid modes in Fig. 2.18. However, the short period and phugoid can be approximated using the step-by-step approximation as described later.

3.6 USAF Digital DATCOM

Using the methods contained in the USAF Stability and Control DATCOM (Data Compendium), USAF Digital DATCOM calculates static stability, high lift and control, and dynamic derivative characteristics. The configuration of the geometry, attitude and Mach range capabilities are available in DATCOM. DATCOM also features a trim option that computes control deflections and aerodynamic increments for vehicle trim at subsonic Mach numbers. The DATCOM stability analysis and calculations outputs are the longitudinal and lateral-directional stability characteristics in stability axes and the pitch, acceleration, roll, and yaw derivatives [27].

However, USAF Digital DATCOM does not have a feature to visualize the aircraft model, which becomes a problem to assess whether the aircraft configuration declared in is correct. The additional tool called drawDATCOMaircraft is used to solve this problem.

3.6.1 drawDATCOMaircraft

drawDATCOMaircraft is a MATLAB-based tool created by Stepen Sahrn, which has capability to read the aircraft configuration data from USAF Digital DATCOM input file and generates an aircraft three-view drawing. It will visualize the top-view, front-view and side-view of the aircraft and the airfoil used by the wing, horizontal and vertical tail, which will help the author to validate the aircraft geometry configuration correctly [28].

The figure shown in Fig. 3.29 is the visualization of Baruna-1 Fire fighting aircraft based on the input aircraft geometry in DATCOM.

3.6.2 USAF Digital DATCOM Input Definition

The Baruna-1 aerodynamic coefficients and stability derivatives calculation using USAF Digital DATCOM requires a set of input data known as a "case" that provides

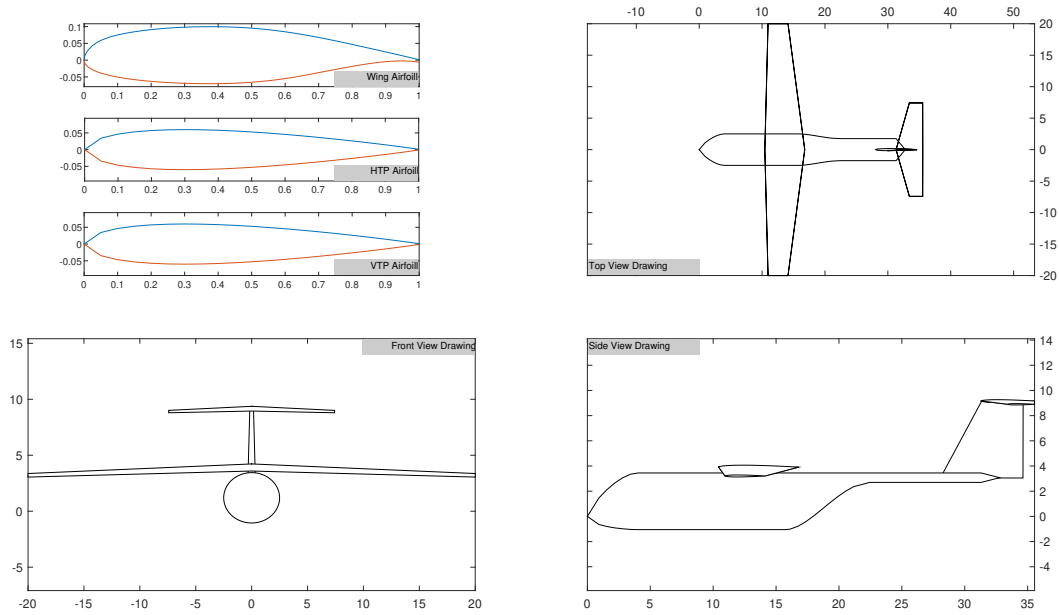


FIGURE 3.29: Baruna-1 Aircraft DATCOM Model

the parameters needed to represent the aircraft configuration and flight conditions. The "case" is generated in a single plain text file with an extension of .INP, which consist of variables groups called namelists and control cards.

There are multiple namelists and control cards available in USAF Digital DATCOM. However, it is classified by the characteristics of aircraft configuration and flight conditions to be designed. For the complete explanations of namelists and control cards available in USAF Digital DATCOM, it is fully available in the USAF Digital DATCOM Manual [27]. The namelists and control cards used in this research are given below, where the complete input files are provided in Appendix 5.3 for Take-off condition and Appendix 5.3.

FLTCON Namelist

In FLTCON namelist, the angle of attack, Mach number and Reynolds number are specified. However, because of the availability of a standard atmospheric model in USAF Digital DATCOM, which accurately simulates the 1962 Standard Atmosphere to compute pressure, temperature, Reynolds number, and other required parameters in the simulation process, the Reynolds number input can be replaced

by altitude. The LOOP variable is required when multiple Mach numbers and altitudes are specified with the maximum Mach number and altitude dimensions of 20. The FLTCON namelist of Baruna-1 is shown in Fig. 3.30.

```
$FLTCON
NMACH=6.0, MACH(1)=0.6,0.5,0.4,0.3,0.2,0.1,
NALPHA=10.0, ALSCHD(1)=-4.0,-2.0,0.0,2.0,4.0,6.0,8.0,10.0,12.0,14.0,
NALT=1.0, ALT(1)=3000.0, LOOP=2.0$
```

FIGURE 3.30: FLTCON Namelist

OPTINS and SYNTHS Namelist

In OPTINS namelist, the reference parameters such as the reference area (SREF), the wing mean aerodynamic chord (CBARR) and the wing span (BLREF) are specified. In SYNTHS namelist, the longitudinal and vertical location of the aircraft center of gravity, wing, horizontal and vertical tail are specified. Additionally, VERTUP =.TRUE. defines the vertical panel is located above the reference plane.

```
$OPTINS
SREF=200.0, CBARR=5.0, BLREF=40.0$
$SYNTHS
XCG=10.93582, ZCG=1.23869, XW=10.4392, ZW=3.9081, ALIW=0.0,
XH=31.3118, ZH=9.1615, ALIH=0.5590, XV=28.0615, ZV=3.0486,
VERTUP=.TRUE.$
```

FIGURE 3.31: OPTINS and SYNTHS Namelists

BODY Namelist

In BODY namelist, the body configurations are specified which consists of several variables as shown in Fig. 3.32. The variables shown in Fig. 3.32 are explained further below.

- NX: Number of longitudinal body station, with the maximum number of 20.
- X: Longitudinal distance measured from the arbitrary location.
- S: Cross-section area at station X_i .

- P: Periphery at station X_i .
- R: Planform half width at station X_i .

However, the additional variables given below are required if the aircraft body is asymmetric.

- ZU: Z-Coordinate at upper surface of the aircraft body at station X_i .
- ZL: Z-Coordinate at lower surface of the aircraft body at station X_i .

The maximum array dimension for each variable is based on the specified number of longitudinal body station (NX).

```
$BODY NX=20.0,  
X(1)=0.0, 0.9081, 1.5414, 2.1747, 2.8079,  
3.4412, 4.0360, 15.7584, 16.1066, 16.7399,  
17.3732, 18.0064, 18.6397, 19.2730, 19.9063,  
20.53952, 21.17279, 22.43933, 31.30507, 32.77775,  
R(1)=0.0, 1.06304, 1.53502, 1.92330, 2.22704,  
2.43145, 2.49990, 2.49935, 2.49234, 2.44719,  
2.37281, 2.28009, 2.17801, 2.07426, 1.97559,  
1.88815, 1.81769, 1.74989, 1.74965, 0.00000,  
S(1)=0.0, 3.50114, 7.02149, 10.75757, 14.20014,  
16.76594, 17.66804, 17.66121, 17.46964, 16.28699,  
14.40578, 12.18224, 10.52271, 8.52722, 7.05941,  
6.12233, 5.47905, 2.04937, 2.05728, 0.00000,  
P(1)=0.0, 6.63316, 9.39662, 11.63553, 13.37271,  
14.53409, 14.92119, 14.91828, 14.83927, 14.34348,  
13.52561, 12.50600, 11.67378, 10.62747, 9.77983,  
9.17430, 8.72474, 6.66860, 6.67252, 0.00000,$  
$BODY  
ZU(1)=0.0, 1.45675, 2.11066, 2.64785, 3.06932,  
3.35319, 3.44831, 3.44808, 3.44830, 3.44830,  
3.44829, 3.44828, 3.44827, 3.44827, 3.44827,  
3.44827, 3.44827, 3.44827, 3.44827, 3.07356,  
ZL(1)=0.0, -0.63997, -0.80136, -0.91294, -0.98611,  
-1.03658, -1.05099, -1.05047, -1.01396, -0.78590,  
-0.41674, 0.04690, 0.55725, 1.07598, 1.56931,  
2.00651, 2.35877, 2.69772, 2.69772, 3.07356,$
```

FIGURE 3.32: BODY Namelist

WGPLNF, HTPLNF and VTPLNF Namelists

In these namelists, the geometry of the wing, horizontal tail and vertical tail are specified which consists of several variables as shown in Fig. 3.33. The variables shown in Fig. 3.33 are explained further below.

- CHRDTP: Tip chord.
- CHRDR: Root chord.
- SSPN: Semi-span theoretical panel from theoretical root chord.
- SSPNE: Semi-span exposed panel.
- SAVSI: Inboard panel sweep angle.
- CHSTAT: Reference chord station (x/c).
- TWISTA: Twist angle.
- DHDADI: Inboard panel dihedral angle.
- DHDADO: Outboard panel dihedral angle.
- TYPE: The planform type, where for straight tapered planform TYPE = 1.

However, TWISTA, DHDADI, and DHDADO are not required in VTPLNF namelist.

```
$WGPLNF CHRDTP=3.17276, SSPNE= 17.5, SSPN=20.0, CHRDR=6.34552,  
  SAVSI=0.0, CHSTAT=0.1604, TWISTA=0.0, DHDADI=-2.0,  
  DHDADO= -2.0, TYPE=1.0$  
$VTPLNF CHRDTP=3.2841, SSPNE=6.1303, SSPN=6.1303, CHRDR=6.5682,  
  SAVSI=22.0, CHSTAT=0.25, TYPE=1.0$  
$HTPLNF CHRDTP=2.1199, SSPNE=7.4196, SSPN=7.4196, CHRDR=4.2398,  
  SAVSI=12.0, CHSTAT=0.25, TWISTA=0.0, DHDADI=-2.0,  
  DHDADO= -2.0, TYPE= 1.0$
```

FIGURE 3.33: WGPLNF, HTPLNF and VTPLNF Namelists

WGSCHR, HTSCHR, VTSCHR Namelists

In these namelists, the characteristics of the wing, horizontal tail and vertical tail are specified. The NACA Control Card can be used to determine the characteristic of the wing, horizontal and vertical tail, where the list of NACA airfoils available in the NACA Control Card are described in Digital DATCOM Manual [27].

However, the other ways to specify the characteristic of the planforms are by defining the airfoil section coordinates which can be obtained from the airfoil

database and specifying the variables input required based on the Digital DAT-COM Manual. In defining the airfoil section coordinates, there are several variables should be specified as shown in Fig. 3.34, where

- TYPEIN: The type of airfoil section coordinates input, where TYPE = 1 is used for determining the upper and lower surface ordinates.
- NPTS: The number of section points input, with the maximum number of 50.
- YUPPER: The ordinates of upper surface.
- YLOWER: The ordinates of upper surface.

```

$WGSCHR TYPEIN=1.0, DWASH=0.0, NPTS=45.0,
XCORD(1)=0.00000, 0.00200, 0.00500, 0.01250, 0.02500,
0.03750, 0.05000, 0.07500, 0.10000, 0.12500,
0.15000, 0.17500, 0.20000, 0.22500, 0.25000,
0.27500, 0.30000, 0.32500, 0.35000, 0.37500,
0.40000, 0.42500, 0.45000, 0.47500, 0.50000,
0.52500, 0.55000, 0.57500, 0.60000, 0.62500,
0.65000, 0.67500, 0.70000, 0.72500, 0.75000,
0.77500, 0.80000, 0.82500, 0.85000, 0.87500,
0.90000, 0.92500, 0.95000, 0.97500, 1.00000,
YUPPER(1)=.00099, .01248, .01950, .03099, .04322,
.05210, .05893, .06840, .07511, .08033, .08454,
.08805, .09096, .09339, .09536, .09694, .09815,
.09901, .09952, .09972, .09956, .09909, .09826,
.09700, .09535, .09323, .09073, .08777, .08448,
.08079, .07672, .07232, .06763, .06269, .05755,
.05225, .04687, .04132, .03576, .03013, .02444,
.01873, .01302, .00720, .00125,
YLOWER(1)=.00099, -.00857, -.01366, -.02105, -.02866,
-.03423, -.03865, -.04541, -.05058, -.05477, -.05817,
-.06099, -.06330, -.06527, -.06685, -.06812, -.06909,
-.06978, -.07021, -.07036, -.07019, -.06967, -.06880,
-.06755, -.06591, -.06389, -.06138, -.05845, -.05501,
-.05106, -.04674, -.04214, -.03735, -.03255, -.02780,
-.02309, -.01857, -.01433, -.01049, -.00719, -.00460,
-.00289, -.00232, -.00324, -.00597$
NACA-H-4-0012
NACA-V-4-0012

```

FIGURE 3.34: WGSCHR, HTSCHR and VTSCHR Namelists

SYMFLP and ASYFLP Namelists

In these namelists, the deflection of the symmetric and asymmetric flight control surfaces used are defined, both flaps and elevators deflection are defined in SYMFLP namelist, while aileron deflections are defined in ASYFLP. However, SYMFLP

and ASYFLP can only be analyzed in a different case. There are several variables required in specifying the SYMFLP and ASYFLP namelists shown in Fig. 3.35 which are explained further below. For SYMFLP namelist,

- NDELTA: Number of flap deflection angles, with the maximum number of 9.
- DELTA: Flap deflection angles.
- PHETE: Tangent of airfoil trailing edge angle based on ordinates at 90% and 99% chord. It can be calculated using

$$\tan_{(\varnothing_{TE}/2)} = \frac{1}{2} \left(\frac{Y_{90} - Y_{99}}{9} \right) \quad (3.88)$$

- PHETEP: Tangent of airfoil trailing edge angle based on ordinates at 95% and 99% chord. It can be calculated using

$$\tan_{(\varnothing_{TE}/2)} = \frac{1}{2} \left(\frac{Y_{95} - Y_{99}}{4} \right) \quad (3.89)$$

- CHRDFI: Flap chord at inboard end of flap.
- CHRDFO: Flap chord at outboard end of flap.
- SPANFI: Span location of inboard end of flap.
- SPANFO: Span location of ioutboard end of flap.
- FTYPE: The type of flap used, FTYPE = 1 for plain flaps.
- CB: Average chord of balance.
- NTYPE: The nose flap type, NTYPE = 1 for Round nose flap.

Furthermore, for ASYFLP namelist,

- STYPE: Type of asymmetric flight control surface used, STYPE = 4 for PLAIN FLAP AILERON.
- NDELTA: Number of control deflection angles, with the maximum number of 9.

- DELTAL: Deflection angles for the left hand plain flap aileron.
- DELTAR: Deflection angles for the right hand plain flap aileron.
- CHRDFI: Flap chord at inboard end of flap.
- CHRDFO: Flap chord at outboard end of flap.
- SPANFI: Span location of inboard end of flap.
- SPANFO: Span location of ioutboard end of flap.

```
$SYMFLP NDELTA=7.0,  
  DELTA(1)=-30.,-20.,-10.,0.0,10.,20.,30.,  
  PHETE=0.002746065556, PHETEP=0.00285082875,  
  CHRDFI=1.4839, CHRDFO=1.4839, CB=0.371,  
  SPANFI=0.0, SPANFO=5.0, FTYPE=1.0, NTYPE=1.0$  
$ASYFLP NDELTA=5.0,  
  DELTAL(1)=5.,10.,20.,30.,40.,  
  DELTAR(1)=-2.,-5.,-10.,-15.,-20.,  
  STYPE=4.0, CHRDFI=1.25, CHRDFO=1.25,  
  SPANFI=28.8, SPANFO=39.2$
```

FIGURE 3.35: SYMFLP and ASYFLP Namelists

Case Control Cards

In case control cards, the optional inputs and outpus and the case control commands are specified which provide additional features and flexibility to the users. The control cards commands shown in Fig. 3.36 are explained further below.

- CASEID BARUNA-1: The name of the case.
- DIM M: Define meter as the length units.
- DERIV RAD: Define rad/s as the static and dynamic stability derivatives output unit
- SAVE: The input data of the case is saved to be used in the following cases.
- DAMP: Provide the results of dynamic derivatives.
- NEXT CASE: Terminate the input data reading and execute the case.

```

CASEID BARUNA-1
DIM M
DERIV RAD
SAVE
DAMP
NEXT CASE
    
```

FIGURE 3.36: Case Control Cards

3.6.3 Output Definitions

The static and dynamic stability of the case is the main output of USAF Digital DATCOM as shown in Fig. 3.37 and Fig. 3.38. The outputs are classified into four categories:

AUTOMATED STABILITY AND CONTROL METHODS PER APRIL 1976 VERSION OF DATCOM
CHARACTERISTICS AT ANGLE OF ATTACK AND IN SIDESLIP
WING-BODY-VERTICAL TAIL-HORIZONTAL TAIL CONFIGURATION
BARUNA-1

FLIGHT CONDITIONS						REFERENCE DIMENSIONS						
MACH NUMBER	ALTITUDE	VELOCITY	PRESSURE	TEMPERATURE	REYNOLDS NUMBER	REF. AREA	REFERENCE LONG.	LENGTH LAT.	MOMENT HORIZ	REF. CENTER VERT		
	M	M/SEC	N/ M**2	DEG K	1/ M	M**2	M	M	M	M		
0	0.600	3000.00	197.13	7.0121E+04	268.659	1.0535E+07	200.000	5.000	40.000	10.936	1.239	
0	ALPHA	CD	CL	CM	CN	CA	XCP	CLA	CMA	CYB	CNB	CLB
0	-4.0	0.018	-0.332	0.2060	-0.332	-0.005	-0.620	5.569E+00	-3.113E+00	-7.313E-01	5.843E-02	-8.968E-02
0	-2.0	0.014	-0.133	0.0860	-0.133	0.010	-0.647	5.833E+00	-3.439E+00			-8.485E-02
0	0.0	0.014	0.075	-0.0341	0.075	0.014	-0.451	5.876E+00	-3.484E+00			-7.987E-02
0	1.3	0.016	0.212	-0.1166	0.212	0.011	-0.549	5.674E+00	-3.401E+00			-7.653E-02
0	2.0	0.017	0.276	-0.1548	0.277	0.008	-0.560	5.562E+00	-3.422E+00			-7.491E-02
0	4.0	0.024	0.466	-0.2823	0.467	-0.008	-0.605	5.119E+00	-3.771E+00			-7.002E-02
0	6.0	0.034	0.634	-0.4181	0.634	-0.032	-0.660	4.216E+00	-3.983E+00			-6.527E-02
0	8.0	0.045	0.760	-0.5604	0.759	-0.061	-0.738	3.875E+00	-4.260E+00			-6.078E-02
0	10.0	0.061	0.904	-0.7155	0.901	-0.097	-0.794	3.967E+00	-4.316E+00			-5.595E-02
0	12.1	0.081	1.043	-0.8678	1.037	-0.139	-0.837	3.947E+00	-4.119E+00			-5.064E-02
0	14.0	0.104	1.179	-1.0034	1.169	-0.184	-0.858	4.198E+00	-4.000E+00			-4.539E-02
0				ALPHA	Q/QINF	EPSLON	D(EPSLON)/D(ALPHA)					
0				-4.0	1.000	-1.173	0.345					
0				-2.0	1.000	-0.483	0.363					
0				0.0	1.000	0.277	0.384					
0				1.3	1.000	0.798	0.419					
0				2.0	1.000	1.082	0.422					
0				4.0	1.000	1.857	0.376					
0				6.0	1.000	2.586	0.342					
0				8.0	1.000	3.225	0.315					
0				10.0	1.000	3.845	0.322					
0				12.1	1.000	4.542	0.340					
0				14.0	1.000	5.203	0.345					

FIGURE 3.37: Aerodynamic Coefficient and Stability Derivatives DATCOM Output

- Static Stability Coefficient and Derivatives.
 - $C_D \triangleq$ The aircraft drag coefficient.
 - $C_L \triangleq$ The aircraft lift coefficient.
 - $C_m \triangleq$ The aircraft pitching moment coefficient.
 - $C_N \triangleq$ The aircraft normal-force coefficient.

STABILITY ANALYSIS AND CONTROL DESIGN OF BARUNA-1

AUTOMATED STABILITY AND CONTROL METHODS PER APRIL 1976 VERSION OF DATCOM
DYNAMIC DERIVATIVES
WING-BODY-VERTICAL TAIL-HORIZONTAL TAIL CONFIGURATION
BARUNA-1

FLIGHT CONDITIONS						REFERENCE DIMENSIONS				
MACH NUMBER	ALTITUDE	VELOCITY	PRESSURE	TEMPERATURE	REYNOLDS NUMBER	REF. AREA	REFERENCE LONG.	LENGTH LAT.	MOMENT HORIZ	REF. CENTER VERT
	M	M/SEC	N/ M**2	DEG K	1/ M	M**2	M	M	M	M
0 0.600	3000.00	197.13	7.0121E+04	268.659	1.0535E+07	200.000	5.000	40.000	10.936	1.239
DYNAMIC DERIVATIVES (PER RADIAN)										
	PITCHING		ACCELERATION		ROLLING			YAWING		
0 ALPHA	CLQ	CMQ	CLAD	CMAD	CLP	CYP	CNP	CNR	CLR	
0	-4.00	1.411E+01	-3.886E+01	3.196E+00	-1.417E+01	-4.617E-01	5.543E-02	2.754E-02	-1.406E-01	NDM
0	-2.00			3.358E+00	-1.489E+01	-4.901E-01	5.169E-02	1.211E-02	-1.439E-01	NDM
0	0.00			3.560E+00	-1.579E+01	-4.966E-01	4.723E-02	-3.966E-03	-1.464E-01	NDM
0	1.34			3.877E+00	-1.720E+01	-4.806E-01	4.451E-02	-1.471E-02	-1.477E-01	NDM
0	2.00			3.913E+00	-1.735E+01	-4.695E-01	4.331E-02	-1.996E-02	-1.482E-01	NDM
0	4.00			3.481E+00	-1.544E+01	-4.136E-01	4.004E-02	-3.641E-02	-1.493E-01	NDM
0	6.00			3.167E+00	-1.405E+01	-3.102E-01	3.840E-02	-5.294E-02	-1.499E-01	NDM
0	8.00			2.915E+00	-1.293E+01	-2.616E-01	4.091E-02	-6.547E-02	-1.504E-01	NDM
0	10.00			2.981E+00	-1.322E+01	-2.617E-01	4.277E-02	-7.796E-02	-1.502E-01	NDM
0	12.00			3.148E+00	-1.396E+01	-2.564E-01	4.574E-02	-9.019E-02	-1.497E-01	NDM
0	14.00			3.195E+00	-1.417E+01	-2.780E-01	4.799E-02	-1.012E-01	-1.487E-01	NDM

0*** NDM PRINTED WHEN NO DATCOM METHODS EXIST

FIGURE 3.38: Aerodynamic Coefficient and Stability Derivatives
DATCOM Output (Cont')

- $C_A \triangleq$ The aircraft axial-force coefficient.
 - $X_{CP} \triangleq$ The location of center of pressure.
 - $C_{L_\alpha} \triangleq$ The lift coefficient derivative in accordance with angle of attack.
 - $C_{m_\alpha} \triangleq$ The pitching moment coefficient derivative in accordance with angle of attack.
 - $C_{y_\beta} \triangleq$ The sideforce coefficient derivative in accordance with sideslip angle.
 - $C_{n_\beta} \triangleq$ The yawing moment coefficient derivative in accordance with sideslip angle.
 - $C_{l_\beta} \triangleq$ The rolling moment coefficient derivative in accordance with sideslip angle.
 - $\frac{\vec{q}}{q_\infty} \triangleq$ The dynamic pressure ratio.
 - $\varepsilon \triangleq$ The horizontal tail downwash angle.
 - $\frac{d\varepsilon}{d\alpha} \triangleq$ The downwash angle derivative in accordance with angle of attack.
- Dynamic Derivatives
 - $C_{L_q} \triangleq$ The lift coefficient derivative in accordance with pitch rate.

- $C_{m_q} \triangleq$ The pitching moment coefficient derivative in accordance with pitch rate.
 - $C_{L_{\dot{\alpha}}} \triangleq$ The lift coefficient derivative in accordance with the angle of attack rate of change.
 - $C_{m_{\dot{\alpha}}} \triangleq$ The pitching moment coefficient derivative in accordance with the angle of attack rate of change.
 - $C_{l_p} \triangleq$ The rolling moment coefficient derivative in accordance with roll rate.
 - $C_{y_p} \triangleq$ The sideforce coefficient derivative in accordance with roll rate.
 - $C_{n_p} \triangleq$ The yawing moment coefficient derivative in accordance with roll rate.
 - $C_{n_r} \triangleq$ The yawing moment coefficient derivative in accordance with yaw rate.
 - $C_{l_r} \triangleq$ The rolling moment coefficient derivative in accordance with yaw rate.
- Symmetrical Deflection of High lift and Control
 - $\delta \triangleq$ The control surface deflection angle.
 - $\Delta C_L \triangleq$ Incremental lift coefficient in the linear-lift angle-of-attack range due to control surface deflection.
 - $\Delta C_m \triangleq$ Incremental pitching moment coefficient in the linear-lift angle-of-attack range due to control surface deflection.
 - $\Delta C_{L_{MAX}} \triangleq$ Incremental maximum-lift coefficient.
 - $\Delta C_{D_{MIN}} \triangleq$ Incremental minimum drag coefficient due to the deflection of control surface.
 - $\Delta C_{D_i} \triangleq$ Incremental induced-drag coefficient due to the deflection of control surface.
 - $(C_{L_\alpha})_\delta \triangleq$ Lift-curve slope of the deflected control surface.
 - $(C_H)_\alpha \triangleq$ Control-surface hinge-moment derivative due to angle of attack.

- $(C_H)_\delta \triangleq$ Control-surface hinge-moment derivative due to control deflection.
- Asymmetrical Control Surfaces.
 - $\delta_L \triangleq$ The deflection angle of the left asymmetrical control surface.
 - $\delta_R \triangleq$ The deflection angle of the right asymmetrical control surface.
 - $C_N \triangleq$ The coefficient of yawing moment due to asymmetrical control surface deflection.
 - $(C_L)_{ROLL} \triangleq$ Incremental rolling moment coefficient due to asymmetrical control surface deflection.

CHAPTER 4

RESULTS AND DISCUSSIONS

4.1 Tail and Control Surfaces Design

The design of the horizontal and vertical tails are shown in Tab. 4.1 and Fig. 4.1

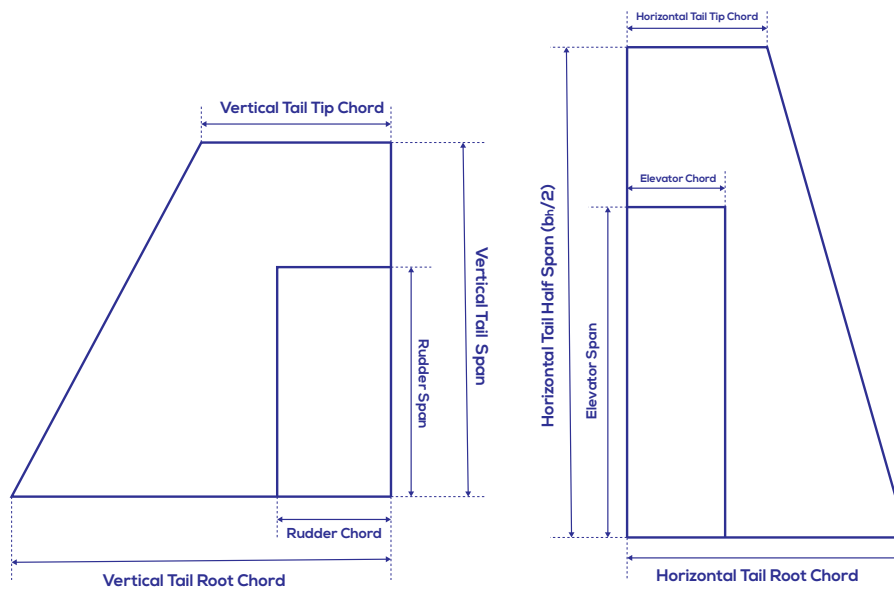


FIGURE 4.1: Elevator and Rudder Design

The design of the aircraft control surfaces (elevators, rudder and ailerons) are shown in Tab. 4.2, for elevators and rudder are shown in Fig. 4.1 and for ailerons are shown in Fig. 4.2

Geometric properties	Horizontal Tail	Vertical Tail
Setting angle ($^{\circ}$)	0	0
Area (m^2)	48.9337	31.3176
Chord (m)	3.2976	5.1086
c_{root} (m)	4.2398	6.5682
c_{tip} (m)	2.1199	3.2841
Span (m)	14.8392	6.1303
Airfoil	NACA-0012	NACA-0012

TABLE 4.1: Geometric Properties of the Horizontal and Vertical Tails

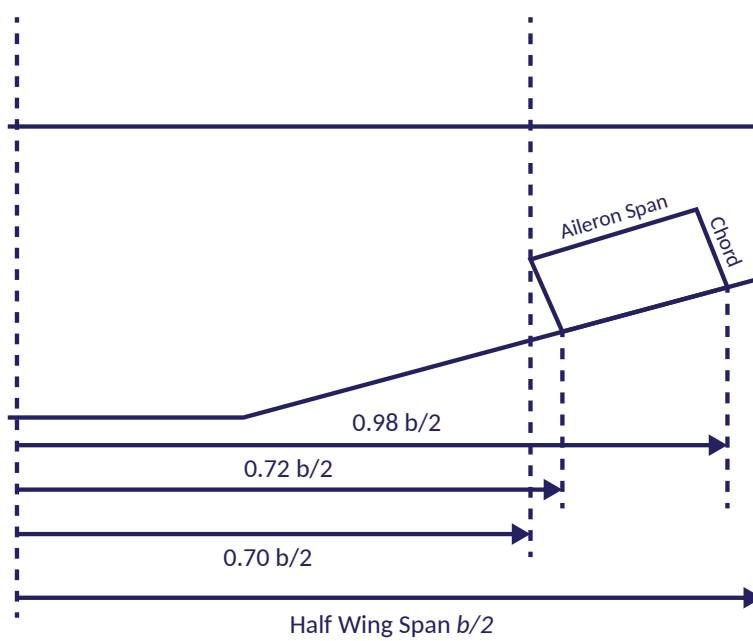


FIGURE 4.2: Aileron Design

Geometric properties	Elevator	Rudder	Aileron
Area (m^2)	7.4196	7.8294	7.5000
Chord (m)	1.4839	1.9705	5.2000
Span (m)	5	3.9734	1.2500

TABLE 4.2: Geometric Properties of the Aircraft Control Surfaces

4.2 Analysis Overview

The steady state aerodynamic coefficients and the stability and control derivatives at take-off and cruise conditions will be calculated using two approach:

- Approach 1: Analytical method based on the Marcello's[16], Snorri's[19], Sadrey's[25], and Roskam's[17] methodologies.
- Approach 2: The combination of Approach 1 and USAF Digital DATCOM data.

The steady state aerodynamic coefficients and the stability and control derivatives are calculated at:

1. Take-off condition:

- Aircraft Mass: 144560 kg
- Altitude: 0 m, at sea level.
- Air Density: 1.225 kg/m^3
- Mach number: 0.2725 (Subsonic Speed)
- Angle of attack α : 12.0856°
- Rate of Climb: 13 m/s

2. Cruise Condition:

- Aircraft Mass: 144560 kg
- Altitude: 3000 m, above sea level.
- Air Density: 0.8634 kg/m^3
- Mach number: 0.6 (Subsonic Speed)
- Angle of attack α : 1.334°
- Rate of Climb: 0 m/s

The rate of climb is purposed to calculate the flight path angle of the aircraft at take-off condition. The flight path angle γ is calculated by using:

$$\frac{dh}{dt} = V \sin(\gamma) \quad (4.1)$$

The application of feedback control to the state space model of Baruna-1 at take-off and cruise conditions are purposed to improve the stability of Baruna-1. The optimum feedback control gain K for longitudinal and lateral directional dynamics is calculated using the Linear Quadratic Regulator method in MATLAB.

4.3 Stability and Control Analysis

4.3.1 The Steady State Aerodynamic Coefficient and the Stability and Control Derivatives

The result of the steady-state aerodynamic coefficient are given in Table 4.3 and the aerodynamic stability and control derivatives are shown in Table 4.4 for the longitudinal dynamic stability derivatives and in Table 4.5 for the lateral directional dynamic stability derivatives.

Steady-State Coefficients	Take-off		Cruise	
	Approach 1	Approach 2	Approach 1	Approach 2
C_{D_1}	0.08248	0.10300	0.00793	0.01600
C_{L_1}	1.32026	1.31300	0.38780	0.21400
C_{m_1}	0.00000	0.00000	0.00000	0.00000
C_{y_1}	0.00000	0.00000	0.00000	0.00000
C_{n_1}	0.00000	0.00000	0.00000	0.00000
C_{l_1}	0.00000	0.00000	0.00000	0.00000

TABLE 4.3: The Steady-State Aerodynamic Coefficient of Baruna-1 at Take-off and Cruise Conditions

4.3.2 Static Stability Analysis

Longitudinal Static Stability and Trim Condition Analysis

The longitudinal static stability of an aircraft is characterized by the pitching moment derivative with respect to the angle of attack α . The requirement for the aircraft is said to be longitudinally stable if:

Longitudinal Derivative	Approach 1		Approach 2	
	Take-off	Cruise	Take-off	Cruise
$C_{D\alpha}$	0.719170	0.211243	0.457030	0.113677
$C_{L\alpha}$	5.818392	5.818392	3.718000	5.674000
$C_{m\alpha}$	-3.866096	-3.866096	-4.425000	-3.414000
C_{D_u}	0.004634	0.010184	0.004634	0.010184
C_{L_u}	0.106324	0.218138	0.105739	0.120375
C_{m_u}	-0.346452	-0.101764	-0.344548	-0.056156
C_{L_q}	14.318421	15.116615	13.170000	14.110000
C_{m_q}	-43.116110	-43.116110	-36.710000	-38.860000
$C_{L\dot{\alpha}}$	3.806559	3.806559	2.817000	3.850000
$C_{m\dot{\alpha}}$	-17.437682	-17.437682	-12.490000	-17.080000
$C_{L\delta_e}$	0.342812	0.342812	0.317369	0.317369
$C_{m\delta_e}$	-1.570409	-1.570409	-1.449848	-1.449848
$C_{T_{X_1}}$	-0.082484	-0.007930	-0.103000	-0.016000
$C_{m_{T_1}}$	0.000000	0.000000	0.000000	0.000000
$C_{T_{X_u}}$	0.247451	0.023789	0.309000	0.048000
$C_{m_{T_u}}$	-0.044335	-0.004262	-0.055362	-0.008600
$C_{m_{T\alpha}}$	0.000000	0.000000	0.000000	0.000000

TABLE 4.4: Longitudinal Stability and Control Derivative of Baruna-1 at Take-off and Cruise Conditions ($\alpha_{to} = 12.0856^\circ$ and $\alpha_{cruise} = 1.344^\circ$)

Longitudinal Derivative	Approach 1		Approach 2	
	Take-off	Cruise	Take-off	Cruise
$C_{y\beta}$	0.278538	0.278400	-0.714800	-0.731300
$C_{l\beta}$	0.023283	-0.018219	-0.054450	-0.076520
$C_{n\beta}$	0.211254	0.206719	0.055320	0.058430
C_{y_p}	-0.006148	-0.090334	0.009313	0.044370
C_{l_p}	-0.466120	-0.466120	-0.234300	-0.480400
C_{n_p}	-0.052200	-0.005956	-0.116800	-0.014820
C_{y_r}	0.452336	0.443267	0.434319	0.425610
C_{l_r}	0.343892	0.161769	0.341895	0.107288
C_{n_r}	-0.572647	-0.245216	-0.138700	-0.147700
$C_{y\delta_a}$	0.000000	0.000000	0.000000	0.000000
$C_{l\delta_a}$	0.050673	0.050673	0.043818	0.043818
$C_{n\delta_a}$	0.001673	0.000491	0.001438	0.000234
$C_{y\delta_r}$	0.156502	0.156502	0.150268	0.150268
$C_{l\delta_r}$	-0.008295	0.016606	-0.007966	0.015946
$C_{n\delta_r}$	-0.132843	-0.132061	-0.127551	-0.126801
$C_{nT\beta}$	0.000000	0.000000	0.000000	0.000000

TABLE 4.5: Lateral Directional Stability and Control Derivative of Baruna-1 at Take-off and Cruise Conditions ($\alpha_{to} = 12.0856^\circ$ and $\alpha_{cruise} = 1.344^\circ$)

$$C_{m_\alpha} = \frac{\partial C_m}{\partial \alpha} < 0$$

The plot shown in Fig. 4.3 describe the pitching moment of Baruna-1 with respect to the angle of attack changes calculated using Approach 1 and Approach 2. However, these plots are presented without the aircraft's elevator for trimming purpose.

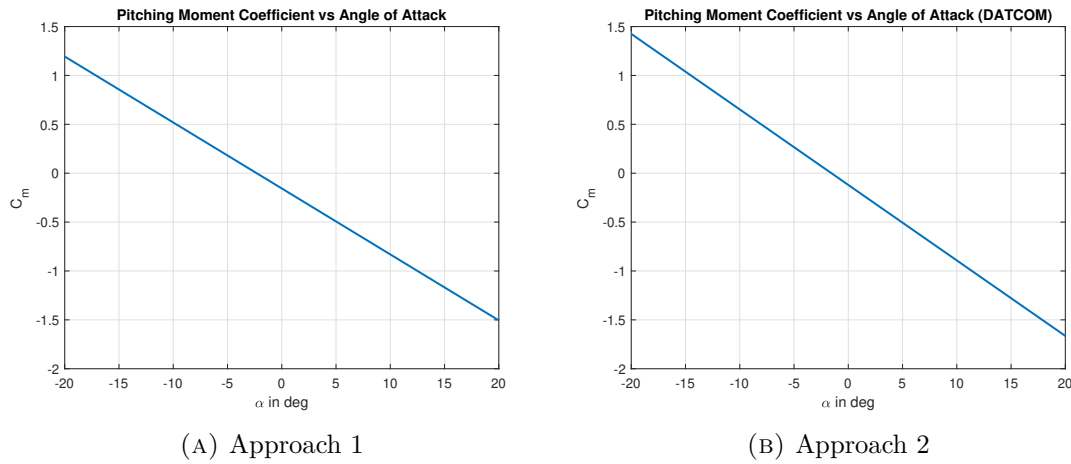


FIGURE 4.3: The Pitching Moment Coefficient vs Angle of Attack

In this thesis, Baruna-1 is used the elevators for the longitudinal control surface for trimming purpose. The figure shown below in Fig. 4.4 describe the correlation between the aircraft angle of attack and the deflection of elevators. At trim condition,

$$C_m = 0$$

The trim angle of attack at given flight conditions are at 12.0856° at take-off conditions and 1.344° at cruise conditions which calculated by using,

$$\alpha_1 = \frac{C_{m_{\delta_E}} (C_{L_1} - C_{L_0}) - C_{L_{\delta_E}} (-C_{m_0})}{(C_{m_{\delta_E}} C_{L_\alpha} - C_{L_{\delta_E}} C_{m_\alpha})}$$

At given trim angle of attack, the deflections of the elevators are at -35.4428° for the Approach 1 and -41.6262° for Approach 2 at take-off condition and -9.0006°

for the Approach 1 and -7.9026° for Approach 2 at cruise condition. which calculated by using,

$$\delta_{e_1} = \frac{C_{L_\alpha} (-C_{m_0}) - C_{m_\alpha} (C_{L_1} - C_{L_0})}{(C_{m_{\delta_E}} C_{L_\alpha} - C_{L_{\delta_E}} C_{m_\alpha})}$$

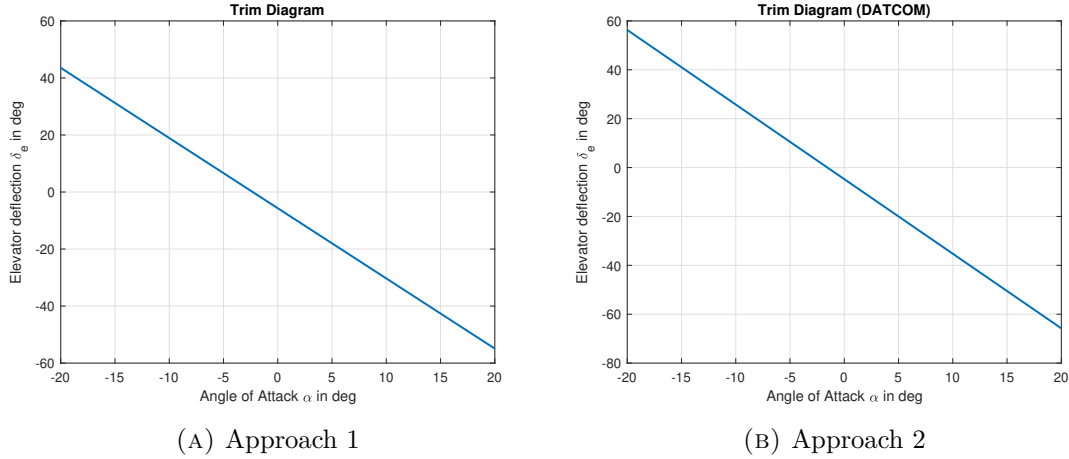


FIGURE 4.4: Trim Diagram for Approach 1 and Approach 2

As shown in Table 4.3, Baruna-1 has negative signs of pitching moment derivative with respect to angle of attack C_{m_α} with the value of $C_{m_\alpha} = -3.866096$ for Approach 1 and $C_{m_\alpha} = -4.425$ and $C_{m_\alpha} = -3.414$ for Approach 2 at take-off and cruise conditions which indicates Baruna-1 is longitudinal statically stable.

The longitudinal static stability of an aircraft is also characterized by the aircraft aerodynamic center and static margin. The static margin is calculated using:

$$SM = -100 (\vec{x}_{CG} - \vec{x}_{AC})$$

Figure 4.5 shows the location of the aircraft aerodynamic center with the value of 0.1404 with respect to \vec{c} or 14.04% of the wing mean aerodynamic chord, where the location of the aircraft center of gravity is -0.1014 with respect to \vec{c} or 10.14% in front of the wing aerodynamic center. The static margin of Baruna-1 is 24.1743% of the wing MAC \vec{c} , where the typical value of Static margin for commercial and military transport aircraft is between 0.15-0.25.

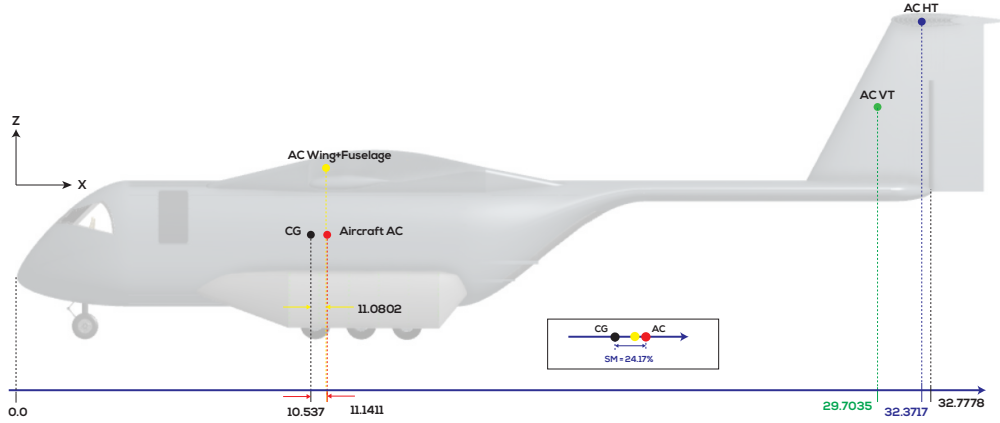


FIGURE 4.5: Location of the CG, AC, Neutral Point and the Static Margin of Baruna-1

Lateral Directional Static Stability Analysis

The lateral and directional static stability of Baruna-1 are evaluated by analyzing the signs of the rolling moment with respect to the sideslip angle C_{l_β} and the yawing moment with respect to the sideslip angle C_{n_β} . With the requirements for lateral and directional static stability, for lateral static stability:

$$C_{l_\beta} = \frac{\partial C_l}{\partial \beta} < 0 \quad \text{and} \quad C_l = 0 \quad \text{if} \quad \beta = 0$$

and for directional static stability:

$$C_{n_\beta} = \frac{\partial C_n}{\partial \beta} > 0 \quad \text{and} \quad C_n = 0 \quad \text{if} \quad \beta = 0$$

In this thesis, the take-off condition is assumed to be without maneuvering, meaning that the bank angle Φ is zero. By this assumptions, the deflection of the ailerons δ_a and rudder δ_r are zero.

As shown in Table 4.4, Baruna-1 has positive signs for both methods at take-off and cruise conditions for C_{n_β} with the results of $C_{n_\beta} = 0.211254$ and $C_{n_\beta} = 0.206719$ for Approach 1 and $C_{n_\beta} = 0.055320$ and $C_{n_\beta} = 0.058430$ for Approach

2 at take-off and cruise condition. By this positive signs of C_{n_β} indicates that Baruna-1 is directional statically stable.

Moreover, the result of C_{l_β} as shown in Table 4.4, shows that Baruna-1 has negative signs for both methods at take-off and cruise conditions, except the Approach 1 at take-off condition. The value of C_{l_β} are $C_{l_\beta} = 0.023283$ and $C_{l_\beta} = -0.018219$ for Approach 1 and $C_{l_\beta} = -0.05445$ and $C_{l_\beta} = -0.07652$ for Approach 2 at take-off and cruise conditions. The C_{l_β} is calculated based on the contribution of the wing, horizontal and vertical tails, where the wing contribution is calculated using the expressions provided by Gudmundsson which based on the digitization of plots [19]. Due to the sweep angle of Baruna-1 is unavailable in the expressions, the author decided to use the nearest value of sweep angle to calculate the sweep angle. By this decision, this may cause the result of C_{l_β} become positive.

4.3.3 Dynamic Stability

The dynamic stability analysis of Baruna-1 is conducted using State Space Model, where the aerodynamic stability and control derivatives as the inputs of the state space model have been calculated using Approach 1 and Approach 2.

$$\begin{aligned}\dot{x} &= Ax + Bu \\ y &= Cx + Du\end{aligned}$$

The purpose of State Space modeling is to obtain the eigenvalues of the characteristic equations, with the following of the damping, undamped natural frequency and time constant, where these parameter will be evaluated based on the flying and handling qualities for each mode.

Longitudinal Dynamic Stability

The state space model for longitudinal dynamics is given by

$$\begin{aligned}\dot{x}_{Long} &= A_{Long}x_{Long} + B_{Long}u_{Long} \\ y_{Long} &= C_{Long}x_{Long} + D_{Long}u_{Long}\end{aligned}$$

$$\begin{bmatrix} \dot{u} \\ \dot{\alpha} \\ \dot{q} \\ \dot{\theta} \end{bmatrix} = \begin{bmatrix} X'_u & X'_\alpha & X'_q & X'_\theta \\ Z'_u & Z'_\alpha & Z'_q & Z'_\theta \\ M'_u & M'_\alpha & M'_q & M'_\theta \\ 0 & 0 & 1 & 0 \end{bmatrix} \begin{bmatrix} u \\ \alpha \\ q \\ \theta \end{bmatrix} + \begin{bmatrix} X'_{\delta_E} \\ Z'_{\delta_E} \\ M'_{\delta_E} \\ 0 \end{bmatrix} (\delta_E)$$

$$\begin{bmatrix} \dot{u} \\ \dot{\alpha} \\ \dot{q} \\ \dot{\theta} \end{bmatrix} = \begin{bmatrix} 1 & 0 & 0 & 0 \\ 0 & 1 & 0 & 0 \\ 0 & 0 & 1 & 0 \\ 0 & 0 & 0 & 1 \end{bmatrix} \begin{bmatrix} u \\ \alpha \\ q \\ \theta \end{bmatrix} + \begin{bmatrix} 0 \\ 0 \\ 0 \\ 0 \end{bmatrix} (\delta_E)$$

The A and B matrices are evaluated using the Baruna-1 longitudinal dynamics stability and control derivatives based on Table 4.3. The state space model for the longitudinal motion of Baruna-1 is evaluated for take-off and cruise conditions using Approach 1 and Approach 2. Calculating the inputs for both A and B matrices, leads to:

1. The longitudinal dynamics state space model and the characteristic equation \vec{D}_1 at take-off condition for Approach 1 are given by

$$\begin{bmatrix} \dot{u} \\ \dot{\alpha} \\ \dot{q} \\ \dot{\theta} \end{bmatrix} = \begin{bmatrix} -0.00691283 & 4.46629833 & 0 & -9.21449565 \\ -0.00230905 & -0.46449135 & 0.96190945 & -0.03565738 \\ 0 & -0.00000622 & -0.00000273 & 0.00000003 \\ 0 & 0 & 1 & 0 \end{bmatrix} \begin{bmatrix} u \\ \alpha \\ q \\ \theta \end{bmatrix} + \begin{bmatrix} 0 \\ -0.02698470 \\ -0.00000265 \\ 0 \end{bmatrix} (\delta_E)$$

$$\vec{D}_1 = s^4 + 0.4714s^3 + 0.01353s^2 - 1.789e - 07s + 1.106e - 07$$

2. The longitudinal dynamics state space model and the characteristic equation \vec{D}_1 at take-off condition for Approach 2 is given by

$$\begin{bmatrix} \dot{u} \\ \dot{\alpha} \\ \dot{q} \\ \dot{\theta} \end{bmatrix} = \begin{bmatrix} -0.00854080 & 6.36018123 & 0 & -9.21449476 \\ -0.00230114 & -0.30139933 & 0.96633250 & -0.03573172 \\ 0 & -0.00000737 & -0.00000222 & 0.00000002 \\ 0 & 0 & 1 & 0 \end{bmatrix} \begin{bmatrix} u \\ \alpha \\ q \\ \theta \end{bmatrix} + \begin{bmatrix} 0 \\ -0.02503401 \\ -0.00000246 \\ 0 \end{bmatrix} (\delta_E)$$

$$\vec{D}_1 = s^4 + 0.3099s^3 + 0.01722s^2 - 1.858e - 07s + 1.388e - 07$$

3. The longitudinal dynamics state space model and the characteristic equation \vec{D}_1 at cruise condition for Approach 1 is given by

$$\begin{bmatrix} \dot{u} \\ \dot{\alpha} \\ \dot{q} \\ \dot{\theta} \end{bmatrix} = \begin{bmatrix} -0.00222656 & 4.46629833 & 0 & -9.80729818 \\ -0.00059017 & -0.71211035 & 0.97190420 & -0.00111235 \\ 0 & -0.00002156 & -0.00000423 & 0 \\ 0 & 0 & 1 & 0 \end{bmatrix} \begin{bmatrix} u \\ \alpha \\ q \\ \theta \end{bmatrix} + \begin{bmatrix} 0 \\ -0.04189954 \\ -0.00000906 \\ 0 \end{bmatrix} (\delta_E)$$

$$\vec{D}_1 = s^4 + 0.7143s^3 + 0.004245s^2 + 2.785e - 08s + 1.097e - 07$$

4. The longitudinal dynamics state space model and the characteristic equation \vec{D}_1 at cruise condition for Approach 2 is given by

$$\begin{bmatrix} \dot{u} \\ \dot{\alpha} \\ \dot{q} \\ \dot{\theta} \end{bmatrix} = \begin{bmatrix} -0.00321853 & 2.53781156 & 0 & -9.80730119 \\ -0.00032565 & -0.69540381 & 0.97333597 & -0.00111166 \\ -0.00000001 & -0.00001897 & -0.00000391 & -0.00000043 \\ 0 & 0 & 1 & 0 \end{bmatrix} \begin{bmatrix} u \\ \alpha \\ q \\ \theta \end{bmatrix} + \begin{bmatrix} 0 \\ -0.03878734 \\ -0.00000837 \\ 0 \end{bmatrix} (\delta_E)$$

$$\vec{D}_1 = s^4 + 0.6986s^3 + 0.003086s^2 + 4.065e - 08s + 5.239e - 08$$

The solution of state space model and characteristic equation for longitudinal dynamics leads to the expression of the Baruna-1's longitudinal transfer functions at take-off and cruise conditions as shown in Table 4.6 for Approach 1 and Approach 2. The roots of the characteristic equation also known as the eigenvalue of the characteristic equations defined the longitudinal dynamic stability of an aircraft. For the longitudinal characteristic equations, the eigenvalues are shown in Table 4.7.

As shown in Table 4.7 and Fig. 4.6, the eigenvalues of Baruna-1 for Approach 1 and Approach 2 at given flight conditions have positive signs which described an instability of the aircraft in lateral directional dynamics. Based on the result, the stability augmentation system will be implemented for both Approach 1 and Approach 2 at take-off and cruise conditions to stabilize the aircraft and improve the dynamic stability characteristic of Baruna-1.

The damping ζ and the natural frequency ω for longitudinal dynamics are shown in Table 4.8. However, due to instability of Baruna-1 in longitudinal dynamics mode, the implementation of the Stability Augmentation System will be conducted.

STABILITY ANALYSIS AND CONTROL DESIGN OF BARUNA-1

Approach 1			
Take-off		Cruise	
$u(s)$	$-0.1205s^2 + 1.273e - 05s + 1.024e - 05$	$u(s)$	$-0.1871s^2 + 4.874e - 05s + 5.446e - 05$
$\bar{\delta}_e(s)$	$s^4 + 0.4714s^3 + 0.01353s^2 - 1.789e - 07s + 1.106e - 07$	$\bar{\delta}_e(s)$	$s^4 + 0.7143s^3 + 0.004245s^2 + 2.785e - 08s + 1.097e - 07$
$\alpha(s)$	$-0.02698s^3 - 0.0001892s^2 + 7.727e - 08s - 5.472e - 08$	$\alpha(s)$	$-0.0419s^3 - 0.0001023s^2 - 9.866e - 09s - 5.154e - 08$
$\bar{\delta}_e(s)$	$s^4 + 0.4714s^3 + 0.01353s^2 - 1.789e - 07s + 1.106e - 07$	$\bar{\delta}_e(s)$	$s^4 + 0.7143s^3 + 0.004245s^2 + 2.785e - 08s + 1.097e - 07$
$q(s)$	$-2.655e - 06s^3 - 1.084e - 06s^2 - 3.421e - 08s + 7.938e - 29$	$q(s)$	$-9.06e - 06s^3 - 5.569e - 06s^2 - 3.584e - 08s - 7.927e - 26$
$\bar{\delta}_e(s)$	$s^4 + 0.4714s^3 + 0.01353s^2 - 1.789e - 07s + 1.106e - 07$	$\bar{\delta}_e(s)$	$s^4 + 0.7143s^3 + 0.004245s^2 + 2.785e - 08s + 1.097e - 07$
$\theta(s)$	$-2.655e - 06s^2 - 1.084e - 06s - 3.421e - 08$	$\theta(s)$	$-9.06e - 06s^2 - 5.569e - 06s - 3.584e - 08$
$\bar{\delta}_e(s)$	$s^4 + 0.4714s^3 + 0.01353s^2 - 1.789e - 07s + 1.106e - 07$	$\bar{\delta}_e(s)$	$s^4 + 0.7143s^3 + 0.004245s^2 + 2.785e - 08s + 1.097e - 07$
Approach 2			
Take-off		Cruise	
$u(s)$	$-0.1592s^2 + 7.185e - 06s + 5.684e - 06$	$u(s)$	$-0.09843s^2 + 6.099e - 05s + 4.986e - 05$
$\bar{\delta}_e(s)$	$s^4 + 0.3099s^3 + 0.01722s^2 - 1.858e - 07s + 1.388e - 07$	$\bar{\delta}_e(s)$	$s^4 + 0.6986s^3 + 0.003086s^2 + 4.065e - 08s + 5.239e - 08$
$\alpha(s)$	$-0.02503s^3 - 0.0002162s^2 + 6.754e - 08s - 5.019e - 08$	$\alpha(s)$	$-0.03879s^3 - 0.0001331s^2 - 1.734e - 08s - 2.623e - 08$
$\bar{\delta}_e(s)$	$s^4 + 0.3099s^3 + 0.01722s^2 - 1.858e - 07s + 1.388e - 07$	$\bar{\delta}_e(s)$	$s^4 + 0.6986s^3 + 0.003086s^2 + 4.065e - 08s + 5.239e - 08$
$q(s)$	$-2.457e - 06s^3 - 5.769e - 07s^2 - 3.991e - 08s + 2.844e - 29$	$q(s)$	$-8.366e - 06s^3 - 5.108e - 06s^2 - 2.315e - 08s - 2.564e - 31$
$\bar{\delta}_e(s)$	$s^4 + 0.3099s^3 + 0.01722s^2 - 1.858e - 07s + 1.388e - 07$	$\bar{\delta}_e(s)$	$s^4 + 0.6986s^3 + 0.003086s^2 + 4.065e - 08s + 5.239e - 08$
$\theta(s)$	$-2.457e - 06s^2 - 5.769e - 07s - 3.991e - 08$	$\theta(s)$	$-8.366e - 06s^2 - 5.108e - 06s - 2.315e - 08$
$\bar{\delta}_e(s)$	$s^4 + 0.3099s^3 + 0.01722s^2 - 1.858e - 07s + 1.388e - 07$	$\bar{\delta}_e(s)$	$s^4 + 0.6986s^3 + 0.003086s^2 + 4.065e - 08s + 5.239e - 08$

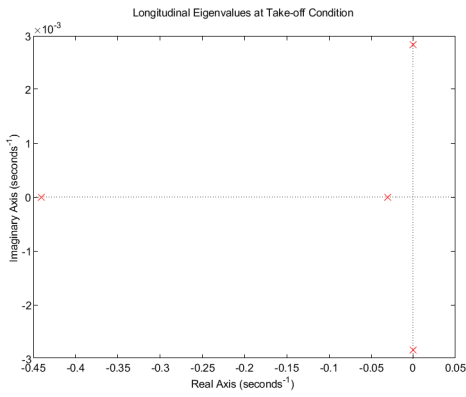
TABLE 4.6: Longitudinal Transfer Function of Baruna-1 at Take-off and Cruise Conditions

Take-off		Cruise	
Approach 1	Approach 2	Approach 1	Approach 2
-0.44070118	-0.23740399	-0.70834747	-0.69418090
-0.03099831	-0.07269361	-0.00827666	-0.00633428
0.00014629 + 0.00284125i	0.00007762 + 0.00283455i	0.00114149 + 0.00417290i	0.00094447 + 0.00332007i
0.00014629 - 0.00284125i	0.00007762 - 0.00283455i	0.00114149 - 0.00417290i	0.00094447 - 0.00332007i

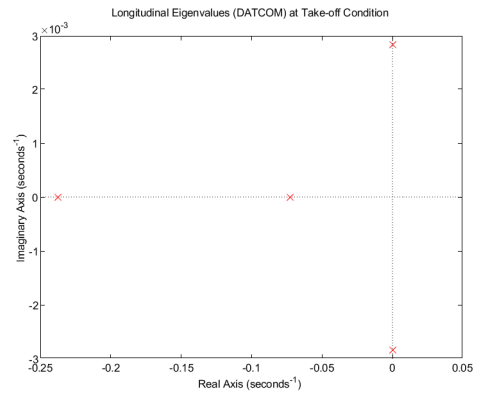
TABLE 4.7: Longitudinal Eigenvalues of Baruna-1 at Take-off and Cruise Conditions

Parameters	Take-off		Cruise	
	Approach 1	Approach 2	Approach 1	Approach 2
ω_{SP}	0.440701	0.237404	0.708347	0.694181
ζ_{SP}	1.000000	1.000000	1.000000	1.000000
ω_{PH}	0.002845	0.002836	0.004326	0.003452
ζ_{PH}	0.051419	0.027375	0.263855	0.273616
ω_{DR}	0.001483	0.000946	0.001144	0.001075
ζ_{DR}	0.015344	0.004554	1.000000	0.001294
T_R	-45.149893	17.627603	-29.351769	11.124909
T_{2s}	293219.691123	-2279279.573041	-356511.947571	6838065.118604

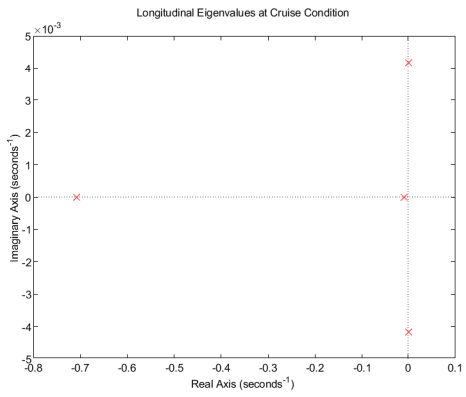
TABLE 4.8: The Natural Frequency ω , Damping ζ and Time Constant T of Baruna-1 at Take-off and Cruise Conditions



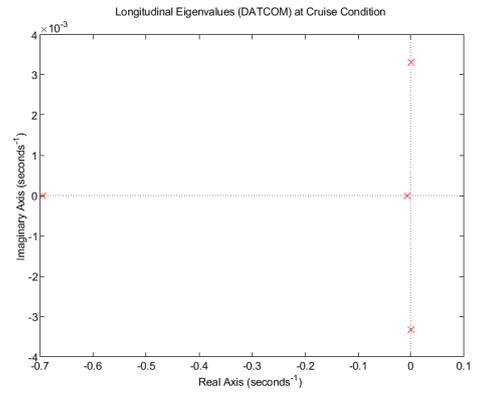
(A) Approach 1 at Take-off Condition



(B) Approach 2 at Take-off Condition



(C) Approach 1 at Cruise Condition



(D) Approach 2 at Cruise Condition

FIGURE 4.6: The Location of Short Period and Phugoid Mode Eigenvalues

The damping ratio that associated with the short period and phugoid mode shown in Table 4.8 will be evaluated in accordance with the Military Specification MIL-F-8785C flying and handling requirements. However, due to instability of the aircraft in longitudinal dynamics the damping associated with the short period and phugoid mode will be evaluated after the implementation of the stability augmentation system.

Lateral Directional Dynamic Stability

The state space model for longitudinal dynamics is given by

$$\begin{aligned} \dot{x}_{Lat Dir} &= A_{Lat Dir} x_{Lat Dir} + B_{Lat Dir} u_{Lat Dir} \\ y_{Lat Dir} &= C_{Lat Dir} x_{Lat Dir} + D_{Lat Dir} u_{Lat Dir} \end{aligned}$$

$$\begin{bmatrix} \dot{\beta} \\ \dot{p} \\ \dot{r} \\ \dot{\phi} \end{bmatrix} = \begin{bmatrix} Y'_\beta & Y'_p & Y'_r & Y'_\phi \\ L'_\beta & L'_p & L'_r & 0 \\ N'_\beta & N'_p & N'_r & 0 \\ 0 & 1 & \tan \Theta_1 & 0 \end{bmatrix} \begin{bmatrix} \beta \\ p \\ r \\ \phi \end{bmatrix} + \begin{bmatrix} Y'_{\delta_A} & Y'_{\delta_R} \\ L'_{\delta_A} & L'_{\delta_R} \\ N'_{\delta_A} & N'_{\delta_R} \\ 0 & 0 \end{bmatrix} \begin{bmatrix} \delta_A \\ \delta_R \end{bmatrix}$$

$$\begin{bmatrix} \dot{\beta} \\ \dot{p} \\ \dot{r} \\ \dot{\phi} \end{bmatrix} = \begin{bmatrix} 1 & 0 & 0 & 0 \\ 0 & 1 & 0 & 0 \\ 0 & 0 & 1 & 0 \\ 0 & 0 & 0 & 1 \end{bmatrix} \begin{bmatrix} \beta \\ p \\ r \\ \phi \end{bmatrix} + \begin{bmatrix} 0 & 0 \\ 0 & 0 \\ 0 & 0 \\ 0 & 0 \end{bmatrix} \begin{bmatrix} \delta_A \\ \delta_R \end{bmatrix}$$

The A and B matrices are evaluated using the Baruna-1 lateral directional dynamics stability and control derivatives based on Table 4.4. The state space model for the lateral directional motion of Baruna-1 is evaluated for take-off and cruise conditions using Approach 1 and Approach 2. Calculating the inputs for both A and B matrices, leads to:

1. The lateral directional dynamics state space model and the lateral directional characteristic equation \bar{D}_2 at take-off condition for Approach 1 is given by

$$\begin{bmatrix} \dot{\beta} \\ \dot{p} \\ \dot{r} \\ \dot{\phi} \end{bmatrix} = \begin{bmatrix} 0.02210210 & -0.00010419 & -0.99233381 & 0.09840341 \\ 0.00000006 & -0.00000079 & 0.00000066 & 0 \\ 0.00000118 & 0 & -0.00000073 & 0 \\ 0 & 1 & 0.36528133 & 0 \end{bmatrix} \begin{bmatrix} \beta \\ p \\ r \\ \phi \end{bmatrix} + \begin{bmatrix} 0 & 0.01241848 \\ 0.00000041 & 0.00000001 \\ -0.00000002 & -0.00000075 \\ 0 & 0 \end{bmatrix} \begin{bmatrix} \delta_A \\ \delta_R \end{bmatrix}$$

$$\vec{D}_2 = s^4 - 0.0221s^3 + 1.139e - 06s^2 - 4.27e - 08s - 1.117e - 13$$

2. The lateral directional dynamics state space model and the lateral directional characteristic equation \vec{D}_2 at take-off condition for Approach 2 is given by

$$\begin{bmatrix} \dot{\beta} \\ \dot{p} \\ \dot{r} \\ \dot{\phi} \end{bmatrix} = \begin{bmatrix} -0.05671969 & 0.00015784 & -0.99263917 & 0.09840340 \\ -0.00000047 & -0.00000039 & 0.00000060 & 0 \\ 0.00000034 & -0.00000011 & 0.30736522 & 0 \\ 0 & 1 & 0.36528163 & 0 \end{bmatrix} \begin{bmatrix} \beta \\ p \\ r \\ \phi \end{bmatrix} + \begin{bmatrix} 0 & 0.01192384 \\ 0.00000035 & 0.00000001 \\ -0.00000002 & -0.00000072 \\ 0 & 0 \end{bmatrix} \begin{bmatrix} \delta_A \\ \delta_R \end{bmatrix}$$

$$\vec{D}_2 = s^4 + 0.05672s^3 + 3.891e - 07s^2 + 5.375e - 08s - 1.449e - 14$$

3. The lateral directional dynamics state space model and the lateral directional characteristic equation \vec{D}_2 at cruise condition for Approach 1 is given by

$$\begin{bmatrix} \dot{\beta} \\ \dot{p} \\ \dot{r} \\ \dot{\phi} \end{bmatrix} = \begin{bmatrix} 0.03422025 & -0.00107908 & -0.99470502 & 0.04765451 \\ -0.00000091 & -0.00000124 & 0.00000048 & 0 \\ 0.00000402 & 0.00000008 & -0.00000049 & 0 \\ 0 & 1 & 0.02347463 & 0 \end{bmatrix} \begin{bmatrix} \beta \\ p \\ r \\ \phi \end{bmatrix} + \begin{bmatrix} 0 & 0.01923683 \\ 0.00000138 & 0.00000072 \\ -0.00000009 & -0.00000258 \\ 0 & 0 \end{bmatrix} \begin{bmatrix} \delta_A \\ \delta_R \end{bmatrix}$$

$$\vec{D}_2 = s^4 - 0.03422s^3 + 3.936e - 06s^2 + 3.887e - 08s - 7.559e - 14$$

4. The lateral directional dynamics state space model and the lateral directional characteristic equation \vec{D}_2 at cruise condition for Approach 2 is given by

$$\begin{bmatrix} \dot{\beta} \\ \dot{p} \\ \dot{r} \\ \dot{\phi} \end{bmatrix} = \begin{bmatrix} -0.08988968 & 0.00053002 & -0.99491594 & 0.04765452 \\ -0.00000221 & -0.00000127 & 0.00000031 & 0 \\ 0.00000128 & 0.00000007 & -0.00000030 & 0 \\ 0 & 1 & 0.02346154 & 0 \end{bmatrix} \begin{bmatrix} \beta \\ p \\ r \\ \phi \end{bmatrix} + \begin{bmatrix} 0 & 0.01847060 \\ 0.00000120 & 0.00000069 \\ -0.00000008 & -0.00000247 \\ 0 & 0 \end{bmatrix} \begin{bmatrix} \delta_A \\ \delta_R \end{bmatrix}$$

$$\vec{D}_2 = s^4 + 0.08989s^3 + 1.414e - 06s^2 + 1.038e - 07s + 1.052e - 14$$

The solution of state space model and characteristic equation for lateral directional dynamics leads to the expression of the Baruna-1's lateral directional transfer functions at take-off and cruise conditions as shown in Table 4.9 and the eigenvalues of the lateral directional characteristic equation are shown in Tab4.10.

As shown in Table 4.10 and Fig. 4.7, the eigenvalues of Baruna-1 for Approach 1 at given flight conditions and for Approach 2 at take-off condition has hasitive signs which described an instability of the aircraft in lateral directional dynamics.

STABILITY ANALYSIS AND CONTROL DESIGN OF BARUNA-1

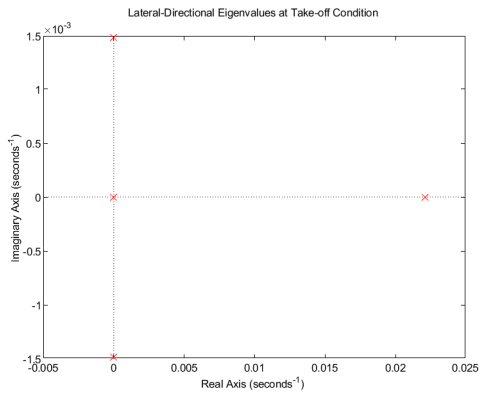
Approach 1			
Take-off		Cruise	
$\beta(s)$	$2e - 08s^2 + 3.921e - 08s + 2.739e - 14$	$\beta(s)$	$8.953e - 08s^2 + 6.586e - 08s + 3.026e - 14$
$\delta_a(s)$	$s^4 - 0.0221s^3 + 1.139e - 06s^2 - 4.87e - 08s - 1.151e - 13$	$\delta_a(s)$	$s^4 - 0.03422s^3 + 3.936e - 06s^2 + 3.887e - 08s - 7.559e - 14$
$p(s)$	$4.059e - 07s^3 - 8.97e - 09s^2 + 4.708e - 13s - 1.728e - 14$	$p(s)$	$1.384e - 06s^3 - 4.736e - 08s^2 + 5.427e - 12s - 6.128e - 15$
$\delta_o(s)$	$s^4 - 0.0221s^3 + 1.139e - 06s^2 - 4.87e - 08s - 1.151e - 13$	$\delta_o(s)$	$s^4 - 0.03422s^3 + 3.936e - 06s^2 + 3.887e - 08s - 7.559e - 14$
$r(s)$	$-2.02e - 08s^3 + 4.463e - 10s^2 + 3.469e - 16s + 4.732e - 14$	$r(s)$	$-9.151e - 08s^3 + 3.131e - 09s^2 - 5.785e - 15s + 2.611e - 13$
$\delta_s(s)$	$s^4 - 0.0221s^3 + 1.139e - 06s^2 - 4.87e - 08s - 1.151e - 13$	$\delta_s(s)$	$s^4 - 0.03422s^3 + 3.936e - 06s^2 + 3.887e - 08s - 7.559e - 14$
$\phi(s)$	$3.985e - 07s^2 - 8.807e - 09s + 4.71e - 13$	$\phi(s)$	$1.382e - 06s^2 - 4.729e - 08s + 5.427e - 12$
$\delta_i(s)$	$s^4 - 0.0221s^3 + 1.139e - 06s^2 - 4.87e - 08s - 1.151e - 13$	$\delta_i(s)$	$s^4 - 0.03422s^3 + 3.936e - 06s^2 + 3.887e - 08s - 7.559e - 14$
$\beta(s)$	$0.01242s^3 + 7.599e - 07s^2 - 2.574e - 08s - 6.907e - 14$	$\beta(s)$	$0.01924s^3 + 2.595e - 06s^2 + 3.129e - 08s - 4.534e - 14$
$\delta_r(s)$	$s^4 - 0.0221s^3 + 1.139e - 06s^2 - 4.87e - 08s - 1.151e - 13$	$\delta_r(s)$	$s^4 - 0.03422s^3 + 3.936e - 06s^2 + 3.887e - 08s - 7.559e - 14$
$p(s)$	$1.115e - 08s^3 + 5.392e - 10s^2 + 8.099e - 14s - 2.173e - 15$	$p(s)$	$7.171e - 07s^3 - 4.204e - 08s^2 + 5.92e - 13s - 6.002e - 16$
$\delta_e(s)$	$s^4 - 0.0221s^3 + 1.139e - 06s^2 - 4.87e - 08s - 1.151e - 13$	$\delta_e(s)$	$s^4 - 0.03422s^3 + 3.936e - 06s^2 + 3.887e - 08s - 7.559e - 14$
$r(s)$	$-7.467e - 07s^3 + 3.118e - 08s^2 + 2.471e - 14s + 5.948e - 15$	$r(s)$	$-2.577e - 06s^3 + 1.655e - 07s^2 + 2.008e - 13s + 2.557e - 14$
$\delta_c(s)$	$s^4 - 0.0221s^3 + 1.139e - 06s^2 - 4.87e - 08s - 1.151e - 13$	$\delta_c(s)$	$s^4 - 0.03422s^3 + 3.936e - 06s^2 + 3.887e - 08s - 7.559e - 14$
$\phi(s)$	$-2.616e - 07s^2 + 1.193e - 08s + 9.002e - 14$	$\phi(s)$	$6.566e - 07s^2 - 3.816e - 08s + 5.967e - 13$
$\delta_r(s)$	$s^4 - 0.0221s^3 + 1.139e - 06s^2 - 4.87e - 08s - 1.151e - 13$	$\delta_r(s)$	$s^4 - 0.03422s^3 + 3.936e - 06s^2 + 3.887e - 08s - 7.559e - 14$

Approach 2			
Take-off		Cruise	
$\beta(s)$	$1.743e - 08s^2 + 3.391e - 08s + 4.57e - 15$	$\beta(s)$	$8.301e - 08s^2 + 5.696e - 08s + 1.569e - 14$
$\delta_a(s)$	$s^4 + 0.05672s^3 + 3.891e - 07s^2 + 5.078e - 08s - 1.544e - 14$	$\delta_a(s)$	$s^4 + 0.08989s^3 + 1.414e - 06s^2 + 1.038e - 07s + 1.052e - 14$
$p(s)$	$3.51e - 07s^3 + 1.991e - 08s^2 + 1.17e - 13s - 4.106e - 15$	$p(s)$	$1.197e - 06s^3 + 1.076e - 07s^2 + 1.37e - 12s - 1.506e - 15$
$\delta_o(s)$	$s^4 + 0.05672s^3 + 3.891e - 07s^2 + 5.078e - 08s - 1.544e - 14$	$\delta_o(s)$	$s^4 + 0.08989s^3 + 1.414e - 06s^2 + 1.038e - 07s + 1.052e - 14$
$r(s)$	$-1.751e - 08s^3 - 9.931e - 10s^2 - 2.593e - 15s + 1.124e - 14$	$r(s)$	$-8.279e - 08s^3 - 7.442e - 09s^2 - 1.736e - 15s + 6.42e - 14$
$\delta_s(s)$	$s^4 + 0.05672s^3 + 3.891e - 07s^2 + 5.078e - 08s - 1.544e - 14$	$\delta_s(s)$	$s^4 + 0.08989s^3 + 1.414e - 06s^2 + 1.038e - 07s + 1.052e - 14$
$\phi(s)$	$3.446e - 07s^2 + 1.954e - 08s + 1.16e - 13$	$\phi(s)$	$1.195e - 06s^2 + 1.074e - 07s + 1.37e - 12$
$\delta_i(s)$	$s^4 + 0.05672s^3 + 3.891e - 07s^2 + 5.078e - 08s - 1.544e - 14$	$\delta_i(s)$	$s^4 + 0.08989s^3 + 1.414e - 06s^2 + 1.038e - 07s + 1.052e - 14$
$\beta(s)$	$0.01192s^3 + 7.188e - 07s^2 - 2.472e - 08s - 5.239e - 14$	$\beta(s)$	$0.01847s^3 + 2.491e - 06s^2 + 3.005e - 08s - 3.069e - 14$
$\delta_r(s)$	$s^4 + 0.05672s^3 + 3.891e - 07s^2 + 5.078e - 08s - 1.544e - 14$	$\delta_r(s)$	$s^4 + 0.08989s^3 + 1.414e - 06s^2 + 1.038e - 07s + 1.052e - 14$
$p(s)$	$1.069e - 08s^3 - 7.106e - 09s^2 - 4.799e - 13s + 1.653e - 14$	$p(s)$	$6.885e - 07s^3 + 2.111e - 08s^2 - 4.616e - 12s + 5.124e - 15$
$\delta_e(s)$	$s^4 + 0.05672s^3 + 3.891e - 07s^2 + 5.078e - 08s - 1.544e - 14$	$\delta_e(s)$	$s^4 + 0.08989s^3 + 1.414e - 06s^2 + 1.038e - 07s + 1.052e - 14$
$r(s)$	$-7.17e - 07s^3 - 3.64e - 08s^2 - 1.337e - 14s - 4.525e - 14$	$r(s)$	$-2.474e - 06s^3 - 1.988e - 07s^2 - 2.542e - 13s - 2.184e - 13$
$\delta_c(s)$	$s^4 + 0.05672s^3 + 3.891e - 07s^2 + 5.078e - 08s - 1.544e - 14$	$\delta_c(s)$	$s^4 + 0.08989s^3 + 1.414e - 06s^2 + 1.038e - 07s + 1.052e - 14$
$\phi(s)$	$-2.512e - 07s^2 - 2.04e - 08s - 4.848e - 13$	$\phi(s)$	$6.305e - 07s^2 + 1.644e - 08s - 4.622e - 12$
$\delta_r(s)$	$s^4 + 0.05672s^3 + 3.891e - 07s^2 + 5.078e - 08s - 1.544e - 14$	$\delta_r(s)$	$s^4 + 0.08989s^3 + 1.414e - 06s^2 + 1.038e - 07s + 1.052e - 14$

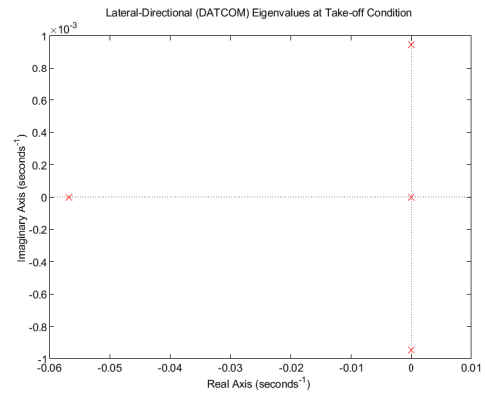
TABLE 4.9: Lateral Directional Transfer Function of Baruna-1 at Take-off and Cruise Conditions

Take-off		Cruise	
Approach 1	Approach 2	Approach 1	Approach 2
0.02214845	-0.05672921	0.03406950	-0.08988837
-0.00002275 + 0.00148268i	0.00000431 + 0.00094613i	0.00114431	-0.00000139 + 0.00107458i
-0.00002275 - 0.00148268i	0.00000431 - 0.00094613i	-0.00099723	-0.00000139 - 0.00107458i
-0.00000236	0.00000030	0.00000194	-0.00000010

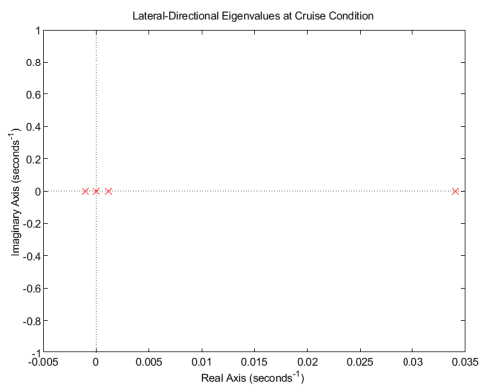
TABLE 4.10: Lateral Directional Eigenvalues of Baruna-1 at Take-off and Cruise Conditions



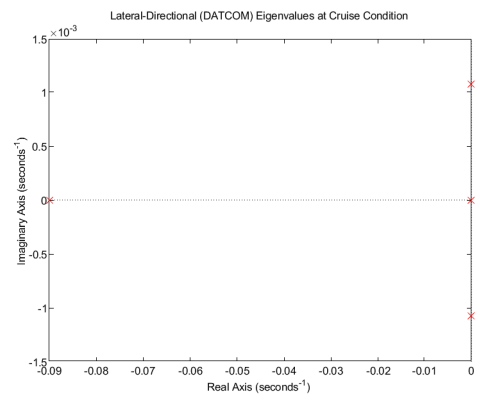
(A) Approach 1 at Take-off Condition



(B) Approach 2 at Take-off Condition



(C) Approach 1 at Cruise Condition



(D) Approach 2 at Cruise Condition

FIGURE 4.7: The Location of Dutch Roll, Rolling and Spiral Mode Eigenvalues

However, for Approach 2 at cruise condition, the negative sign of the eigenvalues indicated that the aircraft is lateral directional dynamically stable. Based on the result, the stability augmentation system will be implemented for both Approach 1 and Approach 2 at take-off and cruise conditions to stabilize the aircraft and improve the dynamic stability characteristic of Baruna-1.

The damping ratio, natural frequency and time constant that associated with the dutch roll, spiral and roll mode shown in Table 4.8 will be evaluated in accordance with the American Military Specification MIL-F-8785C flying and handling requirements. However, due to instability of the aircraft in longitudinal dynamics the damping associated with the short period and phugoid mode will be evaluated after the implementation of the stability augmentation system.

4.4 Application of Stability Augmentation System for Dynamics Stability

The stability augmentation system is applied to the open loop state space model by using a feedback control gain K . The lqr control technique is used to obtain the optimal value of feedback gain K , and once the optimal feedback gains K are obtained, these value are implemented to the state space model by modifying the A matrix as expressed below.

$$\begin{aligned}\dot{x}(t) &= [A - BK]x(t) + Bv(t) \\ y(t) &= [C - DK]x(t) + Dv(t)\end{aligned}$$

which will be implemented for both longitudinal and lateral directional dynamics stability.

4.4.1 Application of Stability Augmentation System for Longitudinal Dynamics Stability

The implementation of lqr control technique to find the optimum feedback control gain k starting from choosing the value of weighting matrices Q and R . The

longitudinal weighting matrices Q and R for Approach 1 and Approach 2 at take-off and cruise conditions are given below, with only one variation of Q and R matrices is applied for both methods at given flight conditions.

$$Q_{long} = \begin{bmatrix} 0.001 & 0 & 0 & 0 \\ 0 & 0.001 & 0 & 0 \\ 0 & 0 & 1000 & 0 \\ 0 & 0 & 0 & 0.0001 \end{bmatrix} \quad R_{long} = \begin{bmatrix} 0.1 \end{bmatrix}$$

The optimum feedback gains K based on the lqr control technique for longitudinal dynamic at take-off and cruise condition for both Approach 1 and Approach 2 are given by

$$K_{long} = \begin{bmatrix} K_u & K_\alpha & K_q & K_\theta \end{bmatrix}$$

1. K for Approach 1 at Take-off Condition:

$$K_{long} = \begin{bmatrix} -0.027835 & -0.165134 & -6742.927300 & -34.957959 \end{bmatrix}$$

2. K for Approach 2 at Take-off Condition:

$$K_{long} = \begin{bmatrix} -0.037600 & -0.623785 & -5046.454980 & -15.754154 \end{bmatrix}$$

3. K for Approach 1 at Cruise Condition:

$$K_{long} = \begin{bmatrix} 0.035912 & 0.459389 & -7419.644823 & -95.031537 \end{bmatrix}$$

4. K for Approach 2 at Cruise Condition:

$$K_{long} = \begin{bmatrix} 0.054420 & 0.381428 & -6663.661927 & -96.344211 \end{bmatrix}$$

The implementation of feedback control gains K to the state space model for Longitudinal Dynamic Stability leads to the closed loop transfer functions, closed loop characteristic equations and the closed loop eigenvalues. The longitudinal closed loop transfer functions are given in Table 4.11 for Approach 1 and Approach 2.

STABILITY ANALYSIS AND CONTROL DESIGN OF BARUNA-1

Approach 1			
Take-off		Cruise	
$\frac{u(s)}{\delta_e(s)}$	$\frac{-0.1205s^2 + 1.273e - 05s + 1.024e - 05}{s^4 + 0.4938s^3 + 0.02432s^2 + 0.000268s + 1.03e - 06}$	$\frac{u(s)}{\delta_e(s)}$	$\frac{-0.1871s^2 + 4.874e - 05s + 5.446e - 05}{s^4 + 0.7623s^3 + 0.03966s^2 + 0.0007969s + 5.447e - 06}$
$\frac{\alpha(s)}{\delta_e(s)}$	$\frac{-0.02698s^3 - 0.0001892s^2 + 7.727e - 08s - 5.472e - 08}{s^4 + 0.4938s^3 + 0.02432s^2 + 0.000268s + 1.03e - 06}$	$\frac{\alpha(s)}{\delta_e(s)}$	$\frac{-0.0419s^3 - 0.0001023s^2 - 9.866e - 09s - 5.154e - 08}{s^4 + 0.7623s^3 + 0.03966s^2 + 0.0007969s + 5.447e - 06}$
$\frac{q(s)}{\delta_e(s)}$	$\frac{-2.655e - 06s^3 - 1.084e - 06s^2 - 3.421e - 08s - 1.077e - 28}{s^4 + 0.4938s^3 + 0.02432s^2 + 0.000268s + 1.03e - 06}$	$\frac{q(s)}{\delta_e(s)}$	$\frac{-9.06e - 06s^3 - 5.569e - 06s^2 - 3.584e - 08s - 2.402e - 29}{s^4 + 0.7623s^3 + 0.03966s^2 + 0.0007969s + 5.447e - 06}$
$\frac{\theta(s)}{\delta_e(s)}$	$\frac{-2.655e - 06s^3 - 1.084e - 06s^2 - 3.421e - 08}{s^4 + 0.4938s^3 + 0.02432s^2 + 0.000268s + 1.03e - 06}$	$\frac{\theta(s)}{\delta_e(s)}$	$\frac{-9.06e - 06s^3 - 5.569e - 06s^2 - 3.584e - 08}{s^4 + 0.7623s^3 + 0.03966s^2 + 0.0007969s + 5.447e - 06}$
$\frac{\delta_e(s)}{\delta_e(s)}$	$\frac{s^4 + 0.4938s^3 + 0.02432s^2 + 0.000268s + 1.03e - 06}{s^4 + 0.4938s^3 + 0.02432s^2 + 0.000268s + 1.03e - 06}$	$\frac{\delta_e(s)}{\delta_e(s)}$	$\frac{s^4 + 0.7623s^3 + 0.03966s^2 + 0.0007969s + 5.447e - 06}{s^4 + 0.7623s^3 + 0.03966s^2 + 0.0007969s + 5.447e - 06}$
Approach 2			
Take-off		Cruise	
$\frac{u(s)}{\delta_e(s)}$	$\frac{-0.1592s^2 + 7.185e - 06s + 5.684e - 06}{s^4 + 0.338s^3 + 0.02629s^2 + 0.00021s + 5.851e - 07}$	$\frac{u(s)}{\delta_e(s)}$	$\frac{-0.09843s^2 + 6.099e - 05s + 4.986e - 05}{s^4 + 0.7396s^3 + 0.03253s^2 + 0.0006498s + 4.986e - 06}$
$\frac{\alpha(s)}{\delta_e(s)}$	$\frac{-0.02503s^3 - 0.0002162s^2 + 6.754e - 08s - 5.019e - 08}{s^4 + 0.338s^3 + 0.02629s^2 + 0.00021s + 5.851e - 07}$	$\frac{\alpha(s)}{\delta_e(s)}$	$\frac{-0.03879s^3 - 0.0001331s^2 - 1.734e - 08s - 2.623e - 08}{s^4 + 0.7396s^3 + 0.03253s^2 + 0.0006498s + 4.986e - 06}$
$\frac{q(s)}{\delta_e(s)}$	$\frac{-2.457e - 06s^3 - 5.769e - 07s^2 - 3.991e - 08s + 1.377e - 28}{s^4 + 0.338s^3 + 0.02629s^2 + 0.00021s + 5.851e - 07}$	$\frac{q(s)}{\delta_e(s)}$	$\frac{-8.366e - 06s^3 - 5.108e - 06s^2 - 2.315e - 08s - 9.133e - 29}{s^4 + 0.7396s^3 + 0.03253s^2 + 0.0006498s + 4.986e - 06}$
$\frac{\theta(s)}{\delta_e(s)}$	$\frac{-2.457e - 06s^3 - 5.769e - 07s^2 - 3.991e - 08}{s^4 + 0.338s^3 + 0.02629s^2 + 0.00021s + 5.851e - 07}$	$\frac{\theta(s)}{\delta_e(s)}$	$\frac{-8.366e - 06s^3 - 5.108e - 06s^2 - 2.315e - 08}{s^4 + 0.7396s^3 + 0.03253s^2 + 0.0006498s + 4.986e - 06}$
$\frac{\delta_e(s)}{\delta_e(s)}$	$\frac{s^4 + 0.338s^3 + 0.02629s^2 + 0.00021s + 5.851e - 07}{s^4 + 0.338s^3 + 0.02629s^2 + 0.00021s + 5.851e - 07}$	$\frac{\delta_e(s)}{\delta_e(s)}$	$\frac{s^4 + 0.7396s^3 + 0.03253s^2 + 0.0006498s + 4.986e - 06}{s^4 + 0.7396s^3 + 0.03253s^2 + 0.0006498s + 4.986e - 06}$

TABLE 4.11: Longitudinal State Feedback Transfer Function of Baruna-1 at Take-off and Cruise Conditions

The closed loop longitudinal characteristic equations for Approach 1 and Approach 2 at given flight conditions are expressed below.

1. Approach 1 at Take-off Condition:

$$\vec{D}_{1aug} = s^4 + 0.4938s^3 + 0.02432s^2 + 0.000268s + 0.00000103$$

2. Approach 2 at Take-off Condition:

$$\vec{D}_{1aug} = s^4 + 0.338s^3 + 0.02629s^2 + 0.00021s + 0.0000005851$$

3. Approach 1 at Cruise Condition:

$$\vec{D}_{1aug} = s^4 + 0.7623s^3 + 0.03966s^2 + 0.0007969s + 0.000005447$$

4. Approach 2 at Cruise Condition:

$$\vec{D}_{1aug} = s^4 + 0.7396s^3 + 0.03253s^2 + 0.0006498s + 0.000004986$$

As shown in Table 4.12 and shown in Fig. 4.8, all of the eigenvalues of the closed loop longitudinal characteristic equation are had a negative sign and located on the

left side of the axis. This indicates that the application of the optimum feedback control gains to the state space model using lqr control technique leads the aircraft to be longitudinal dynamically stable.

Take-off		Cruise	
Approach 1	Approach 2	Approach 1	Approach 2
-0.43985345	-0.22540743	-0.70786706	-0.69404726
-0.04039713	-0.10393529	-0.02018116 + 0.01178961i	-0.014913801 + 0.01533393i
-0.00675742 + 0.00350988i	-0.00430658 + 0.00253574i	-0.02018116 - 0.01178961i	-0.014913801 - 0.01533393i
-0.00675742 - 0.00350988i	-0.00430658 - 0.00253574i	-0.01408724	-0.01570179

TABLE 4.12: Longitudinal State Feedback Eigenvalues of Baruna-1 at Take-off and Cruise Conditions

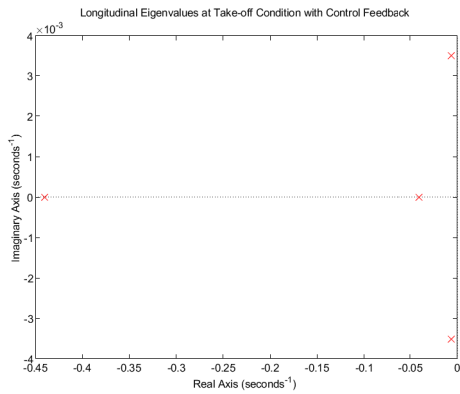
The dynamic's behaviour of the short period and phugoid mode for the closed loop longitudinal transfer functions are highlighted in the aircraft time response due to step inputs as shown below.

The plots in Fig. 4.9 represent the changes of the velocity in accordance with the trim condition following a 1° elevator step input. At take-off condition as shown in Fig. 4.9a and Fig. 4.9b, the velocity initially decreases and converges to the value of nearly 10 m/s at 1000 s and 1600 s respectively. At cruise condition, as shown in Fig. 4.9c and Fig. 4.9d, the velocity converge to the value of 10 m/s at 500 s and 450 s respectively.

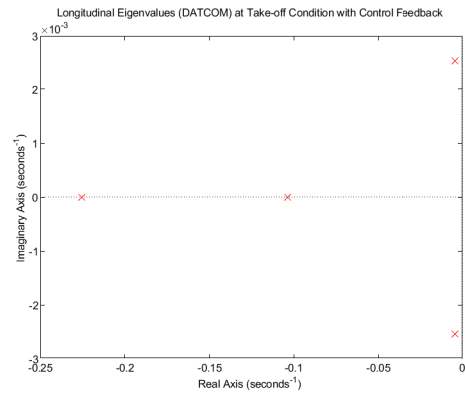
The plots in Fig. 4.10 represent the changes of the angle of attack in accordance with the trim condition following a 1° elevator step input. At take-off condition as shown in Fig. 4.10a and Fig. 4.10b the short period mode occur in less than 10 s and the angle of attack converges to the value of -0.0531 rads and -0.088 rads respectively. At cruise condition as shown in Fig. 4.10c and Fig. 4.10d, the short period mode occur in less than 10 s and the angle of attack converges to the value of -0.01 rads and -0.005 rads respectively.

The plots in Fig. 4.11 represent the changes of the pitch rate in accordance with the trim condition following a 1° elevator step input. At all conditions, the pitch rate initially decreases and converges to the initial trim condition at 1000 s (Fig. 4.11a) and 1600 s (Fig. 4.11b) at take-off condition, and at 500 s (Fig. 4.11c) and 450 s (Fig. 4.11d) at cruise condition.

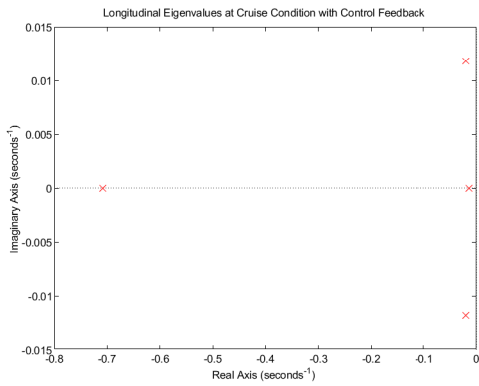
The plots in Fig. 4.12 represent the changes of the pitch angle in accordance with the trim condition following a 1° elevator step input. At take-off condition



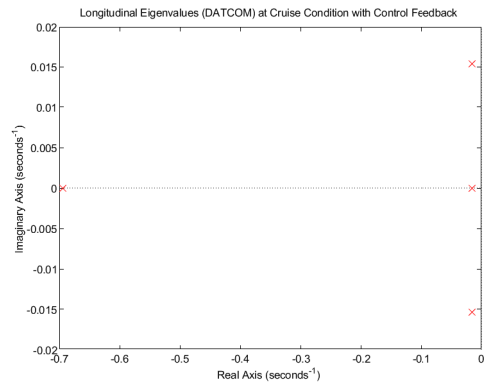
(A) Approach 1 at Take-off Condition



(B) Approach 2 at Take-off Condition

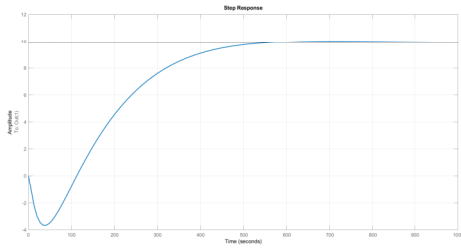


(C) Approach 1 at Cruise Condition

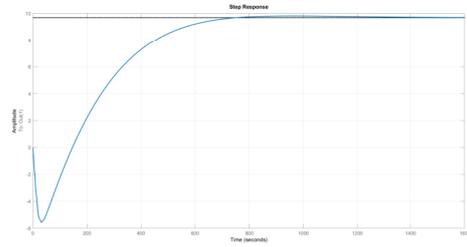


(D) Approach 2 at Cruise Condition

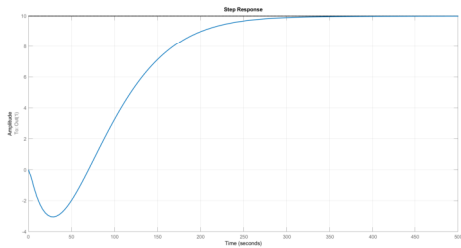
FIGURE 4.8: The Location of Short Period and Phugoid Mode State Feedback Eigenvalues



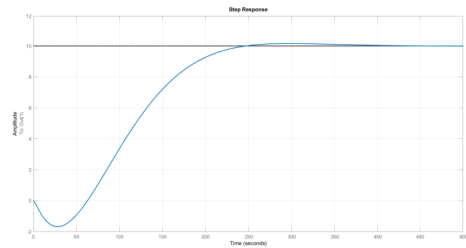
(A) Approach 1 at Take-off Condition



(B) Approach 2 at Take-off Condition

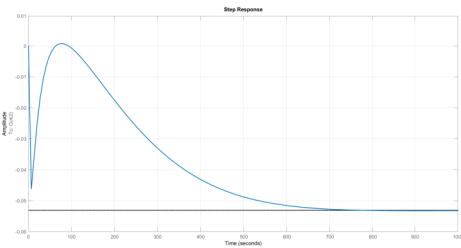


(C) Approach 1 at Cruise Condition

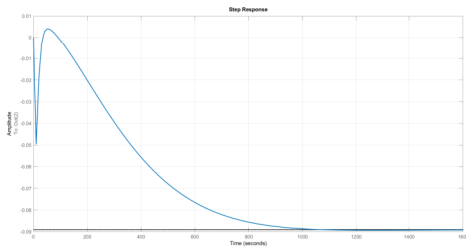


(D) Approach 2 at Cruise Condition

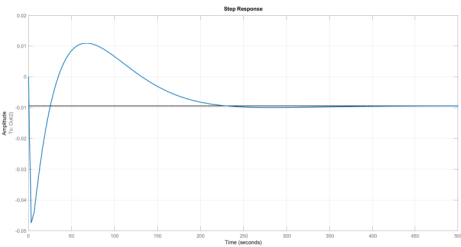
FIGURE 4.9: The Response of Speed Perturbation $u(s)$ to Elevator $\delta_e(s)$ Step Input



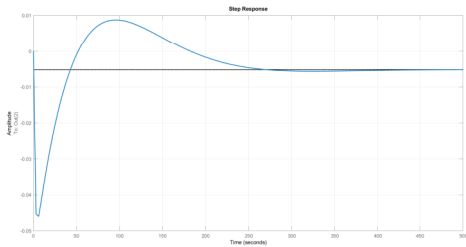
(A) Approach 1 at Take-off Condition



(B) Approach 2 at Take-off Condition

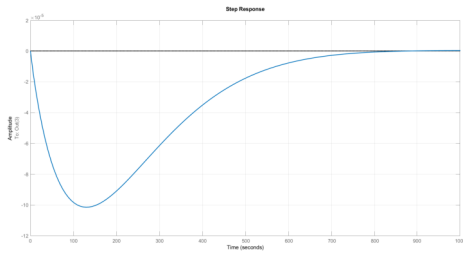


(C) Approach 1 at Cruise Condition

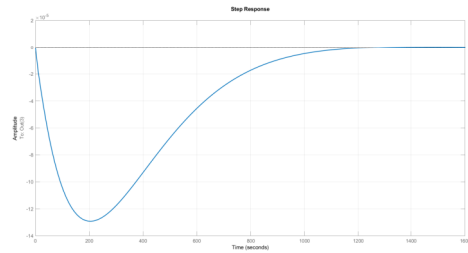


(D) Approach 2 at Cruise Condition

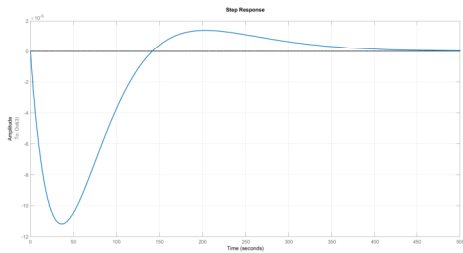
FIGURE 4.10: The Response of Angle of Attack $\alpha(s)$ to Elevator $\delta_e(s)$ Step Input



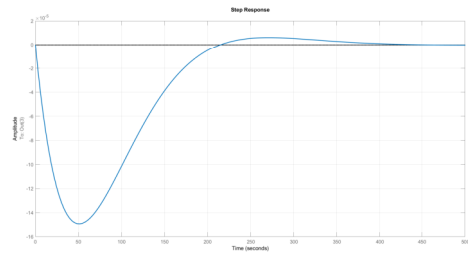
(A) Approach 1 at Take-off Condition



(B) Approach 2 at Take-off Condition

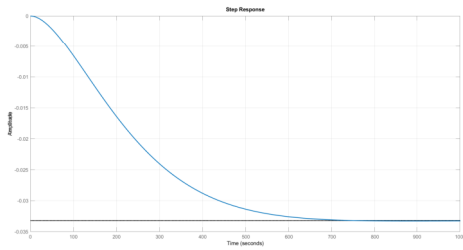


(C) Approach 1 at Cruise Condition

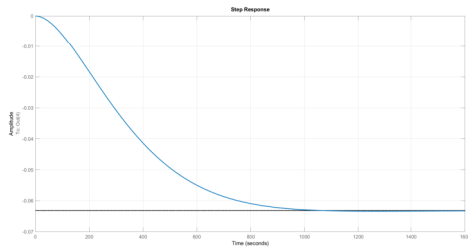


(D) Approach 2 at Cruise Condition

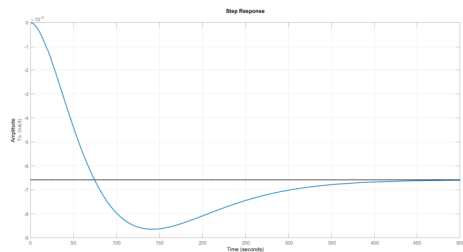
FIGURE 4.11: The Response of Pitch Rate $q(s)$ to Elevator $\delta_e(s)$ Step Input



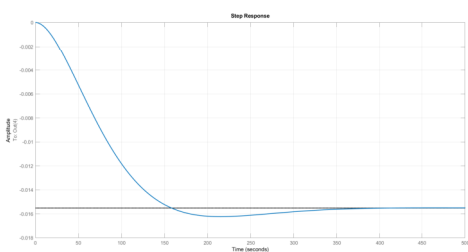
(A) Approach 1 at Take-off Condition



(B) Approach 2 at Take-off Condition



(C) Approach 1 at Cruise Condition



(D) Approach 2 at Cruise Condition

FIGURE 4.12: The Response of Pitch Angle $\theta(s)$ to Elevator $\delta_e(s)$ Step Input

as shown in Fig. 4.12a and Fig. 4.12b the pitch angle decreases and converges to the value of -0.0332 rads and -0.0682 at 1000 s and 1600 s respectively. At cruise condition as shown in Fig. 4.12c and Fig. 4.12d, the pitch angle decreases to the value of ± 0.0085 rads following an increment of the pitch angle to the value of -0.00658 rads and -0.00464 rads at 500 s and 450 s respectively.

The damping ratio for the closed loop longitudinal dynamics that associated with the short period and phugoid modes as shown in Table 4.13 will be evaluated based on the regulation available in the Military specification MIL-F-8785C to satisfy the level of flying qualities.

Parameter	Take-off		Cruise	
	Approach 1	Approach 2	Approach 1	Approach 2
ω_{SP}	0.439853	0.225407	0.707867	0.694047
ζ_{SP}	1.000000	1.000000	1.000000	1.000000
ω_{PH}	0.007615	0.004998	0.023373	0.021390
ζ_{PH}	0.887430	0.861719	0.863457	0.697218
ω_{DR}	0.006473	0.006137	0.010799	0.010255
ζ_{DR}	0.603028	0.595956	0.772421	0.755838
T_R	0.080524	0.083863	0.051979	0.054135
T_{2s}	121.038523	125.799247	93.208810	97.244902

TABLE 4.13: The State Feedback Natural Frequency ω , Damping ζ and Time Constant T of Baruna-1 at Take-off and Cruise Conditions

4.4.2 Application of Stability Augmentation System for Lateral Directional Dynamics Stability

The lateral directional weighting matrices Q and R for Approach 1 and Approach 2 at take-off and cruise conditions are given below, with only one variation of Q and R matrices is applied for both methods at given flight conditions.

$$Q_{latdir} = \begin{bmatrix} 0.1 & 0 & 0 & 0 \\ 0 & 1 & 0 & 0 \\ 0 & 0 & 1000 & 0 \\ 0 & 0 & 0 & 0.00001 \end{bmatrix} \quad R_{latdir} = [0.0000001]$$

The result of the optimum feedback gains K based on the lqr control technique for lateral directional dynamic for both Approach 1 and Approach 2 at given flight condition are given by

$$K_{latdir} = \begin{bmatrix} K_{\beta_{\delta_a}} & K_{p_{\delta_a}} & K_{r_{\delta_a}} & K_{\phi_{\delta_a}} \\ K_{\beta_{\delta_r}} & K_{p_{\delta_r}} & K_{r_{\delta_r}} & K_{\phi_{\delta_r}} \end{bmatrix}$$

1. K for Approach 1 at Take-off Condition:

$$K_{latdir} = \begin{bmatrix} 6.694420 & 38688.536443 & 111523.511303 & 219.610515 \\ 1002.341585 & 1162.140829 & 8924.289044 & 18.109771 \end{bmatrix}$$

2. K for Approach 2 at Take-off Condition:

$$K_{latdir} = \begin{bmatrix} 6.676616 & 41845.288800 & 112165.712855 & 228.523342 \\ 994.481572 & -1688.958001 & -13321.321424 & -5.947193 \end{bmatrix}$$

3. K for Approach 1 at Cruise Condition:

$$K_{latdir} = \begin{bmatrix} 11.860187 & 23462.124357 & 94725.471652 & 167.372508 \\ 1004.624386 & 2038.332789 & 21008.812310 & 21.711838 \end{bmatrix}$$

4. K for Approach 2 at Cruise Condition:

$$K_{latdir} = \begin{bmatrix} 11.386859 & 24904.632848 & 92282.742248 & 170.589922 \\ 991.346182 & -2776.902321 & -29987.348457 & -22.859238 \end{bmatrix}$$

The implementation of feedback control gains K to the state space model for Lateral Directional Dynamic Stability leads to the closed loop transfer functions, closed loop characteristic equations and the closed loop eigenvalues. The lateral directional closed loop transfer functions are given in Table 4.14 for Approach 1 and Approach 2.

The closed loop lateral directional characteristic equations for Approach 1 and Approach 2 at given flight conditions are expressed below.

STABILITY ANALYSIS AND CONTROL DESIGN OF BARUNA-1

Approach 1			
Take-off		Cruise	
$\beta(s)$	$-3.599e - 06s^2 - 5.076e - 08s - 2.588e - 10$	$\beta(s)$	$-1.72e - 05s^2 - 5.184e - 07s - 3.573e - 09$
$\delta_a(s)$	$s^4 + 12.43s^3 + 0.1682s^2 + 0.001076s + 2.98e - 06$	$\delta_a(s)$	$s^4 + 19.26s^3 + 0.4643s^2 + 0.004631s + 1.668e - 05$
$p(s)$	$4.059e - 07s^3 + 5.04e - 06s^2 + 4.163e - 10s - 1.084e - 11$	$p(s)$	$1.384e - 06s^3 + 2.663e - 05s^2 + 8.245e - 09s - 3.826e - 12$
$\delta_a(s)$	$s^4 + 12.43s^3 + 0.1682s^2 + 0.001076s + 2.98e - 06$	$\delta_a(s)$	$s^4 + 19.26s^3 + 0.4643s^2 + 0.004631s + 1.668e - 05$
$r(s)$	$-2.02e - 08s^3 - 2.506e - 07s^2 - 9.489e - 12s + 2.969e - 11$	$r(s)$	$-9.151e - 08s^3 - 1.758e - 06s^2 - 3.869e - 10s + 1.63e - 10$
$\delta_a(s)$	$s^4 + 12.43s^3 + 0.1682s^2 + 0.001076s + 2.98e - 06$	$\delta_a(s)$	$s^4 + 19.26s^3 + 0.4643s^2 + 0.004631s + 1.668e - 05$
$\phi(s)$	$3.985e - 07s^2 + 4.949e - 06s + 4.128e - 10$	$\phi(s)$	$1.382e - 06s^2 + 2.659e - 05s + 8.236e - 09$
$\delta_a(s)$	$s^4 + 12.43s^3 + 0.1682s^2 + 0.001076s + 2.98e - 06$	$\delta_a(s)$	$s^4 + 19.26s^3 + 0.4643s^2 + 0.004631s + 1.668e - 05$
$\beta(s)$	$0.01242s^3 + 0.0001678s^2 + 1.073e - 06s + 2.969e - 09$	$\beta(s)$	$0.01924s^3 + 0.0004606s^2 + 4.563e - 06s + 1.63e - 08$
$\delta_r(s)$	$s^4 + 12.43s^3 + 0.1682s^2 + 0.001076s + 2.98e - 06$	$\delta_r(s)$	$s^4 + 19.26s^3 + 0.4643s^2 + 0.004631s + 1.668e - 05$
$p(s)$	$1.115e - 08s^3 + 5.708e - 10s^2 - 1.39e - 09s - 9.452e - 13$	$p(s)$	$7.171e - 07s^3 - 2.622e - 08s^2 - 2.136e - 08s - 8.389e - 13$
$\delta_r(s)$	$s^4 + 12.43s^3 + 0.1682s^2 + 0.001076s + 2.98e - 06$	$\delta_r(s)$	$s^4 + 19.26s^3 + 0.4643s^2 + 0.004631s + 1.668e - 05$
$r(s)$	$-7.467e - 07s^3 + 2.114e - 08s^2 + 4.235e - 10s + 2.588e - 12$	$r(s)$	$-2.577e - 06s^3 + 1.042e - 07s^2 + 4.697e - 09s + 3.574e - 11$
$\delta_r(s)$	$s^4 + 12.43s^3 + 0.1682s^2 + 0.001076s + 2.98e - 06$	$\delta_r(s)$	$s^4 + 19.26s^3 + 0.4643s^2 + 0.004631s + 1.668e - 05$
$\phi(s)$	$-2.616e - 07s^2 + 8.292e - 09s - 1.235e - 09$	$\phi(s)$	$6.566e - 07s^2 - 2.377e - 08s - 2.125e - 08$
$\delta_r(s)$	$s^4 + 12.43s^3 + 0.1682s^2 + 0.001076s + 2.98e - 06$	$\delta_r(s)$	$s^4 + 19.26s^3 + 0.4643s^2 + 0.004631s + 1.668e - 05$
Approach 2			
Take-off		Cruise	
$\beta(s)$	$4.209e - 06s^2 + 5.818e - 08s + 3.167e - 10$	$\beta(s)$	$8.301e - 08s^2 + 5.696e - 08s + 1.569e - 14$
$\delta_a(s)$	$s^4 + 11.94s^3 + 0.153s^2 + 0.0009299s + 2.475e - 06$	$\delta_a(s)$	$s^4 + 0.08989s^3 + 1.414e - 06s^2 + 1.038e - 07s + 1.052e - 14$
$p(s)$	$3.51e - 07s^3 + 4.185e - 06s^2 + 4.215e - 10s - 8.964e - 12$	$p(s)$	$1.197e - 06s^3 + 1.076e - 07s^2 + 1.37e - 12s - 1.506e - 15$
$\delta_a(s)$	$s^4 + 11.94s^3 + 0.153s^2 + 0.0009299s + 2.475e - 06$	$\delta_a(s)$	$s^4 + 0.08989s^3 + 1.414e - 06s^2 + 1.038e - 07s + 1.052e - 14$
$r(s)$	$-1.751e - 08s^3 - 2.09e - 07s^2 - 2.379e - 11s + 2.454e - 11$	$r(s)$	$-8.279e - 08s^3 - 7.442e - 09s^2 - 1.736e - 15s + 6.42e - 14$
$\delta_a(s)$	$s^4 + 11.94s^3 + 0.153s^2 + 0.0009299s + 2.475e - 06$	$\delta_a(s)$	$s^4 + 0.08989s^3 + 1.414e - 06s^2 + 1.038e - 07s + 1.052e - 14$
$\phi(s)$	$3.446e - 07s^2 + 4.109e - 06s + 4.128e - 10$	$\phi(s)$	$1.195e - 06s^2 + 1.074e - 07s + 1.37e - 12$
$\delta_a(s)$	$s^4 + 11.94s^3 + 0.153s^2 + 0.0009299s + 2.475e - 06$	$\delta_a(s)$	$s^4 + 0.08989s^3 + 1.414e - 06s^2 + 1.038e - 07s + 1.052e - 14$
$\beta(s)$	$0.01192s^3 + 0.0001524s^2 + 9.246e - 07s + 2.454e - 09$	$\beta(s)$	$0.01847s^3 + 2.491e - 06s^2 + 3.005e - 08s - 3.069e - 14$
$\delta_r(s)$	$s^4 + 11.94s^3 + 0.153s^2 + 0.0009299s + 2.475e - 06$	$\delta_r(s)$	$s^4 + 0.08989s^3 + 1.414e - 06s^2 + 1.038e - 07s + 1.052e - 14$
$p(s)$	$1.069e - 08s^3 - 6.844e - 09s^2 + 1.466e - 09s + 1.154e - 12$	$p(s)$	$6.885e - 07s^3 + 2.111e - 08s^2 - 4.616e - 12s + 5.124e - 15$
$\delta_r(s)$	$s^4 + 11.94s^3 + 0.153s^2 + 0.0009299s + 2.475e - 06$	$\delta_r(s)$	$s^4 + 0.08989s^3 + 1.414e - 06s^2 + 1.038e - 07s + 1.052e - 14$
$r(s)$	$-7.17e - 07s^3 - 4.553e - 08s^2 - 5.973e - 10s - 3.158e - 12$	$r(s)$	$-2.474e - 06s^3 - 1.988e - 07s^2 - 2.542e - 13s - 2.184e - 13$
$\delta_r(s)$	$s^4 + 11.94s^3 + 0.153s^2 + 0.0009299s + 2.475e - 06$	$\delta_r(s)$	$s^4 + 0.08989s^3 + 1.414e - 06s^2 + 1.038e - 07s + 1.052e - 14$
$\phi(s)$	$-2.512e - 07s^2 - 2.347e - 08s + 1.248e - 09$	$\phi(s)$	$6.305e - 07s^2 + 1.644e - 08s - 4.622e - 12$
$\delta_r(s)$	$s^4 + 11.94s^3 + 0.153s^2 + 0.0009299s + 2.475e - 06$	$\delta_r(s)$	$s^4 + 0.08989s^3 + 1.414e - 06s^2 + 1.038e - 07s + 1.052e - 14$

TABLE 4.14: Lateral Directional State Feedback Transfer Function of Baruna-1 at Take-off and Cruise Conditions

1. Approach 1 at Take-off Condition:

$$\vec{D}_{2aug} = s^4 + 12.43s^3 + 0.1682s^2 + 0.001076s + 0.00000298$$

2. Approach 2 at Take-off Condition:

$$\vec{D}_{2aug} = s^4 + 11.94s^3 + 0.153s^2 + 0.0009299s + 0.000002475$$

3. Approach 1 at Cruise Condition:

$$\vec{D}_{2aug} = s^4 + 19.26s^3 + 0.4643s^2 + 0.004631s + 0.00001668$$

4. Approach 2 at Cruise Condition:

$$\vec{D}_{2aug} = s^4 + 0.08989s^3 + 1.414e - 06s^2 + 1.038e - 07s + 1.052e - 14$$

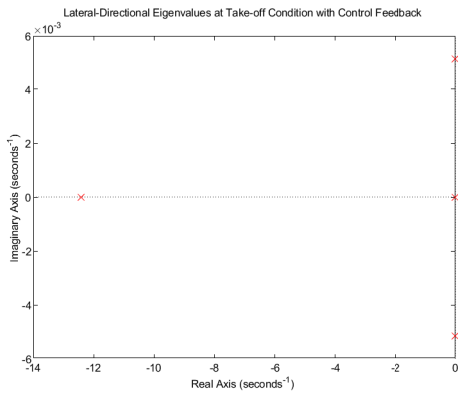
As shown in Table 4.15 and shown in Fig. 4.9, all of the eigenvalues of the closed loop lateral directional characteristic equations are had a negative sign and located on the left side of the axis. This indicates that Baruna-1 is lateral directional dynamically stable after the application of the feedback control gains K based on the lqr control technique.

Take-off		Cruise	
Approach 1	Approach 2	Approach 1	Approach 2
-12.41872805	-11.92418855	-19.23858738	-18.47247675
-0.00391349 + 0.00521297i	-0.00366597 + 0.00497608i	-0.00834147 + 0.00685863i	-0.00775090 + 0.00671436i
-0.00391349 - 0.00521297i	-0.00366597 + 0.00497608i	-0.00834147 - 0.00685863i	-0.00775090 - 0.00671436i
-0.00574743	-0.00552807	-0.00743650	-0.00712785

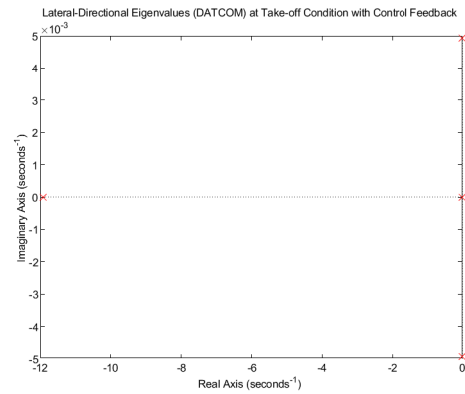
TABLE 4.15: Lateral Directional State Feedback Eigenvalues of Baruna-1 at Take-off and Cruise Conditions

The dynamic's behaviour of the dutch roll, rolling and spiral modes for the closed loop lateral directional dynamics are highlighted in the aircraft time response due to step inputs as shown below.

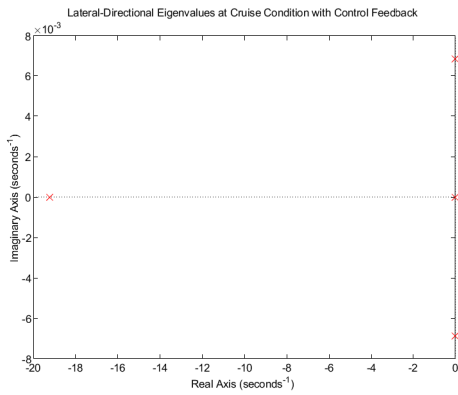
The plots in Fig. 4.14 represent the changes of the sideslip angle in accordance with the trim condition following a 1° ailerons step input. At take-off condition



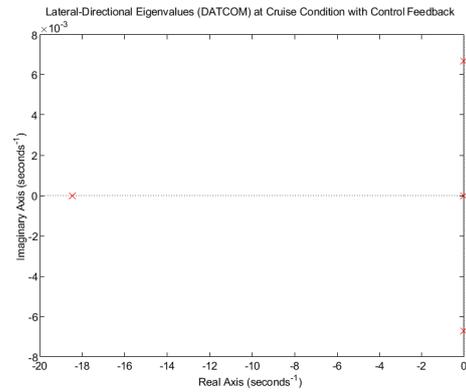
(A) Approach 1 at Take-off Condition



(B) Approach 2 at Take-off Condition



(C) Approach 1 at Cruise Condition



(D) Approach 2 at Cruise Condition

FIGURE 4.13: The Location of Dutch Roll, Rolling and Spiral Mode State Feedback Eigenvalues

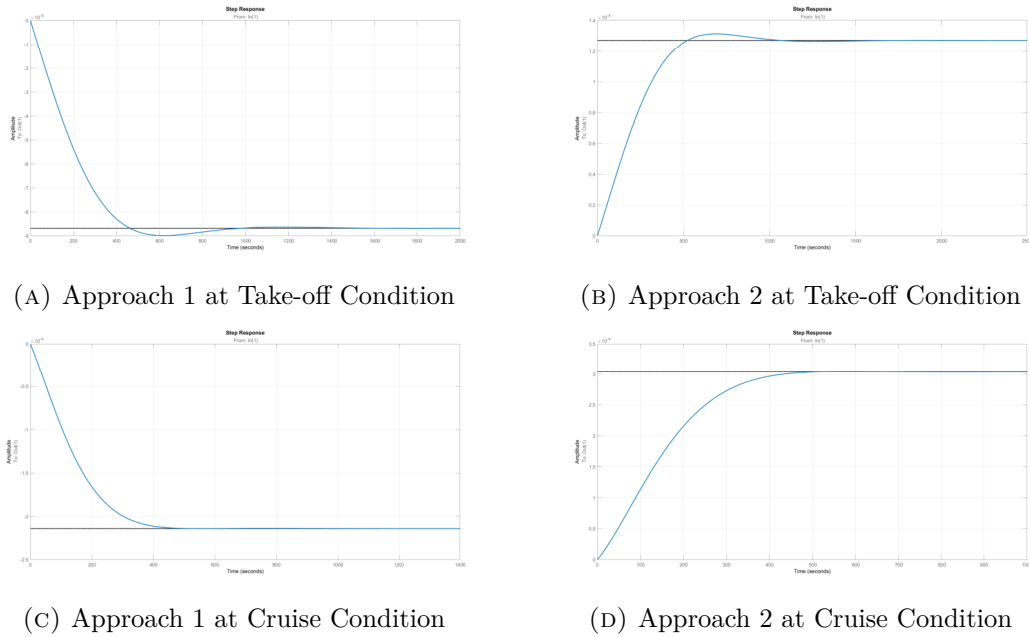
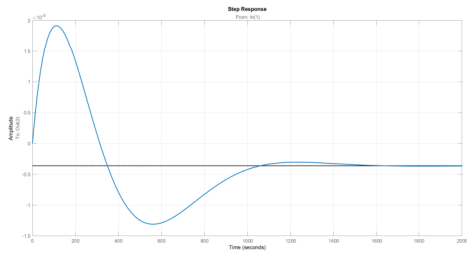


FIGURE 4.14: The Response of Sideslip Angle $\beta(s)$ to Aileron $\delta_a(s)$ Step Input

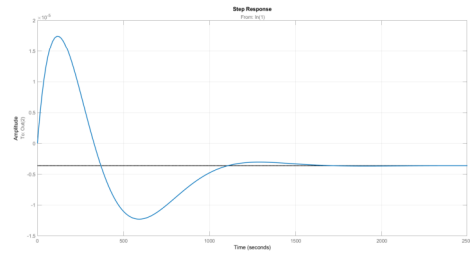
for Approach 1 as shown in Fig. 4.14a the sideslip angle decreases and converges to the value of -0.000087 rads at 2000 s and for Approach 2 as shown in Fig. 4.14b the sideslip angle increases and converges with the value of 0.000128 rads at 2500 s. At cruise condition for Approach 1 as shown in Fig. 4.14c the sideslip angle decreases and converges to the value of -0.000214 rads at 1400 s and for Approach 2 as shown in Fig. 4.14d the sideslip angle increases and converges to the value of 0.000304 rads at 1000 s.

The plots in Fig. 4.15 represent the changes of the roll rate in accordance with the trim condition following a 1° ailerons step input. At take off condition as shown in Fig. 4.15a and Fig. 4.15b, the roll rate converges to the value of -0.0000036 rad/s at 2000 s and 2500 s respectively. At cruise condition as shown in Fig. 4.15c and Fig. 4.15d, the roll rate initially increases and converges to the initial trim condition rad/s at 1400 s and 1000 s respectively.

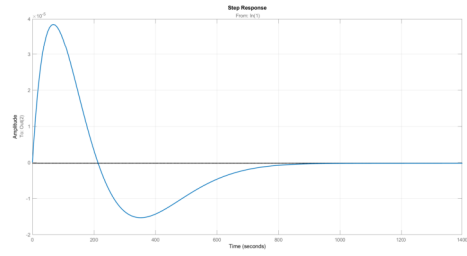
The plots in Fig. 4.16 represent the changes of the yaw rate in accordance with the trim condition following a 1° ailerons step input. At take-off condition as shown in Fig. 4.16a and Fig. 4.16b, the yaw rate converges to the value of 0.00001 rad/s at 2000 s and 2500 s respectively. At cruise condition as shown in Fig. 4.16c and



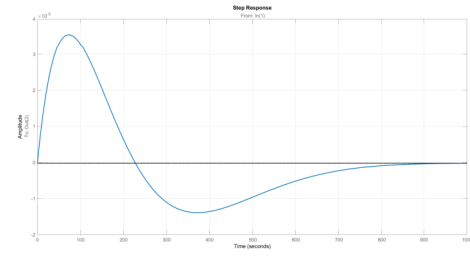
(A) Approach 1 at Take-off Condition



(B) Approach 2 at Take-off Condition

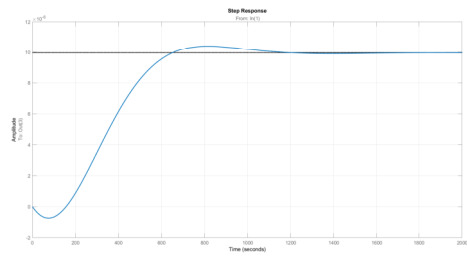


(C) Approach 1 at Cruise Condition

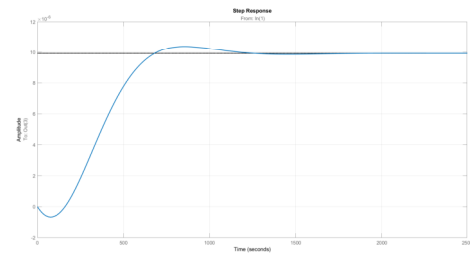


(D) Approach 2 at Cruise Condition

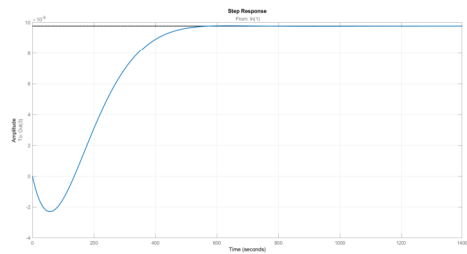
FIGURE 4.15: The Response of Roll Rate $p(s)$ to Aileron $\delta_a(s)$ Step Input



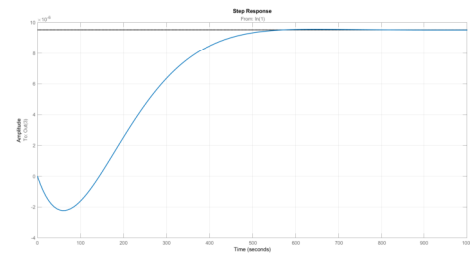
(A) Approach 1 at Take-off Condition



(B) Approach 2 at Take-off Condition



(C) Approach 1 at Cruise Condition



(D) Approach 2 at Cruise Condition

FIGURE 4.16: The Response of Yaw Rate $r(s)$ to Aileron $\delta_a(s)$ Step Input

Fig. 4.16d, the yaw rate converges to the value of nearly 0.00001 rad/s at 1400 s and 1000 s respectively.

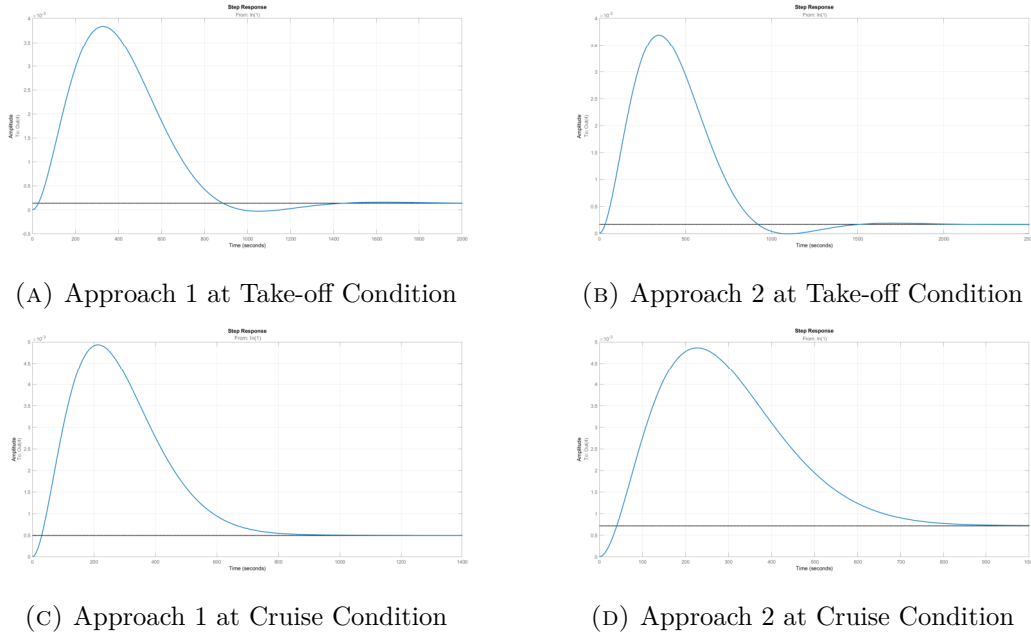
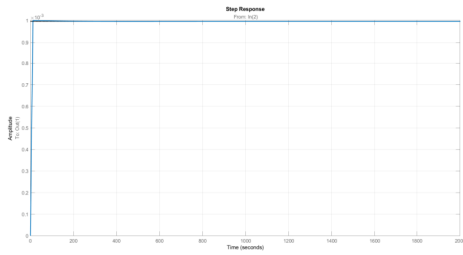


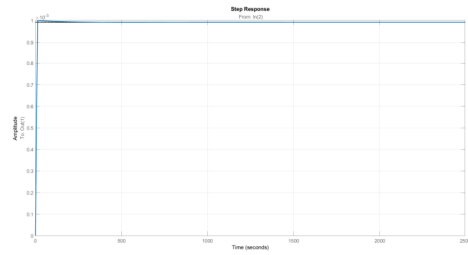
FIGURE 4.17: The Response of Bank Angle $\phi(s)$ to Aileron $\delta_a(s)$ Step Input

The plots in Fig. 4.17 represent the changes of the bank angle in accordance with the trim condition following a 1° ailerons step input. At take-off condition as shown in Fig. 4.17a and Fig. 4.17b, the bank angle angle is initially increases and converges to the value of 0.00015 rads at 2000 s and 2500 s respectively. At cruise condition as shown in Fig. 4.17c and Fig. 4.17d the bank angle increases initially and converges to the value of 0.0005 rads and 0.0007 rads at 1400 s and 1000 s respectively.

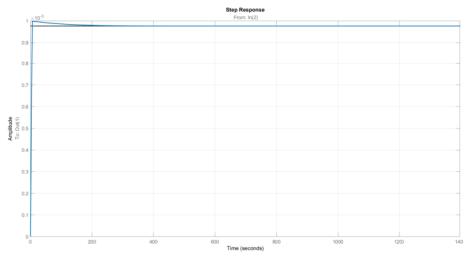
The plots in Fig. 4.18 represent the changes of the sideslip angle in accordance with the trim condition following a 1° rudder step input. At take-off condition as shown in Fig. 4.18a and Fig. 4.18b, the short period mode initially occur and the sideslip angle increases and converges to the value of nearly 0.001 rads at 2000 s and for Approach 2 as shown in Fig. 4.18b, the bank angle converges to the value of nearly 0.000005 rads at 2500 s. At cruise condition as shown in Fig. 4.18c and Fig. 4.18d, the short period occur initially during cruise condition and converges to the value of ± 0.00098 rads and 0.00096 at 1400 s and 1000 s respectively.



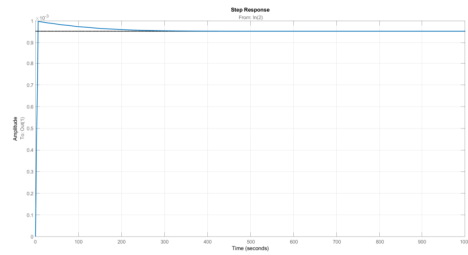
(A) Approach 1 at Take-off Condition



(B) Approach 2 at Take-off Condition

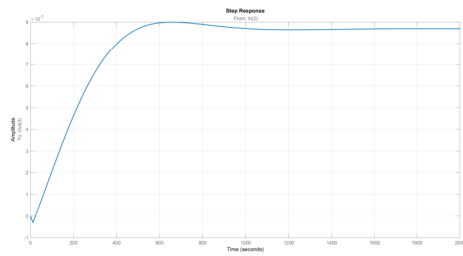


(C) Approach 1 at Cruise Condition

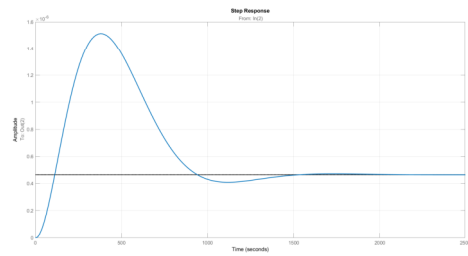


(D) Approach 2 at Cruise Condition

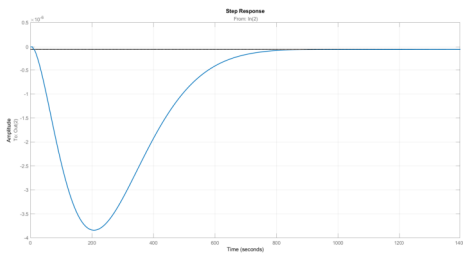
FIGURE 4.18: The Response of Sideslip Angle $\beta(s)$ to Rudder $\delta_r(s)$ Step Input



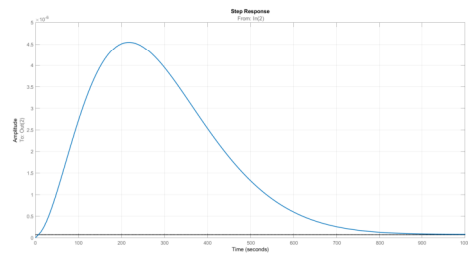
(A) Approach 1 at Take-off Condition



(B) Approach 2 at Take-off Condition



(C) Approach 1 at Cruise Condition



(D) Approach 2 at Cruise Condition

FIGURE 4.19: The Response of Roll Rate $p(s)$ to Rudder $\delta_r(s)$ Step Input

The plots in Fig. 4.19 represent the changes of the roll rate in accordance with the trim condition following a 1° rudder step input. At take-off condition for Approach 1 as shown in Fig. 4.19a, the roll rate initially increases and converges to the value of nearly 0.0000003 rad/s at 2000 s and for Approach 2 as shown in Fig. 4.19b, the pitch rate converges to the value of 0.00000045 rad/s at 2500 s. At cruise condition as shown in Fig. 4.19c and Fig. 4.19d, the roll rate converges to the value of nearly to initial trim condition at 1400 s and 1000 s respectively.

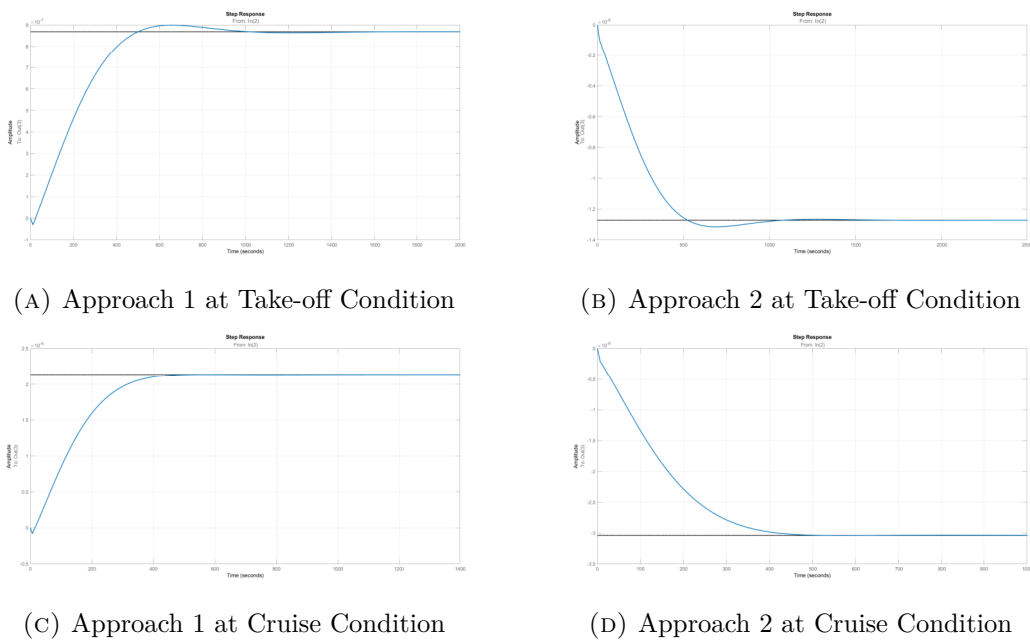


FIGURE 4.20: The Response of Yaw Rate $r(s)$ to Rudder $\delta_r(s)$ Step Input

The plots in Fig. 4.20 represent the changes of the yaw rate in accordance with the trim condition following a 1° rudder step input. At take-off condition for Approach 1 as shown in Fig. 4.20a the short period occur at the beginning and the yaw rate converges to the value of 0.00000088 rad/s at 2000 s and for Approach 2 as shown in Fig. 4.20b the short period occurred with the following of a decrement of yaw rate to the value of -0.00000146 rad/s at 2500 s. At cruise condition for Approach 1 as shown in Fig. 4.20c the short period occur at the beginning with the following of an increment of the yaw rate and converges to the value of 0.0000022 rad/s at 1400 s and for Approach 2 as shown in Fig. 4.20d the short period occurred

with the following of a decrement of yaw rate to the value of -0.0000028 rad/s at 1000 s.

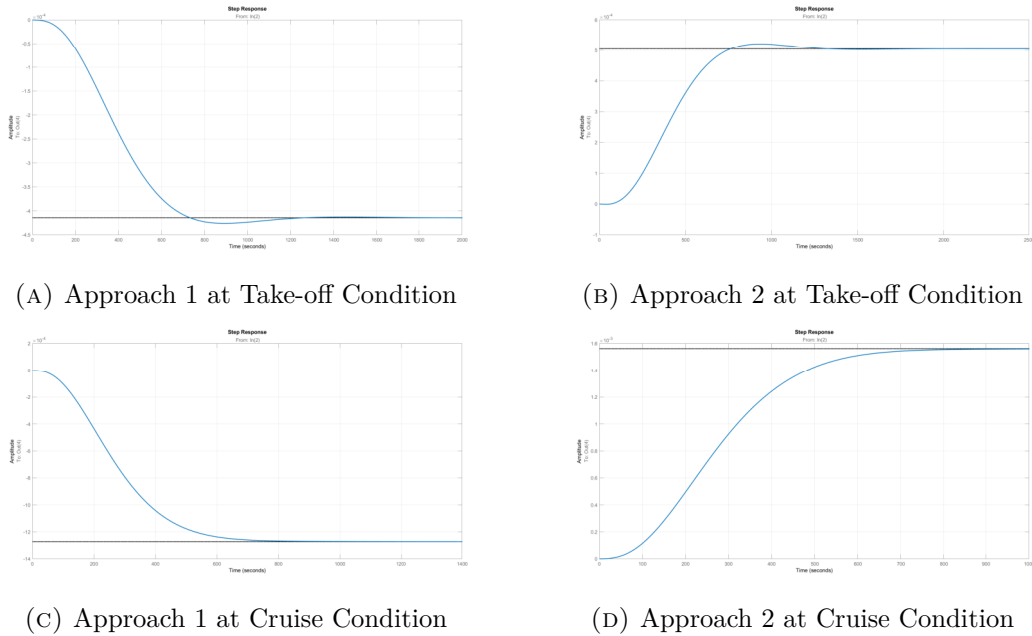


FIGURE 4.21: The Response of Bank Angle $\phi(s)$ to Rudder $\delta_r(s)$ Step Input

The plots in Fig. 4.21 represent the changes of the bank angle in accordance with the trim condition following a 1° rudder step input. At take-off condition for Approach 1 as shown in Fig. 4.21a the bank angle decreases and converges to the value of -0.00042 rads at 2000 s and for Approach 2 as shown in Fig. 4.21b, the bank angle increases and converges to the value of nearly 0.00005 rads at 2500 s. At cruise condition for Approach 1 as shown in Fig. 4.21c, the bank angle decreases and converges to the value of -0.00124 rads at 1400 s and for Approach 2 as shown in Fig. 4.21b, the bank angle increases and converges to the value of nearly 0.0016 rads at 1000 s.

The damping ratio, natural frequency and time constant for the closed loop lateral directional dynamics that associated with the dutch roll, spiral and roll modes as shown in Table 4.13 will be evaluated based on the regulation available in the Military specification MIL-F-8785C to satisfy the level of flying qualities.

4.5 Baruna-1 Flying and Handling Quality Evaluation

The result of the closed loop damping, natural frequency and time constant for longitudinal and lateral directional modes must be evaluated to the regulation available to satisfy the flying qualities requirements. The Military specification MIL-F-8785C reference is the main reference for the evaluation of Baruna-1 flying and handling qualities.

The mission profile of Baruna-1 analyzed in this thesis are take-off and cruise. Based on the design specifications, Baruna-1 is categorized as:

- Class III aircraft, a large, heavy aircraft with low-to-medium maneuverability.
- Category B for Cruise mission and Category C for Take-off mission.

These Baruna-1 classifications leads to the analysis of each mode for the longitudinal and lateral directional dynamics stability.

4.5.1 Baruna-1 Short Period Mode Flying Qualities

For the short period mode, the damping ratio ζ_{SP} requirements flying of Baruna-1 is shown below. At both flight conditions, Baruna-1 meets the Level I flying and handling requirements.

Category C	Take-off		Category B	Cruise	
	Approach 1	Approach 2		Approach 1	Approach 2
Level I $\zeta_{SP} > 0.35$	$\zeta_{SP} = 1.0000$	$\zeta_{SP} = 1.0000$	Level I $\zeta_{SP} > 0.35$	$\zeta_{SP} = 1.0000$	$\zeta_{SP} = 1.0000$
Level II $\zeta_{SP} > 0.25$	-	-	Level II $\zeta_{SP} > 0.20$	-	-
Level III $\zeta_{SP} > 0.15$	-	-	Level III $\zeta_{SP} > 0.15$	-	-

TABLE 4.16: Baruna-1 Short Period Mode Damping Evaluation at Take-off and Cruise Conditions

4.5.2 Baruna-1 Phugoid Mode Flying Qualities

For the phugoid mode, the damping ratio ζ_{PH} flying qualities of Baruna-1 is shown below. At both flight conditions, Baruna-1 meets the Level I flying and handling requirements.

Category C	Take-off		Category B	Cruise	
	Approach 1	Approach 2		Approach 1	Approach 2
Level I $\zeta_{PH} \geq 0.04$	$\zeta_{PH} = 0.887430$	$\zeta_{PH} = 0.861719$	Level I $\zeta_{PH} \geq 0.04$	$\zeta_{PH} = 0.863457$	$\zeta_{PH} = 0.697218$
Level II $\zeta_{PH} \geq 0$	-	-	Level II $\zeta_{PH} \geq 0$	-	-
Level III $T_{2PH} \geq 55$ sec	-	-	Level III $T_{2PH} \geq 55$ sec	-	-

TABLE 4.17: Baruna-1 Phugoid Mode Damping Evaluation at Take-off and Cruise Conditions

4.5.3 Baruna-1 Dutch Roll Mode Flying Qualities

For the dutch roll mode, the damping ratio ζ_{DR} flying qualities of Baruna-1 is shown below. At both flight conditions, Baruna-1 meets the Level I flying and handling requirements.

Category C	Take-off		Category B	Cruise	
	Approach 1	Approach 2		Approach 1	Approach 2
Level I $\zeta_{DR} \geq 0.08$	$\zeta_{DR} = 0.603028$	$\zeta_{DR} = 0.595956$	Level I $\zeta_{DR} \geq 0.08$	$\zeta_{DR} = 0.772421$	$\zeta_{DR} = 0.755838$
Level II $\zeta_{DR} \geq 0.05$	-	-	Level II $\zeta_{DR} \geq 0.05$	-	-
Level III $\zeta_{DR} \geq 0$	-	-	Level III $\zeta_{DR} \geq 0$	-	-

TABLE 4.18: Baruna-1 Dutch Roll Mode Damping Evaluation at Take-off and Cruise Conditions

For the dutch roll mode, the natural frequency ω_{DR} flying qualities of Baruna-1 is shown below. At both flight condition, Baruna-1 did not meet any flying and handling requirements where the value of the natural frequency ω_{DR} are 0.006473 and 0.006137 at take-off mission and 0.010799 and 0.010255 at cruise mission.

Category C	Take-off		Category B	Cruise	
	Approach 1	Approach 2		Approach 1	Approach 2
Level I $\omega_{DR} \geq 0.4$	DMR	DMR	Level I $\omega_{DR} \geq 0.4$	DMR	DMR
Level II $\omega_{DR} \geq 0.4$	DMR	DMR	Level II $\omega_{DR} \geq 0.4$	DMR	DMR
Level III $\omega_{DR} \geq 0.4$	DMR	DMR	Level III $\omega_{DR} \geq 0.4$	DMR	DMR

TABLE 4.19: Baruna-1 Dutch Roll Mode Natural Frequency Evaluation at Take-off and Cruise Conditions

4.5.4 Baruna-1 Roll Mode Flying Qualities

For the roll mode, the time constant T_R flying qualities of Baruna-1 is shown below. At both flight condition, Baruna-1 meets the Level I flying and handling requirements.

Category C	Take-off		Category B	Cruise	
	Approach 1	Approach 2		Approach 1	Approach 2
Level I $T_R < 1.4$ sec	$T_R = 0.080524$ sec	$T_R = 0.083863$ sec	Level I $T_R < 1.4$ sec	$T_R = 0.051979$ sec	$T_R = 0.054135$ sec
Level II $T_R < 3.0$ sec	-	-	Level II $T_R < 3.0$ sec	-	-
Level III -	-	-	Level III $T_R < 10.0$ sec	-	-

TABLE 4.20: Baruna-1 Rolling Mode Time Constant Evaluation at Take-off and Cruise Conditions

4.5.5 Baruna-1 Spiral Mode Flying Qualities

For the spiral mode, the time constant T_{2s} flying qualities of Baruna-1 is shown below. At both flight condition, Baruna-1 meets the Level I flying and handling requirements.

Category C	Take-off		Category B	Cruise	
	Approach 1	Approach 2		Approach 1	Approach 2
Level I $T_{2s} > 12$ sec	$T_{2s} = 121.038523$ sec	$T_{2s} = 125.799247$ sec	Level I $T_{2s} > 20$ sec	$T_{2s} = 93.208810$ sec	$T_{2s} = 97.244902$ sec
Level II $T_{2s} > 8$ sec	-	-	Level II $T_{2s} > 12$ sec	-	-
Level III $T_{2s} > 4$ sec	-	-	Level III $T_{2s} > 12$ sec	-	-

TABLE 4.21: Baruna-1 Spiral Mode Double Amplitude Time Constant Evaluation at Take-off and Cruise Conditions

CHAPTER 5

SUMMARY, CONCLUSION, RECOMMENDATION

5.1 Summary

In this thesis, Baruna-1 is chosen as the model of interest. The primary objectives of this thesis are to design the Baruna-1 control surfaces and analyze the stability and control of Baruna-1 at take-off and cruise conditions. The State Space Model is used to analyze the dynamic stability.

The stability and control derivatives of Baruna-1 are calculated using two approaches:

1. Approach 1: Analytical method based on the Marcello's[16], Snorri's[19], Sadrey's[25], and Roskam's[17] methodologies.
2. Approach 2: The combination of Approach 1 and USAF Digital DATCOM data.

The following steps are done in MATLAB to support the numerical calculation and analysis:

1. Aerodynamic coefficients and stability and control derivatives;
2. State Space and dynamics modeling;
3. The LQR optimal feedback gain K calculation;

Furthermore, the static and dynamic stability of Baruna-1 is analyzed at 1.344° angle of attack, 0.6 Mach number and 3500 m altitude for cruise condition and 12.0856° angle of attack, 0.2725 Mach number at sea level for take-off condition.

5.2 Conclusion

The conclusion of this thesis are given by:

1. The dimension of the Baruna-1 control surfaces based on the wing and body configurations:

- Elevators: $S_{elev} = 7.4196m^2$, $b_{elev} = 1.4839m$, $c_{elev} = 5$;
- Rudder: $S_{rud} = 7.8294m^2$, $b_{rud} = 1.9705m$, $c_{rud} = 3.9734$;
- Ailerons: $S_{ail} = 7.5m^2$, $b_{ail} = 5.2m$, $c_{ail} = 1.25$;

2. Baruna-1 is natural longitudinal statically stable with the value of C_{m_α} and the Static Margin:

- $C_{m_\alpha} = -3.866096$ at take-off and cruise conditions calculated using Approach 1; and
- $C_{m_\alpha} = -4.425$ and $C_{m_\alpha} = -3.414$ at take-off and cruise conditions calculated using Approach 2.
- The static margin of Baruna-1 is 24.1743% \bar{c} wing mean aerodynamic chord.

3. Baruna-1 is natural lateral statically stable with the value of C_{l_β} :

- $C_{l_\beta} = -0.018219$ at cruise condition calculated using Approach 1.
- $C_{l_\beta} = -0.05445$ and $C_{l_\beta} = -0.07652$ at take-off and cruise conditions calculated using Approach 2.

However, Baruna-1 is natural lateral statically unstable at take-off condition calculated using Approach 1 with the value of $C_{l_\beta} = 0.023283$.

4. Baruna-1 is directional statically stable with the value of C_{n_β} :

- $C_{n_\beta} = 0.211254$ and $C_{n_\beta} = 0.206719$ at cruise condition calculated using Approach 1.
- $C_{n_\beta} = 0.05532$ and $C_{l_\beta} = 0.05843$ at take-off and cruise conditions calculated using Approach 2.

5. Baruna-1 is natural longitudinal dynamically unstable for Approach 1 and Approach 2 at take-off and cruise conditions indicated by the positive sign of the eigenvalues.
- Approach 1: $0.00014629 \pm 0.00284125i$ at take-off condition and $0.00114149 \pm 0.00417290i$ at cruise condition.
 - Approach 2: $0.00007762 \pm 0.00283455i$ at take-off condition and $0.00094447 \pm 0.00332007i$ at cruise condition.

6. Baruna-1 is natural lateral directional dynamically unstable for Approach 1 at take-off and cruise conditions and for Approach 2 at take-off condition indicated by the positive sign of the eigenvalues.

- Approach 1: 0.02214845 at take-off condition and 0.03406950, 0.00114431, 0.00000194 at cruise condition.
- Approach 2: $0.00000431 \pm 0.00094613i$ at take-off condition.

However, Baruna-1 is natural lateral directional dynamically stable for Approach 2 at cruise condition indicated by the negative signs of the eigenvalues.

7. Baruna-1 is longitudinal and lateral directional dynamically stable after the implementation of the stability augmentation system with the conditions:

- All of the eigenvalues for Approach 1 and Approach 2 at take-off and cruise conditions have a negative sign.
- Baruna-1's dynamic behaviour for Approach 1 and Approach 2 at take-off and cruise conditions described that the aircraft is asymptotically stable with the curve converges to the steady state condition.

8. The flying and handling quality evaluations of Baruna-1 based on MIL-F-8785C:,

- Baruna-1 have met the Level I for Class III Category B and C for the longitudinal and lateral directional damping and time constant.
- However, the dutch roll natural frequency of Baruna-1 did not meet the minimum level of natural frequency with the value of $\omega_{DR} = 0.006518$

and $\omega_{DR} = 0.006181$ for Approach 1 and $\omega_{DR} = 0.010799$ and $\omega_{DR} = 0.010255$ for Approach 2.

5.3 Recommendations

Based on the outcome of this thesis, several recommendations can be made:

1. Analyzing the stability of Baruna-1 at landing condition.
2. Design evaluation and modification of Baruna-1, due to its natural longitudinal and lateral directional dynamically unstable before the application of feedback control.
3. Vary the missions of the aircraft for the static and dynamic stability along with the speed and angle of attack.
4. Vary the Q and R matrices to find the optimum feedback control gain K that fully meets the Level I flying and handling quality requirements.

Bibliography

- [1] O. Pechony and D. T. Shindell, “Driving forces of global wildfires over the past millennium and the forthcoming century,” *Proceedings of the National Academy of Sciences*, vol. 107, no. 45, pp. 19 167–19 170, 2010.
- [2] A. M. Gill, S. L. Stephens, and G. J. Cary, “The worldwide wildfire problem,” *Ecological applications*, vol. 23, no. 2, pp. 438–454, 2013.
- [3] *Multi-decade global fire dataset set to support trend analysis*. [Online]. Available: <https://climate.esa.int/de/news-events/multi-decade-global-fire-dataset-set-support-trend-analysis/>.
- [4] N. Andela, D. C. Morton, L. Giglio, Y. Chen, G. R. van der Werf, P. S. Kasibhatla, R. S. DeFries, G. Collatz, S. Hantson, S. Kloster, *et al.*, “A human-driven decline in global burned area,” *Science*, vol. 356, no. 6345, pp. 1356–1362, 2017.
- [5] D. H. A. Darmawan, “Fuelling the fires: Practical steps towards wildfires in indonesia,” *IOP Conference Series: Earth and Environmental Science*, vol. 504, no. 1, p. 012021, May 2020. DOI: [10.1088/1755-1315/504/1/012021](https://doi.org/10.1088/1755-1315/504/1/012021). [Online]. Available: <https://doi.org/10.1088/1755-1315/504/1/012021>.
- [6] A. Krasovskii, N. Khabarov, J. Pirker, F. Kraxner, P. Yowargana, D. Schepaschenko, and M. Obersteiner, “Modeling burned areas in indonesia: The flam approach,” *Forests*, vol. 9, no. 7, p. 437, 2018.
- [7] W. B. Group, “The cost of fire: An economic analysis of indonesia’s 2015 fire crisis,” *Technical Report, Indonesia Sustainable Landscapes Knowledge*, no. 1, 2016.
- [8] B. N. P. Bencana, *Luas lahan terbakar seluruh indonesia capai 857 ribu ha*, id, Oct. 2019. [Online]. Available: <https://bnpb.go.id/berita/luas-lahan-terbakar-seluruh-indonesia-capai-857-ribu-ha> (visited on 06/30/2022).

- [9] S. E. Finlay, A. Moffat, R. Gazzard, D. Baker, and V. Murray, “Health impacts of wildfires,” *PLoS currents*, vol. 4, 2012.
- [10] M. Plucinski, G. McCarthy, J. Hollis, and J. Gould, “The effect of aerial suppression on the containment time of australian wildfires estimated by fire management personnel,” *International Journal of Wildland Fire*, vol. 21, no. 3, pp. 219–229, 2011.
- [11] P. Kalavský, P. Petříček, M. Kelemen, R. Rozenberg, J. Jevčák, R. Tomaško, and B. Mikula, “The efficiency of aerial firefighting in varying flying conditions,” in *2019 International Conference on Military Technologies (ICMT)*, IEEE, 2019, pp. 1–5.
- [12] C. Bil, “C-17 Conversion System for Fire Fighting Operations,” in *53rd AIAA Aerospace Sciences Meeting*, Kissimmee, Florida: American Institute of Aeronautics and Astronautics, Jan. 2015, ISBN: 978-1-62410-343-8. DOI: [10.2514/6.2015-1904](https://doi.org/10.2514/6.2015-1904).
- [13] A. Aircraft Design Competition Technical Committee, *Request for proposal: Responsive aerial fire fighting aircraft*, 2021-2022.
- [14] A. B, *Boeing 747-132(sf) - evergreen international airlines*, 2009. [Online]. Available: <https://www.airliners.net/photo/Evergreen-International-Airlines/Boeing-747-132-SF/1564646/L>.
- [15] M. V. Cook, *Flight dynamics principles: a linear systems approach to aircraft stability and control*. Butterworth-Heinemann, 2012.
- [16] M. R. Napolitano, *Aircraft dynamics: from modeling to simulation*. J. Wiley, 2012.
- [17] J. Roskam, *Airplane Design Part VI : Preliminary Calculation of Aerodynamic Thrust and Power Characteristics*. DARcorporation, 2004.
- [18] M. Tuna, S. Inel, and S. Ozdemir, “Longitudinal stability analysis of aircrafts,” *The Journal of Scientific and Engineering Research*, vol. 7, pp. 45–51, Oct. 2020.
- [19] S. Gudmundsson, *General aviation aircraft design: Applied Methods and Procedures*. Butterworth-Heinemann, 2013.

- [20] R. J. Moorhouse David J. Woodcock, “Background information and user guide for mil-f-8785c, military specification - flying qualities of piloted airplanes,” 1982.
- [21] R. M. M. Karl Johan Astrom, *Feedback Systems: An Introduction for Scientists and Engineers, Second Edition*, 2nd ed. Princeton University Press, 2021, ISBN: 0691193983,9780691193984.
- [22] M. A. Usta, Ö. Akyazi, and A. S. Akpinar, “Aircraft roll control system using lqr and fuzzy logic controller,” in *2011 International Symposium on Innovations in Intelligent Systems and Applications*, IEEE, 2011, pp. 223–227.
- [23] C. Hajiyev and S. Y. Vural, “Lqr controller with kalman estimator applied to uav longitudinal dynamics,” 2013.
- [24] O. A. Dhewa, A. Dharmawan, and T. K. Priyambodo, “Model of linear quadratic regulator (lqr) control method in hovering state of quadrotor,” *vol*, vol. 9, pp. 135–143, 2017.
- [25] M. H. Sadraey, *Aircraft design: a systems engineering approach*. J. Wiley, 2013.
- [26] E. Torenbeek, *Synthesis of subsonic airplane design: an introduction to the preliminary design of subsonic general aviation and transport aircraft, with emphasis on layout, aerodynamic design, propulsion and performance*. Springer Science & Business Media, 2013.
- [27] V. S. Williams J., *The USAF Stability and Control Digital Datcom*. 1979, vol. 1.
- [28] S. Sahrin, *Drawdatcomaircraft*, <https://www.mathworks.com/matlabcentral/fileexchange/34035-drawdatcomaircraft>, en, 2014. [Online]. Available: <https://www.mathworks.com/matlabcentral/fileexchange/34035-drawdatcomaircraft> (visited on 06/15/2022).

Appendices

Appendix A: MATLAB Code for Approach 1

```
1  clc
2  clear;
3  deg2rad = 0.0174533;
4  rad2deg = 57.3;
5
6  % Flight Condition
7  e = 0.85; % Oswald efficiency
8  % rho = 1.225; % Air Density at take-off condition in kg/m3
9  rho = 0.86341; % Air Density at cruise condition in kg/m3
10 g = 9.81; % gravitational acceleration in m/s2
11 pi = 3.1416;
12 % V = 93.64; % Aircraft Take-off Velocity in m/s
13 V = 205.8; % Aircraft Cruise Velocity in m/s
14 Mach = V * 0.00291545; % Mach number
15 q1 = 1/2*rho*V^2; % Dynamic Pressure
16 roc = 13; % rate of climb m/s
17
18 % Fuselage geometry
19 m = 144560.00911369; % Aircraft mass in kg
20 df = 5; % Maximum diameter of fuselage in m
21 hf = 4.5; % Fuselage diameter in m
22 a_FUS_deg = 1; % Angle of attack of the Fuselage in deg
23 a_FUS = a_FUS_deg * deg2rad; % Angle of attack of the Fuselage in
    rad
24 L_F = 32.77775; % Fuselage length in m
25
26 % Inertia
27 I_XX = 5391992711550.996;
28 I_XZ = -557802990253.2191;
29 I_YY = 3151300757404.5815;
30 I_ZZ = 7652161022155.232;
31
32 % Wing geometry
```

```

33 AR_W = 8; % Wing Aspect Ratio
34 S_W = 200; % Wing Planform Area in m2
35 c_W = 5; % Mean Aerodynamic Chord Wing in m
36 b_W = S_W / c_W; % Wing span in m
37 lambda = 0.5; % Taper ratio of the Wing, HT and VT
38 c_Wr = ((3*c_W)/2)*((1+lambda)/(1+lambda+lambda^2));
39 c_Wt = lambda * c_Wr;
40 Dih_deg = -2; % Dihedral angle of the Wing and Horizontal Tail in
    deg
41 Dih_rad = Dih_deg * deg2rad; % Dihedral angle of the Wing and
    Horizontal Tail in rad
42 i_w0 = 0; % Wing Setting Angle in deg
43 i_w = i_w0 * deg2rad; % Wing Setting Angle in rad
44 a_W_deg = a_FUS_deg + i_w0; % Wing AoA in deg
45 a_W = a_W_deg * deg2rad; % Wing AoA in rad
46 ew_deg = 0; % Wing Twist Angle in deg
47 ew_rad = ew_deg * deg2rad; % Wing Twist Angle in rad
48 wapex = 10.4392; % Wing Apex in m
49
50 % Wing Sweep Angle
51 SA_WLE_deg = 0; % Wing Sweep Angle at Leading Edge in deg
52 SA_WLE_rad = SA_WLE_deg * deg2rad; % Wing Sweep Angle at Leading
    Edge in rad
53
54 tanSA_W50 = tan(SA_WLE_rad)-((4*0.5*(1-lambda))/(AR_W*(1+lambda)))
    ;
55 SA_W50_rad = atan(tanSA_W50); % Wing Sweep Angle at 50% Chord in
    rad
56 SA_W50_deg = SA_W50_rad*rad2deg; % Wing Sweep Angle at 50% Chord
    in deg
57
58 tanSA_W25 = tan(SA_WLE_rad)-((4*0.25*(1-lambda))/(AR_W*(1+lambda))
    );
59 SA_W25_rad = atan(tanSA_W25); % Wing Sweep Angle at 25% Chord in
    rad
60 SA_W25_deg = SA_W25_rad * rad2deg; % Wing Sweep Angle at 25% Chord
    in deg
61
62 % Horizontal Tail Geometry
63 AR_HT = 4.5; % HT Aspect Ratio

```

```
64 S_HT = 48.9337; % HT Planform area
65 b_HT = sqrt(AR_HT*S_HT); % HT Span in m
66 c_HT = b_HT/AR_HT; %HT MAC in m
67 c_HTr = ((3*c_HT)/2)*((1+lambda)/(1+lambda+lambda^2)); % HT Root
    Chord
68 c_HTt = c_HTr * lambda; % HT Tip Chord
69
70 % HT Sweep Angle
71 SA_HTLE_deg = 12; % HT Sweep Angle at Leading Edge in deg
72 SA_HTLE_rad = SA_HTLE_deg * deg2rad; % HT Sweep Angle at Leading
    Edge in rad
73 tanSA_HT50 = tan(SA_HTLE_rad)-((4*0.5*(1-lambda))/(AR_HT*(1+lambda
    )));
74 SA_HT50_rad = atan(tanSA_HT50); % HT Sweep Angle at 50% Chord in
    rad
75 SA_HT50_deg = SA_HT50_rad * rad2deg; %HT Sweep Angle at 50% Chord
    in deg
76 tanSA_HT25 = tan(SA_HTLE_rad)-((4*0.25*(1-lambda))/(AR_HT*(1+
    lambda)));
77 SA_HT25_rad = atan(tanSA_HT25); % HT Sweep Angle at 25% Chord in
    rad
78 SA_HT25_deg = SA_HT25_rad * rad2deg; %HT Sweep Angle at 25% Chord
    in deg
79
80 % Vertical Tail Geometry
81 AR_VT = 1.2; % VT Aspect Ratio
82 S_VT = 31.3176; % VT Plaform Area in m2
83 b_VT = sqrt(AR_VT*S_VT); %VT Span in m
84 c_VT = b_VT/AR_VT; %VT MAC in m
85 c_VTr = ((3*c_VT)/2)*((1+lambda)/(1+lambda+lambda^2)); % VT Root
    Chord
86 c_VTt = c_VTr * lambda; % VT Tip Chord
87
88 % VT Sweep Angle
89 SA_VTLE_deg = 22; % VT Sweep Angle at Leading Edge in deg
90 SA_VTLE_rad = SA_VTLE_deg * deg2rad; % VT Sweep Angle at Leading
    Edge in rad
91
92 % Control Surface Geom
93 % Elevator
```

STABILITY ANALYSIS AND CONTROL DESIGN OF BARUNA-1

```

94 b_elev = 5; % Elevator Span in m
95 c_elev = 0.35*c_HTr; % Elevator chord in m
96 S_elev = b_elev*c_elev; % Elevator Area in m2
97 % Aileron
98 b_ail = 0.26*(b_W/2); % Aileron Span in m
99 c_ail = 0.25*c_W; % Aileron chord in m
100 S_ail = b_ail*c_ail*2; % Aileron Area in m2
101 % Rudder
102 S_rud = 0.25*S_VT; % Rudder Area in m2
103 c_rud = 0.3*c_VTr; % Rudder chord in m
104 b_rud = S_rud/c_rud; % Rudder Span in m
105
106 % Location of Wing, HT and VT
107 z_W = 3.908076; % Location of Wing in Z axis
108 x_W = 10.439200; % Location of Wing in X axis
109 z_HT = 9.161455; % Location of HT in Z axis
110 x_HT = 31.311799; % Location of HT in X axis
111 z_VT = 3.048570; % Location of VT in Z axis
112 x_VT = 28.061452; % Location of VT in X axis
113
114 % Wing Lift Coefficient
115 Cla_W_deg = 0.1212; % Wing Airfoil Lift Curve Slope in /deg
116 Cla_W_rad = Cla_W_deg * rad2deg; % Wing Airfoil Lift Curve Slope
    in /rad
117 Cl0 = 0.4046; % Zero AoA Wing Airfoil Lift Coefficient
118 a_zerolift = -Cl0/Cla_W_rad; % Wing Airfoil Zero AoA in rad
119 CLa_W = Cla_W_rad/(1+(Cla_W_rad/(pi*AR_W*e))); % Wing Lift Curve
    Slope in /rad
120 CLa_WMO = CLa_W;
121 K_WB = 1+0.025*(df/b_W)-0.25*(df/b_W)^2;
122 CLa_WB = K_WB * CLa_W; % Wing-Fuselage Lift Curve Slope in /rad
123 CL0_W = abs(a_zerolift)*CLa_WB; % Zero AoA Wing Lift Coefficient
124
125 % Location of Aircraft Center of Gravity and Aerodynamic Center
126 x_CG = 10.57338; % Location of CG X-axis from Nose in m
127 z_CG = 1.56417636; % Location of CG Z-axis from Nose in m
128
129 Xac_W = 0.22; % Wing AC based on Torenbeek
130 Df1_Xac = -(1.8/CLa_WB)*((df*hf*wapex)/(S_W*c_W)); % Correction
    factor

```

STABILITY ANALYSIS AND CONTROL DESIGN OF BARUNA-1

```

131 Df2_Xac = (0.273/(1+lambda))*((df*x_CG*(b_W-df))/(c_W^2*(b_W+2.15*
      df)))*tanSA_W25; % Correction factor
132 Xac_WB = Xac_W+Df1_Xac+Df2_Xac; % Location of AC Wing-Fuselage in
      terms of MAC
133 Xac_MAC_WB = Xac_WB * c_W; % Location of AC Wing-Fuselage wrt MAC
      from Wing Leading edge in m
134 xac_WB = wapex + Xac_MAC_WB; %Location of Wing AC from nose in m
135
136 Xac_HT = 0.25; % Location of AC HT wrt HT MAC
137 Xac_MAC_HT = Xac_HT * c_HT; % Location of AC HT in m
138 x_MAC_HT = (b_HT/6)*((1+2*lambda)/(1+lambda))*tan(SA_HTLE_rad); %
      Location of HT MAC from HT Leading edge in m
139 xac_MAC_HT = x_MAC_HT + Xac_MAC_HT; % Location of AC HT wrt MAC
      from HT Leading edge in m
140 xac_HT = x_HT + xac_MAC_HT; % Location of HT AC from nose in m
141 Xac_H = (xac_HT - wapex)/c_W;
142
143 Xac_VT = 0.25; % Location of AC VT wrt VT MAC
144 Xac_MAC_VT = Xac_VT * c_VT; % Location of AC VT in m
145 x_MAC_VT = (b_VT/6)*((1+2*lambda)/(1+lambda))*tan(SA_VTLE_rad); %
      Location of VT MAC from VT Leading edge in m
146 xac_MAC_VT = x_MAC_VT + Xac_MAC_VT; % Location of AC VT wrt MAC
      from VT Leading edge in m
147 xac_VT = x_VT + xac_MAC_VT; % Location of VT AC from nose in m
148 zac_VT = x_MAC_VT/tan(SA_VTLE_rad); % Location of VT AC from VT
      Root Chord Z axis.
149
150 X_CG_WRT_ACWB = x_CG-xac_WB; % Location of from AC Wing-Fuselage
      in m
151 X_CG = X_CG_WRT_ACWB/c_W; % Location of CG in terms of MAC
152
153 X_V = xac_VT - x_CG;
154 Z_V = z_VT + zac_VT;
155
156 Z_R = (z_VT)+(b_rud/2);
157 X_R = x_VT+(c_VTr-(c_rud/2));
158
159 % Lift Coefficient
160 % HT Lift Coefficient NACA 0012
161 Cla_HT_deg = 0.1076; % HT Airfoil Lift Curve Slope in /deg

```

STABILITY ANALYSIS AND CONTROL DESIGN OF BARUNA-1

```

162 Cla_HT_rad = Cla_HT_deg*rad2deg; % HT Airfoil Lift Curve Slope in
    /rad
163 CLa_HT = Cla_HT_rad/(1+(Cla_HT_rad/(pi*AR_HT*e))); % HT Lift Curve
    Slope in /rad
164 de_da = (2*CLa_WB)/(pi*AR_W);
165 nHT = 1; % HT Effectiveness for T-Tail=1
166 CLO_HT = 0; %Zero AoA HT Lift Coefficient
167
168 % VT Lift Coefficient NACA 0012
169 Cla_VT_deg = 0.1076; % VT Airfoil Lift Curve Slope in /deg
170 Cla_VT_rad = Cla_VT_deg*rad2deg; % VT Airfoil Lift Curve Slope in
    /rad
171 CLa_VT = Cla_VT_rad/(1+(Cla_VT_rad/(pi*AR_VT*e))); % VT Lift Curve
    Slope in /rad
172
173 % General Expression for Lift Stability
174 CLO = CLO_W;
175 CLa = (CLa_WB)+CLa_HT*nHT*(S_HT/S_W)*(1-de_da); % Aircraft Lift
    Curve Slope
176 re = S_elev/S_HT;
177 tau_e = -4.66*re^4+8.79*re^3-6.44*re^2+2.85*re+0.0316;
178 CLde = nHT*(S_HT/S_W)*CLa_HT*tau_e;
179
180 CL1 = (m*g)/(q1*S_W);
181
182 % Pitching Moment Coefficient
183 Cmac_W = -0.0859; % for MS-0317 extracted from airfoil graph
184 Cmac_HT = 0; % symmetrical
185 Cm0_W = Cmac_W + CLO*(X_CG - Xac_WB);
186 Cm0_HT = Cmac_HT + CLO_HT * (Xac_H);
187 Cm0 = Cm0_W + Cm0_HT;
188 Cma = CLa_WB*(X_CG-Xac_WB)-CLa_HT*nHT*(S_HT/S_W)*(1-de_da)*(Xac_H-
    X_CG);
189 Cmde = -CLa_HT*nHT*(S_HT/S_W)*(Xac_H-X_CG)*tau_e;
190
191 % AoA
192 a1 = (Cmde*(CL1-CLO)-CLde*(-Cm0))/(CLa*Cmde-Cma*CLde);
193 a1_deg = a1 * rad2deg;
194
195 % Elevator Deflection

```

STABILITY ANALYSIS AND CONTROL DESIGN OF BARUNA-1

```

196 % de1 = (CLa*(-Cm0)-Cma*(CL1-CL0))/(CLa*Cmde-Cma*CLde);
197 de1 = (Cm0 + Cma*a1)/(-Cmde);
198 de1_deg = de1*rad2deg;
199
200 % Cm1
201 Cm1 = Cm0 + Cma*a1 + Cmde*de1; % at Take-off Condition
202
203 % Drag Coefficient
204 CD0 = 0.00089; % Baruna-1 Paper
205 CDa = ((2*CL1)/(pi*AR_W*e))*CLa;
206 CDde = 0;
207 CD1 = CD0 + ((CL1^2)/(pi*AR_W*e));
208
209 % Longitudinal Small Perturbation
210 dCD_dMach = 0.0169741004; % from DATCOM
211 CDu = Mach * dCD_dMach;
212 dXacWB_dMach = 0.2624126747; % from DATCOM
213 Cmu = -CL1*dXacWB_dMach;
214 CLu = (Mach^2/(1-Mach^2))*CL1;
215
216 CDad = 0.0;
217 CLad = 2*CLa_HT*nHT*(S_HT/S_W)*(Xac_H-X_CG)*de_da;
218 Cmad = -CLad*(Xac_H-X_CG);
219
220 % Pitch rate perturbation
221 CDq = 0.0;
222 B_CLq = sqrt(1-Mach^2*(cos(SA_W25_rad))^2);
223 CLq_WM0 = (1/2+2*abs(Xac_WB-X_CG))*CLa_WM0;
224 CLq_W = ((AR_W+2*cos(SA_W25_rad))/(AR_W*B_CLq+2*cos(SA_W25_rad)))*
        CLq_WM0;
225 CLq_HT = 2*CLa_HT*nHT*(S_HT/S_W)*(Xac_H-X_CG);
226 CLq = CLq_W+CLq_HT;
227
228 Kq = 0.8;
229 C_Cmq = (((AR_W*(0.5*abs(Xac_WB-X_CG)+2*abs(Xac_WB-X_CG)^2))/(AR_W
        +2*cos(SA_W25_rad)))+(1/24*((AR_W^3*tanSA_W25^2)/(AR_W+6*cos(
        SA_W25_rad))))+1/8);
230 Cmq_WM0 = -Kq*CLa_WM0*cos(SA_W25_rad)*C_Cmq;
231 Cmq_HT = -2*CLa_HT*nHT*(S_HT/S_W)*(Xac_H-X_CG)^2;
232 Cmq = Cmq_WM0+Cmq_HT;

```

```

233
234 % Thrust Coefficient
235 CTX1 = -CD1;
236 CmT1 = -Cm1;
237 CTXu = -3*CTX1;
238 dT0 = -2.46; % from centerline in m
239 dT = dT0+z_CG;
240 CmTu = (dT/c_W)*CTXu;
241 CmTa = 0;
242
243 % Thrust Force
244 LT1 = 0;
245 FTY1 = 0;
246 NT1 = 0;
247
248 % Lateral-Directional Stability Derivatives Coefficients
249
250 % Cy0
251 Cy0 = 0;
252
253 % Cyb
254 Cyb_W = -0.00573*abs(Dih_deg)+ (CL1^2/30)*((tan(SA_W25_rad)*sin(
        SA_W25_rad))/AR_W*(AR_W+4*cos(SA_W25_rad))) ;
255 nHT_depsdb = 0.724+3.06*((S_HT/S_W)/(1+cos(SA_W25_rad)))+0.4*(z_W/
        hf)+0.009*AR_W;
256 Cyb_HT = -0.00573*abs(Dih_deg)*nHT_depsdb*(S_HT/S_W);
257 bv_2r1 = b_VT/(2*0.75);
258 KY_VT = 1;
259 nVT_depsdb = 0.724+3.06*((S_VT/S_W)/(1+cos(SA_W25_rad)))+0.4*(z_W/
        hf)+0.009*AR_W;
260 Cyb_VT = -KY_VT*abs(CLa_VT)*nVT_depsdb*(S_VT/S_W);
261 X1_lF = 16/L_F;
262 XO_LF = 0.64;
263 Kint = -1;
264 S_PV = ((1.051*4)/2)+(4*3.448/2)+(11.758*4.5)+((1.907+4.5)*4.11/2)
        ;
265 Cyb_B = -2*Kint*(S_PV/S_W);
266 Cyb = (Cyb_W+Cyb_B)+Cyb_HT+Cyb_VT;
267
268 % Cyda

```

```
269 Cyda = 0;
270
271 % Cydr
272 D_KR = 0.79;
273 cr_cVT = c_rud/c_VT;
274 tau_r = 0.6;
275 nVT = 1;
276 Cydr = CLa_VT*nVT*(S_VT/S_W)*D_KR*tau_r;
277
278 % Clb
279 Clb_CL1SA50 = (2.8639*10^-8)*SA_W50_deg^3+(5.7675*10^-7)*
      SA_W50_deg^2-(7.4987*10^-5)*SA_W50_deg-8.2421*10^-5;
280 KM_SA = 0.7766+1.3372*(Mach*cos(SA_W50_deg))-2.3077*(Mach*cos(
      SA_W50_deg))^2+2.0271*(Mach*cos(SA_W50_deg))^3;
281 Clb_CLAR = -(0.009804/AR_W)+(0.001/AR_W^0.005);
282 Clb_Dih = (-2.786-(50.46*AR_W)+(2.653*AR_W^2))*10^-6;
283 KM_Dih = 1+(-0.1969*(Mach*cos(SA_W50_deg))+1.6231*(Mach*cos(
      SA_W50_deg))^2-2.8513*(Mach*cos(SA_W50_deg))^3+2.1992*(Mach*cos
      (SA_W50_deg))^4)*(0.1193*AR_W-0.1961);
284 Clb_W_deg = CL1*(Clb_CL1SA50*KM_SA+Clb_CLAR)+Dih_deg*(Clb_Dih*
      KM_Dih);
285 Clb_WB = Clb_W_deg*1/deg2rad;
286 Clb_HT = 0;
287 Clb_VT = Cyb_VT*((Z_V*cos(a1)-X_V*sin(a1))/b_W);
288 Clb = Clb_WB+Clb_HT+Clb_VT;
289
290 % Clda
291 b = sqrt(1-Mach^2);
292 b1 = b * rad2deg;
293 k = (CLa_W*b)/(2*pi);
294 SA_bW_rad = atan(tanSA_W25/b);
295 SA_bW_deg = SA_bW_rad * rad2deg;
296 DRME = 0.79-0.52;
297 ta = 0.45;
298 cld = DRME*k/b;
299 Cld = ta*cld;
300 Clda = Cld/2;
301
302 % Cldr
303 Cldr = Cydr*((Z_R*cos(a1)-X_R*sin(a1))/b_W);
```

```
304
305 % Cnb
306 SB_S = ((1.051*4)/2)+(4*3.448/2)+(11.758*4.5)+((1.108+4.5)
      *5.736/2)+((0.75+1.108)*1.267/2)+(8.904*0.75);
307 wmax = 5;
308 L_B25 = 0.25*L_F;
309 L_B75 = 0.75*L_F;
310 z1_LB25 = 4.5;
311 z2_LB75 = 0.745570;
312 zmax_wmax = z1_LB25/wmax;
313 sqrtz1_z2 = sqrt(z1_LB25/z2_LB75);
314 lb2_SBS = L_F^2/SB_S;
315 lcg_lb = x_CG/L_F;
316 KN = 0.0005;
317 KR_f = 1.48;
318 Cnb_B = -57.3*KN*KR_f*(SB_S/S_W)*(L_F/b_W);
319 Cnb_W = 0;
320 Cnb_HT = 0;
321 Cnb_VT = -Cyb_VT*((X_V*cos(a1)+Z_V*sin(a1))/b_W);
322 Cnb = Cnb_B + Cnb_W + Cnb_HT + Cnb_VT;
323
324 % Cnda
325 D_Kn_a = 0.025;
326 Cnda = D_Kn_a*CL1*Cllda;
327
328 % Cndr
329 Cndr = -Cydr*((X_R*cos(a1)+Z_R*sin(a1))/b_W);
330
331 % Cyp
332 Cyp = 2*Cyb_VT*((Z_V*cos(a1)-X_V*sin(a1))/b_W);
333
334 % Clp
335 k1 = CLa_W*b/(2*pi);
336 bARW_k = b*AR_W/k1;
337 RDP_W = -0.54;
338 Clp_WB = RDP_W*k1/b;
339 k2 = CLa_HT*b/(2*pi);
340 SA_bHT0 = atan(tanSA_HT25/b);
341 SA_bHT = SA_bHT0 * rad2deg;
342 bARHT_k = b*AR_HT/k2;
```

```

343 RDP_HT = -0.42;
344 Clp_WHT = RDP_HT*k2/b;
345 Clp_HT = 1/2*Clp_WHT*(S_HT/S_W)*(b_HT/b_W)^2;
346 Clp_VT = 2*Cyb_VT*(Z_V/b_W)^2;
347 Clp = Clp_WB+Clp_HT+Clp_VT;
348
349 % Cnp
350 B_Cnp = sqrt(1-Mach^2*cos(SA_W25_rad)*cos(SA_W25_rad));
351 C_Cnp = ((AR_W+4*cos(SA_W25_rad))/(AR_W*B_Cnp+4*cos(SA_W25_rad)))
          *((AR_W*B_Cnp+(1/2)*(AR_W*B_Cnp+4*cos(SA_W25_rad))*tanSA_W25^2)
          /(AR_W+(1/2)*(AR_W+4*cos(SA_W25_rad))*tanSA_W25^2));
352 Cnp_CLMOCL0 = -(1/6)*(((AR_W+6*(AR_W+cos(SA_W25_rad)))*((X_CG -
          Xac_WB)*(tanSA_W25/AR_W)+(tanSA_W25^2/12)))/(AR_W+cos(
          SA_W25_rad)));
353 Cnp_CLMCL0 = C_Cnp*Cnp_CLMOCL0;
354 Cnp_W = -Clp_WB*tan(a1)+Clp*tan(a1)+Cnp_CLMCL0*CL1;
355 Cnp_VT = -2*Cyb_VT*((X_V*cos(a1)+Z_V*sin(a1))/b_W)*((Z_V*cos(a1)-
          X_V*sin(a1)-Z_V)/b_W);
356 Cnp = Cnp_W + Cnp_VT;
357
358 % Cyr
359 Cyr = -2*Cyb_VT*((X_V*cos(a1)+Z_V*sin(a1))/b_W);
360
361 % Clr
362 Clr_CLMOCL0 = 0.25;
363 B_Clr = sqrt(1-Mach^2*cos(SA_W25_rad)*cos(SA_W25_rad));
364 D_num = 1+((AR_W*(1-B_Clr^2))/(2*B_Clr*(AR_W*B_Clr+2*cos(
          SA_W25_rad))))+((AR_W*B_Clr+2*cos(SA_W25_rad))/(AR_W*B_Clr+4*
          cos(SA_W25_rad)))*(tanSA_W25^2/8);
365 D_den = 1+((AR_W+2*cos(SA_W25_rad))/(AR_W+4*cos(SA_W25_rad)))*
          (tanSA_W25^2/8);
366 D_Clr = D_num/D_den;
367 Clr_CLMCL0 = D_Clr * Clr_CLMOCL0;
368 DClr_Dih = 1/12*((pi*AR_W*sin(SA_W25_rad))/(AR_W+4*cos(SA_W25_rad)
          ));
369 Clr_W = Clr_CLMCL0*CL1+DClr_Dih*Dih_rad;
370 Clr_VT = -2*Cyb_VT*((X_V*cos(a1)+Z_V*sin(a1))/b_W)*((Z_V*cos(a1)-
          X_V*sin(a1))/b_W);
371 Clr = Clr_W + Clr_VT;
372

```

```

373 % Cnr
374 Cnr_CL1 = -0.2;
375 Cnr_W = Cnr_CL1*CL1^2;
376 Cnr_VT = 2*Cyb_VT*((X_V*cos(a1)+Z_V*sin(a1))^2/b_W^2);
377 Cnr = Cnr_W + Cnr_VT;
378
379 % CnTb
380 CnTb = 0;
381
382 %% Location of AC Aircraft
383 Xac = ((Xac_WB+(CLa_HT/CLa_W)*nHT*(S_HT/S_W)*(1-de_da)*Xac_HT)
        /(1+(CLa_HT/CLa_W)*nHT*(S_HT/S_W)*(1-de_da)));
384 xac = wapex+Xac*c_W;
385 SM = -100*(X_CG-Xac);
386
387 % Simulation
388 % gamma = asin(roc/V); % take-off in rads
389 gamma = 0; % cruise in degs
390 Gamma = gamma*rad2deg; % in deg
391 phi = 0; % Cruise in degs
392 % phi = 5; % Takeoff in degs
393 Phi = phi*deg2rad; % in rad
394 theta = a1_deg + Gamma; % in degs
395 Theta = theta * deg2rad; % in rads
396
397 % sideslip, ailerons and rudder deflection
398 A_Latdir = (-(m*g*cos(gamma)*sin(Phi)+FTY1))/(q1*S_W);
399 B_Latdir = (-LT1/(q1*S_W*b_W));
400 C_Latdir = (-NT1/(q1*S_W*b_W));
401
402 b_1 = (A_Latdir*(Clda*Cndr-Cnda*Clldr)+B_Latdir*(Cnda*Cydr-Cyda*
        Cndr)+C_Latdir*(Cyda*Clldr-Clda*Cydr))/(Cyb*(Clda*Cndr-Cnda*Clldr)
        +Cyda*(Clldr*Cnb-Clb*Cndr)+Cydr*(Clb*Cnda-Cnb*Clda));
403 b1_deg = b_1*rad2deg;
404 da_1 = (Cyb*(B_Latdir*Cndr-C_Latdir*Clldr)+A_Latdir*(Cnb*Clldr-Clb*
        Cndr)+Cydr*(Clb*C_Latdir-Cnb*B_Latdir))/(Cyb*(Clda*Cndr-Cnda*
        Clldr)+Cyda*(Clldr*Cnb-Clb*Cndr)+Cydr*(Clb*Cnda-Cnb*Clda));
405 da1_deg = da_1*rad2deg;

```

```

406 dr_1 = (Cyb*(Clda*C_Latdir-Cnda*B_Latdir)+Cyda*(Clb*C_Latdir-Cnb*
      B_Latdir)+A_Latdir*(Clb*Cnda-Cnb*Clda))/(Cyb*(Clda*Cndr-Cnda*
      Cldr)+Cyda*(Cldr*Cnb-Clb*Cndr)+Cydr*(Clb*Cnda-Cnb*Clda));
407 dr1_deg = dr_1*rad2deg;
408
409 % Steady State LatDir Coefficient
410 % Cy1
411 Cy1 = Cy0 + Cyb*b_1 + Cyda*da_1 + Cydr*dr_1;
412 % Cl1
413 Cl0 = 0;
414 Cl1 = Cl0 + Clb*b_1 + Clda*da_1 + Cldr*dr_1;
415 % Cn1
416 Cn0 = 0;
417 Cn1 = Cn0 + Cnb*b_1 + Cnda*da_1 + Cndr*dr_1;
418
419 D_1 = CD1*q1*S_W;
420 L_1 = CL1*q1*S_W;
421 M_1 = Cm1*q1*S_W*c_W;
422 FAY_1 = Cy1*q1*S_W;
423 LA_1 = Cl1*q1*S_W*b_W;
424 NA_1 = Cn1*q1*S_W*b_W;
425
426 % Longitudinal Stability and Control Derivatives
427 Xu = (-q1*S_W*(CDu+2*CD1))/(m*V);
428 Xa = (-q1*S_W*(CDa-CL1))/m;
429 XTu = (q1*S_W*(CTXu+2*CTX1))/(m*V);
430 Xde = (-q1*S_W*CDde)/m;
431 % Z
432 Zu = -(q1*S_W*(CLu+2*CL1))/(m*V);
433 Za = -(q1*S_W*(CLa+CD1))/(m);
434 Zad = -(q1*S_W*c_W*CLad)/(2*m*V);
435 Zq = -(q1*S_W*c_W*CLq)/(2*m*V);
436 Zde = (-q1*S_W*CLde)/(m);
437 % M
438 Mu = (q1*S_W*c_W*(Cmu+2*Cm1))/(V*I_YY);
439 Ma = (q1*S_W*c_W*Cma)/(I_YY);
440 Mad = ((q1*S_W*c_W*Cmad)/(I_YY))*(c_W/(2*V));
441 Mde = (q1*S_W*c_W*Cmde)/(I_YY);
442 MTu = (q1*S_W*c_W*(CmTu+2*CmT1))/(V*I_YY);
443 MTa = (q1*S_W*c_W*CmTa)/(I_YY);

```

```

444 Mq = ((q1*S_W*c_W*Cmq)/(I_YY))*(c_W/(2*V));
445
446 % State Matrix Input
447 Xu_1 = (Xu+XTu);
448 Xa_1 = Xa;
449 Xtheta_1 = -g*cos(Theta);
450 Xq_1 = 0;
451 Xde_1 = Xde;
452 Zad_1 = Zad;
453 Zu_1 = Zu/(V-Zad_1);
454 Za_1 = Za/(V-Zad_1);
455 Zq_1 = (Zq+V)/(V-Zad_1);
456 Ztheta_1 = -((g*sin(Theta))/(V-Zad_1));
457 Zde_1 = Zde/(V-Zad_1);
458 Mu_1 = Mad*Zu_1+Mu;
459 Ma_1 = Mad*Za_1+Ma;
460 Mtheta_1 = Mad*Ztheta_1;
461 Mq_1 = Mad*Zq_1+Mq;
462 Mde_1 = Mad*Zde_1+Mde;
463
464 Zu_2 = Zu_1*V;
465 Za_2 = Za_1*V-g*sin(Theta);
466 Zq_2 = (Zq_1-1)*V;
467 Ztheta_2 = Ztheta_1*V+g*sin(Theta);
468 Zde_2 = Zde_1*V;
469
470 % Longitudinal Characteristic Equations
471 % Numu(s)
472 Au = Xde*(V-Zad);
473 Bu = -Xde*((V-Za)*Mq+Za+Mad*(V-Zq))+Zde*Xa;
474 Cu = Xde*(Mq*Za+Mad*g*sin(Theta)-(Ma+MTa)*(V-Zq));
475 Du = g*sin(Theta)*Xde*(Ma+MTa)-g*cos(Theta)*Zde*(Ma+MTa)+Mde*(g*
      cos(Theta)*Za-g*sin(Theta)*Xa);
476 Numu = [Au,Bu,Cu,Du];
477 % Numa(s)
478 Aa = Zde;
479 Ba = Xde*Zu - Zde*((Xu+XTu)+Mq)+Mde*(Zq+V);
480 Ca = Xde*((Zq+V)*(Mu+MTu)-Mq*Zu)+Zde*Mq*(Xu+XTu)-Mde*(g*sin(Theta)
      +(Zq+V)*(Xu+XTu));

```

```

481 Da = -g*sin(Theta)*Xde*(Mu+MTu)+g*cos(Theta)*Zde*(Mu+MTu)+Mde*(g*
      sin(Theta)*(Xu+XTu)-g*cos(Theta)*Zu);
482 Numa = [Aa,Ba,Ca,Da];
483 % Numt(s)
484 At = Zde*Mad+Mde*(V-Zad);
485 Bt = Xde*(Zu*Mad+(V-Zad)*(Mu+MTu))+Zde*((Ma+MTa)-Mad*(Xu+XTu))-Mde
      *((V-Zad)*(Xu+XTu)-Za);
486 Ct = Xde*((Ma+MTa)*Zu-(Mu+MTu)*Za)-Zde*((Ma+MTa)*(Xu+XTu)+Xa*(Mu+
      MTu))+Mde*((Xu+XTu)*Za-Xa*Zu);
487 Numt = [At,Bt,Ct];
488 % D1(s)
489 A1 = (V-Zad);
490 B1 = -(V-Zad)*(Xu+XTu+Mq)-Za-Mad*(Zq+V);
491 C1 = (Xu+XTu)*(Mq*(V-Zad)+Za+Mad*(V+Zq))+Mq*Za-Zu*Xa+Mad*g*sin(
      Theta)-(Ma+MTa)*(V-Zq);
492 D1 = g*sin(Theta)*((Ma+MTa)-Mad*(Xu+XTu))+g*cos(Theta)*(Mad*Zu+(Mu
      +MTu)*(V-Zad))-Xa*(Mu+MTu)*(Zq+V)+Zu*Xa*Mq+(Xu+XTu)*((Ma+MTa)*
      (Zq+V)-Mq*Za);
493 E1 = g*cos(Theta)*(Zu*(Ma+MTa)-Za*(Mu+MTu))+g*sin(Theta)*((Mu+MTu)
      *Xa-(Xu+XTu)*(Ma+MTa));
494 D1s = [A1,B1,C1,D1,E1];
495
496 % SV matrix
497 A_long = [Xu_1, Xa_1, Xq_1, Xtheta_1; Zu_1, Za_1, Zq_1, Ztheta_1;
      Mu_1, Ma_1, Mq_1, Mtheta_1; 0,0,1,0];
498 B_long = [Xde_1; Zde_1;Mde_1;0];
499 C_long = [1,0,0,0;0,1,0,0;0,0,1,0;0,0,0,1];
500 D_long = [0;0;0;0];
501
502 % Lateral-Directional Dynamic Stability and Control Derivatives
503 % ratios
504 I1 = I_XZ/I_XX;
505 I2 = I_XZ/I_ZZ;
506 % Y
507 Yb = (q1*S_W*Cyb)/m;
508 Yr = ((q1*S_W*Cyr)/m)*(b_W/(2*V));
509 Yp = ((q1*S_W*Cyp)/m)*(b_W/(2*V));
510 Ydr = (q1*S_W*Cydr)/m;
511 Yda = (q1*S_W*Cyda)/m;
512 % L

```

```
513 Lb = (q1*S_W*Clb*b_W)/I_XX;
514 Lr = ((q1*S_W*Clr*b_W)/I_XX)*(b_W/(2*V));
515 Lp = ((q1*S_W*Clp*b_W)/I_XX)*(b_W/(2*V));
516 Lda = (q1*S_W*Clda*b_W)/I_XX;
517 Ldr = (q1*S_W*Cldr*b_W)/I_XX;
518 % N
519 Nb = (q1*S_W*Cnb*b_W)/I_ZZ;
520 NTb = (q1*S_W*CnTb*b_W)/I_ZZ;
521 Np = ((q1*S_W*Cnp*b_W)/I_ZZ)*(b_W/(2*V));
522 Nr = ((q1*S_W*Cnr*b_W)/I_ZZ)*(b_W/(2*V));
523 Ndr = (q1*S_W*Cndr*b_W)/I_ZZ;
524 Nda = (q1*S_W*Cnda*b_W)/I_ZZ;
525
526 % State-Space Inputs
527 Yb_1 = Yb/V;
528 Yp_1 = Yp/V;
529 Yr_1 = (Yr-V)/V;
530 Yphi_1 = (g*cos(Theta))/V;
531 Yda_1 = Yda/V;
532 Ydr_1 = Ydr/V;
533
534 Lb_1 = (Lb+I1*Nb)/(1-I1*I2);
535 Lp_1 = (Lp+I1*Np)/(1-I1*I2);
536 Lr_1 = (Lr+I1*Nr)/(1-I1*I2);
537 Lda_1 = (Lda+I1*Nda)/(1-I1*I2);
538 Ldr_1 = (Ldr+I1*Ndr)/(1-I1*I2);
539
540 Nb_1 = (I2*Lb+Nb)/(1-I1*I2);
541 Np_1 = (I2*Lp+Np)/(1-I1*I2);
542 Nr_1 = (I2*Lr+Nr)/(1-I1*I2);
543 Nda_1 = (I2*Lda+Nda)/(1-I1*I2);
544 Ndr_1 = (I2*Ldr+Ndr)/(1-I1*I2);
545
546 Yb_2 = Yb_1*V;
547 Yp_2 = Yp_1*V;
548 Yr_2 = V*(Yr_1+1);
549 Yphi_2 = Yphi_1*V -g*cos(Theta);
550 Yda_2 = Yda_1*V;
551 Ydr_2 = Ydr_1*V;
552
```

```
553 % SV Lateral-Directional Matrix
554 A_latdir = [Yb_1, Yp_1, Yr_1, Yphi_1; Lb_1, Lp_1, Lr_1, 0; Nb_1,
             Np_1, Nr_1, 0; 0,1,tan(Theta),0];
555 B_latdir = [Yda_1, Ydr_1; Lda_1, Ldr_1; Nda_1, Ndr_1; 0,0];
556 C_latdir = [1,0,0,0;0,1,0,0;0,0,1,0;0,0,0,1];
557 D_latdir = [0,0;0,0;0,0;0,0];
558
559 % Output
560 % Longitudinal Output
561 sys_long = ss(A_long, B_long, C_long, D_long);
562 tf_long = tf(sys_long)
563 eig_long = eig(sys_long);
564
565 % % LQR at Take-off Condition
566 % Q_long = [0.001,0,0,0;0,0.001,0,0;0,0,1000,0;0,0,0,0.0001];
567 % R_long = 0.1;
568 % K_long = lqr(A_long, B_long, Q_long, R_long);
569
570 % LQR at Cruise Condition
571 Q_long = [0.001,0,0,0;0,0.001,0,0;0,0,1000,0;0,0,0,0.0001];
572 R_long = 0.1;
573 K_long = lqr(A_long, B_long, Q_long, R_long);
574
575 cl_long = ss((A_long-B_long*K_long),B_long,C_long,D_long);
576 cltf_long = tf(cl_long)
577 eiglong_cl = eig(cl_long);
578
579 omega_sp = sqrt(abs(eig_long(1,1)^2));
580 omega_ph = sqrt(abs(eig_long(3,1)^2));
581 damp_sp = abs(real(eig_long(1,1)))/omega_sp;
582 damp_ph = abs(real(eig_long(3,1)))/omega_ph;
583
584 omega_sp_cl = sqrt(abs(eiglong_cl(1,1)^2));
585 omega_ph_cl = sqrt(abs(eiglong_cl(3,1)^2));
586 damp_sp_cl = abs(real(eiglong_cl(1,1)))/omega_sp_cl;
587 damp_ph_cl = abs(real(eiglong_cl(3,1)))/omega_ph_cl;
588
589 % Lateral Directional Output
590 sys_latdir = ss(A_latdir, B_latdir, C_latdir, D_latdir);
591 tf_latdir = tf(sys_latdir)
```

```
592 eig_latdir = eig(sys_latdir);
593
594 % % LQR For at Take-off Condition
595 % Q_latdir = [0.1,0,0,0;0,1,0,0;0,0,1000,0;0,0,0,0.00001];
596 % R_latdir = 0.0000001;
597 % K_latdir = lqr(A_latdir, B_latdir, Q_latdir, R_latdir);
598
599 % LQR For at Cruise Condition
600 Q_latdir = [0.1,0,0,0;0,1,0,0;0,0,1000,0;0,0,0,0.00001];
601 R_latdir = 0.0000001;
602 K_latdir = lqr(A_latdir, B_latdir, Q_latdir, R_latdir);
603
604 cl_latdir = ss((A_latdir-B_latdir*K_latdir),B_latdir,C_latdir,
        D_latdir);
605 cltf_latdir = tf(cl_latdir)
606 eiglatdir_cl = eig(cl_latdir);
607
608 omega_dr = sqrt(abs(eig_latdir(2,1)^2));
609 damp_dr = abs(real(eig_latdir(2,1)))/omega_dr;
610 t_roll = -1/(eig_latdir(1,1));
611 t_spiral = -1/(eig_latdir(4,1));
612 log_e_2 = 0.69314718055995;
613 t2_spiral = t_spiral*log_e_2;
614
615 omega_dr_cl = sqrt(abs(eiglatdir_cl(2,1)^2));
616 damp_dr_cl = abs(real(eiglatdir_cl(2,1)))/omega_dr_cl;
617 t_roll_cl = -1/(eiglatdir_cl(1,1));
618 t_spiral_cl = -1/(eiglatdir_cl(4,1));
619 t2_spiral_cl = t_spiral_cl*log_e_2;
620
621 % Plotting
622 % Plot Eigenvalues Open Loop
623 % Longitudinal
624 figure(1)
625 plotoptions = pzoptions;
626 % plotoptions.Title.String = 'Longitudinal Eigenvalues at Take-off
        Condition';
627 plotoptions.Title.String = 'Longitudinal Eigenvalues at Cruise
        Condition';
628 pzplot_long = pzplot(sys_long,plotoptions,'r');
```

```
629 % Lateral Directional
630 figure(2)
631 plotoptions = pzoptions;
632 % plotoptions.Title.String = 'Lateral-Directional Eigenvalues at
    Take-off Condition';
633 plotoptions.Title.String = 'Lateral-Directional Eigenvalues at
    Cruise Condition';
634 pzplot_latdir = pzplot(sys_latdir,plotoptions,'r');
635
636 % Plot Eigenvalues Closed-Loop
637 % Longitudinal
638 figure(10)
639 plotoptions = pzoptions;
640 % plotoptions.Title.String = 'Longitudinal Eigenvalues at Take-off
    Condition with Control Feedback';
641 plotoptions.Title.String = 'Longitudinal Eigenvalues at Cruise
    Condition with Control Feedback';
642 pzplot_cllong = pzplot(cl_long,plotoptions,'r');
643 % Lateral Directional
644 figure(11)
645 plotoptions = pzoptions;
646 % plotoptions.Title.String = 'Lateral-Directional Eigenvalues at
    Take-off Condition with Control Feedback';
647 plotoptions.Title.String = 'Lateral-Directional Eigenvalues at
    Cruise Condition with Control Feedback';
648 pzplot_cllatdir = pzplot(cl_latdir,plotoptions,'r');
649
650 % Closed Loop Step Response Plot
651 figure(8)
652 cltflong_step = stepplot(cltf_long);
653 grid on;
654 set(findall(gcf,'type','line'),'linewidth',1.5);
655
656 figure(9)
657 cltflatdir_step = stepplot(cltf_latdir);
658 grid on;
659 set(findall(gcf,'type','line'),'linewidth',1.5);
660
661 % Plot Trim diagram
662 Cma_deg = Cma*deg2rad;
```

```
663 Cmde_deg = Cmde*deg2rad;
664 a1deg = -20:0.1:20;
665 de1deg = (Cm0 + Cma_deg*a1deg)/(-Cmde_deg);
666 figure(5)
667 plot(a1deg,de1deg,'LineWidth', 1.5);
668 grid on;
669 title('Trim Diagram');
670 xlabel('Angle of Attack \alpha in deg');
671 ylabel('Elevator deflection \delta_e in deg');
672
673 % Plot Cm vs Alpha
674 Cma_deg = Cma*deg2rad;
675 Cm1_plot = Cm0 + Cma_deg*a1deg;
676 figure(7)
677 plot(a1deg,Cm1_plot,'LineWidth', 1.5);
678 grid on;
679 title('Pitching Moment Coefficient vs Angle of Attack');
680 xlabel('\alpha in deg');
681 ylabel('C_m');
682
683 % Store DATA
684 SD = table(CDa,CLa,Cma,CDu,CLu,Cmu,CLq,Cmq,CLad,Cmad,CLde,Cmde,
            CTX1,CmT1,CTXu,CmTu,CmTa,Cyb,Clb,Cnb,Cyp,Clp,Cnp,Cyr,Clr,Cnr,
            Cyda,Cllda,Cnda,Cydr,Cldr,Cndr);
685 dft_ol = table(omega_sp,damp_sp,omega_ph,damp_ph,omega_dr,damp_dr,
            t_roll,t2_spiral);
686 dft_cl = table(omega_sp_cl,damp_sp_cl,omega_ph_cl,damp_ph_cl,
            omega_dr_cl,damp_dr_cl,t_roll_cl,t2_spiral_cl);
687
688 matrix_long = table(A_long,B_long);
689 matrix_latdir = table(A_latdir,B_latdir);
690 kgain_long = table(K_long);
691 kgain_latdir = table(K_latdir);
692 Stability_Derivative = rows2vars(SD);
693 eigenvalues = table(eig_long,eig_latdir,eiglong_cl,eiglatdir_cl);
694 Damp_NF_TC_OL = rows2vars(dft_ol);
695 Damp_NF_TC_CL = rows2vars(dft_cl);
696 SSC = table(CD1,CL1,Cm1,Cy1,Cn1,Cl1,a1_deg,de1_deg,b1_deg,da1_deg,
            dr1_deg);
697 SteadyStateCoeff = rows2vars(SSC);
```

```
698 S_long = stepinfo(cltf_long);  
699 S_latdir = stepinfo(cltf_latdir);
```

Appendix B: MATLAB Code for Approach 2

```
1  clc
2  clear;
3  deg2rad = 0.0174533;
4  rad2deg = 57.3;
5
6  % Flight Condition
7  e = 0.85; % Oswald efficiency
8  % rho = 1.225; % Air Density at take-off condition in kg/m3
9  rho = 0.86341; % Air Density at cruise condition in kg/m3
10 g = 9.81; % gravitational acceleration in m/s2
11 pi = 3.1416;
12 % V = 93.64; % Aircraft Take-off Velocity in m/s
13 V = 205.8; % Aircraft Cruise Velocity in m/s
14 Mach = V * 0.00291545; % Mach number
15 q1 = 1/2*rho*V^2; % Dynamic Pressure
16 roc = 13 % rate of climb m/s
17
18 % Fuselage geometry
19 m = 144560.00911369; % Aircraft mass in kg
20 df = 5; % Maximum diameter of fuselage in m
21 hf = 4.5; % Fuselage diameter in m
22 a_FUS_deg = 1; % Angle of attack of the Fuselage in deg
23 a_FUS = a_FUS_deg * deg2rad; % Angle of attack of the Fuselage in
    rad
24 L_F = 32.77775; % Fuselage length in m
25
26 % Inertia
27 I_XX = 5391992711550.996;
28 I_XZ = -557802990253.2191;
29 I_YY = 3151300757404.5815;
30 I_ZZ = 7652161022155.232;
31
32 % Wing geometry
```

```

33 AR_W = 8; % Wing Aspect Ratio
34 S_W = 200; % Wing Planform Area in m2
35 c_W = 5; % Mean Aerodynamic Chord Wing in m
36 b_W = S_W / c_W; % Wing span in m
37 lambda = 0.5; % Taper ratio of the Wing, HT and VT
38 c_Wr = ((3*c_W)/2)*((1+lambda)/(1+lambda+lambda^2));
39 c_Wt = lambda * c_Wr;
40 Dih_deg = -2; % Dihedral angle of the Wing and Horizontal Tail in
    deg
41 Dih_rad = Dih_deg * deg2rad; % Dihedral angle of the Wing and
    Horizontal Tail in rad
42 i_w0 = 0; % Wing Setting Angle in deg
43 i_w = i_w0 * deg2rad; % Wing Setting Angle in rad
44 a_W_deg = a_FUS_deg + i_w0; % Wing AoA in deg
45 a_W = a_W_deg * deg2rad; % Wing AoA in rad
46 ew_deg = 0; % Wing Twist Angle in deg
47 ew_rad = ew_deg * deg2rad; % Wing Twist Angle in rad
48 wapex = 10.4392; % Wing Apex in m
49
50 % Wing Sweep Angle
51 SA_WLE_deg = 0; % Wing Sweep Angle at Leading Edge in deg
52 SA_WLE_rad = SA_WLE_deg * deg2rad; % Wing Sweep Angle at Leading
    Edge in rad
53
54 tanSA_W50 = tan(SA_WLE_rad)-((4*0.5*(1-lambda))/(AR_W*(1+lambda)))
    ;
55 SA_W50_rad = atan(tanSA_W50); % Wing Sweep Angle at 50% Chord in
    rad
56 SA_W50_deg = SA_W50_rad*rad2deg; % Wing Sweep Angle at 50% Chord
    in deg
57
58 tanSA_W25 = tan(SA_WLE_rad)-((4*0.25*(1-lambda))/(AR_W*(1+lambda))
    );
59 SA_W25_rad = atan(tanSA_W25); % Wing Sweep Angle at 25% Chord in
    rad
60 SA_W25_deg = SA_W25_rad * rad2deg; % Wing Sweep Angle at 25% Chord
    in deg
61
62 % Horizontal Tail Geometry
63 AR_HT = 4.5; % HT Aspect Ratio

```

```
64 S_HT = 48.9337; % HT Planform area
65 b_HT = sqrt(AR_HT*S_HT); % HT Span in m
66 c_HT = b_HT/AR_HT; %HT MAC in m
67 c_HTr = ((3*c_HT)/2)*((1+lambda)/(1+lambda+lambda^2)); % HT Root
    Chord
68 c_HTt = c_HTr * lambda; % HT Tip Chord
69
70 % HT Sweep Angle
71 SA_HTLE_deg = 12; % HT Sweep Angle at Leading Edge in deg
72 SA_HTLE_rad = SA_HTLE_deg * deg2rad; % HT Sweep Angle at Leading
    Edge in rad
73 tanSA_HT50 = tan(SA_HTLE_rad)-((4*0.5*(1-lambda))/(AR_HT*(1+lambda
    )));
74 SA_HT50_rad = atan(tanSA_HT50); % HT Sweep Angle at 50% Chord in
    rad
75 SA_HT50_deg = SA_HT50_rad * rad2deg; %HT Sweep Angle at 50% Chord
    in deg
76 tanSA_HT25 = tan(SA_HTLE_rad)-((4*0.25*(1-lambda))/(AR_HT*(1+
    lambda)));
77 SA_HT25_rad = atan(tanSA_HT25); % HT Sweep Angle at 25% Chord in
    rad
78 SA_HT25_deg = SA_HT25_rad * rad2deg; %HT Sweep Angle at 25% Chord
    in deg
79
80 % Vertical Tail Geometry
81 AR_VT = 1.2; % VT Aspect Ratio
82 S_VT = 31.3176; % VT Plaform Area in m2
83 b_VT = sqrt(AR_VT*S_VT); %VT Span in m
84 c_VT = b_VT/AR_VT; %VT MAC in m
85 c_VTr = ((3*c_VT)/2)*((1+lambda)/(1+lambda+lambda^2)); % VT Root
    Chord
86 c_VTt = c_VTr * lambda; % VT Tip Chord
87
88 % VT Sweep Angle
89 SA_VTLE_deg = 22; % VT Sweep Angle at Leading Edge in deg
90 SA_VTLE_rad = SA_VTLE_deg * deg2rad; % VT Sweep Angle at Leading
    Edge in rad
91
92 % Control Surface Geom
93 % Elevator
```

```
94 b_elev = 5; % Elevator Span in m
95 c_elev = 0.35*c_HTr; % Elevator chord in m
96 S_elev = b_elev*c_elev; % Elevator Area in m2
97 % Aileron
98 b_ail = 0.26*(b_W/2); % Aileron Span in m
99 c_ail = 0.25*c_W; % Aileron chord in m
100 S_ail = b_ail*c_ail*2; % Aileron Area in m2
101 % Rudder
102 S_rud = 0.25*S_VT; % Rudder Area in m2
103 c_rud = 0.3*c_VTr; % Rudder chord in m
104 b_rud = S_rud/c_rud; % Rudder Span in m
105
106 % Location of Wing, HT and VT
107 z_W = 3.908076; % Location of Wing in Z axis
108 x_W = 10.439200; % Location of Wing in X axis
109 z_HT = 9.161455; % Location of HT in Z axis
110 x_HT = 31.311799; % Location of HT in X axis
111 z_VT = 3.048570; % Location of VT in Z axis
112 x_VT = 28.061452; % Location of VT in X axis
113
114 % Wing Lift Coefficient
115 Cla_W_deg = 0.10039; % Wing Airfoil Lift Curve Slope in /deg
116 Cla_W_rad = Cla_W_deg * rad2deg; % Wing Airfoil Lift Curve Slope
    in /rad
117 a_zerolift = -2.10390*deg2rad; % Wing Airfoil Zero AoA in rad
118 CLa_W = Cla_W_rad/(1+(Cla_W_rad/(pi*AR_W*e))); % Wing Lift Curve
    Slope in /rad
119 CLa_WMO = CLa_W;
120 K_WB = 1+0.025*(df/b_W)-0.25*(df/b_W)^2;
121 CLa_WB = K_WB * CLa_W; % Wing-Fuselage Lift Curve Slope in /rad
122 CLO_W = abs(a_zerolift)*CLa_WB; % Zero AoA Wing Lift Coefficient
123
124 % Location of Aircraft Center of Gravity and Aerodynamic Center
125 x_CG = 10.57338; % Location of CG X-axis from Nose in m
126 z_CG = 1.56417636; % Location of CG Z-axis from Nose in m
127
128 Xac_W = 0.22; % Wing AC based on Torenbeek
129 Df1_Xac = -(1.8/CLa_WB)*((df*hf*wapex)/(S_W*c_W)); % Correction
    factor
```

STABILITY ANALYSIS AND CONTROL DESIGN OF BARUNA-1

```

130 Df2_Xac = (0.273/(1+lambda))*((df*x_CG*(b_W-df))/(c_W^2*(b_W+2.15*
      df)))*tanSA_W25; % Correction factor
131 Xac_WB = Xac_W+Df1_Xac+Df2_Xac; % Location of AC Wing-Fuselage in
      terms of MAC
132 Xac_MAC_WB = Xac_WB * c_W; % Location of AC Wing-Fuselage wrt MAC
      from Wing Leading edge in m
133 xac_WB = wapex + Xac_MAC_WB; %Location of Wing AC from nose in m
134
135 Xac_HT = 0.25; % Location of AC HT wrt HT MAC
136 Xac_MAC_HT = Xac_HT * c_HT; % Location of AC HT in m
137 x_MAC_HT = (b_HT/6)*((1+2*lambda)/(1+lambda))*tan(SA_HTLE_rad); %
      Location of HT MAC from HT Leading edge in m
138 xac_MAC_HT = x_MAC_HT + Xac_MAC_HT; % Location of AC HT wrt MAC
      from HT Leading edge in m
139 xac_HT = x_HT + xac_MAC_HT; % Location of HT AC from nose in m
140 Xac_H = (xac_HT - wapex)/c_W;
141
142 Xac_VT = 0.25; % Location of AC VT wrt VT MAC
143 Xac_MAC_VT = Xac_VT * c_VT; % Location of AC VT in m
144 x_MAC_VT = (b_VT/6)*((1+2*lambda)/(1+lambda))*tan(SA_VTLE_rad); %
      Location of VT MAC from VT Leading edge in m
145 xac_MAC_VT = x_MAC_VT + Xac_MAC_VT; % Location of AC VT wrt MAC
      from VT Leading edge in m
146 xac_VT = x_VT + xac_MAC_VT; % Location of VT AC from nose in m
147 zac_VT = x_MAC_VT/tan(SA_VTLE_rad); % Location of VT AC from VT
      Root Chord Z axis.
148
149 X_CG_WRT_ACWB = x_CG-xac_WB; % Location of from AC Wing-Fuselage
      in m
150 X_CG = X_CG_WRT_ACWB/c_W; % Location of CG in terms of MAC
151
152 X_V = xac_VT - x_CG;
153 Z_V = z_VT + zac_VT;
154
155 Z_R = (z_VT)+(b_rud/2);
156 X_R = x_VT+(c_VTr-(c_rud/2));
157
158 % Lift Coefficient
159 % HT Lift Coefficient NACA 0012
160 Cla_HT_deg = 0.09596; % HT Airfoil Lift Curve Slope in /deg

```

STABILITY ANALYSIS AND CONTROL DESIGN OF BARUNA-1

```

161 Cla_HT_rad = Cla_HT_deg*rad2deg; % HT Airfoil Lift Curve Slope in
    /rad
162 CLa_HT = Cla_HT_rad/(1+(Cla_HT_rad/(pi*AR_HT*e))); % HT Lift Curve
    Slope in /rad
163 de_da = (2*CLa_WB)/(pi*AR_W);
164 nHT = 1; % HT Effectiveness for T-Tail=1
165 CLO_HT = 0; %Zero AoA HT Lift Coefficient
166
167 % VT Lift Coefficient NACA 0012
168 Cla_VT_deg = 0.09596; % VT Airfoil Lift Curve Slope in /deg
169 Cla_VT_rad = Cla_VT_deg*rad2deg; % VT Airfoil Lift Curve Slope in
    /rad
170 CLa_VT = Cla_VT_rad/(1+(Cla_VT_rad/(pi*AR_VT*e))); % VT Lift Curve
    Slope in /rad
171
172 % General Expression for Lift Stability
173 CLO = CLO_W;
174 CLa = 5.674; % DATCOM at Cruise Condition
175 % CLa = 3.718; % DATCOM at Take-off Condition
176 re = S_elev/S_HT;
177 tau_e = -4.66*re^4+8.79*re^3-6.44*re^2+2.85*re+0.0316;
178 CLde = nHT*(S_HT/S_W)*CLa_HT*tau_e;
179
180 CL1 = 0.214; % DATCOM at Cruise Condition
181 % CL1 = 1.313; % DATCOM at Take-off Condition
182
183 % Pitching Moment Coefficient
184 Cmac_W = -0.0859; % for MS-0317 extracted from airfoil graph
185 Cmac_HT = 0; % symmetrical
186 Cm0_W = Cmac_W + CLO*(X_CG - Xac_WB);
187 Cm0_HT = Cmac_HT + CLO_HT * (Xac_H);
188 Cm0 = Cm0_W + Cm0_HT;
189 Cma = -3.414; % DATCOM at Cruise Condition
190 % Cma = -4.425; % DATCOM at Take-off Condition
191 Cmde = -CLa_HT*nHT*(S_HT/S_W)*(Xac_H-X_CG)*tau_e;
192
193 % AoA
194 % a1 = (Cmde*(CL1-CLO)-CLde*(-Cm0))/(CLa*Cmde-Cma*CLde);
195 a1_deg = 1.344; % DATCOM at Cruise Condition
196 % a1_deg = 12.0856; % DATCOM at Take-off Condition

```

STABILITY ANALYSIS AND CONTROL DESIGN OF BARUNA-1

```

197 a1 = a1_deg * deg2rad;
198
199 % Elevator Deflection
200 % de1 = (CLa*(-Cm0)-Cma*(CL1-CL0))/(CLa*Cmde-Cma*CLde);
201 de1 = (Cm0 + Cma*a1)/(-Cmde);
202 de1_deg = de1*rad2deg;
203
204 % Cm1
205 Cm1 = Cm0 + Cma*a1 + Cmde*de1;
206
207 % Drag Coefficient
208 CD0 = 0.00089; % Baruna-1 Paper
209 CDa = ((2*CL1)/(pi*AR_W*e))*CLa;
210 CDde = 0;
211 % CD1 = 0.016; % DATCOM at Cruise Condition
212 CD1 = 0.103; % DATCOM at Take-off Condition
213
214 % Longitudinal Small Perturbation
215 dCD_dMach = 0.0169741004; % from DATCOM
216 CDu = Mach * dCD_dMach;
217 dXacWB_dMach = 0.2624126747; % from DATCOM
218 Cmu = -CL1*dXacWB_dMach;
219 CLu = (Mach^2/(1-Mach^2))*CL1;
220
221 CDad = 0.0;
222 CLad = 3.850; % DATCOM at Cruise Condition
223 Cmad = -17.08; % DATCOM at Cruise Condition
224
225 % CLad = 2.817; % DATCOM at Take-off Condition
226 % Cmad = -12.49; % DATCOM at Take-off Condition
227
228 % Pitch rate perturbation
229 CDq = 0.0;
230 B_CLq = sqrt(1-Mach^2*(cos(SA_W25_rad))^2);
231 CLq_WMO = (1/2+2*abs(Xac_WB-X_CG))*CLa_WMO;
232 CLq_W = ((AR_W+2*cos(SA_W25_rad))/(AR_W*B_CLq+2*cos(SA_W25_rad)))*
        CLq_WMO;
233 CLq_HT = 2*CLa_HT*nHT*(S_HT/S_W)*(Xac_H-X_CG);
234 CLq = 14.11; % DATCOM at Cruise Condition
235 % CLq = 13.17; % DATCOM at Take-off Condition

```

STABILITY ANALYSIS AND CONTROL DESIGN OF BARUNA-1

```

236
237 Kq = 0.8;
238 C_Cmq = (((AR_W*(0.5*abs(Xac_WB-X_CG)+2*abs(Xac_WB-X_CG)^2))/(AR_W
      +2*cos(SA_W25_rad)))+(1/24*((AR_W^3*tanSA_W25^2)/(AR_W+6*cos(
      SA_W25_rad))))+1/8);
239 Cmq_WM0 = -Kq*CLa_WM0*cos(SA_W25_rad)*C_Cmq;
240 Cmq_HT = -2*CLa_HT*nHT*(S_HT/S_W)*(Xac_H-X_CG)^2;
241 Cmq = -38.86; % DATCOM at Cruise Condition
242 % Cmq = -36.71; % DATCOM at Take-off Condition
243
244 % Thrust Coefficient
245 CTX1 = -CD1;
246 CmT1 = -Cm1;
247 CTXu = -3*CTX1;
248 dT0 = -2.46; % from centerline in m
249 dT = dT0+z_CG;
250 CmTu = (dT/c_W)*CTXu;
251 CmTa = 0;
252
253 % Thrust Force
254 LT1 = 0;
255 FTY1 = 0;
256 NT1 = 0;
257
258 % Lateral-Directional Stability Derivatives Coefficients
259
260 % Cy0
261 Cy0 = 0;
262
263 % Cyb
264 Cyb_W = -0.00573*abs(Dih_deg)+ (CL1^2/30)*((tan(SA_W25_rad)*sin(
      SA_W25_rad))/AR_W*(AR_W+4*cos(SA_W25_rad))) ;
265 nHT_depsdb = 0.724+3.06*((S_HT/S_W)/(1+cos(SA_W25_rad)))+0.4*(z_W/
      hf)+0.009*AR_W;
266 Cyb_HT = -0.00573*abs(Dih_deg)*nHT_depsdb*(S_HT/S_W);
267 bv_2r1 = b_VT/(2*0.75);
268 KY_VT = 1;
269 nVT_depsdb = 0.724+3.06*((S_VT/S_W)/(1+cos(SA_W25_rad)))+0.4*(z_W/
      hf)+0.009*AR_W;
270 Cyb_VT = -KY_VT*abs(CLa_VT)*nVT_depsdb*(S_VT/S_W);

```

STABILITY ANALYSIS AND CONTROL DESIGN OF BARUNA-1

```

271 X1_LF = 16/L_F;
272 XO_LF = 0.64;
273 Kint = -1;
274 S_PV = ((1.051*4)/2)+(4*3.448/2)+(11.758*4.5)+((1.907+4.5)*4.11/2)
      ;
275 Cyb_B = -2*Kint*(S_PV/S_W);
276 Cyb = -0.7313; % DATCOM at Cruise Condition
277 % Cyb = -0.7148; % DATCOM at Take-off Condition
278
279 % Cyda
280 Cyda = 0;
281
282 % Cydr
283 D_KR = 0.79;
284 cr_cVT = c_rud/c_VT;
285 tau_r = 0.6;
286 nVT = 1;
287 Cydr = CLa_VT*nVT*(S_VT/S_W)*D_KR*tau_r;
288
289 % Clb
290 Clb_CL1SA50 = (2.8639*10^-8)*SA_W50_deg^3+(5.7675*10^-7)*
      SA_W50_deg^2-(7.4987*10^-5)*SA_W50_deg-8.2421*10^-5;
291 KM_SA = 0.7766+1.3372*(Mach*cos(SA_W50_deg))-2.3077*(Mach*cos(
      SA_W50_deg))^2+2.0271*(Mach*cos(SA_W50_deg))^3;
292 Clb_CLAR = -(0.009804/AR_W)+(0.001/AR_W^0.005);
293 Clb_Dih = (-2.786-(50.46*AR_W)+(2.653*AR_W^2))*10^-6;
294 KM_Dih = 1+(-0.1969*(Mach*cos(SA_W50_deg))+1.6231*(Mach*cos(
      SA_W50_deg))^2-2.8513*(Mach*cos(SA_W50_deg))^3+2.1992*(Mach*cos
      (SA_W50_deg))^4)*(0.1193*AR_W-0.1961);
295 Clb_W0 = CL1*(Clb_CL1SA50*KM_SA+Clb_CLAR)+Dih_deg*(Clb_Dih*KM_Dih)
      ;
296 Clb_WB = Clb_W0*1/deg2rad;
297 Clb_HT = 0;
298 Clb_VT = Cyb_VT*((Z_V*cos(a1)-X_V*sin(a1))/b_W);
299 Clb = -0.07652; % DATCOM at Cruise Condition
300 % Clb = -0.05445; % DATCOM at Take-off Condition
301
302 % Clda
303 b = sqrt(1-Mach^2);
304 b1 = b * rad2deg;

```

```
305 k = (CLa_W*b)/(2*pi);
306 SA_bW_rad = atan(tanSA_W25/b);
307 SA_bW_deg = SA_bW_rad * rad2deg;
308 DRME = 0.79-0.52;
309 ta = 0.45;
310 cld = DRME*k/b;
311 Cld = ta*cld;
312 Clda = Cld/2;
313
314 % Cldr
315 Cldr = Cydr*((Z_R*cos(a1)-X_R*sin(a1))/b_W);
316
317 % Cnb
318 SB_S = ((1.051*4)/2)+(4*3.448/2)+(11.758*4.5)+((1.108+4.5)
          *5.736/2)+((0.75+1.108)*1.267/2)+(8.904*0.75);
319 wmax = 5;
320 L_B25 = 0.25*L_F;
321 L_B75 = 0.75*L_F;
322 z1_LB25 = 4.5;
323 z2_LB75 = 0.745570;
324 zmax_wmax = z1_LB25/wmax;
325 sqrtz1_z2 = sqrt(z1_LB25/z2_LB75);
326 lb2_SBS = L_F^2/SB_S;
327 lcg_lb = x_CG/L_F;
328 KN = 0.0005;
329 KR_f = 1.48;
330 Cnb_B = -57.3*KN*KR_f*(SB_S/S_W)*(L_F/b_W);
331 Cnb_W = 0;
332 Cnb_HT = 0;
333 Cnb_VT = -Cyb_VT*((X_V*cos(a1)+Z_V*sin(a1))/b_W);
334 Cnb = 0.05843; % DATCOM at Cruise Condition
335 % Cnb = 0.05532; % DATCOM at Take-off Condition
336
337 % Cnda
338 D_Kn_a = 0.025;
339 Cnda = D_Kn_a*CL1*Clda;
340
341 % Cndr
342 Cndr = -Cydr*((X_R*cos(a1)+Z_R*sin(a1))/b_W);
343
```

STABILITY ANALYSIS AND CONTROL DESIGN OF BARUNA-1

```

344 % Cyp
345 Cyp = 0.04437; % DATCOM at Cruise Condition
346 % Cyp = 0.009313; % DATCOM at Take-off Condition
347
348 % Clp
349 k1 = CLa_W*b/(2*pi);
350 bARW_k = b*AR_W/k1;
351 RDP_W = -0.54;
352 Clp_WB = RDP_W*k1/b;
353 k2 = CLa_HT*b/(2*pi);
354 SA_bHT0 = atan(tanSA_HT25/b);
355 SA_bHT = SA_bHT0 * rad2deg;
356 bARHT_k = b*AR_HT/k2;
357 RDP_HT = -0.42;
358 Clp_WHT = RDP_HT*k2/b;
359 Clp_HT = 1/2*Clp_WHT*(S_HT/S_W)*(b_HT/b_W)^2;
360 Clp_VT = 2*Cyb_VT*(Z_V/b_W)^2;
361 Clp = -0.4804; % DATCOM at Cruise Condition
362 % Clp = -0.2343; % DATCOM at Take-off Condition
363
364 % Cnp
365 B_Cnp = sqrt(1-Mach^2*cos(SA_W25_rad)*cos(SA_W25_rad));
366 C_Cnp = ((AR_W+4*cos(SA_W25_rad))/(AR_W*B_Cnp+4*cos(SA_W25_rad)))
          *((AR_W*B_Cnp+(1/2)*(AR_W*B_Cnp+4*cos(SA_W25_rad))*tanSA_W25^2)
          /(AR_W+(1/2)*(AR_W+4*cos(SA_W25_rad))*tanSA_W25^2));
367 Cnp_CLMOCL0 = -(1/6)*(((AR_W+6*(AR_W*cos(SA_W25_rad)))*((X_CG -
          Xac_WB)*(tanSA_W25/AR_W)+(tanSA_W25^2/12)))/(AR_W*cos(
          SA_W25_rad)));
368 Cnp_CLMCL0 = C_Cnp*Cnp_CLMOCL0;
369 Cnp_W = -Clp_WB*tan(a1)+Clp*tan(a1)+Cnp_CLMCL0*CL1;
370 Cnp_VT = -2*Cyb_VT*((X_V*cos(a1)+Z_V*sin(a1))/b_W)*((Z_V*cos(a1)-
          X_V*sin(a1)-Z_V)/b_W);
371 Cnp = -0.01482; % DATCOM at Cruise Condition
372 % Cnp = -0.1168; % DATCOM at Take-off Condition
373
374 % Cyr
375 Cyr = -2*Cyb_VT*((X_V*cos(a1)+Z_V*sin(a1))/b_W);
376
377 % Clr
378 Clr_CLMOCL0 = 0.25;

```

```
379 B_Clr = sqrt(1-Mach^2*cos(SA_W25_rad)*cos(SA_W25_rad));
380 D_num = 1+((AR_W*(1-B_Clr^2))/(2*B_Clr*(AR_W*B_Clr+2*cos(
      SA_W25_rad))))+((AR_W*B_Clr+2*cos(SA_W25_rad))/(AR_W*B_Clr+4*
      cos(SA_W25_rad)))*(tanSA_W25^2/8);
381 D_den = 1+((AR_W+2*cos(SA_W25_rad))/(AR_W+4*cos(SA_W25_rad)))*(
      tanSA_W25^2/8);
382 D_Clr = D_num/D_den;
383 Clr_CLMCL0 = D_Clr * Clr_CLMOCL0;
384 DClr_Dih = 1/12*((pi*AR_W*sin(SA_W25_rad))/(AR_W+4*cos(SA_W25_rad)
      ));
385 Clr_W = Clr_CLMCL0*CL1+DClr_Dih*Dih_rad;
386 Clr_VT = -2*Cyb_VT*((X_V*cos(a1)+Z_V*sin(a1))/b_W)*((Z_V*cos(a1)-
      X_V*sin(a1))/b_W);
387 Clr = Clr_W + Clr_VT;
388
389 % Cnr
390 Cnr_CL1 = -0.2;
391 Cnr_W = Cnr_CL1*CL1^2;
392 Cnr_VT = 2*Cyb_VT*((X_V*cos(a1)+Z_V*sin(a1))^2/b_W^2);
393 Cnr = -0.1477; % DATCOM at Cruise Condition
394 % Cnr = -0.1387; % DATCOM at Take-off Condition
395
396 % CnTb
397 CnTb = 0;
398
399 % % Location of AC Aircraft
400 Xac = ((Xac_WB+(CLa_HT/CLa_W)*nHT*(S_HT/S_W)*(1-de_da)*Xac_HT)
      /(1+(CLa_HT/CLa_W)*nHT*(S_HT/S_W)*(1-de_da)));
401 xac = wapex+Xac*c_W;
402 SM = -100*(X_CG-Xac);
403
404 % Simulation
405 % gamma = asin(roc/V); % take-off in rads
406 gamma = 0; % cruise in degs
407 Gamma = gamma*rad2deg; % in deg
408 phi = 0; % Cruise in degs
409 % phi = 5; % Takeoff in degs
410 Phi = phi*deg2rad; % in rad
411 theta = a1_deg + Gamma; % in degs
412 Theta = theta * deg2rad; % in rads
```

```

413
414 % sideslip, ailerons and rudder deflection
415 A_Latdir = (-(m*g*cos(gamma)*sin(Phi)+FTY1))/(q1*S_W);
416 B_Latdir = (-LT1/(q1*S_W*b_W));
417 C_Latdir = (-NT1/(q1*S_W*b_W));
418
419 b_1 = (A_Latdir*(Clda*Cndr-Cnda*Clldr)+B_Latdir*(Cnda*Cydr-Cyda*
        Cndr)+C_Latdir*(Cyda*Clldr-Clda*Cydr))/(Cyb*(Clda*Cndr-Cnda*Clldr
        )+Cyda*(Clldr*Cnb-Clb*Cndr)+Cydr*(Clb*Cnda-Cnb*Clda));
420 b1_deg = b_1*rad2deg;
421 da_1 = (Cyb*(B_Latdir*Cndr-C_Latdir*Clldr)+A_Latdir*(Cnb*Clldr-Clb*
        Cndr)+Cydr*(Clb*C_Latdir-Cnb*B_Latdir))/(Cyb*(Clda*Cndr-Cnda*
        Clldr)+Cyda*(Clldr*Cnb-Clb*Cndr)+Cydr*(Clb*Cnda-Cnb*Clda));
422 da1_deg = da_1*rad2deg;
423 dr_1 = (Cyb*(Clda*C_Latdir-Cnda*B_Latdir)+Cyda*(Clb*C_Latdir-Cnb*
        B_Latdir)+A_Latdir*(Clb*Cnda-Cnb*Clda))/(Cyb*(Clda*Cndr-Cnda*
        Clldr)+Cyda*(Clldr*Cnb-Clb*Cndr)+Cydr*(Clb*Cnda-Cnb*Clda));
424 dr1_deg = dr_1*rad2deg;
425
426 % Steady State LatDir Coefficient
427 % Cy1
428 Cy1 = Cy0 + Cyb*b_1 + Cyda*da_1 + Cydr*dr_1;
429 % Cl1
430 Cl0 = 0;
431 Cl1 = Cl0 + Clb*b_1 + Clda*da_1 + Clldr*dr_1;
432 % Cn1
433 Cn0 = 0;
434 Cn1 = Cn0 + Cnb*b_1 + Cnda*da_1 + Cndr*dr_1;
435
436 D_1 = CD1*q1*S_W;
437 L_1 = CL1*q1*S_W;
438 M_1 = Cm1*q1*S_W*c_W;
439 FAY_1 = Cy1*q1*S_W;
440 LA_1 = Cl1*q1*S_W*b_W;
441 NA_1 = Cn1*q1*S_W*b_W;
442
443 % Longitudinal Stability and Control Derivatives
444 Xu = (-q1*S_W*(CDu+2*CD1))/(m*V);
445 Xa = (-q1*S_W*(CDa-CL1))/m;
446 XTu = (q1*S_W*(CTXu+2*CTX1))/(m*V);

```

```
447 Xde = (-q1*S_W*CDde)/m;
448 % Z
449 Zu = -(q1*S_W*(CLu+2*CL1))/(m*V);
450 Za = -(q1*S_W*(CLa+CD1))/(m);
451 Zad = -(q1*S_W*c_W*CLad)/(2*m*V);
452 Zq = -(q1*S_W*c_W*CLq)/(2*m*V);
453 Zde = (-q1*S_W*CLde)/(m);
454 % M
455 Mu = (q1*S_W*c_W*(Cmu+2*Cm1))/(V*I_YY);
456 Ma = (q1*S_W*c_W*Cma)/(I_YY);
457 Mad = ((q1*S_W*c_W*Cmad)/(I_YY))*(c_W/(2*V));
458 Mde = (q1*S_W*c_W*Cmde)/(I_YY);
459 MTu = (q1*S_W*c_W*(CmTu+2*CmT1))/(V*I_YY);
460 MTa = (q1*S_W*c_W*CmTa)/(I_YY);
461 Mq = ((q1*S_W*c_W*Cmq)/(I_YY))*(c_W/(2*V));
462
463 % State Matrix Input
464 Xu_1 = (Xu+XTu);
465 Xa_1 = Xa;
466 Xtheta_1 = -g*cos(Theta);
467 Xq_1 = 0;
468 Xde_1 = Xde;
469 Zad_1 = Zad;
470 Zu_1 = Zu/(V-Zad_1);
471 Za_1 = Za/(V-Zad_1);
472 Zq_1 = (Zq+V)/(V-Zad_1);
473 Ztheta_1 = -((g*sin(Theta))/(V-Zad_1));
474 Zde_1 = Zde/(V-Zad_1);
475 Mu_1 = Mad*Zu_1+Mu;
476 Ma_1 = Mad*Za_1+Ma;
477 Mtheta_1 = Mad*Ztheta_1;
478 Mq_1 = Mad*Zq_1+Mq;
479 Mde_1 = Mad*Zde_1+Mde;
480
481 Zu_2 = Zu_1*V;
482 Za_2 = Za_1*V-g*sin(Theta);
483 Zq_2 = (Zq_1-1)*V;
484 Ztheta_2 = Ztheta_1*V+g*sin(Theta);
485 Zde_2 = Zde_1*V;
486
```

```

487 % Longitudinal Characteristic Equations
488 % Numu(s)
489 Au = Xde*(V-Zad);
490 Bu = -Xde*((V-Za)*Mq+Za+Mad*(V-Zq))+Zde*Xa;
491 Cu = Xde*(Mq*Za+Mad*g*sin(Theta)-(Ma+MTa)*(V-Zq));
492 Du = g*sin(Theta)*Xde*(Ma+MTa)-g*cos(Theta)*Zde*(Ma+MTa)+Mde*(g*
      cos(Theta)*Za-g*sin(Theta)*Xa);
493 Numu = [Au,Bu,Cu,Du];
494 % Numa(s)
495 Aa = Zde;
496 Ba = Xde*Zu - Zde*((Xu+XTu)+Mq)+Mde*(Zq+V);
497 Ca = Xde*((Zq+V)*(Mu+MTu)-Mq*Zu)+Zde*Mq*(Xu+XTu)-Mde*(g*sin(Theta)
      +(Zq+V)*(Xu+XTu));
498 Da = -g*sin(Theta)*Xde*(Mu+MTu)+g*cos(Theta)*Zde*(Mu+MTu)+Mde*(g*
      sin(Theta)*(Xu+XTu)-g*cos(Theta)*Zu);
499 Numa = [Aa,Ba,Ca,Da];
500 % Numt(s)
501 At = Zde*Mad+Mde*(V-Zad);
502 Bt = Xde*(Zu*Mad+(V-Zad)*(Mu+MTu))+Zde*((Ma+MTa)-Mad*(Xu+XTu))-Mde
      *((V-Zad)*(Xu+XTu)-Za);
503 Ct = Xde*((Ma+MTa)*Zu-(Mu+MTu)*Za)-Zde*((Ma+MTa)*(Xu+XTu)+Xa*(Mu+
      MTu))+Mde*((Xu+XTu)*Za-Xa*Zu);
504 Numt = [At,Bt,Ct];
505 % D1(s)
506 A1 = (V-Zad);
507 B1 = -(V-Zad)*(Xu+XTu+Mq)-Za-Mad*(Zq+V);
508 C1 = (Xu+XTu)*(Mq*(V-Zad)+Za+Mad*(V+Zq))+Mq*Za-Zu*Xa+Mad*g*sin(
      Theta)-(Ma+MTa)*(V-Zq);
509 D1 = g*sin(Theta)*((Ma+MTa)-Mad*(Xu+XTu))+g*cos(Theta)*(Mad*Zu+(Mu
      +MTu)*(V-Zad))-Xa*(Mu+MTu)*(Zq+V)+Zu*Xa*Mq+(Xu+XTu)*((Ma+MTa)*
      (Zq+V)-Mq*Za);
510 E1 = g*cos(Theta)*(Zu*(Ma+MTa)-Za*(Mu+MTu))+g*sin(Theta)*((Mu+MTu)
      *Xa-(Xu+XTu)*(Ma+MTa));
511 D1s = [A1,B1,C1,D1,E1];
512
513 % SV matrix
514 A_long = [Xu_1, Xa_1, Xq_1, Xtheta_1; Zu_1, Za_1, Zq_1, Ztheta_1;
      Mu_1, Ma_1, Mq_1, Mtheta_1; 0,0,1,0];
515 B_long = [Xde_1; Zde_1;Mde_1;0];
516 C_long = [1,0,0,0;0,1,0,0;0,0,1,0;0,0,0,1];

```

```
517 D_long = [0;0;0;0];
518
519 % Lateral-Directional Dynamic Stability and Control Derivatives
520 % ratios
521 I1 = I_XZ/I_XX;
522 I2 = I_XZ/I_ZZ;
523 % Y
524 Yb = (q1*S_W*Cyb)/m;
525 Yr = ((q1*S_W*Cyr)/m)*(b_W/(2*V));
526 Yp = ((q1*S_W*Cyp)/m)*(b_W/(2*V));
527 Ydr = (q1*S_W*Cydr)/m;
528 Yda = (q1*S_W*Cyda)/m;
529 % L
530 Lb = (q1*S_W*Clb*b_W)/I_XX;
531 Lr = ((q1*S_W*Clr*b_W)/I_XX)*(b_W/(2*V));
532 Lp = ((q1*S_W*Clp*b_W)/I_XX)*(b_W/(2*V));
533 Lda = (q1*S_W*Clda*b_W)/I_XX;
534 Ldr = (q1*S_W*Cldr*b_W)/I_XX;
535 %N
536 Nb = (q1*S_W*Cnb*b_W)/I_ZZ;
537 NTb = (q1*S_W*CnTb*b_W)/I_ZZ;
538 Np = ((q1*S_W*Cnp*b_W)/I_ZZ)*(b_W/(2*V));
539 Nr = ((q1*S_W*Cnr*b_W)/I_ZZ)*(b_W/(2*V));
540 Ndr = (q1*S_W*Cndr*b_W)/I_ZZ;
541 Nda = (q1*S_W*Cnda*b_W)/I_ZZ;
542
543 % State-Space Inputs
544 Yb_1 = Yb/V;
545 Yp_1 = Yp/V;
546 Yr_1 = (Yr-V)/V;
547 Yphi_1 = (g*cos(Theta))/V;
548 Yda_1 = Yda/V;
549 Ydr_1 = Ydr/V;
550
551 Lb_1 = (Lb+I1*Nb)/(1-I1*I2);
552 Lp_1 = (Lp+I1*Np)/(1-I1*I2);
553 Lr_1 = (Lr+I1*Nr)/(1-I1*I2);
554 Lda_1 = (Lda+I1*Nda)/(1-I1*I2);
555 Ldr_1 = (Ldr+I1*Ndr)/(1-I1*I2);
556
```

```
557 Nb_1 = (I2*Lb+Nb)/(1-I1*I2);
558 Np_1 = (I2*Lp+Np)/(1-I1*I2);
559 Nr_1 = (I2*Lr+Nr)/(1-I1*I2);
560 Nda_1 = (I2*Lda+Nda)/(1-I1*I2);
561 Ndr_1 = (I2*Ldr+Ndr)/(1-I1*I2);
562
563 Yb_2 = Yb_1*V;
564 Yp_2 = Yp_1*V;
565 Yr_2 = V*(Yr_1+1);
566 Yphi_2 = Yphi_1*V -g*cos(Theta);
567 Yda_2 = Yda_1*V;
568 Ydr_2 = Ydr_1*V;
569
570 % SV Lateral-Directional Matrix
571 A_latdir = [Yb_1, Yp_1, Yr_1, Yphi_1; Lb_1, Lp_1, Lr_1, 0; Nb_1,
             Np_1, Nr_1, 0; 0,1,tan(Theta),0];
572 B_latdir = [Yda_1, Ydr_1; Lda_1, Ldr_1; Nda_1, Ndr_1; 0,0];
573 C_latdir = [1,0,0,0;0,1,0,0;0,0,1,0;0,0,0,1];
574 D_latdir = [0,0;0,0;0,0;0,0];
575
576 % Output
577 % Longitudinal Output
578 sys_long = ss(A_long, B_long, C_long, D_long);
579 tf_long = tf(sys_long)
580 eig_long = eig(sys_long);
581
582 % % LQR at Take-off Condition
583 % Q_long = [0.001,0,0,0;0,0.001,0,0;0,0,1000,0;0,0,0,0.0001];
584 % R_long = 0.1;
585 % K_long = lqr(A_long, B_long, Q_long, R_long);
586
587 % LQR at Cruise Condition
588 Q_long = [0.001,0,0,0;0,0.001,0,0;0,0,1000,0;0,0,0,0.0001];
589 R_long = 0.1;
590 K_long = lqr(A_long, B_long, Q_long, R_long);
591
592 cl_long = ss((A_long-B_long*K_long),B_long,C_long,D_long);
593 cltf_long = tf(cl_long)
594 eiglong_cl = eig(cl_long);
595
```

```
596 omega_sp = sqrt(abs(eig_long(1,1)^2));
597 omega_ph = sqrt(abs(eig_long(3,1)^2));
598 damp_sp = abs(real(eig_long(1,1)))/omega_sp;
599 damp_ph = abs(real(eig_long(3,1)))/omega_ph;
600
601 omega_sp_cl = sqrt(abs(eiglong_cl(1,1)^2));
602 omega_ph_cl = sqrt(abs(eiglong_cl(3,1)^2));
603 damp_sp_cl = abs(real(eiglong_cl(1,1)))/omega_sp_cl;
604 damp_ph_cl = abs(real(eiglong_cl(3,1)))/omega_ph_cl;
605
606 % Lateral Directional Output
607 sys_latdir = ss(A_latdir, B_latdir, C_latdir, D_latdir);
608 tf_latdir = tf(sys_latdir)
609 eig_latdir = eig(sys_latdir);
610
611 % % LQR For at Take-off Condition
612 % Q_latdir = [0.1,0,0,0;0,1,0,0;0,0,1000,0;0,0,0,0.00001];
613 % R_latdir = 0.0000001;
614 % K_latdir = lqr(A_latdir, B_latdir, Q_latdir, R_latdir);
615
616 % LQR For at Cruise Condition
617 Q_latdir = [0.1,0,0,0;0,1,0,0;0,0,1000,0;0,0,0,0.00001];
618 R_latdir = 0.0000001;
619 K_latdir = lqr(A_latdir, B_latdir, Q_latdir, R_latdir);
620
621 cl_latdir = ss((A_latdir-B_latdir*K_latdir),B_latdir,C_latdir,
    D_latdir);
622 cltf_latdir = tf(cl_latdir)
623 eiglatdir_cl = eig(cl_latdir);
624
625 omega_dr = sqrt(abs(eig_latdir(2,1)^2));
626 damp_dr = abs(real(eig_latdir(2,1)))/omega_dr;
627 t_roll = -1/(eig_latdir(1,1));
628 t_spiral = -1/(eig_latdir(4,1));
629 log_e_2 = 0.69314718055995;
630 t2_spiral = t_spiral*log_e_2;
631
632 omega_dr_cl = sqrt(abs(eiglatdir_cl(2,1)^2));
633 damp_dr_cl = abs(real(eiglatdir_cl(2,1)))/omega_dr_cl;
634 t_roll_cl = -1/(eiglatdir_cl(1,1));
```

```
635 t_spiral_cl = -1/(eiglatdir_cl(4,1));
636 t2_spiral_cl = t_spiral_cl*log_e_2;
637
638 % Plotting
639 % Plot Eigenvalues Open Loop
640 % Longitudinal
641 figure(1)
642 plotoptions = pzoptions;
643 % plotoptions.Title.String = 'Longitudinal Eigenvalues (DATCOM) at
        Take-off Condition';
644 plotoptions.Title.String = 'Longitudinal Eigenvalues (DATCOM) at
        Cruise Condition';
645 pzplot_long = pzplot(sys_long,plotoptions,'r');
646 % Lateral Directional
647 figure(2)
648 plotoptions = pzoptions;
649 % plotoptions.Title.String = 'Lateral-Directional (DATCOM)
        Eigenvalues at Take-off Condition';
650 plotoptions.Title.String = 'Lateral-Directional (DATCOM)
        Eigenvalues at Cruise Condition';
651 pzplot_latdir = pzplot(sys_latdir,plotoptions,'r');
652
653 % Plot Eigenvalues Closed-Loop
654 % Longitudinal
655 figure(10)
656 plotoptions = pzoptions;
657 % plotoptions.Title.String = 'Longitudinal Eigenvalues (DATCOM) at
        Take-off Condition with Control Feedback';
658 plotoptions.Title.String = 'Longitudinal Eigenvalues (DATCOM) at
        Cruise Condition with Control Feedback';
659 pzplot_cllong = pzplot(cl_long,plotoptions,'r');
660 % Lateral Directional
661 figure(11)
662 plotoptions = pzoptions;
663 % plotoptions.Title.String = 'Lateral-Directional Eigenvalues (
        DATCOM) at Take-off Condition with Control Feedback';
664 plotoptions.Title.String = 'Lateral-Directional Eigenvalues (
        DATCOM) at Cruise Condition with Control Feedback';
665 pzplot_cllatdir = pzplot(cl_latdir,plotoptions,'r');
666
```

```
667 % Closed Loop Step Response Plot
668 figure(8)
669 cltflong_step = stepplot(cltf_long);
670 grid on;
671 set(findall(gcf,'type','line'),'linewidth',1.5);
672
673 figure(9)
674 cltflatdir_step = stepplot(cltf_latdir);
675 grid on;
676 set(findall(gcf,'type','line'),'linewidth',1.5);
677
678 % Plot Trim diagram
679 Cma_deg = Cma*deg2rad;
680 Cmde_deg = Cmde*deg2rad;
681 a1deg = -20:0.1:20;
682 de1deg = (Cm0 + Cma_deg*a1deg)/(-Cmde_deg);
683 figure(5)
684 plot(a1deg,de1deg,'LineWidth', 1.5);
685 grid on;
686 title('Trim Diagram (DATCOM)');
687 xlabel('Angle of Attack \alpha in deg');
688 ylabel('Elevator deflection \delta_e in deg');
689
690 % Plot Cm vs Alpha
691 Cma_deg = Cma*deg2rad;
692 Cm1_plot = Cm0 + Cma_deg*a1deg;
693 figure(7)
694 plot(a1deg,Cm1_plot,'LineWidth', 1.5);
695 grid on;
696 title('Pitching Moment Coefficient vs Angle of Attack (DATCOM)');
697 xlabel('\alpha in deg');
698 ylabel('C_m');
699
700 % Store DATA
701 SD = table(CDa,CLa,Cma,CDu,CLu,Cmu,CLq,Cmq,CLad,Cmad,CLde,Cmde,
            CTX1,CmT1,CTXu,CmTu,CmTa,Cyb,Clb,Cnb,Cyp,Clp,Cnp,Cyr,Clr,Cnr,
            Cyda,Clda,Cnda,Cydr,Cldr,Cndr);
702 dft_ol = table(omega_sp,damp_sp,omega_ph,damp_ph,omega_dr,damp_dr,
                t_roll,t2_spiral);
```

STABILITY ANALYSIS AND CONTROL DESIGN OF BARUNA-1

```
703 dft_cl = table(omega_sp_cl,damp_sp_cl,omega_ph_cl,damp_ph_cl,
    omega_dr_cl,damp_dr_cl,t_roll_cl,t2_spiral_cl);
704
705 matrix_long = table(A_long,B_long);
706 matrix_latdir = table(A_latdir,B_latdir);
707 kgain_long = table(K_long);
708 kgain_latdir = table(K_latdir);
709 Stability_Derivative = rows2vars(SD);
710 eigenvalues = table(eig_long,eig_latdir,eiglong_cl,eiglatdir_cl);
711 Damp_NF_TC_OL = rows2vars(dft_ol);
712 Damp_NF_TC_CL = rows2vars(dft_cl);
713 SSC = table(CD1,CL1,Cm1,Cy1,Cn1,Cl1,a1_deg,de1_deg,b1_deg,da1_deg,
    dr1_deg);
714 SteadyStateCoeff = rows2vars(SSC);
715 S_long = stepinfo(cltf_long);
716 S_latdir = stepinfo(cltf_latdir);
```

Appendix C: DATCOM Output at Take-off Condition

```

1  THIS SOFTWARE AND ANY ACCOMPANYING DOCUMENTATION
2  IS RELEASED "AS IS".  THE U.S. GOVERNMENT MAKES NO
3  WARRANTY OF ANY KIND, EXPRESS OR IMPLIED, CONCERNING
4  THIS SOFTWARE AND ANY ACCOMPANYING DOCUMENTATION,
5  INCLUDING, WITHOUT LIMITATION, ANY WARRANTIES OF
6  MERCHANTABILITY OR FITNESS FOR A PARTICULAR PURPOSE.
7  IN NO EVENT WILL THE U.S. GOVERNMENT BE LIABLE FOR ANY
8  DAMAGES, INCLUDING LOST PROFITS, LOST SAVINGS OR OTHER
9  INCIDENTAL OR CONSEQUENTIAL DAMAGES ARISING OUT OF THE
10 USE, OR INABILITY TO USE, THIS SOFTWARE OR ANY
11 ACCOMPANYING DOCUMENTATION, EVEN IF INFORMED IN ADVANCE
12 OF THE POSSIBILITY OF SUCH DAMAGES.
13 *****
14 *   USAF STABILITY AND CONTROL  DIGITAL DATCOM   *
15 *   PROGRAM REV. JAN 96   DIRECT INQUIRIES TO:   *
16 *   WRIGHT LABORATORY (WL/FIGC)  ATTN: W. BLAKE  *
17 *   WRIGHT PATTERSON AFB, OHIO  45433           *
18 *   PHONE (513) 255-6764,   FAX (513) 258-4054  *
19 *****
20 Preparing to start the big loop
21 At 1000
22 1          CONERR - INPUT ERROR CHECKING
23 0 ERROR CODES - N* DENOTES THE NUMBER OF OCCURENCES OF EACH ERROR
24 0 A - UNKNOWN VARIABLE NAME
25 0 B - MISSING EQUAL SIGN FOLLOWING VARIABLE NAME
26 0 C - NON-ARRAY VARIABLE HAS AN ARRAY ELEMENT DESIGNATION - (N)
27 0 D - NON-ARRAY VARIABLE HAS MULTIPLE VALUES ASSIGNED
28 0 E - ASSIGNED VALUES EXCEED ARRAY DIMENSION
29 0 F - SYNTAX ERROR
30
31 0***** INPUT DATA CARDS *****
32
33 $FLTCN
34   NMACH=1.0, MACH(1)=0.273,
35   NALPHA=11.0, ALSCHD(1)=-4.0,-2.0,0.0,1.3447,2.0,4.0,6.0,8.0,
36   10.0,12.0856,14.0, NALT=1.0, ALT(1)=0.0$
37 $OPTINS SREF=200.0, CBARR=5.0, BLREF=40.0$
38 $SYNTHS
39   XCG=10.93582, ZCG=1.23869, XW=10.4392, ZW=3.9081, ALIW=0.0,
40   XH=31.3118, ZH=9.1615, ALIH=0.5590, XV=28.0615, ZV=3.0486,
41   VERTUP=.TRUE.$
42 $BODY NX=20.0,
43   X(1)=0.0, 0.9081, 1.5414, 2.1747, 2.8079,
44   3.4412, 4.0360, 15.7584, 16.1066, 16.7399,
45   17.3732, 18.0064, 18.6397, 19.2730, 19.9063,
46   20.53952, 21.17279, 22.43933, 31.30507, 32.77775,
47   R(1)=0.0, 1.06304, 1.53502, 1.92330, 2.22704,
48   2.43145, 2.49990, 2.49935, 2.49234, 2.44719,
49   2.37281, 2.28009, 2.17801, 2.07426, 1.97559,
50   1.88815, 1.81769, 1.74989, 1.74965, 0.00000,
51   S(1)=0.0, 3.50114, 7.02149, 10.75757, 14.20014,
52   16.76594, 17.66804, 17.66121, 17.46964, 16.28699,
53   14.40578, 12.18224, 10.52271, 8.52722, 7.05941,
54   6.12233, 5.47905, 2.04937, 2.05728, 0.00000,

```

STABILITY ANALYSIS AND CONTROL DESIGN OF BARUNA-1

```

55 P(1)=0.0, 6.63316, 9.39662, 11.63553, 13.37271,
56 14.53409, 14.92119, 14.91828, 14.83927, 14.34348,
57 13.52561, 12.50600, 11.67378, 10.62747, 9.77983,
58 9.17430, 8.72474, 6.66860, 6.67252, 0.00000,$
59 SBODY
60 ZU(1)=0.0, 1.45675, 2.11066, 2.64785, 3.06932,
61 3.35319, 3.44831, 3.44808, 3.44830, 3.44830,
62 3.44829, 3.44828, 3.44827, 3.44827, 3.44827,
63 3.44827, 3.44827, 3.44827, 3.44827, 3.07356,
64 ZL(1)=0.0, -0.63997, -0.80136, -0.91294, -0.98611,
65 -1.03658, -1.05099, -1.05047, -1.01396, -0.78590,
66 -0.41674, 0.04690, 0.55725, 1.07598, 1.56931,
67 2.00651, 2.35877, 2.69772, 2.69772, 3.07356,$
68 $SWGPNF CHRDTP=3.17276, SSPNE= 17.5, SSPN=20.0, CHRDR=6.34552,
69 SAVSI=0.0, CHSTAT=0.1604, TWISTA=0.0, DHDADI=-2.0,
70 DHDADO= -2.0, TYPE=1.0$
71 $WGSCHR TYPEIN=1.0, DWASH=0.0, NPTS=45.0,
72 XCORD(1)=0.00000, 0.00200, 0.00500, 0.01250, 0.02500,
73 0.03750, 0.05000, 0.07500, 0.10000, 0.12500,
74 0.15000, 0.17500, 0.20000, 0.22500, 0.25000,
75 0.27500, 0.30000, 0.32500, 0.35000, 0.37500,
76 0.40000, 0.42500, 0.45000, 0.47500, 0.50000,
77 0.52500, 0.55000, 0.57500, 0.60000, 0.62500,
78 0.65000, 0.67500, 0.70000, 0.72500, 0.75000,
79 0.77500, 0.80000, 0.82500, 0.85000, 0.87500,
80 0.90000, 0.92500, 0.95000, 0.97500, 1.00000,
81 YUPPER(1)=.00099, .01248, .01950, .03099, .04322,
82 .05210, .05893, .06840, .07511, .08033, .08454,
83 .08805, .09096, .09339, .09536, .09694, .09815,
84 .09901, .09952, .09972, .09956, .09909, .09826,
85 .09700, .09535, .09323, .09073, .08777, .08448,
86 .08079, .07672, .07232, .06763, .06269, .05755,
87 .05225, .04687, .04132, .03576, .03013, .02444,
88 .01873, .01302, .00720, .00125,
89 YLOWER(1)=.00099, -.00857, -.01366, -.02105, -.02866,
90 -.03423, -.03865, -.04541, -.05058, -.05477, -.05817,
91 -.06099, -.06330, -.06527, -.06685, -.06812, -.06909,
92 -.06978, -.07021, -.07036, -.07019, -.06967, -.06880,
93 -.06755, -.06591, -.06389, -.06138, -.05845, -.05501,
94 -.05106, -.04674, -.04214, -.03735, -.03255, -.02780,
95 -.02309, -.01857, -.01433, -.01049, -.00719, -.00460,
96 -.00289, -.00232, -.00324, -.00597$
97 NACA-H-4-0012
98 NACA-V-4-0012
99 $VTPLNF CHRDTP=3.2841, SSPNE=6.1303, SSPN=6.1303, CHRDR=6.5682,
100 SAVSI=22.0, CHSTAT=0.25, TYPE=1.0$
101 $HTPLNF CHRDTP=2.1199, SSPNE=7.4196, SSPN=7.4196, CHRDR=4.2398,
102 SAVSI=12.0, CHSTAT=0.25, TWISTA=0.0, DHDADI=-2.0,
103 DHDADO= -2.0, TYPE= 1.0$
104 $$SYMFLP NDELTA=7.0, DELTA(1)=-30.,-20.,-10.,0.0,10.,20.,30.,
105 PHETE=0.002746065556, CHRDFI=1.4839, CHRDFO=1.4839, SPANFI=0.0,
106 SPANFO=5.0, FTYPE=1.0, CB=0.371, PHETEP=0.00285082875, NTYPE=1.0$
107 CASEID BARUNA-1
108 DIM M
109 DERIV RAD
110 SAVE
111 DAMP
112 NEXT CASE
113 $ASYFLP NDELTA=5.0, DELTAL(1)=5.,10.,20.,30.,40.,
114 DELTAR(1)=-2.,-5.,-10.,-15.,-20.,
115 STYPE=4.0, CHRDFI=1.25, CHRDFO=1.25,
116 SPANFI=28.8, SPANFO=39.2$
117 CASEID BARUNA-1 AILERONS ON WING
118 DERIV RAD
119 NEXT CASE
120 1 THE FOLLOWING IS A LIST OF ALL INPUT CARDS FOR THIS CASE.
121 0
122 $FLTCON

```

STABILITY ANALYSIS AND CONTROL DESIGN OF BARUNA-1

```

123     NMACH=1.0, MACH(1)=0.273,
124     NALPHA=11.0, ALSCHD(1)=-4.0,-2.0,0.0,1.3447,2.0,4.0,6.0,8.0,
125     10.0,12.0856,14.0, NALT=1.0, ALT(1)=0.0$
126     $OPTINS SREF=200.0, CBARR=5.0, BLREF=40.0$
127     $SYNTHS
128     XCG=10.93582, ZCG=1.23869, XW=10.4392, ZW=3.9081, ALIW=0.0,
129     XH=31.3118, ZH=9.1615, ALIH=0.5590, XV=28.0615, ZV=3.0486,
130     VERTUP=.TRUE.$
131     $BODY NX=20.0,
132     X(1)=0.0, 0.9081, 1.5414, 2.1747, 2.8079,
133     3.4412, 4.0360, 15.7584, 16.1066, 16.7399,
134     17.3732, 18.0064, 18.6397, 19.2730, 19.9063,
135     20.53952, 21.17279, 22.43933, 31.30507, 32.77775,
136     R(1)=0.0, 1.06304, 1.53502, 1.92330, 2.22704,
137     2.43145, 2.49990, 2.49935, 2.49234, 2.44719,
138     2.37281, 2.28009, 2.17801, 2.07426, 1.97559,
139     1.88815, 1.81769, 1.74989, 1.74965, 0.00000,
140     S(1)=0.0, 3.50114, 7.02149, 10.75757, 14.20014,
141     16.76594, 17.66804, 17.66121, 17.46964, 16.28699,
142     14.40578, 12.18224, 10.52271, 8.52722, 7.05941,
143     6.12233, 5.47905, 2.04937, 2.05728, 0.00000,
144     P(1)=0.0, 6.63316, 9.39662, 11.63553, 13.37271,
145     14.53409, 14.92119, 14.91828, 14.83927, 14.34348,
146     13.52561, 12.50600, 11.67378, 10.62747, 9.77983,
147     9.17430, 8.72474, 6.66860, 6.67252, 0.00000,$
148     $BODY
149     ZU(1)=0.0, 1.45675, 2.11066, 2.64785, 3.06932,
150     3.35319, 3.44831, 3.44808, 3.44830, 3.44830,
151     3.44829, 3.44828, 3.44827, 3.44827, 3.44827,
152     3.44827, 3.44827, 3.44827, 3.44827, 3.07356,
153     ZL(1)=0.0, -0.63997, -0.80136, -0.91294, -0.98611,
154     -1.03658, -1.05099, -1.05047, -1.01396, -0.78590,
155     -0.41674, 0.04690, 0.55725, 1.07598, 1.56931,
156     2.00651, 2.35877, 2.69772, 2.69772, 3.07356,$
157     $WGPLNF CHRDTIP=3.17276, SSPNE= 17.5, SSPN=20.0, CHRDR=6.34552,
158     $AVSI=0.0, CHSTAT=0.1604, TWISTA=0.0, DHDADI=-2.0,
159     DHDADO= -2.0, TYPE=1.0$
160     $WGSCHR TYPEIN=1.0, DWASH=0.0, NPTS=45.0,
161     XCORD(1)=0.00000, 0.00200, 0.00500, 0.01250, 0.02500,
162     0.03750, 0.05000, 0.07500, 0.10000, 0.12500,
163     0.15000, 0.17500, 0.20000, 0.22500, 0.25000,
164     0.27500, 0.30000, 0.32500, 0.35000, 0.37500,
165     0.40000, 0.42500, 0.45000, 0.47500, 0.50000,
166     0.52500, 0.55000, 0.57500, 0.60000, 0.62500,
167     0.65000, 0.67500, 0.70000, 0.72500, 0.75000,
168     0.77500, 0.80000, 0.82500, 0.85000, 0.87500,
169     0.90000, 0.92500, 0.95000, 0.97500, 1.00000,
170     YUPPER(1)=.00099, .01248, .01950, .03099, .04322,
171     .05210, .05893, .06840, .07511, .08033, .08454,
172     .08805, .09096, .09339, .09536, .09694, .09815,
173     .09901, .09952, .09972, .09956, .09909, .09826,
174     .09700, .09535, .09323, .09073, .08777, .08448,
175     .08079, .07672, .07232, .06763, .06269, .05755,
176     .05225, .04687, .04132, .03576, .03013, .02444,
177     .01873, .01302, .00720, .00125,
178     YLOWER(1)=.00099, -.00857, -.01366, -.02105, -.02866,
179     -.03423, -.03865, -.04541, -.05058, -.05477, -.05817,
180     -.06099, -.06330, -.06527, -.06685, -.06812, -.06909,
181     -.06978, -.07021, -.07036, -.07019, -.06967, -.06880,
182     -.06755, -.06591, -.06389, -.06138, -.05845, -.05501,
183     -.05106, -.04674, -.04214, -.03735, -.03255, -.02780,
184     -.02309, -.01857, -.01433, -.01049, -.00719, -.00460,
185     -.00289, -.00232, -.00324, -.00597$
186     NACA-H-4-0012
187     NACA-V-4-0012
188     $VTPLNF CHRDTIP=3.2841, SSPNE=6.1303, SSPN=6.1303, CHRDR=6.5682,
189     $AVSI=22.0, CHSTAT=0.25, TYPE=1.0$
190     $HTPLNF CHRDTIP=2.1199, SSPNE=7.4196, SSPN=7.4196, CHRDR=4.2398,

```

STABILITY ANALYSIS AND CONTROL DESIGN OF BARUNA-1

```

191 SAVSI=12.0, CHSTAT=0.25, TWISTA=0.0, DHDADI=-2.0,
192 DHDADO= -2.0, TYPE= 1.0$
193 $SYMFPLP NDELTA=7.0, DELTA(1) = -30., -20., -10.,0.0,10.,20.,30.,
194 PHETE=0.002746065556, CHRDFI=1.4839, CHRDFO=1.4839, SPANFI=0.0,
195 SPANFO=5.0, FTYPE=1.0, CB=0.371, PHETEP=0.00285082875, NTYPE=1.0$
196 CASEID BARUNA-1
197 DIM M
198 DERIV RAD
199 SAVE
200 DAMP
201 NEXT CASE
202 0 INPUT DIMENSIONS ARE IN M , SCALE FACTOR IS 1.0000
203
204 Return to main program from M01O01
205 1 AUTOMATED STABILITY AND CONTROL METHODS PER APRIL 1976 VERSION OF
    DATCOM
206
207          USER DEFINED WING SECTION
    UPPER ABSCISSA      UPPER ORDINATE      LOWER ABSCISSA      LOWER ORDINATE      X-FRACTION
      CHORD      MEAN LINE      THICKNESS
208      0.00000      0.00000      0.00000      0.00000      0.00000
209      -0.00412      0.01052      0.00812      -0.00661      0.00200
210      0.00012      0.01877      0.00988      -0.01293      0.00500
211      0.00642      0.03027      0.01858      -0.02033      0.01250
212      0.01937      0.04278      0.03063      -0.02822      0.02500
213      0.03259      0.05182      0.04241      -0.03395      0.03750
214      0.04600      0.05877      0.05400      -0.03849      0.05000
215      0.07258      0.06835      0.07742      -0.04536      0.07500
216      0.09839      0.07509      0.10161      -0.05056      0.10000
217      0.12376      0.08032      0.12624      -0.05476      0.12500
218      0.14893      0.08453      0.15107      -0.05816      0.15000
219      0.17404      0.08804      0.17596      -0.06098      0.17500
220      0.19918      0.09096      0.20082      -0.06330      0.20000
221      0.22433      0.09339      0.22567      -0.06527      0.22500
222      0.24943      0.09536      0.25057      -0.06685      0.25000
223      0.27455      0.09694      0.27545      -0.06812      0.27500
224      0.29966      0.09815      0.30034      -0.06909      0.30000
225      0.32479      0.09901      0.32521      -0.06978      0.32500
226      0.34989      0.09952      0.35011      -0.07021      0.35000
227      0.37495      0.09972      0.37505      -0.07036      0.37500
228      0.39995      0.09956      0.40005      -0.07019      0.40000
229      0.42492      0.09909      0.42508      -0.06967      0.42500
230      0.44997      0.09826      0.45003      -0.06880      0.45000
231      0.47502      0.09700      0.47498      -0.06755      0.47500
    0.01472      0.16455

```

STABILITY ANALYSIS AND CONTROL DESIGN OF BARUNA-1

232	0.50009	0.09535	0.49991	-0.06591	0.50000
		0.01472	0.16126		
233	0.52507	0.09323	0.52493	-0.06389	0.52500
		0.01467	0.15712		
234	0.55002	0.09073	0.54998	-0.06138	0.55000
		0.01467	0.15211		
235	0.57491	0.08777	0.57509	-0.05845	0.57500
		0.01466	0.14622		
236	0.59971	0.08448	0.60029	-0.05501	0.60000
		0.01473	0.13949		
237	0.62466	0.08079	0.62534	-0.05106	0.62500
		0.01486	0.13185		
238	0.64972	0.07672	0.65028	-0.04674	0.65000
		0.01499	0.12346		
239	0.67483	0.07232	0.67517	-0.04214	0.67500
		0.01509	0.11446		
240	0.70002	0.06763	0.69998	-0.03735	0.70000
		0.01514	0.10498		
241	0.72525	0.06269	0.72475	-0.03255	0.72500
		0.01507	0.09524		
242	0.75042	0.05755	0.74958	-0.02780	0.75000
		0.01487	0.08535		
243	0.77555	0.05225	0.77445	-0.02309	0.77500
		0.01458	0.07534		
244	0.80071	0.04686	0.79929	-0.01856	0.80000
		0.01415	0.06544		
245	0.82584	0.04131	0.82416	-0.01432	0.82500
		0.01350	0.05565		
246	0.85094	0.03574	0.84906	-0.01047	0.85000
		0.01264	0.04625		
247	0.87601	0.03010	0.87399	-0.00716	0.87500
		0.01147	0.03732		
248	0.90103	0.02440	0.89897	-0.00456	0.90000
		0.00992	0.02904		
249	0.92598	0.01869	0.92402	-0.00285	0.92500
		0.00792	0.02162		
250	0.95090	0.01297	0.94910	-0.00227	0.95000
		0.00535	0.01534		
251	0.97556	0.00717	0.97444	-0.00321	0.97500
		0.00198	0.01044		
252	1.00000	0.00000	1.00000	0.00000	1.00000
		0.00000	0.00000		
253	1	AUTOMATED STABILITY AND CONTROL METHODS PER APRIL 1976 VERSION OF			
	DATCOM				
254		WING SECTION DEFINITION			
255	0	IDEAL ANGLE OF ATTACK = 1.77118 DEG.			
256					
257		ZERO LIFT ANGLE OF ATTACK = -2.10390 DEG.			
258					
259		IDEAL LIFT COEFFICIENT = 0.45392			
260					
261		ZERO LIFT PITCHING MOMENT COEFFICIENT = -0.05514			
262					
263		MACH ZERO LIFT-CURVE-SLOPE = 0.10039 /DEG.			
264					
265		LEADING EDGE RADIUS = 0.02869 FRACTION CHORD			
266					
267		MAXIMUM AIRFOIL THICKNESS = 0.17008 FRACTION CHORD			
268					
269		DELTA-Y = 4.41423 PERCENT CHORD			
270					
271					
272	0	MACH= 0.2730 LIFT-CURVE-SLOPE = 0.10337 /DEG. XAC = 0.25958			
273	1	AUTOMATED STABILITY AND CONTROL METHODS PER APRIL 1976 VERSION OF			
	DATCOM				
274		HORIZONTAL TAIL SECTION DEFINITION			
275	0	IDEAL ANGLE OF ATTACK = 0.00000 DEG.			
276					

STABILITY ANALYSIS AND CONTROL DESIGN OF BARUNA-1

```

277             ZERO LIFT ANGLE OF ATTACK = 0.00000 DEG.
278
279             IDEAL LIFT COEFFICIENT = 0.00000
280
281             ZERO LIFT PITCHING MOMENT COEFFICIENT = 0.00000
282
283             MACH ZERO LIFT-CURVE-SLOPE = 0.09596 /DEG.
284
285             LEADING EDGE RADIUS = 0.01587 FRACTION CHORD
286
287             MAXIMUM AIRFOIL THICKNESS = 0.12000 FRACTION CHORD
288
289             DELTA-Y = 3.16898 PERCENT CHORD
290
291
292 0             MACH= 0.2730 LIFT-CURVE-SLOPE = 0.09913 /DEG.      XAC = 0.25912
293 1             AUTOMATED STABILITY AND CONTROL METHODS PER APRIL 1976 VERSION OF
                DATCOM
294
295 0             VERTICAL TAIL SECTION DEFINITION
                IDEAL ANGLE OF ATTACK = 0.00000 DEG.
296
297             ZERO LIFT ANGLE OF ATTACK = 0.00000 DEG.
298
299             IDEAL LIFT COEFFICIENT = 0.00000
300
301             ZERO LIFT PITCHING MOMENT COEFFICIENT = 0.00000
302
303             MACH ZERO LIFT-CURVE-SLOPE = 0.09596 /DEG.
304
305             LEADING EDGE RADIUS = 0.01587 FRACTION CHORD
306
307             MAXIMUM AIRFOIL THICKNESS = 0.12000 FRACTION CHORD
308
309             DELTA-Y = 3.16898 PERCENT CHORD
310
311
312 0             MACH= 0.2730 LIFT-CURVE-SLOPE = 0.09913 /DEG.      XAC = 0.25912
313 Return to main program from M50O62
314 Return to main program from M02O02
315 Return to main program from M51O63
316 1             AUTOMATED STABILITY AND CONTROL METHODS PER APRIL 1976 VERSION
                OF DATCOM
317
318             CHARACTERISTICS AT ANGLE OF ATTACK AND IN SIDESLIP
319             WING-BODY-VERTICAL TAIL-HORIZONTAL TAIL CONFIGURATION
320             BARUNA-1
321
322             _____ FLIGHT CONDITIONS _____
                REFERENCE DIMENSIONS _____
                MACH ALTITUDE VELOCITY PRESSURE TEMPERATURE REYNOLDS REF.
                REFERENCE LENGTH MOMENT REF. CENTER
323 NUMBER NUMBER AREA
                LONG. LAT. HORIZ VERT
324 M M M/SEC N/ M**2 DEG K 1/ M M**2
                M M M M
325 0 0.273 0.00 92.89 1.0133E+05 288.150 6.3308E+06 200.000
                5.000 40.000 10.936 1.239
326 0
                _____ DERIVATIVE (
                PER RADIAN)_____
327 0 ALPHA CD CL CM CN CA XCP CLA CMA
                CYB CNB CLB
328 0
329 -4.0 0.016 -0.210 0.2108 -0.210 0.001 -1.002 5.560E+00 -2.990E+00
                -7.157E-01 5.532E-02 -8.920E-02
330 -2.0 0.013 -0.016 0.0978 -0.016 0.013 -6.004 5.547E+00 -3.200E+00
                -8.493E-02
331 0.0 0.015 0.177 -0.0126 0.177 0.015 -0.071 5.586E+00 -3.204E+00
                -8.055E-02

```

STABILITY ANALYSIS AND CONTROL DESIGN OF BARUNA-1

332	1.3	0.018	0.309	-0.0885	0.310	0.010	-0.286	5.657E+00	-3.312E+00
					-7.759E-02				
333	2.0	0.020	0.374	-0.1268	0.375	0.006	-0.338	5.687E+00	-3.360E+00
					-7.615E-02				
334	4.0	0.028	0.574	-0.2449	0.575	-0.012	-0.426	5.804E+00	-3.527E+00
					-7.176E-02				
335	6.0	0.041	0.779	-0.3731	0.779	-0.040	-0.479	5.909E+00	-3.813E+00
					-6.736E-02				
336	8.0	0.059	0.986	-0.5111	0.985	-0.079	-0.519	5.456E+00	-4.077E+00
					-6.297E-02				
337	10.0	0.079	1.160	-0.6577	1.157	-0.123	-0.569	4.604E+00	-4.269E+00
					-5.873E-02				
338	12.1	0.103	1.314	-0.8157	1.306	-0.175	-0.625	3.716E+00	-4.425E+00
					-5.444E-02				
339	14.0	0.125	1.423	-0.9661	1.411	-0.223	-0.685	2.808E+00	-4.575E+00
					-5.030E-02				
340	0				ALPHA	Q/QINF	EPSLON	D(EPSLON)/D(ALPHA)	
341	0								
342					-4.0	1.000	-0.666	0.352	
343					-2.0	1.000	0.038	0.362	
344					0.0	1.000	0.782	0.383	
345					1.3	1.000	1.307	0.389	
346					2.0	1.000	1.561	0.396	
347					4.0	1.000	2.394	0.426	
348					6.0	1.000	3.266	0.437	
349					8.0	1.000	4.142	0.421	
350					10.0	1.000	4.951	0.373	
351					12.1	1.000	5.662	0.319	
352					14.0	1.000	6.235	0.299	
353	1				AUTOMATED STABILITY AND CONTROL METHODS PER APRIL 1976 VERSION				
		OF DATCOM							
354					DYNAMIC DERIVATIVES				
355					WING-BODY-VERTICAL TAIL-HORIZONTAL TAIL CONFIGURATION				
356					BARUNA-1				
357									
358					FLIGHT CONDITIONS				
		REFERENCE DIMENSIONS							
359	MACH	ALTITUDE	VELOCITY	PRESSURE	TEMPERATURE	REYNOLDS		REF.	
		REFERENCE LENGTH	MOMENT REF. CENTER						
360	NUMBER					NUMBER		AREA	
	LONG.	LAT.	HORIZ	VERT					
361		M	M/SEC	N/ M**2	DEG K	1/ M		M**2	
		M	M	M	M				
362	0 0.273	0.00	92.89	1.0133E+05	288.150	6.3308E+06		200.000	
	5.000	40.000	10.936	1.239					
363									
364	0				DYNAMIC DERIVATIVES (PER RADIAN)				
		PITCHING		ACCELERATION			ROLLING		
		YAWING							
365	0	ALPHA	CLQ	CMQ	CLAD	CMAD	CLP	CYP	
		CNP	CNR	CLR					
366	0								
367		-4.00	1.317E+01	-3.675E+01	3.106E+00	-1.377E+01	-4.692E-01	4.277E-02	
		1.979E-02	-1.341E-01	NDM					
368		-2.00	4.183E-03	-1.369E-01	3.195E+00	-1.417E+01	-4.713E-01	3.825E-02	
				NDM					
369		0.00	-1.153E-02	-1.390E-01	3.379E+00	-1.498E+01	-4.784E-01	3.377E-02	
				NDM					
370		1.34	-2.224E-02	-1.401E-01	3.434E+00	-1.523E+01	-4.857E-01	3.063E-02	
				NDM					
371		2.00	-2.750E-02	-1.405E-01	3.491E+00	-1.548E+01	-4.884E-01	2.907E-02	
				NDM					
372		4.00	-4.371E-02	-1.413E-01	3.760E+00	-1.667E+01	-4.938E-01	2.423E-02	
				NDM					
373		6.00	-6.032E-02	-1.413E-01	3.857E+00	-1.710E+01	-4.916E-01	1.925E-02	
				NDM					
374		8.00	-7.951E-02	-1.406E-01	3.719E+00	-1.649E+01	-4.330E-01	1.372E-02	
				NDM					

STABILITY ANALYSIS AND CONTROL DESIGN OF BARUNA-1

```

375      10.00      -9.853E-02  -1.398E-01      3.295E+00  -1.461E+01  -3.355E-01  1.049E-02
376      12.09      -1.168E-01  -1.387E-01      2.816E+00  -1.249E+01  -2.340E-01  9.286E-03
377      14.00      -1.296E-01  -1.378E-01      2.639E+00  -1.170E+01  -1.302E-01  1.210E-02
378 0*** NDM PRINTED WHEN NO DATCOM METHODS EXIST
379 1          AUTOMATED STABILITY AND CONTROL METHODS PER APRIL 1976 VERSION OF
      DATCOM
380                                     CHARACTERISTICS OF HIGH LIFT AND CONTROL DEVICES
381                                     TAIL PLAIN TRAILING-EDGE FLAP CONFIGURATION
382                                     BARUNA-1
383 ----- FLIGHT CONDITIONS -----
      REFERENCE DIMENSIONS
384 MACH ALTITUDE VELOCITY PRESSURE TEMPERATURE REYNOLDS REF.
      REFERENCE LENGTH MOMENT REF. CENTER
385 NUMBER NUMBER AREA
      LONG. LAT. HORIZ VERT
386 M M M/SEC N/ M**2 DEG K 1/ M M**2
387 0 0.273 0.00 92.89 4.4198E+01 933.606 5.8815E+05 200.000
      5.000 40.000 10.936 1.239
388 0 -----INCREMENTS DUE TO DEFLECTION----- ---DERIVATIVES (PER
      DEGREE)---
389 0 DELTA D(CL) D(CM) D(CL MAX) D(CD MIN) (CLA)D (CH)A
      (CH)D
390
391
392 -30.0 -0.215 0.8585 0.130 0.03196 NDM -5.680E-03
      -8.006E-03
393 -20.0 -0.185 0.7362 0.098 0.01586 NDM
      -7.560E-03
394 -10.0 -0.126 0.4982 0.057 0.00594 NDM
      -6.850E-03
395 0.0 0.000 -0.0005 0.000 0.00000 NDM
      -6.850E-03
396 10.0 0.126 -0.4982 0.057 0.00594 NDM
      -6.850E-03
397 20.0 0.185 -0.7362 0.098 0.01586 NDM
      -7.560E-03
398 30.0 0.215 -0.8585 0.130 0.03196 NDM
      -8.006E-03
399 0 *** NOTE * HINGE MOMENT DERIVATIVES ARE BASED ON TWICE THE AREA-MOMENT OF THE CONTROL ABOUT
      ITS HINGE LINE
400
401 0 ----- INDUCED DRAG COEFFICIENT INCREMENT , D(CDI) , DUE TO DEFLECTION
      -----
402 0 DELTA = -30.0 -20.0 -10.0 0.0 10.0 20.0 30.0
403 ALPHA
404 0
405 -4.0 1.31E-02 9.86E-03 4.79E-03 -7.05E-07 3.37E-03 7.78E-03 1.07E-02
406 -2.0 1.08E-02 7.85E-03 3.42E-03 6.65E-07 4.74E-03 9.79E-03 1.30E-02
407 0.0 8.49E-03 5.90E-03 2.10E-03 1.99E-06 6.07E-03 1.17E-02 1.53E-02
408 1.3 7.01E-03 4.62E-03 1.23E-03 2.86E-06 6.94E-03 1.30E-02 1.67E-02
409 2.0 6.29E-03 4.00E-03 8.07E-04 3.28E-06 7.36E-03 1.36E-02 1.75E-02
410 4.0 4.19E-03 2.19E-03 -4.27E-04 4.51E-06 8.59E-03 1.54E-02 1.96E-02
411 6.0 2.15E-03 4.38E-04 -1.62E-03 5.71E-06 9.79E-03 1.72E-02 2.16E-02
412 8.0 1.27E-04 -1.31E-03 -2.81E-03 6.90E-06 1.10E-02 1.89E-02 2.36E-02
413 10.0 -2.02E-03 -3.16E-03 -4.06E-03 8.15E-06 1.22E-02 2.08E-02 2.58E-02
414 12.1 -4.50E-03 -5.29E-03 -5.52E-03 9.61E-06 1.37E-02 2.29E-02 2.83E-02
415 14.0 -6.91E-03 -7.37E-03 -6.94E-03 1.10E-05 1.51E-02 2.50E-02 3.07E-02
416 0***NDM PRINTED WHEN NO DATCOM METHODS EXIST
417 Return to main program from M57O1
418 1 THE FOLLOWING IS A LIST OF ALL INPUT CARDS FOR THIS CASE.
419 0
420 $ASYFLP NDELTA=5.0, DELTAL(1)=5.,10.,20.,30.,40.,
421 DELTAR(1)=-2.,-5.,-10.,-15.,-20.,
422 STYPE=4.0, CHRDFI=1.25, CHRDFO=1.25,

```

STABILITY ANALYSIS AND CONTROL DESIGN OF BARUNA-1

```

423     SPANFI=28.8, SPANFO=39.2$
424     CASEID BARUNA-1 AILERONS ON WING
425     DERIV RAD
426     NEXT CASE
427     0 INPUT DIMENSIONS ARE IN M , SCALE FACTOR IS 1.0000
428
429     Return to main program from M01O01
430     1          AUTOMATED STABILITY AND CONTROL METHODS PER APRIL 1976 VERSION OF
          DATCOM
431
          USER DEFINED WING SECTION
432     UPPER ABSCISSA      UPPER ORDINATE      LOWER ABSCISSA      LOWER ORDINATE      X-FRACTION
          CHORD      MEAN LINE      THICKNESS
433     0.00000      0.00000      0.00000      0.00000      0.00000
          0.00000      0.00000
434     -0.00412      0.01052      0.00812      -0.00661      0.00200
          0.00196      0.02105
435     0.00012      0.01877      0.00988      -0.01293      0.00500
          0.00292      0.03316
436     0.00642      0.03027      0.01858      -0.02033      0.01250
          0.00497      0.05204
437     0.01937      0.04278      0.03063      -0.02822      0.02500
          0.00728      0.07188
438     0.03259      0.05182      0.04241      -0.03395      0.03750
          0.00894      0.08633
439     0.04600      0.05877      0.05400      -0.03849      0.05000
          0.01014      0.09758
440     0.07258      0.06835      0.07742      -0.04536      0.07500
          0.01149      0.11381
441     0.09839      0.07509      0.10161      -0.05056      0.10000
          0.01226      0.12569
442     0.12376      0.08032      0.12624      -0.05476      0.12500
          0.01278      0.13510
443     0.14893      0.08453      0.15107      -0.05816      0.15000
          0.01318      0.14271
444     0.17404      0.08804      0.17596      -0.06098      0.17500
          0.01353      0.14904
445     0.19918      0.09096      0.20082      -0.06330      0.20000
          0.01383      0.15426
446     0.22433      0.09339      0.22567      -0.06527      0.22500
          0.01406      0.15866
447     0.24943      0.09536      0.25057      -0.06685      0.25000
          0.01425      0.16221
448     0.27455      0.09694      0.27545      -0.06812      0.27500
          0.01441      0.16506
449     0.29966      0.09815      0.30034      -0.06909      0.30000
          0.01453      0.16724
450     0.32479      0.09901      0.32521      -0.06978      0.32500
          0.01461      0.16879
451     0.34989      0.09952      0.35011      -0.07021      0.35000
          0.01466      0.16973
452     0.37495      0.09972      0.37505      -0.07036      0.37500
          0.01468      0.17008
453     0.39995      0.09956      0.40005      -0.07019      0.40000
          0.01469      0.16975
454     0.42492      0.09909      0.42508      -0.06967      0.42500
          0.01471      0.16876
455     0.44997      0.09826      0.45003      -0.06880      0.45000
          0.01473      0.16706
456     0.47502      0.09700      0.47498      -0.06755      0.47500
          0.01472      0.16455
457     0.50009      0.09535      0.49991      -0.06591      0.50000
          0.01472      0.16126
458     0.52507      0.09323      0.52493      -0.06389      0.52500
          0.01467      0.15712
459     0.55002      0.09073      0.54998      -0.06138      0.55000
          0.01467      0.15211
460     0.57491      0.08777      0.57509      -0.05845      0.57500
          0.01466      0.14622

```

STABILITY ANALYSIS AND CONTROL DESIGN OF BARUNA-1

461	0.59971	0.08448	0.60029	-0.05501	0.60000
		0.01473	0.13949		
462	0.62466	0.08079	0.62534	-0.05106	0.62500
		0.01486	0.13185		
463	0.64972	0.07672	0.65028	-0.04674	0.65000
		0.01499	0.12346		
464	0.67483	0.07232	0.67517	-0.04214	0.67500
		0.01509	0.11446		
465	0.70002	0.06763	0.69998	-0.03735	0.70000
		0.01514	0.10498		
466	0.72525	0.06269	0.72475	-0.03255	0.72500
		0.01507	0.09524		
467	0.75042	0.05755	0.74958	-0.02780	0.75000
		0.01487	0.08535		
468	0.77555	0.05225	0.77445	-0.02309	0.77500
		0.01458	0.07534		
469	0.80071	0.04686	0.79929	-0.01856	0.80000
		0.01415	0.06544		
470	0.82584	0.04131	0.82416	-0.01432	0.82500
		0.01350	0.05565		
471	0.85094	0.03574	0.84906	-0.01047	0.85000
		0.01264	0.04625		
472	0.87601	0.03010	0.87399	-0.00716	0.87500
		0.01147	0.03732		
473	0.90103	0.02440	0.89897	-0.00456	0.90000
		0.00992	0.02904		
474	0.92598	0.01869	0.92402	-0.00285	0.92500
		0.00792	0.02162		
475	0.95090	0.01297	0.94910	-0.00227	0.95000
		0.00535	0.01534		
476	0.97556	0.00717	0.97444	-0.00321	0.97500
		0.00198	0.01044		
477	1.00000	0.00000	1.00000	0.00000	1.00000
		0.00000	0.00000		
478	1	AUTOMATED STABILITY AND CONTROL METHODS PER APRIL 1976 VERSION OF			
	DATCOM				
479		WING SECTION DEFINITION			
480	0	IDEAL ANGLE OF ATTACK = 1.77118 DEG.			
481					
482		ZERO LIFT ANGLE OF ATTACK = -2.10390 DEG.			
483					
484		IDEAL LIFT COEFFICIENT = 0.45392			
485					
486		ZERO LIFT PITCHING MOMENT COEFFICIENT = -0.05514			
487					
488		MACH ZERO LIFT-CURVE-SLOPE = 0.10039 /DEG.			
489					
490		LEADING EDGE RADIUS = 0.02869 FRACTION CHORD			
491					
492		MAXIMUM AIRFOIL THICKNESS = 0.17008 FRACTION CHORD			
493					
494		DELTA-Y = 4.41423 PERCENT CHORD			
495					
496					
497	0	MACH= 0.2730 LIFT-CURVE-SLOPE = 0.10337 /DEG. XAC = 0.25958			
498	1	AUTOMATED STABILITY AND CONTROL METHODS PER APRIL 1976 VERSION OF			
	DATCOM				
499		HORIZONTAL TAIL SECTION DEFINITION			
500	0	IDEAL ANGLE OF ATTACK = 0.00000 DEG.			
501					
502		ZERO LIFT ANGLE OF ATTACK = 0.00000 DEG.			
503					
504		IDEAL LIFT COEFFICIENT = 0.00000			
505					
506		ZERO LIFT PITCHING MOMENT COEFFICIENT = 0.00000			
507					
508		MACH ZERO LIFT-CURVE-SLOPE = 0.09596 /DEG.			
509					

STABILITY ANALYSIS AND CONTROL DESIGN OF BARUNA-1

```

510             LEADING EDGE RADIUS = 0.01587 FRACTION CHORD
511
512             MAXIMUM AIRFOIL THICKNESS = 0.12000 FRACTION CHORD
513
514             DELTA-Y = 3.16898 PERCENT CHORD
515
516
517 0             MACH= 0.2730 LIFT-CURVE-SLOPE = 0.09913 /DEG.      XAC = 0.25912
518 1             AUTOMATED STABILITY AND CONTROL METHODS PER APRIL 1976 VERSION OF
                    DATCOM
519
520             VERTICAL TAIL SECTION DEFINITION
521             IDEAL ANGLE OF ATTACK = 0.00000 DEG.
522
523             ZERO LIFT ANGLE OF ATTACK = 0.00000 DEG.
524
525             IDEAL LIFT COEFFICIENT = 0.00000
526
527             ZERO LIFT PITCHING MOMENT COEFFICIENT = 0.00000
528
529             MACH ZERO LIFT-CURVE-SLOPE = 0.09596 /DEG.
530
531             LEADING EDGE RADIUS = 0.01587 FRACTION CHORD
532
533             MAXIMUM AIRFOIL THICKNESS = 0.12000 FRACTION CHORD
534
535             DELTA-Y = 3.16898 PERCENT CHORD
536
537 0             MACH= 0.2730 LIFT-CURVE-SLOPE = 0.09913 /DEG.      XAC = 0.25912
538 Return to main program from M50O62
539 Return to main program from M02O02
540 Return to main program from M51O63
541 1             AUTOMATED STABILITY AND CONTROL METHODS PER APRIL 1976 VERSION
                    OF DATCOM
542
543             CHARACTERISTICS AT ANGLE OF ATTACK AND IN SIDESLIP
544             WING-BODY-VERTICAL TAIL-HORIZONTAL TAIL CONFIGURATION
545             BARUNA-1 AILERONS ON WING
546
547 ----- FLIGHT CONDITIONS -----
548
549 REFERENCE DIMENSIONS -----
550 MACH ALTITUDE VELOCITY PRESSURE TEMPERATURE REYNOLDS REF.
551 NUMBER REFERENCE LENGTH MOMENT REF. CENTER NUMBER AREA
552 LONG. LAT. HORIZ VERT
553 M M/SEC N/ M**2 DEG K 1/ M M**2
554 M M M M M M
555 0 0.273 0.00 92.89 1.0133E+05 288.150 6.3308E+06 200.000
556 5.000 40.000 10.936 1.239
557
558 -----DERIVATIVE (
559 PER RADIAN)-----
560 ALPHA CD CL CM CN CA XCP CLA CMA
561 CYB CNB CLB
562 0
563 -4.0 0.016 -0.210 0.2108 -0.210 0.001 -1.002 5.560E+00 -2.990E+00
564 -7.157E-01 5.532E-02 -8.920E-02
565 -2.0 0.013 -0.016 0.0978 -0.016 0.013 -6.004 5.547E+00 -3.200E+00
566 -8.493E-02
567 0.0 0.015 0.177 -0.0126 0.177 0.015 -0.071 5.586E+00 -3.204E+00
568 -8.055E-02
569 1.3 0.018 0.309 -0.0885 0.310 0.010 -0.286 5.657E+00 -3.312E+00
570 -7.759E-02
571 2.0 0.020 0.374 -0.1268 0.375 0.006 -0.338 5.687E+00 -3.360E+00
572 -7.615E-02
573 4.0 0.028 0.574 -0.2449 0.575 -0.012 -0.426 5.804E+00 -3.527E+00
574 -7.176E-02
575 6.0 0.041 0.779 -0.3731 0.779 -0.040 -0.479 5.909E+00 -3.813E+00
576 -6.736E-02

```

STABILITY ANALYSIS AND CONTROL DESIGN OF BARUNA-1

```

561      8.0      0.059      0.986      -0.5111      0.985      -0.079      -0.519      5.456E+00      -4.077E+00
                    -6.297E-02
562     10.0      0.079      1.160      -0.6577      1.157      -0.123      -0.569      4.604E+00      -4.269E+00
                    -5.873E-02
563     12.1      0.103      1.314      -0.8157      1.306      -0.175      -0.625      3.716E+00      -4.425E+00
                    -5.444E-02
564     14.0      0.125      1.423      -0.9661      1.411      -0.223      -0.685      2.808E+00      -4.575E+00
                    -5.030E-02
565 0
566 0
567
568
569
570
571
572
573
574
575
576
577
578 1
                    ALPHA      Q/QINF      EPSLON      D(EPSLON)/D(ALPHA)
                    -4.0      1.000      -0.666      0.352
                    -2.0      1.000      0.038      0.362
                    0.0      1.000      0.782      0.383
                    1.3      1.000      1.307      0.389
                    2.0      1.000      1.561      0.396
                    4.0      1.000      2.394      0.426
                    6.0      1.000      3.266      0.437
                    8.0      1.000      4.142      0.421
                    10.0     1.000      4.951      0.373
                    12.1     1.000      5.662      0.319
                    14.0     1.000      6.235      0.299
579 1
                    DATCOM
                    AUTOMATED STABILITY AND CONTROL METHODS PER APRIL 1976 VERSION OF
580
581
582
                    CHARACTERISTICS OF HIGH LIFT AND CONTROL DEVICES
                    WING PLAIN TRAILING-EDGE FLAP CONFIGURATION
                    BARUNA-1 AILERONS ON WING
                    _____ FLIGHT CONDITIONS _____
                    REFERENCE DIMENSIONS
583 MACH      ALTITUDE      VELOCITY      PRESSURE      TEMPERATURE      REYNOLDS      REF.
                    REFERENCE LENGTH      MOMENT REF. CENTER
584 NUMBER
                    LONG.      LAT.      HORIZ      VERT      NUMBER      AREA
                    M      M      M/SEC      N/ M**2      DEG K      1/ M      M**2
                    M      M      M      M      M
585 0 0.273      0.00      92.89      4.4198E+01      933.606      5.8815E+05      200.000
                    5.000      40.000      10.936      1.239
586 0
587 0
                    _____YAWING MOMENT COEFFICIENT,CN,DUE TO CONTROL DEFLECTION
588 0(DALTAL-DELTAR)= 7.0      15.0      30.0      45.0      60.0
589 0ALPHA
590 0
591 -4.0      0.000E+00      0.000E+00      0.000E+00      0.000E+00      0.000E+00
592 -2.0      -0.000E+00      -0.000E+00      -0.000E+00      -0.000E+00      -0.000E+00
593 0.0      -0.000E+00      -0.000E+00      -0.000E+00      -0.000E+00      -0.000E+00
594 1.3      -0.000E+00      -0.000E+00      -0.000E+00      -0.000E+00      -0.000E+00
595 2.0      -0.000E+00      -0.000E+00      -0.000E+00      -0.000E+00      -0.000E+00
596 4.0      -0.000E+00      -0.000E+00      -0.000E+00      -0.000E+00      -0.000E+00
597 6.0      -0.000E+00      -0.000E+00      -0.000E+00      -0.000E+00      -0.000E+00
598 8.0      -0.000E+00      -0.000E+00      -0.000E+00      -0.000E+00      -0.000E+00
599 10.0     -0.000E+00      -0.000E+00      -0.000E+00      -0.000E+00      -0.000E+00
600 12.1     -0.000E+00      -0.000E+00      -0.000E+00      -0.000E+00      -0.000E+00
601 14.0     -0.000E+00      -0.000E+00      -0.000E+00      -0.000E+00      -0.000E+00
602 0
603 0
604 0
605
606
607
608
609
610
611
612
613
                    DELTAL      DELTAR      (CL)ROLL
                    5.0      -2.0      0.0000E+00
                    10.0     -5.0      0.0000E+00
                    20.0     -10.0     0.0000E+00
                    30.0     -15.0     0.0000E+00
                    40.0     -20.0     0.0000E+00
610 Return to main program from M57O71
611 1 THE FOLLOWING IS A LIST OF ALL INPUT CARDS FOR THIS CASE.
612 0
613 1 END OF JOB.

```

Appendix D: DATCOM Output at Cruise Condition

```

1  THIS SOFTWARE AND ANY ACCOMPANYING DOCUMENTATION
2  IS RELEASED "AS IS".  THE U.S. GOVERNMENT MAKES NO
3  WARRANTY OF ANY KIND, EXPRESS OR IMPLIED, CONCERNING
4  THIS SOFTWARE AND ANY ACCOMPANYING DOCUMENTATION,
5  INCLUDING, WITHOUT LIMITATION, ANY WARRANTIES OF
6  MERCHANTABILITY OR FITNESS FOR A PARTICULAR PURPOSE.
7  IN NO EVENT WILL THE U.S. GOVERNMENT BE LIABLE FOR ANY
8  DAMAGES, INCLUDING LOST PROFITS, LOST SAVINGS OR OTHER
9  INCIDENTAL OR CONSEQUENTIAL DAMAGES ARISING OUT OF THE
10 USE, OR INABILITY TO USE, THIS SOFTWARE OR ANY
11 ACCOMPANYING DOCUMENTATION, EVEN IF INFORMED IN ADVANCE
12 OF THE POSSIBILITY OF SUCH DAMAGES.
13 *****
14 *   USAF STABILITY AND CONTROL  DIGITAL DATCOM   *
15 *   PROGRAM REV. JAN 96   DIRECT INQUIRIES TO:   *
16 *   WRIGHT LABORATORY (WL/FIGC)  ATTN: W. BLAKE *
17 *   WRIGHT PATTERSON AFB, OHIO  45433           *
18 *   PHONE (513) 255-6764,   FAX (513) 258-4054  *
19 *****
20 Preparing to start the big loop
21 At 1000
22 1          CONERR - INPUT ERROR CHECKING
23 0 ERROR CODES - N* DENOTES THE NUMBER OF OCCURENCES OF EACH ERROR
24 0 A - UNKNOWN VARIABLE NAME
25 0 B - MISSING EQUAL SIGN FOLLOWING VARIABLE NAME
26 0 C - NON-ARRAY VARIABLE HAS AN ARRAY ELEMENT DESIGNATION - (N)
27 0 D - NON-ARRAY VARIABLE HAS MULTIPLE VALUES ASSIGNED
28 0 E - ASSIGNED VALUES EXCEED ARRAY DIMENSION
29 0 F - SYNTAX ERROR
30
31 0***** INPUT DATA CARDS *****
32
33 $FLTCN
34 NMACH=1.0, MACH(1)=0.6,
35 NALPHA=11.0, ALSCHD(1)=-4.0,-2.0,0.0,1.3447,2.0,4.0,6.0,8.0,
36 10.0,12.0856,14.0, NALT=1.0, ALT(1)=3000.0$
37 $OPTINS SREF=200.0, CBARR=5.0, BLREF=40.0$
38 $$SYNTHS
39 XCG=10.93582, ZCG=1.23869, XW=10.4392, ZW=3.9081, ALIW=0.0,
40 XH=31.3118, ZH=9.1615, ALIH=0.5590, XV=28.0615, ZV=3.0486,
41 VERTUP=.TRUE.$
42 $BODY NX=20.0,
43 X(1)=0.0, 0.9081, 1.5414, 2.1747, 2.8079,
44 3.4412, 4.0360, 15.7584, 16.1066, 16.7399,
45 17.3732, 18.0064, 18.6397, 19.2730, 19.9063,
46 20.53952, 21.17279, 22.43933, 31.30507, 32.77775,
47 R(1)=0.0, 1.06304, 1.53502, 1.92330, 2.22704,
48 2.43145, 2.49990, 2.49935, 2.49234, 2.44719,
49 2.37281, 2.28009, 2.17801, 2.07426, 1.97559,
50 1.88815, 1.81769, 1.74989, 1.74965, 0.00000,
51 S(1)=0.0, 3.50114, 7.02149, 10.75757, 14.20014,
52 16.76594, 17.66804, 17.66121, 17.46964, 16.28699,
53 14.40578, 12.18224, 10.52271, 8.52722, 7.05941,
54 6.12233, 5.47905, 2.04937, 2.05728, 0.00000,

```

STABILITY ANALYSIS AND CONTROL DESIGN OF BARUNA-1

```

55 P(1)=0.0, 6.63316, 9.39662, 11.63553, 13.37271,
56 14.53409, 14.92119, 14.91828, 14.83927, 14.34348,
57 13.52561, 12.50600, 11.67378, 10.62747, 9.77983,
58 9.17430, 8.72474, 6.66860, 6.67252, 0.00000,$
59 SBODY
60 ZU(1)=0.0, 1.45675, 2.11066, 2.64785, 3.06932,
61 3.35319, 3.44831, 3.44808, 3.44830, 3.44830,
62 3.44829, 3.44828, 3.44827, 3.44827, 3.44827,
63 3.44827, 3.44827, 3.44827, 3.44827, 3.07356,
64 ZL(1)=0.0, -0.63997, -0.80136, -0.91294, -0.98611,
65 -1.03658, -1.05099, -1.05047, -1.01396, -0.78590,
66 -0.41674, 0.04690, 0.55725, 1.07598, 1.56931,
67 2.00651, 2.35877, 2.69772, 2.69772, 3.07356,$
68 $SWGPNF CHRDTP=3.17276, SSPNE= 17.5, SSPN=20.0, CHRDR=6.34552,
69 SAVSI=0.0, CHSTAT=0.1604, TWISTA=0.0, DHDADI=-2.0,
70 DHDADO= -2.0, TYPE=1.0$
71 $WGSCHR TYPEIN=1.0, DWASH=0.0, NPTS=45.0,
72 XCORD(1)=0.00000, 0.00200, 0.00500, 0.01250, 0.02500,
73 0.03750, 0.05000, 0.07500, 0.10000, 0.12500,
74 0.15000, 0.17500, 0.20000, 0.22500, 0.25000,
75 0.27500, 0.30000, 0.32500, 0.35000, 0.37500,
76 0.40000, 0.42500, 0.45000, 0.47500, 0.50000,
77 0.52500, 0.55000, 0.57500, 0.60000, 0.62500,
78 0.65000, 0.67500, 0.70000, 0.72500, 0.75000,
79 0.77500, 0.80000, 0.82500, 0.85000, 0.87500,
80 0.90000, 0.92500, 0.95000, 0.97500, 1.00000,
81 YUPPER(1)=.00099, .01248, .01950, .03099, .04322,
82 .05210, .05893, .06840, .07511, .08033, .08454,
83 .08805, .09096, .09339, .09536, .09694, .09815,
84 .09901, .09952, .09972, .09956, .09909, .09826,
85 .09700, .09535, .09323, .09073, .08777, .08448,
86 .08079, .07672, .07232, .06763, .06269, .05755,
87 .05225, .04687, .04132, .03576, .03013, .02444,
88 .01873, .01302, .00720, .00125,
89 YLOWER(1)=.00099, -.00857, -.01366, -.02105, -.02866,
90 -.03423, -.03865, -.04541, -.05058, -.05477, -.05817,
91 -.06099, -.06330, -.06527, -.06685, -.06812, -.06909,
92 -.06978, -.07021, -.07036, -.07019, -.06967, -.06880,
93 -.06755, -.06591, -.06389, -.06138, -.05845, -.05501,
94 -.05106, -.04674, -.04214, -.03735, -.03255, -.02780,
95 -.02309, -.01857, -.01433, -.01049, -.00719, -.00460,
96 -.00289, -.00232, -.00324, -.00597$
97 NACA-H-4-0012
98 NACA-V-4-0012
99 $VTPLNF CHRDTP=3.2841, SSPNE=6.1303, SSPN=6.1303, CHRDR=6.5682,
100 SAVSI=22.0, CHSTAT=0.25, TYPE=1.0$
101 $HTPLNF CHRDTP=2.1199, SSPNE=7.4196, SSPN=7.4196, CHRDR=4.2398,
102 SAVSI=12.0, CHSTAT=0.25, TWISTA=0.0, DHDADI=-2.0,
103 DHDADO= -2.0, TYPE= 1.0$
104 $SYMFLP NDELTA=7.0, DELTA(1)=-30.,-20.,-10.,0.0,10.,20.,30.,
105 PHETE=0.002746065556, CHRDFI=1.4839, CHRDFO=1.4839, SPANFI=0.0,
106 SPANFO=5.0, FTYPE=1.0, CB=0.371, PHETEP=0.00285082875, NTYPE=1.0$
107 CASEID BARUNA-1
108 DIM M
109 DERIV RAD
110 SAVE
111 DAMP
112 NEXT CASE
113 $ASYFLP NDELTA=5.0, DELTAL(1)=5.,10.,20.,30.,40.,
114 DELTAR(1)=-2.,-5.,-10.,-15.,-20.,
115 STYPE=4.0, CHRDFI=1.25, CHRDFO=1.25,
116 SPANFI=28.8, SPANFO=39.2$
117 CASEID BARUNA-1 AILERONS ON WING
118 DERIV RAD
119 NEXT CASE
120 1 THE FOLLOWING IS A LIST OF ALL INPUT CARDS FOR THIS CASE.
121 0
122 $FLTCON

```

STABILITY ANALYSIS AND CONTROL DESIGN OF BARUNA-1

```

123     NMACH=1.0, MACH(1)=0.6,
124     NALPHA=11.0, ALSCHD(1)=-4.0,-2.0,0.0,1.3447,2.0,4.0,6.0,8.0,
125     10.0,12.0856,14.0, NALT=1.0, ALT(1)=3000.0$
126     $OPTINS SREF=200.0, CBARR=5.0, BLREF=40.0$
127     $SYNTHS
128     XCG=10.93582, ZCG=1.23869, XW=10.4392, ZW=3.9081, ALIW=0.0,
129     XH=31.3118, ZH=9.1615, ALIH=0.5590, XV=28.0615, ZV=3.0486,
130     VERTUP=.TRUE.$
131     $BODY NX=20.0,
132     X(1)=0.0, 0.9081, 1.5414, 2.1747, 2.8079,
133     3.4412, 4.0360, 15.7584, 16.1066, 16.7399,
134     17.3732, 18.0064, 18.6397, 19.2730, 19.9063,
135     20.53952, 21.17279, 22.43933, 31.30507, 32.77775,
136     R(1)=0.0, 1.06304, 1.53502, 1.92330, 2.22704,
137     2.43145, 2.49990, 2.49935, 2.49234, 2.44719,
138     2.37281, 2.28009, 2.17801, 2.07426, 1.97559,
139     1.88815, 1.81769, 1.74989, 1.74965, 0.00000,
140     S(1)=0.0, 3.50114, 7.02149, 10.75757, 14.20014,
141     16.76594, 17.66804, 17.66121, 17.46964, 16.28699,
142     14.40578, 12.18224, 10.52271, 8.52722, 7.05941,
143     6.12233, 5.47905, 2.04937, 2.05728, 0.00000,
144     P(1)=0.0, 6.63316, 9.39662, 11.63553, 13.37271,
145     14.53409, 14.92119, 14.91828, 14.83927, 14.34348,
146     13.52561, 12.50600, 11.67378, 10.62747, 9.77983,
147     9.17430, 8.72474, 6.66860, 6.67252, 0.00000,$
148     $BODY
149     ZU(1)=0.0, 1.45675, 2.11066, 2.64785, 3.06932,
150     3.35319, 3.44831, 3.44808, 3.44830, 3.44830,
151     3.44829, 3.44828, 3.44827, 3.44827, 3.44827,
152     3.44827, 3.44827, 3.44827, 3.44827, 3.07356,
153     ZL(1)=0.0, -0.63997, -0.80136, -0.91294, -0.98611,
154     -1.03658, -1.05099, -1.05047, -1.01396, -0.78590,
155     -0.41674, 0.04690, 0.55725, 1.07598, 1.56931,
156     2.00651, 2.35877, 2.69772, 2.69772, 3.07356,$
157     $WGTLNF CHRDTIP=3.17276, SSPNE= 17.5, SSPN=20.0, CHRDR=6.34552,
158     $SAVSI=0.0, CHSTAT=0.1604, TWISTA=0.0, DHDADI=-2.0,
159     DHDADO= -2.0, TYPE=1.0$
160     $WGSCHR TYPEIN=1.0, DWASH=0.0, NPTS=45.0,
161     XCORD(1)=0.00000, 0.00200, 0.00500, 0.01250, 0.02500,
162     0.03750, 0.05000, 0.07500, 0.10000, 0.12500,
163     0.15000, 0.17500, 0.20000, 0.22500, 0.25000,
164     0.27500, 0.30000, 0.32500, 0.35000, 0.37500,
165     0.40000, 0.42500, 0.45000, 0.47500, 0.50000,
166     0.52500, 0.55000, 0.57500, 0.60000, 0.62500,
167     0.65000, 0.67500, 0.70000, 0.72500, 0.75000,
168     0.77500, 0.80000, 0.82500, 0.85000, 0.87500,
169     0.90000, 0.92500, 0.95000, 0.97500, 1.00000,
170     YUPPER(1)=.00099, .01248, .01950, .03099, .04322,
171     .05210, .05893, .06840, .07511, .08033, .08454,
172     .08805, .09096, .09339, .09536, .09694, .09815,
173     .09901, .09952, .09972, .09956, .09909, .09826,
174     .09700, .09535, .09323, .09073, .08777, .08448,
175     .08079, .07672, .07232, .06763, .06269, .05755,
176     .05225, .04687, .04132, .03576, .03013, .02444,
177     .01873, .01302, .00720, .00125,
178     YLOWER(1)=.00099, -.00857, -.01366, -.02105, -.02866,
179     -.03423, -.03865, -.04541, -.05058, -.05477, -.05817,
180     -.06099, -.06330, -.06527, -.06685, -.06812, -.06909,
181     -.06978, -.07021, -.07036, -.07019, -.06967, -.06880,
182     -.06755, -.06591, -.06389, -.06138, -.05845, -.05501,
183     -.05106, -.04674, -.04214, -.03735, -.03255, -.02780,
184     -.02309, -.01857, -.01433, -.01049, -.00719, -.00460,
185     -.00289, -.00232, -.00324, -.00597$
186     NACA-H-4-0012
187     NACA-V-4-0012
188     $VTPLNF CHRDTIP=3.2841, SSPNE=6.1303, SSPN=6.1303, CHRDR=6.5682,
189     $SAVSI=22.0, CHSTAT=0.25, TYPE=1.0$
190     $HTPLNF CHRDTIP=2.1199, SSPNE=7.4196, SSPN=7.4196, CHRDR=4.2398,

```

STABILITY ANALYSIS AND CONTROL DESIGN OF BARUNA-1

```

191 SAVSI=12.0, CHSTAT=0.25, TWISTA=0.0, DHDADI=-2.0,
192 DHDADO= -2.0, TYPE= 1.0$
193 $SYMFPLP NDELTA=7.0, DELTA(1) = -30., -20., -10.,0.0,10.,20.,30.,
194 PHETE=0.002746065556, CHRDFI=1.4839, CHRDFO=1.4839, SPANFI=0.0,
195 SPANFO=5.0, FTYPE=1.0, CB=0.371, PHETEP=0.00285082875, NTYPE=1.0$
196 CASEID BARUNA-1
197 DIM M
198 DERIV RAD
199 SAVE
200 DAMP
201 NEXT CASE
202 0 INPUT DIMENSIONS ARE IN M , SCALE FACTOR IS 1.0000
203
204 Return to main program from M01O01
205 1 AUTOMATED STABILITY AND CONTROL METHODS PER APRIL 1976 VERSION OF
    DATCOM
206
207          USER DEFINED WING SECTION
    UPPER ABSCISSA      UPPER ORDINATE      LOWER ABSCISSA      LOWER ORDINATE      X-FRACTION
      CHORD      MEAN LINE      THICKNESS
208      0.00000      0.00000      0.00000      0.00000      0.00000
209      -0.00412      0.01052      0.00812      -0.00661      0.00200
210      0.00012      0.01877      0.00988      -0.01293      0.00500
211      0.00642      0.03027      0.01858      -0.02033      0.01250
212      0.01937      0.04278      0.03063      -0.02822      0.02500
213      0.03259      0.05182      0.04241      -0.03395      0.03750
214      0.04600      0.05877      0.05400      -0.03849      0.05000
215      0.07258      0.06835      0.07742      -0.04536      0.07500
216      0.09839      0.07509      0.10161      -0.05056      0.10000
217      0.12376      0.08032      0.12624      -0.05476      0.12500
218      0.14893      0.08453      0.15107      -0.05816      0.15000
219      0.17404      0.08804      0.17596      -0.06098      0.17500
220      0.19918      0.09096      0.20082      -0.06330      0.20000
221      0.22433      0.09339      0.22567      -0.06527      0.22500
222      0.24943      0.09536      0.25057      -0.06685      0.25000
223      0.27455      0.09694      0.27545      -0.06812      0.27500
224      0.29966      0.09815      0.30034      -0.06909      0.30000
225      0.32479      0.09901      0.32521      -0.06978      0.32500
226      0.34989      0.09952      0.35011      -0.07021      0.35000
227      0.37495      0.09972      0.37505      -0.07036      0.37500
228      0.39995      0.09956      0.40005      -0.07019      0.40000
229      0.42492      0.09909      0.42508      -0.06967      0.42500
230      0.44997      0.09826      0.45003      -0.06880      0.45000
231      0.47502      0.09700      0.47498      -0.06755      0.47500
    0.01472      0.16455

```

STABILITY ANALYSIS AND CONTROL DESIGN OF BARUNA-1

232	0.50009	0.09535	0.49991	-0.06591	0.50000
		0.01472	0.16126		
233	0.52507	0.09323	0.52493	-0.06389	0.52500
		0.01467	0.15712		
234	0.55002	0.09073	0.54998	-0.06138	0.55000
		0.01467	0.15211		
235	0.57491	0.08777	0.57509	-0.05845	0.57500
		0.01466	0.14622		
236	0.59971	0.08448	0.60029	-0.05501	0.60000
		0.01473	0.13949		
237	0.62466	0.08079	0.62534	-0.05106	0.62500
		0.01486	0.13185		
238	0.64972	0.07672	0.65028	-0.04674	0.65000
		0.01499	0.12346		
239	0.67483	0.07232	0.67517	-0.04214	0.67500
		0.01509	0.11446		
240	0.70002	0.06763	0.69998	-0.03735	0.70000
		0.01514	0.10498		
241	0.72525	0.06269	0.72475	-0.03255	0.72500
		0.01507	0.09524		
242	0.75042	0.05755	0.74958	-0.02780	0.75000
		0.01487	0.08535		
243	0.77555	0.05225	0.77445	-0.02309	0.77500
		0.01458	0.07534		
244	0.80071	0.04686	0.79929	-0.01856	0.80000
		0.01415	0.06544		
245	0.82584	0.04131	0.82416	-0.01432	0.82500
		0.01350	0.05565		
246	0.85094	0.03574	0.84906	-0.01047	0.85000
		0.01264	0.04625		
247	0.87601	0.03010	0.87399	-0.00716	0.87500
		0.01147	0.03732		
248	0.90103	0.02440	0.89897	-0.00456	0.90000
		0.00992	0.02904		
249	0.92598	0.01869	0.92402	-0.00285	0.92500
		0.00792	0.02162		
250	0.95090	0.01297	0.94910	-0.00227	0.95000
		0.00535	0.01534		
251	0.97556	0.00717	0.97444	-0.00321	0.97500
		0.00198	0.01044		
252	1.00000	0.00000	1.00000	0.00000	1.00000
		0.00000	0.00000		
253	1	AUTOMATED STABILITY AND CONTROL METHODS PER APRIL 1976 VERSION OF			
	DATCOM				
254		WING SECTION DEFINITION			
255	0	IDEAL ANGLE OF ATTACK = 1.77118 DEG.			
256					
257		ZERO LIFT ANGLE OF ATTACK = -2.10390 DEG.			
258					
259		IDEAL LIFT COEFFICIENT = 0.45392			
260					
261		ZERO LIFT PITCHING MOMENT COEFFICIENT = -0.05514			
262					
263		MACH ZERO LIFT-CURVE-SLOPE = 0.10039 /DEG.			
264					
265		LEADING EDGE RADIUS = 0.02869 FRACTION CHORD			
266					
267		MAXIMUM AIRFOIL THICKNESS = 0.17008 FRACTION CHORD			
268					
269		DELTA-Y = 4.41423 PERCENT CHORD			
270					
271					
272	0	MACH= 0.6000 LIFT-CURVE-SLOPE = 0.11977 /DEG. XAC = 0.26313			
273	1	AUTOMATED STABILITY AND CONTROL METHODS PER APRIL 1976 VERSION OF			
	DATCOM				
274		HORIZONTAL TAIL SECTION DEFINITION			
275	0	IDEAL ANGLE OF ATTACK = 0.00000 DEG.			
276					

STABILITY ANALYSIS AND CONTROL DESIGN OF BARUNA-1

```

277             ZERO LIFT ANGLE OF ATTACK = 0.00000 DEG.
278
279             IDEAL LIFT COEFFICIENT = 0.00000
280
281             ZERO LIFT PITCHING MOMENT COEFFICIENT = 0.00000
282
283             MACH ZERO LIFT-CURVE-SLOPE = 0.09596 /DEG.
284
285             LEADING EDGE RADIUS = 0.01587 FRACTION CHORD
286
287             MAXIMUM AIRFOIL THICKNESS = 0.12000 FRACTION CHORD
288
289             DELTA-Y = 3.16898 PERCENT CHORD
290
291
292 0             MACH= 0.6000 LIFT-CURVE-SLOPE = 0.11639 /DEG.      XAC = 0.26186
293 1             AUTOMATED STABILITY AND CONTROL METHODS PER APRIL 1976 VERSION OF
                DATCOM
294
295 0             VERTICAL TAIL SECTION DEFINITION
                IDEAL ANGLE OF ATTACK = 0.00000 DEG.
296
297             ZERO LIFT ANGLE OF ATTACK = 0.00000 DEG.
298
299             IDEAL LIFT COEFFICIENT = 0.00000
300
301             ZERO LIFT PITCHING MOMENT COEFFICIENT = 0.00000
302
303             MACH ZERO LIFT-CURVE-SLOPE = 0.09596 /DEG.
304
305             LEADING EDGE RADIUS = 0.01587 FRACTION CHORD
306
307             MAXIMUM AIRFOIL THICKNESS = 0.12000 FRACTION CHORD
308
309             DELTA-Y = 3.16898 PERCENT CHORD
310
311
312 0             MACH= 0.6000 LIFT-CURVE-SLOPE = 0.11639 /DEG.      XAC = 0.26186
313 Return to main program from M50O62
314 Return to main program from M02O02
315 Return to main program from M51O63
316 1             AUTOMATED STABILITY AND CONTROL METHODS PER APRIL 1976 VERSION
                OF DATCOM
317
318             CHARACTERISTICS AT ANGLE OF ATTACK AND IN SIDESLIP
319             WING-BODY-VERTICAL TAIL-HORIZONTAL TAIL CONFIGURATION
320             BARUNA-1
321
322             _____ FLIGHT CONDITIONS _____
                REFERENCE DIMENSIONS
                MACH ALTITUDE VELOCITY PRESSURE TEMPERATURE REYNOLDS REF.
                REFERENCE LENGTH MOMENT REF. CENTER
323 NUMBER NUMBER AREA
                LONG. LAT. HORIZ VERT
324 M M M/SEC N/ M**2 DEG K 1/ M M**2
                M M M M
325 0 0.600 3000.00 197.13 7.0121E+04 268.659 1.0535E+07 200.000
                5.000 40.000 10.936 1.239
326 0
                _____ DERIVATIVE (
                PER RADIAN)_____
327 0 ALPHA CD CL CM CN CA XCP CLA CMA
                CYB CNB CLB
328 0
329 -4.0 0.018 -0.332 0.2060 -0.332 -0.005 -0.620 5.569E+00 -3.113E+00
                -7.313E-01 5.843E-02 -8.968E-02
330 -2.0 0.014 -0.133 0.0860 -0.133 0.010 -0.647 5.833E+00 -3.439E+00
                -8.485E-02
331 0.0 0.014 0.075 -0.0341 0.075 0.014 -0.451 5.876E+00 -3.484E+00
                -7.987E-02

```

STABILITY ANALYSIS AND CONTROL DESIGN OF BARUNA-1

332	1.3	0.016	0.212	-0.1166	0.212	0.011	-0.549	5.674E+00	-3.401E+00
					-7.653E-02				
333	2.0	0.017	0.276	-0.1548	0.277	0.008	-0.560	5.562E+00	-3.422E+00
					-7.491E-02				
334	4.0	0.024	0.466	-0.2823	0.467	-0.008	-0.605	5.119E+00	-3.771E+00
					-7.002E-02				
335	6.0	0.034	0.634	-0.4181	0.634	-0.032	-0.660	4.216E+00	-3.983E+00
					-6.527E-02				
336	8.0	0.045	0.760	-0.5604	0.759	-0.061	-0.738	3.875E+00	-4.260E+00
					-6.078E-02				
337	10.0	0.061	0.904	-0.7155	0.901	-0.097	-0.794	3.967E+00	-4.316E+00
					-5.595E-02				
338	12.1	0.081	1.043	-0.8678	1.037	-0.139	-0.837	3.947E+00	-4.119E+00
					-5.064E-02				
339	14.0	0.104	1.179	-1.0034	1.169	-0.184	-0.858	4.198E+00	-4.000E+00
					-4.539E-02				
340	0				ALPHA	Q/QINF	EPSLON	D(EPSLON)/D(ALPHA)	
341	0								
342					-4.0	1.000	-1.173	0.345	
343					-2.0	1.000	-0.483	0.363	
344					0.0	1.000	0.277	0.384	
345					1.3	1.000	0.798	0.419	
346					2.0	1.000	1.082	0.422	
347					4.0	1.000	1.857	0.376	
348					6.0	1.000	2.586	0.342	
349					8.0	1.000	3.225	0.315	
350					10.0	1.000	3.845	0.322	
351					12.1	1.000	4.542	0.340	
352					14.0	1.000	5.203	0.345	
353	1				AUTOMATED STABILITY AND CONTROL METHODS PER APRIL 1976 VERSION				
		OF DATCOM							
354								DYNAMIC DERIVATIVES	
355								WING-BODY-VERTICAL TAIL-HORIZONTAL TAIL CONFIGURATION	
356								BARUNA-1	
357									
358					FLIGHT CONDITIONS				
		REFERENCE DIMENSIONS							
359	MACH	ALTITUDE	VELOCITY	PRESSURE	TEMPERATURE	REYNOLDS		REF.	
360	NUMBER	REFERENCE LENGTH	MOMENT REF. CENTER			NUMBER		AREA	
361	LONG.	LAT.	HORIZ	VERT					
		M	M/SEC	N/ M**2	DEG K	1/ M		M**2	
		M	M	M	M				
362	0	0.600	3000.00	197.13	7.0121E+04	268.659	1.0535E+07	200.000	
		5.000	40.000	10.936	1.239				
363								DYNAMIC DERIVATIVES (PER RADIAN)	
364	0								
		PITCHING			ACCELERATION			ROLLING	
		YAWING							
365	0	ALPHA	CLQ	CMQ	CLAD	CMAD	CLP	CYP	
		CNP	CNR	CLR					
366	0								
367		-4.00	1.411E+01	-3.886E+01	3.196E+00	-1.417E+01	-4.617E-01	5.543E-02	
			2.754E-02	-1.406E-01	NDM				
368		-2.00			3.358E+00	-1.489E+01	-4.901E-01	5.169E-02	
			1.211E-02	-1.439E-01	NDM				
369		0.00			3.560E+00	-1.579E+01	-4.966E-01	4.723E-02	
			-3.966E-03	-1.464E-01	NDM				
370		1.34			3.877E+00	-1.720E+01	-4.806E-01	4.451E-02	
			-1.471E-02	-1.477E-01	NDM				
371		2.00			3.913E+00	-1.735E+01	-4.695E-01	4.331E-02	
			-1.996E-02	-1.482E-01	NDM				
372		4.00			3.481E+00	-1.544E+01	-4.136E-01	4.004E-02	
			-3.641E-02	-1.493E-01	NDM				
373		6.00			3.167E+00	-1.405E+01	-3.102E-01	3.840E-02	
			-5.294E-02	-1.499E-01	NDM				
374		8.00			2.915E+00	-1.293E+01	-2.616E-01	4.091E-02	
			-6.547E-02	-1.504E-01	NDM				

STABILITY ANALYSIS AND CONTROL DESIGN OF BARUNA-1

```

375      10.00      -7.796E-02  -1.502E-01      2.981E+00  -1.322E+01  -2.617E-01  4.277E-02
376      12.09      -9.019E-02  -1.497E-01      3.148E+00  -1.396E+01  -2.564E-01  4.574E-02
377      14.00      -1.012E-01  -1.487E-01      3.195E+00  -1.417E+01  -2.780E-01  4.799E-02
378 0*** NDM PRINTED WHEN NO DATCOM METHODS EXIST
379 1          AUTOMATED STABILITY AND CONTROL METHODS PER APRIL 1976 VERSION OF
      DATCOM
380                                     CHARACTERISTICS OF HIGH LIFT AND CONTROL DEVICES
381                                     TAIL PLAIN TRAILING-EDGE FLAP CONFIGURATION
382                                     BARUNA-1
383 ----- FLIGHT CONDITIONS -----
      REFERENCE DIMENSIONS
384 MACH ALTITUDE VELOCITY PRESSURE TEMPERATURE REYNOLDS REF.
      REFERENCE LENGTH MOMENT REF. CENTER
385 NUMBER NUMBER AREA
      LONG. LAT. HORIZ VERT
386 M M M/SEC N/ M**2 DEG K 1/ M M**2
387 0 0.600 3000.00 197.13 3.0587E+01 870.455 9.7872E+05 200.000
      5.000 40.000 10.936 1.239
388 0 -----INCREMENTS DUE TO DEFLECTION----- ---DERIVATIVES (PER
      DEGREE)---
389 0 DELTA D(CL) D(CM) D(CL MAX) D(CD MIN) (CLA)D (CH)A
      (CH)D
390
391
392 -30.0 -0.193 0.8140 0.130 0.03120 NDM -6.828E-03
      -9.883E-03
393 -20.0 -0.166 0.6979 0.098 0.01530 NDM
      -9.427E-03
394 -10.0 -0.113 0.4721 0.057 0.00568 NDM
      -8.700E-03
395 0.0 0.000 -0.0005 0.000 0.00000 NDM
      -8.700E-03
396 10.0 0.113 -0.4721 0.057 0.00568 NDM
      -8.700E-03
397 20.0 0.166 -0.6979 0.098 0.01530 NDM
      -9.427E-03
398 30.0 0.193 -0.8140 0.130 0.03120 NDM
      -9.883E-03
399 0 *** NOTE * HINGE MOMENT DERIVATIVES ARE BASED ON TWICE THE AREA-MOMENT OF THE CONTROL ABOUT
      ITS HINGE LINE
400
401 0 ----- INDUCED DRAG COEFFICIENT INCREMENT , D(CDI) , DUE TO DEFLECTION
      -----
402 0 DELTA = -30.0 -20.0 -10.0 0.0 10.0 20.0 30.0
403 ALPHA
404 0
405 -4.0 1.34E-02 1.03E-02 5.33E-03 -1.72E-06 1.90E-03 5.28E-03 7.58E-03
406 -2.0 1.10E-02 8.20E-03 3.88E-03 -2.65E-07 3.35E-03 7.41E-03 1.01E-02
407 0.0 8.63E-03 6.18E-03 2.51E-03 1.11E-06 4.72E-03 9.43E-03 1.24E-02
408 1.3 7.07E-03 4.84E-03 1.60E-03 2.02E-06 5.63E-03 1.08E-02 1.39E-02
409 2.0 6.37E-03 4.24E-03 1.19E-03 2.43E-06 6.04E-03 1.14E-02 1.46E-02
410 4.0 4.06E-03 2.25E-03 -1.69E-04 3.79E-06 7.40E-03 1.34E-02 1.70E-02
411 6.0 1.66E-03 1.78E-04 -1.58E-03 5.19E-06 8.80E-03 1.54E-02 1.94E-02
412 8.0 -9.09E-04 -2.04E-03 -3.08E-03 6.70E-06 1.03E-02 1.76E-02 2.19E-02
413 10.0 -3.51E-03 -4.28E-03 -4.61E-03 8.23E-06 1.18E-02 1.99E-02 2.45E-02
414 12.1 -6.14E-03 -6.54E-03 -6.15E-03 9.76E-06 1.34E-02 2.21E-02 2.72E-02
415 14.0 -8.50E-03 -8.58E-03 -7.53E-03 1.12E-05 1.48E-02 2.42E-02 2.95E-02
416 0***NDM PRINTED WHEN NO DATCOM METHODS EXIST
417 Return to main program from M57O1
418 1 THE FOLLOWING IS A LIST OF ALL INPUT CARDS FOR THIS CASE.
419 0
420 $ASYFLP NDELTA=5.0, DELTAL(1)=5.,10.,20.,30.,40.,
421 DELTAR(1)=-2.,-5.,-10.,-15.,-20.,
422 STYPE=4.0, CHRDFI=1.25, CHRDFO=1.25,

```

STABILITY ANALYSIS AND CONTROL DESIGN OF BARUNA-1

```

423     SPANFI=28.8, SPANFO=39.2$
424     CASEID BARUNA-1 AILERONS ON WING
425     DERIV RAD
426     NEXT CASE
427     0 INPUT DIMENSIONS ARE IN M , SCALE FACTOR IS 1.0000
428
429     Return to main program from M01O01
430     1          AUTOMATED STABILITY AND CONTROL METHODS PER APRIL 1976 VERSION OF
          DATCOM
431
          USER DEFINED WING SECTION
432     UPPER ABSCISSA      UPPER ORDINATE      LOWER ABSCISSA      LOWER ORDINATE      X-FRACTION
          CHORD      MEAN LINE      THICKNESS
433     0.00000      0.00000      0.00000      0.00000      0.00000
          0.00000      0.00000
434     -0.00412      0.01052      0.00812      -0.00661      0.00200
          0.00196      0.02105
435     0.00012      0.01877      0.00988      -0.01293      0.00500
          0.00292      0.03316
436     0.00642      0.03027      0.01858      -0.02033      0.01250
          0.00497      0.05204
437     0.01937      0.04278      0.03063      -0.02822      0.02500
          0.00728      0.07188
438     0.03259      0.05182      0.04241      -0.03395      0.03750
          0.00894      0.08633
439     0.04600      0.05877      0.05400      -0.03849      0.05000
          0.01014      0.09758
440     0.07258      0.06835      0.07742      -0.04536      0.07500
          0.01149      0.11381
441     0.09839      0.07509      0.10161      -0.05056      0.10000
          0.01226      0.12569
442     0.12376      0.08032      0.12624      -0.05476      0.12500
          0.01278      0.13510
443     0.14893      0.08453      0.15107      -0.05816      0.15000
          0.01318      0.14271
444     0.17404      0.08804      0.17596      -0.06098      0.17500
          0.01353      0.14904
445     0.19918      0.09096      0.20082      -0.06330      0.20000
          0.01383      0.15426
446     0.22433      0.09339      0.22567      -0.06527      0.22500
          0.01406      0.15866
447     0.24943      0.09536      0.25057      -0.06685      0.25000
          0.01425      0.16221
448     0.27455      0.09694      0.27545      -0.06812      0.27500
          0.01441      0.16506
449     0.29966      0.09815      0.30034      -0.06909      0.30000
          0.01453      0.16724
450     0.32479      0.09901      0.32521      -0.06978      0.32500
          0.01461      0.16879
451     0.34989      0.09952      0.35011      -0.07021      0.35000
          0.01466      0.16973
452     0.37495      0.09972      0.37505      -0.07036      0.37500
          0.01468      0.17008
453     0.39995      0.09956      0.40005      -0.07019      0.40000
          0.01469      0.16975
454     0.42492      0.09909      0.42508      -0.06967      0.42500
          0.01471      0.16876
455     0.44997      0.09826      0.45003      -0.06880      0.45000
          0.01473      0.16706
456     0.47502      0.09700      0.47498      -0.06755      0.47500
          0.01472      0.16455
457     0.50009      0.09535      0.49991      -0.06591      0.50000
          0.01472      0.16126
458     0.52507      0.09323      0.52493      -0.06389      0.52500
          0.01467      0.15712
459     0.55002      0.09073      0.54998      -0.06138      0.55000
          0.01467      0.15211
460     0.57491      0.08777      0.57509      -0.05845      0.57500
          0.01466      0.14622

```

STABILITY ANALYSIS AND CONTROL DESIGN OF BARUNA-1

461	0.59971	0.08448	0.60029	-0.05501	0.60000
		0.01473	0.13949		
462	0.62466	0.08079	0.62534	-0.05106	0.62500
		0.01486	0.13185		
463	0.64972	0.07672	0.65028	-0.04674	0.65000
		0.01499	0.12346		
464	0.67483	0.07232	0.67517	-0.04214	0.67500
		0.01509	0.11446		
465	0.70002	0.06763	0.69998	-0.03735	0.70000
		0.01514	0.10498		
466	0.72525	0.06269	0.72475	-0.03255	0.72500
		0.01507	0.09524		
467	0.75042	0.05755	0.74958	-0.02780	0.75000
		0.01487	0.08535		
468	0.77555	0.05225	0.77445	-0.02309	0.77500
		0.01458	0.07534		
469	0.80071	0.04686	0.79929	-0.01856	0.80000
		0.01415	0.06544		
470	0.82584	0.04131	0.82416	-0.01432	0.82500
		0.01350	0.05565		
471	0.85094	0.03574	0.84906	-0.01047	0.85000
		0.01264	0.04625		
472	0.87601	0.03010	0.87399	-0.00716	0.87500
		0.01147	0.03732		
473	0.90103	0.02440	0.89897	-0.00456	0.90000
		0.00992	0.02904		
474	0.92598	0.01869	0.92402	-0.00285	0.92500
		0.00792	0.02162		
475	0.95090	0.01297	0.94910	-0.00227	0.95000
		0.00535	0.01534		
476	0.97556	0.00717	0.97444	-0.00321	0.97500
		0.00198	0.01044		
477	1.00000	0.00000	1.00000	0.00000	1.00000
		0.00000	0.00000		
478	1	AUTOMATED STABILITY AND CONTROL METHODS PER APRIL 1976 VERSION OF			
		DATCOM			
479		WING SECTION DEFINITION			
480	0	IDEAL ANGLE OF ATTACK = 1.77118 DEG.			
481					
482		ZERO LIFT ANGLE OF ATTACK = -2.10390 DEG.			
483					
484		IDEAL LIFT COEFFICIENT = 0.45392			
485					
486		ZERO LIFT PITCHING MOMENT COEFFICIENT = -0.05514			
487					
488		MACH ZERO LIFT-CURVE-SLOPE = 0.10039 /DEG.			
489					
490		LEADING EDGE RADIUS = 0.02869 FRACTION CHORD			
491					
492		MAXIMUM AIRFOIL THICKNESS = 0.17008 FRACTION CHORD			
493					
494		DELTA-Y = 4.41423 PERCENT CHORD			
495					
496					
497	0	MACH= 0.6000 LIFT-CURVE-SLOPE = 0.11977 /DEG. XAC = 0.26313			
498	1	AUTOMATED STABILITY AND CONTROL METHODS PER APRIL 1976 VERSION OF			
		DATCOM			
499		HORIZONTAL TAIL SECTION DEFINITION			
500	0	IDEAL ANGLE OF ATTACK = 0.00000 DEG.			
501					
502		ZERO LIFT ANGLE OF ATTACK = 0.00000 DEG.			
503					
504		IDEAL LIFT COEFFICIENT = 0.00000			
505					
506		ZERO LIFT PITCHING MOMENT COEFFICIENT = 0.00000			
507					
508		MACH ZERO LIFT-CURVE-SLOPE = 0.09596 /DEG.			
509					

STABILITY ANALYSIS AND CONTROL DESIGN OF BARUNA-1

```

510             LEADING EDGE RADIUS = 0.01587 FRACTION CHORD
511
512             MAXIMUM AIRFOIL THICKNESS = 0.12000 FRACTION CHORD
513
514             DELTA-Y = 3.16898 PERCENT CHORD
515
516
517 0             MACH= 0.6000 LIFT-CURVE-SLOPE = 0.11639 /DEG.      XAC = 0.26186
518 1             AUTOMATED STABILITY AND CONTROL METHODS PER APRIL 1976 VERSION OF
                    DATCOM
519
520             VERTICAL TAIL SECTION DEFINITION
521             IDEAL ANGLE OF ATTACK = 0.00000 DEG.
522
523             ZERO LIFT ANGLE OF ATTACK = 0.00000 DEG.
524
525             IDEAL LIFT COEFFICIENT = 0.00000
526
527             ZERO LIFT PITCHING MOMENT COEFFICIENT = 0.00000
528
529             MACH ZERO LIFT-CURVE-SLOPE = 0.09596 /DEG.
530
531             LEADING EDGE RADIUS = 0.01587 FRACTION CHORD
532
533             MAXIMUM AIRFOIL THICKNESS = 0.12000 FRACTION CHORD
534
535             DELTA-Y = 3.16898 PERCENT CHORD
536
537 0             MACH= 0.6000 LIFT-CURVE-SLOPE = 0.11639 /DEG.      XAC = 0.26186
538 Return to main program from M50O62
539 Return to main program from M02O02
540 Return to main program from M51O63
541 1             AUTOMATED STABILITY AND CONTROL METHODS PER APRIL 1976 VERSION
                    OF DATCOM
542
543             CHARACTERISTICS AT ANGLE OF ATTACK AND IN SIDESLIP
544             WING-BODY-VERTICAL TAIL-HORIZONTAL TAIL CONFIGURATION
545             BARUNA-1 AILERONS ON WING
546
547 ----- FLIGHT CONDITIONS -----
548
549 REFERENCE DIMENSIONS -----
550 MACH ALTITUDE VELOCITY PRESSURE TEMPERATURE REYNOLDS REF.
551 NUMBER REFERENCE LENGTH MOMENT REF. CENTER NUMBER AREA
552 LONG. LAT. HORIZ VERT DEG K 1/ M M**2
553 M M M N/ M**2 M M
554 0 0.600 3000.00 197.13 7.0121E+04 268.659 1.0535E+07 200.000
555 5.000 40.000 10.936 1.239
556
557 -----DERIVATIVE (
558 PER RADIAN)-----
559 ALPHA CD CL CM CN CA XCP CLA CMA
560 CYB CNB CLB
561
562 0 -4.0 0.018 -0.332 0.2060 -0.332 -0.005 -0.620 5.569E+00 -3.113E+00
563 -7.313E-01 5.843E-02 -8.968E-02
564 555 -2.0 0.014 -0.133 0.0860 -0.133 0.010 -0.647 5.833E+00 -3.439E+00
565 -8.485E-02
566 556 0.0 0.014 0.075 -0.0341 0.075 0.014 -0.451 5.876E+00 -3.484E+00
567 -7.987E-02
568 557 1.3 0.016 0.212 -0.1166 0.212 0.011 -0.549 5.674E+00 -3.401E+00
569 -7.653E-02
570 558 2.0 0.017 0.276 -0.1548 0.277 0.008 -0.560 5.562E+00 -3.422E+00
571 -7.491E-02
572 559 4.0 0.024 0.466 -0.2823 0.467 -0.008 -0.605 5.119E+00 -3.771E+00
573 -7.002E-02
574 560 6.0 0.034 0.634 -0.4181 0.634 -0.032 -0.660 4.216E+00 -3.983E+00
575 -6.527E-02

```

STABILITY ANALYSIS AND CONTROL DESIGN OF BARUNA-1

```

561      8.0      0.045      0.760      -0.5604      0.759      -0.061      -0.738      3.875E+00      -4.260E+00
                    -6.078E-02
562     10.0      0.061      0.904      -0.7155      0.901      -0.097      -0.794      3.967E+00      -4.316E+00
                    -5.595E-02
563     12.1      0.081      1.043      -0.8678      1.037      -0.139      -0.837      3.947E+00      -4.119E+00
                    -5.064E-02
564     14.0      0.104      1.179      -1.0034      1.169      -0.184      -0.858      4.198E+00      -4.000E+00
                    -4.539E-02
565 0
566 0
567
568
569
570
571
572
573
574
575
576
577
578 1
                    ALPHA      Q/QINF      EPSLON      D(EPSLON)/D(ALPHA)
                    -4.0      1.000      -1.173      0.345
                    -2.0      1.000      -0.483      0.363
                    0.0      1.000      0.277      0.384
                    1.3      1.000      0.798      0.419
                    2.0      1.000      1.082      0.422
                    4.0      1.000      1.857      0.376
                    6.0      1.000      2.586      0.342
                    8.0      1.000      3.225      0.315
                    10.0     1.000      3.845      0.322
                    12.1     1.000      4.542      0.340
                    14.0     1.000      5.203      0.345
579 1
                    DATCOM
                    AUTOMATED STABILITY AND CONTROL METHODS PER APRIL 1976 VERSION OF
580
581
582
                    CHARACTERISTICS OF HIGH LIFT AND CONTROL DEVICES
                    WING PLAIN TRAILING-EDGE FLAP CONFIGURATION
                    BARUNA-1 AILERONS ON WING
                    _____ FLIGHT CONDITIONS _____
                    REFERENCE DIMENSIONS
583  MACH      ALTITUDE      VELOCITY      PRESSURE      TEMPERATURE      REYNOLDS      REF.
                    REFERENCE LENGTH      MOMENT REF. CENTER
584  NUMBER
                    LONG.      LAT.      HORIZ      VERT      NUMBER      AREA
                    M      M      M/SEC      N/ M**2      DEG K      1/ M      M**2
                    M      M
585  0 0.600      3000.00      197.13      3.0587E+01      870.455      9.7872E+05      200.000
                    5.000      40.000      10.936      1.239
586 0
587 0
                    _____YAWING MOMENT COEFFICIENT,CN,DUE TO CONTROL DEFLECTION
588 0(DALTAL-DELTAR)= 7.0      15.0      30.0      45.0      60.0
589 0ALPHA
590 0
591 -4.0      0.000E+00      0.000E+00      0.000E+00      0.000E+00      0.000E+00
592 -2.0      0.000E+00      0.000E+00      0.000E+00      0.000E+00      0.000E+00
593 0.0      -0.000E+00      -0.000E+00      -0.000E+00      -0.000E+00      -0.000E+00
594 1.3      -0.000E+00      -0.000E+00      -0.000E+00      -0.000E+00      -0.000E+00
595 2.0      -0.000E+00      -0.000E+00      -0.000E+00      -0.000E+00      -0.000E+00
596 4.0      -0.000E+00      -0.000E+00      -0.000E+00      -0.000E+00      -0.000E+00
597 6.0      -0.000E+00      -0.000E+00      -0.000E+00      -0.000E+00      -0.000E+00
598 8.0      -0.000E+00      -0.000E+00      -0.000E+00      -0.000E+00      -0.000E+00
599 10.0     -0.000E+00      -0.000E+00      -0.000E+00      -0.000E+00      -0.000E+00
600 12.1     -0.000E+00      -0.000E+00      -0.000E+00      -0.000E+00      -0.000E+00
601 14.0     -0.000E+00      -0.000E+00      -0.000E+00      -0.000E+00      -0.000E+00
602 0
603 0
604 0
                    DELTAL      DELTAR      (CL)ROLL
605      5.0      -2.0      0.0000E+00
606     10.0     -5.0      0.0000E+00
607     20.0    -10.0      0.0000E+00
608     30.0    -15.0      0.0000E+00
609     40.0    -20.0      0.0000E+00
610 Return to main program from M57O71
611 1 THE FOLLOWING IS A LIST OF ALL INPUT CARDS FOR THIS CASE.
612 0
613 1 END OF JOB.

```

Turnitin Report

Made's Thesis

ORIGINALITY REPORT

19%	15%	10%	6%
SIMILARITY INDEX	INTERNET SOURCES	PUBLICATIONS	STUDENT PAPERS

PRIMARY SOURCES

1	www.scribd.com Internet Source	5%
2	aerocastle.files.wordpress.com Internet Source	1%
3	Submitted to Cranfield University Student Paper	1%
4	Bandu N. Pamadi. "Performance, Stability, Dynamics, and Control of Airplanes, Second Edition", American Institute of Aeronautics and Astronautics (AIAA), 2004 Publication	<1%
5	hdl.handle.net Internet Source	<1%
6	researchrepository.wvu.edu Internet Source	<1%
7	mafiadoc.com Internet Source	<1%
8	Jia-Horng Yang, Hua-Kai Xu. "Robust Controller Design for Non-Minimum Phase	<1%

Curriculum Vitae



Basic Information	
Name	I Made Pradana Kusuma Putra
Place of Birth	Denpasar
Date of Birth	5 February 2000
Address	Jl. Padma Gg. 1B No. 17 Denpasar

Year	Education
2018 - present	International University Liaison Indonesia (IULI)
2015 - 2018	SMA Negeri 3 Denpasar
2012 - 2015	SMP Negeri 3 Denpasar
2006 - 2012	SD Negeri 1 Penatih

Year	Work Experiences
2022	Flight Control Engineer in Baruna-1 Firefighting Aircraft Design Project for AIAA Undergraduate Aircraft Design Competition 2022
2021	A Quadcopter Design Project Member in the part of Internship at Badan Tenaga Nuklir Nasional
2020	Internship at Merpati Maintenance Facility
2020	Member of Koba Airport Masterplan Project
2020	Internship at Merpati Maintenance Facility
2020	Head of The Fundamental Amphibious Aircraft System Design Project
2019	Head of Aeromodelling Aviation Engineering Club
2019	Chairman of Student Executive Board International University Liaison Indonesia
